

MOUNTAIN-PLAINS CONSORTIUM

MPC 17-329 | N. Wehbe, A. Ghadban, and T. Pauly

Seismic Performance of
Self-Consolidating Concrete
Bridge Columns



A University Transportation Center sponsored by the U.S. Department of Transportation serving the Mountain-Plains Region. Consortium members:

Colorado State University
North Dakota State University
South Dakota State University

University of Colorado Denver
University of Denver
University of Utah

Utah State University
University of Wyoming

Seismic Performance of Self-Consolidating Concrete Bridge Columns

Nadim I. Wehbe
Professor and Department Head
Department of Civil and Environmental Engineering
South Dakota State University
Brooking, SD 57007
Phone: (605) 688-5427
Email: nadim.wehbe@sdstate.edu

Ahmad A. Ghadban
Post-Doctoral Research Associate
Department of Civil and Environmental Engineering
South Dakota State University
Brooking, SD 57007
Phone: (605) 688-6627
Email: ahmad.ghadban@sdstate.edu

Todd Pauly
Graduate Student
Department of Civil and Environmental Engineering
South Dakota State University
Brooking, SD 57007
Phone: (605) 688-5427
Email: todd.pauly@sdstate.edu

Acknowledgment

The authors would like to acknowledge the financial support of the Mountain-Plains Consortium (MPC) for funding this study through project MPC-402.

Disclaimer

The contents of this report reflect the views of the authors, who are responsible for the facts and the accuracy of the information presented. This document is disseminated under the sponsorship of the Department of Transportation, University Transportation Centers Program, in the interest of information exchange. The U.S. Government assumes no liability for the contents or use thereof.

NDSU does not discriminate in its programs and activities on the basis of age, color, gender expression/identity, genetic information, marital status, national origin, participation in lawful off-campus activity, physical or mental disability, pregnancy, public assistance status, race, religion, sex, sexual orientation, spousal relationship to current employee, or veteran status, as applicable. Direct inquiries to Vice Provost for Title IX/ADA Coordinator, Old Main 201, NDSU Main Campus, 701-231-7708, ndsu.eoaa@ndsu.edu.

ABSTRACT

The high amount of confining lateral steel required by seismic design provisions for rectangular bridge columns can cause steel congestion. The high amount of confining steel may hinder the placement of conventional concrete (CC). Self-consolidating concrete (SCC) eliminates or reduces concrete placement and consolidation issues in concrete members with steel congestion. There are limited data, however, on the seismic performance of SCC bridge columns. This study included experimental investigations to assess the stress-strain relationships of SCC mixes and the seismic performance of rectangular SCC bridge columns. SCC mixes, control CC mixes, and rectangular columns were tested. Experimental results of the concrete mixes showed that the strain at strength and the ultimate strain of SCC are higher than those of CC, while concrete ductility and the elastic modulus of SCC are lower than those of CC. Experimental results of the column tests showed that the use of SCC reduces displacement ductility and energy dissipation but increases drift ratio at failure. The SCC column performance under inelastic cyclic lateral loading was found to be satisfactory and comparable to that of CC columns.

TABLE OF CONTENTS

1. INTRODUCTION.....	1
1.1 Project Description.....	1
1.2 Objectives	2
2. LITERATURE REVIEW	3
2.1 Strength and Ductility of Reinforced Concrete Columns	3
2.1.1 Summary of Code Confinement Reinforcement Requirements	3
2.1.1.1 ACI Building Code Requirements for Structural Concrete (ACI 318-2011).....	3
2.1.1.2 AASHTO LRFD Bridge Design Specifications (AASHTO 2012).....	5
2.1.1.3 AASHTO Guide Specifications for LRFD Seismic Bridge Design (AASHTO 2011).....	5
2.2 Previous Studies.....	8
2.2.1 SCC Stress-Strain Relationship.....	8
2.2.2 Reinforced SCC Columns	9
3. METHODOLOGY	12
3.1 Stress-Strain Relationship Study.....	12
3.1.1 Concrete Mixtures.....	12
3.1.1.1 Mix Designs	12
3.1.1.2 Concrete Constituents	13
3.1.2 Mixing and Batching.....	14
3.1.3 Curing Methods.....	14
3.1.4 Fresh Properties.....	15
3.1.4.1 Slump Flow Test	15
3.1.4.2 Passing Ability Test	16
3.1.4.3 Other Fresh Tests	17
3.1.5 Hardened Properties	17
3.1.5.1 Uniaxial Compression Test.....	17
3.1.5.2 Stress-Strain Relationship	18
3.2 Column Study	19
3.2.1 Design of Specimens.....	19
3.2.1.1 Column Height.....	22
3.2.1.2 Column Cross Section.....	22
3.2.1.3 Transverse Reinforcement	23
3.2.1.4 Footing Design.....	24
3.2.2 Instrumentation	25
3.2.3 Construction	26
3.2.4 Material Properties.....	28
3.2.4.1 Hardened Concrete Properties.....	28
3.2.4.2 Reinforcing Steel Properties	28
3.2.5 Test Setup	28
3.2.6 Experimental Procedure	32
3.2.6.1 Other Considerations.....	34
3.2.7 Theoretical Analysis.....	36
3.2.7.1 Deflection Due to Flexure.....	36
3.2.7.2 Deflection Due to Shear	41
3.2.7.3 Deflection Due to Bond Slip.....	42

4. RESULTS AND DISCUSSIONS	46
4.1 Stress-Strain Relationship Study.....	46
4.1.1 Fresh Concrete Properties	46
4.1.2 Hardened Properties	47
4.2 Column Study	51
4.2.1 Material Properties	51
4.2.1.1 Fresh Concrete Properties	51
4.2.1.2 Hardened Concrete Properties.....	52
4.2.1.3 Reinforcing Steel Properties	52
4.2.2 Testing Results.....	53
4.2.2.1 Specimen CC1.....	53
4.2.2.2 Specimen CC2.....	59
4.2.2.3 Specimen SCC1	64
4.2.2.4 Specimen SCC2	69
4.2.3 Remarks and Observations.....	76
4.2.4 Analytical Results	78
4.2.4.1 Calculated Deflections	78
4.2.4.2 Comparison between Experimental and Analytical Results	81
5. SUMMARY, FINDINGS, AND CONCLUSIONS.....	83
5.1 Summary	83
5.2 Findings	83
5.2.1 SCC Stress-Strain Relationship.....	83
5.2.2 Column Performance	84
5.3 Conclusions.....	84
6. REFERENCES.....	85
APPENDIX A. CONCRETE CONSTITUENT TEST DATA.....	88
A-1. GCC Type III Cement Data Sheet.....	88
A-2. Coal Creek Class F Fly Ash Data Sheet.....	89
A-3. Aggregate Testing Data.....	90
A-3.1 Aggregate Gradations	90
A-3.2 Fine Aggregate Data Sheet.....	93
A-3.3 Coarse Aggregate Data Sheet.....	94
A-4 Steel Reinforcement Mill Certificates	96
APPENDIX B: ADMIXTURE LITERATURE	98
B-1. Superplasticizer - ADVA® Cast 575	98
B-2. Air Entrainer – Daravair® M	100
APPENDIX C: MEASURED COLUMN RESPONSE.....	102
C-1. Specimen CC1	102
C-2. Specimen CC2.....	105
C-3. Specimen SCC1.....	108
C-4. Specimen SCC2.....	110
APPENDIX D: PLOTS OF EXPERIMENTAL MEASUREMENTS	112
D-1. Specimen CC1.....	113

LIST OF TABLES

Table 3.1	Mix Design Matrix for CC	12
Table 3.2	Mix Design Matrix for SCC	13
Table 4.1	Measured Fresh Properties	46
Table 4.2	Measured Compressive Strength.....	47
Table 4.3	Measured Concrete Strain at Strength.....	49
Table 4.4	Measured Concrete Ultimate Strain	49
Table 4.5	Measured Concrete Ductility.....	49
Table 4.6	Measured Concrete Elastic Modulus.....	50
Table 4.7	Comparison of Measured and Theoretical (ACI Empirical) Elastic Moduli.....	50
Table 4.8	Fresh Concrete Properties of the Column Concrete	51
Table 4.9	Hardened Concrete Properties of the Columns Concrete.....	52
Table 4.10	Measured Steel Properties	52
Table 4.11	Target and Measured Axial Load Information	53
Table 4.12	Summary of Experimental Results.....	77
Table 4.13	Analytical Lateral Deflections for Group 1 Specimens.....	79
Table 4.14	Analytical Lateral Deflections for Group 2 Specimens.....	80
Table 4.15	Calculated Deflections due to Flexure, Bond Slip, and Shear.....	81
Table 4.16	Comparison between Experimental and Analytical Displacements	81
Table 4.17	Ratios of Experimental to Analytical Displacements.....	81

LIST OF FIGURES

Figure 1.1	Placement of Conventional Concrete in a Highly Congested Bridge Column-Footing Connection	2
Figure 3.1	Portable Concrete Mixer	14
Figure 3.2	Slump Flow Test	15
Figure 3.3	J-Ring Test	17
Figure 3.4	SCC Standard Cylinder Specimen at Failure	18
Figure 3.5	Prototype Column and Corresponding Test Column	20
Figure 3.6	Details of Column Specimens	21
Figure 3.7	Longitudinal Bar Designations.....	22
Figure 3.8	Reinforcement Cage Configuration at the Top of the Column	23
Figure 3.9	Footing Details	24
Figure 3.10	3-D Representation of Specimen Reinforcement	25
Figure 3.11	Locations of the Strain Gages.....	26
Figure 3.12	Steel Reinforcement Cage	27
Figure 3.13	Plan View of Test Setup.....	29
Figure 3.14	Elevation Views of Test Setup	30
Figure 3.15	3-D View of Test Setup.....	31
Figure 3.16	Test Setup.....	32
Figure 3.17	Typical Moment-Curvature of the Experimental R/C Cross Sections	33
Figure 3.18	System of Forces Acting on the (a) Un-deflected Specimen, (b) Deflected Specimen.....	34
Figure 3.19	Typical Curvature along Column Height at the Ultimate State.....	40
Figure 3.20	Typical Bond Slip Rotation of a Specimen	42
Figure 3.21	Bond Slip of Developed Bars	43
Figure 4.1	Measured Stress-Strain for the Conventional and SCC Mixes.....	47
Figure 4.2	Comparison between SCC and CC Measured Stress-Strain Curves	48
Figure 4.3	Theoretical (ACI Empirical) and Measured Elastic Moduli	51
Figure 4.4	Measured Stress-Strain Relationship of the Column Concrete	52
Figure 4.5	Measured Stress-Strain Relationship of Steel Bars	53
Figure 4.6	Lateral Load History for Specimen CC1	54
Figure 4.7	Measured Load-Displacement for Specimen CC1	55
Figure 4.8	Visual Inspection of Specimen CC1 (1st Excursion)	56
Figure 4.9	Measured Lateral Load-Strain in Longitudinal Steel Below Column-Footing Interface of Specimen CC1.....	57
Figure 4.10	Measured Lateral Load-Strain in Longitudinal Steel of at and Above Column-Footing Interface of Specimen CC1	58
Figure 4.11	Measured Lateral Load-Strain in Transverse Steel of Specimen CC1	59
Figure 4.12	Lateral Load History for Specimen CC2.....	60
Figure 4.13	Measured Load-Displacement for Specimen CC2	60
Figure 4.14	Visual Inspection of Specimen CC2 (1st Excursion)	61
Figure 4.15	Measured Lateral Load-Strain in Longitudinal Steel Below Column-Footing Interface of Specimen CC2.....	62

Figure 4.16 Measured Lateral Load-Strain in Longitudinal Steel of at and Above Column-Footing Interface of Specimen CC2	63
Figure 4.17 Measured Lateral Load-Strain in Transverse Steel of Specimen CC2	64
Figure 4.18 Lateral Load History for Specimen SCC1	65
Figure 4.19 Measured Load-Displacement for Specimen SCC1	65
Figure 4.20 Visual Inspection of Specimen SCC1 (1st Excursion)	66
Figure 4.21 Measured Lateral Load-Strain in Longitudinal Steel Below Column-Footing Interface of Specimen SCC1	67
Figure 4.22 Measured Lateral Load-Strain in Longitudinal Steel of at and Above Column-Footing Interface of Specimen SCC1	68
Figure 4.23 Measured Lateral Load-Strain in Transverse Steel of Specimen SCC1	69
Figure 4.24 Specimen SCC2 Plastic Hinge Region Concrete Defects (Looking North)	70
Figure 4.25 Lateral Load History for Specimen SCC2	70
Figure 4.26 Measured Lateral Load-Displacement for Specimen SCC2	71
Figure 4.27 Visual Inspection of Specimen SCC2 (1st Excursion)	73
Figure 4.28 Measured Lateral Load-Strain in Longitudinal Steel Below Column-Footing Interface of Specimen SCC2	74
Figure 4.29 Measured Lateral Load-Strain in Longitudinal Steel of at and Above Column-Footing Interface of Specimen SCC2	75
Figure 4.30 Measured Lateral Load-Strain in Transverse Steel of Specimen SCC2	76
Figure 4.31 Response Envelopes	77
Figure 4.32 Analytical Lateral Load-Deflection Envelopes	79
Figure 4.33 Experimental and Analytical Response Envelopes	82

LIST OF ACRONYMS

AASHTO	American Association of State Highway and Transportation Officials
ACI	American Concrete Institute
ASTM	American Society for Testing and Materials
Caltrans	California Department of Transportation
CC	Conventional Concrete
CFRP	Carbon Fiber Reinforced Polymer
DOT	Department of Transportation
FRP	Fiber Reinforced Polymer
GFRP	Glass Fiber Reinforced Polymer
PCI	Precast/Prestressed Concrete Institute
PEER	Pacific Earthquake Engineering Research
SCC	Self-Consolidating Concrete
SDC	Seismic Design Category
SDDOT	South Dakota Department of Transportation
VSI	Visual Stability Index

EXECUTIVE SUMMARY

Self-consolidating concrete (SCC) is a specially proportioned hydraulic cement concrete that enables the fresh concrete to flow without segregation. Because of its high workability, SCC flows into narrow spaces to form corners, and around closely spaced steel reinforcement without the need for mechanical vibration. In seismic regions such as Utah and parts of Colorado in Transportation Region 8, the need for a large amount of confinement reinforcement to provide the required ductility often results in columns with excessive steel congestion. Steel congestion hinders the placement and proper consolidation of conventional concrete (CC). There are also cases when concrete repair and/or replacement are needed to fix localized damage in bridge structural elements following a seismic event. The high flowability and robustness of SCC make it ideal for the construction and repair of bridge columns designed to meet seismic detailing. There is lack of data on the performance of rectangular SCC bridge columns under seismic loads. In this study, experimental work was performed on SCC and CC mixes and bridge column specimens. The study covered in this report had two main objectives: 1) to assess stress-strain relationships of SCC under uniaxial compression, and 2) to evaluate the seismic performance of rectangular SCC bridge columns under inelastic load reversal. To accomplish the first objective, three SCC and four CC mixtures were designed, batched, and tested under uniaxial compression. Fresh and hardened properties were measured, and typical stress-strain parameters were evaluated to compare SCC to CC mixes. To fulfill the second objective, four one-third scale rectangular bridge column specimens were designed, fabricated, instrumented, and tested. The specimens were identical in geometry and reinforcement. The column's cross section was 12-in. square and the column's aspect ratio was 5.08. The reinforcement consisted of 1.72% longitudinal reinforcement and 1.5% transverse reinforcement. Two of the specimens were constructed with SCC, while the other two were constructed with CC. The specimens were tested under combined axial and lateral loads. One of the SCC and one of the CC column specimens were subjected to axial compressive load equal to $0.075f'_cA_g$ while the other SCC and CC column specimens were subjected to axial compressive load equal to $0.15f'_cA_g$. The results of the material testing showed that, for the same concrete strength, SCC attained higher strain at strength and ultimate strain, lower material ductility, and lower elastic modulus than conventional concrete. The results of the structural tests of the column specimens showed that SCC bridge columns provide adequate performance under high inelastic lateral load reversals. Compared with CC columns, SCC columns exhibited lower displacement ductility, higher drift ratio, and lower energy dissipation.

1. INTRODUCTION

1.1 Project Description

Self-consolidating concrete (SCC) is a type that fills formwork and encompasses steel reinforcement in its fresh state under its own weight without the need for mechanical vibration while still maintaining a homogeneous composition (Goodier 2003). In typical concrete construction, conventional concrete (CC) requires the use of an external means of mechanical vibration in order to fully consolidate during placement and to ensure that the formwork is thoroughly filled without excessive voids. This is especially important in structural applications to ensure that steel reinforcement is completely embedded in concrete. SCC was developed in Japan in the late 1980s in response to the diminishing durability and overall quality of concrete structures due to a decrease in the availability of skilled workers needed to place concrete that meets code requirements (Okamura 1998). Since SCC does not require mechanical vibration, it reduces the number of necessary workers and speeds up concrete placement, thereby reducing the overall labor cost on projects. Additionally, SCC ensures peace of mind knowing that steel reinforcement in the structure is fully embedded in concrete, and that the appearance of the structure will be satisfactory following formwork removal. SCC eliminates voids on the surface known as “bug-holes” or “honeycombing,” a problem common in some structures constructed with improperly consolidated CC. These surfaces require subsequent patching or grouting.

SCC has been used extensively in European and Asian countries during the past two decades, but has had limited application in the United States until the last decade. SCC use in the United States began in the precast concrete industry where smoothness of the finished concrete surface was an architectural requirement. More recently, SCC has been utilized on a greater variety of projects, including drilled shafts, bridge pier and abutment repairs, and other structural applications where reinforcement congestion and restricted access during placement and consolidation is common (ACI 2007).

In seismic regions of the United States, design code provisions for reinforced concrete columns require increased amounts of confinement steel reinforcement in comparison with other regions of the country. Increased amounts of reinforcement can lead to excessive steel congestion, as seen in **Figure** . This figure demonstrates casting of CC in a highly reinforced column-footing connection. Additionally, reinforced concrete columns often suffer localized damage from seismic events. Damaged columns require repairs that are only possible with highly flowable concrete. SCC would be an ideal alternative to CC in these applications due to its fresh properties.



Figure 1.1 Placement of Conventional Concrete in a Highly Congested Bridge Column-Footing Connection

There is a lack of experimental data to assess the performance of SCC columns under seismic loads. This research includes experimental and analytical studies conducted to evaluate the structural performance of SCC bridge column specimens under inelastic cyclic lateral loading. Conclusions drawn from the results of this research project will be made available to state DOTs for their use in determining if SCC should be implemented in bridge columns in seismic regions.

1.2 Objectives

Two main objectives were addressed during the course of this study. The first was to evaluate the stress-strain relationship of SCC and compare it with CC under uniaxial compression. The second was to evaluate the ductility of reinforced SCC bridge columns under combined axial and reverse cyclic lateral loads and compare it with CC bridge columns.

2. LITERATURE REVIEW

2.1 Strength and Ductility of Reinforced Concrete Columns

In seismic design of reinforced concrete structures, column critical sections, known as plastic hinges, are detailed for inelastic flexural response in order to dissipate energy from earthquakes. A column's ability to undergo large deformation past its elastic limit and still maintain a large portion of its initial strength is known as ductility (Paulay and Priestley 1992). Increased column ductility is required in seismic regions in order to prevent bridge failures and maintain functionality of roadways (Priestley et al. 1996). In columns designed for moment connections at the footing and bent-cap, plastic hinge regions are located above the column-footing interface and below the column-bent-cap interface. Column transverse confinement steel in these regions is vital in attaining ductile response. Confinement steel prevents premature buckling of compression bars, confines compressed concrete cores, provides clamping of lap-splices, and resists shear forces from lateral loads (Paulay and Priestley 1992).

2.1.1 Summary of Code Confinement Reinforcement Requirements

In order to provide required ductility in the plastic hinge regions of reinforced concrete columns in seismic regions, design codes specify a minimum amount of confinement steel reinforcement. Three design codes were summarized in this review of confinement requirements: the American Concrete Institute Building Code Requirements for Structural Concrete (ACI 2011), the American Association of State Highway and Transportation Officials LRFD Bridge Design Specifications (AASHTO 2012), and the American Association of State Highway and Transportation Officials Guide Specifications for LRFD Seismic Bridge Design (AASHTO 2011). A square column cross section was used for the experimental testing conducted in this study; therefore, only tied rectangular column requirements were summarized in this review. The California Department of Transportation (Caltrans) Bridge Design Specifications were not included because Caltrans currently only permits the use of circular transverse steel reinforcement consisting of butt-welded hoops or continuous spirals in bridge column design in California.

The code equations presented in this summary are in United States Customary Units (e.g., pounds, inches). Throughout this review, the amount of confinement reinforcement can be taken as the area of the transverse tie bars, A_{sh} , required in the direction of applied lateral loads, within a spacing s , along the height of the column. Tie bars can consist of rectangular hoops and crossties. A_{sh} must be satisfied in both directions of the column cross section. Variables that are equivalent and used throughout this section include specified concrete compressive strength, f'_c , specified yield strength of transverse reinforcement, f_{yt} , and gross cross-sectional area of the concrete section, A_g .

2.1.1.1 ACI Building Code Requirements for Structural Concrete (ACI 318-2011)

Throughout the potential plastic hinge region of the column, A_{sh} shall not be less than the greater of the values given by Equation and Equation (§ 21.6.4.4).

$$A_{sh} = 0.3 \frac{s b_c f'_c}{f_{yt}} \left[\left(\frac{A_g}{A_{ch}} \right) - 1 \right] \quad \text{Equation 2.1}$$

$$A_{sh} = 0.09 \frac{s b_c f'_c}{f_{yt}} \quad \text{Equation 2.2}$$

Where:

b_c = cross-sectional dimension of member core measured to the outside edges of the transverse reinforcement composing area A_{sh}

A_{ch} = cross-sectional area of structural member measured to the outside edges of the transverse reinforcement

A_{sh} shall be provided throughout the plastic hinge length, l_o , which shall not be taken less than the greater of the member depth at the joint face or the section where flexural yielding is likely to occur, one-sixth of the column clear span, or 18 inches (§ 21.6.4.1). Tie set spacing, s , inside the plastic hinge region shall not exceed the smaller of one-quarter of the minimum member dimension, six times the smallest longitudinal reinforcement nominal bar diameter ($6d_b$), or s_o , defined by Equation 2.3 (§ 21.6.4.3). The conditions that prohibit s from exceeding the smaller of one-quarter of the minimum member dimension and s_o were set to maintain concrete confinement. The condition that prohibits s from exceeding $6d_b$ was set to prevent longitudinal bar buckling.

$$s_o = 4 + \left(\frac{14 - h_x}{3} \right) \quad \text{Equation 2.3}$$

Where:

$$4 \text{ in.} \leq s_o \leq 6 \text{ in.}$$

h_x = maximum center-to-center horizontal spacing of crossties or hoop legs on all faces of the column
Transverse reinforcement shall consist of rectangular hoops with or without crossties of the same or smaller size bar diameter as that of the hoop (§ 21.6.4.2). A hoop has seismic hooks at both ends and can be either a closed tie made up of several reinforcing elements, or a continuously wound tie. A tie is a loop of reinforcing bar that encloses longitudinal reinforcement. A seismic hook is the end of a reinforcing bar that has a bend of 135 degrees or greater and an extension of $6d_b$ but not less than 3 inches extending into the column core. A crosstie is a reinforcing bar that has a seismic hook at one end and a 90-degree bend with a $6d_b$ extension at the other (§ 7.1.4). The inside diameter of the bend for ties is $4d_b$ for #5 and smaller bars (§ 7.2.2).

Crossties must engage an outside longitudinal bar at both ends. Crossties in consecutive tie-sets must be alternated end-for-end in order to provide sufficient confinement. The spacing between hoop legs and crossties within the member cross section must not exceed 14 inches center-to-center (§ 21.6.4.2). Transverse bar sizes shall be at least #3 for longitudinal bar sizes #10 and under, and #4 for longitudinal bar sizes #11, #14, #18, and bundled bars (§ 7.10.5.1). Tie sets must be arranged so that every corner and every alternating longitudinal bar is supported by the corner of a tie with an angle less than 135 degrees, while maintaining a distance between supported and unsupported bars of less than 6 inches (§ 7.10.5.3). Additionally, the first tie set above the footing cannot be located greater than one-half of a tie spacing above the column-footing interface (§ 7.10.5.5). Outside of the plastic hinge region, vertical tie set spacing shall not exceed the smaller of six times the smallest nominal bar diameter of the longitudinal reinforcement ($6d_b$) and 6 in. This requirement is in place to provide reasonable ductility along the length of the column (§ 21.6.4.5).

2.1.1.2 AASHTO LRFD Bridge Design Specifications (AASHTO 2012)

Transverse reinforcement requirements for AASHTO specifications are similar to those of ACI specifications with the exception of the factor preceding the variables in Equation 2.5. Throughout the potential plastic hinge region, A_{sh} for both principal axes shall be taken as the greater area obtained from Equation 2.4 and Equation 2.5 (§ 5.10.11.4.1d).

$$A_{sh} \geq 0.3sh_c \frac{f'_c}{f_{yt}} \left[\frac{A_g}{A_{ch}} - 1 \right] \quad \text{Equation 2.4}$$

$$A_{sh} \geq 0.12sh_c \frac{f'_c}{f_{yt}} \quad \text{Equation 2.5}$$

Where:

A_c = area of column core

h_c = core dimension of tied column in the direction under consideration, measured to the outside of the perimeter hoop

Similar to requirements provided by ACI, the length of the plastic hinge region shall not be less than the greatest among the maximum cross-sectional column dimension, one-sixth of the clear height of the column, or 18 inches (§ 5.10.11.4.1e). The spacing of transverse reinforcement throughout the plastic hinge shall not exceed one-quarter of the minimum member dimension, or 4 inches center-to-center (§ 5.10.11.4.1e). The spacing of ties outside of the plastic hinge region shall not exceed the least dimension of the member, or 12 inches (§ 5.10.6.3). At connections, the column transverse reinforcement should continue into the adjoining member a distance not less than one-half of the greater column dimension or 18 inches (§ 5.10.11.4.3). All other AASHTO transverse reinforcement details for hoops and cross-ties are the same as those presented in the ACI specifications summary.

2.1.1.3 AASHTO Guide Specifications for LRFD Seismic Bridge Design (AASHTO 2011)

For columns requiring a displacement ductility demand greater than 4, transverse reinforcement shall be either butt-welded hoops or spirals (§ 8.8.7). In this project, rectangular hoops with seismic hooks were used in order to create higher steel congestion, compared with using circular confinement reinforcement. This project focused on directly comparing the seismic performance of SCC to CC; therefore, a target displacement ductility demand was not defined.

The volume of transverse confinement reinforcement in the plastic hinge region of columns is based upon the shear capacity of the column utilizing ductility demand. The shear capacity, V_n , of columns is determined using Equation 2.6 (§ 8.6.1).

$$\phi_s V_n \geq V_u \quad \text{Equation 2.6}$$

Where:

$\phi_s = 0.9$ for shear in reinforced concrete

The shear demand, V_u for columns in Seismic Design Category (SDC) B, is based upon the lesser of the force obtained from linear-elastic seismic analysis or the force, V_{po} , corresponding to the overstrength moment, M_{po} . V_u for columns in SDCs C and D is based upon V_{po} , which can be determined using Equation 2.7 (§ 8.5).

$$M_{po} = \lambda_{mo} M_p \quad \text{Equation 2.7}$$

Where:

M_p = idealized plastic moment capacity of reinforced concrete member based upon the expected material properties; M_p is obtained from moment-curvature analysis of the reinforced concrete section

λ_{mo} = steel overstrength magnifier = 1.2 for ASTM A706 reinforcement or 1.4 for ASTM A615 Grade 60 reinforcement

The nominal shear capacity, V_n , of reinforced concrete members is determined from Equation 2.8 (§ 8.6.1).

$$V_n = V_c + V_s \quad \text{Equation 2.8}$$

Where:

V_c = concrete contribution to shear capacity

V_s = steel reinforcement contribution to shear capacity

The nominal shear capacity of concrete, V_c , decreases in a section as ductility demand increases, but increases as additional confinement reinforcement is added. In SDCs B, C, and D, V_c is determined using Equation 2.9 (§ 8.6.2).

$$V_c = v_c A_e \quad \text{Equation 2.9}$$

Where:

A_e = effective area of cross section for shear resistance = $0.8A_g$

v_c = shear stress in concrete

If the ultimate compressive force, P_u , acting on the section is compressive, then Equation 2.10 through Equation 2.13 are used to calculate v_c . If P_u is tensile, $v_c = 0$.

$$v_c = 0.032\alpha' \left(1 + \frac{P_u}{2A_g} \right) \sqrt{f'_c} \leq \min \begin{cases} 0.11\sqrt{f'_c} \\ 0.47\alpha' \sqrt{f'_c} \end{cases} \quad \text{Equation 2.10}$$

$$\alpha' = \frac{f_w}{0.15} + 3.67 - \mu_D \quad \text{Equation 2.11}$$

$$f_w = 2\rho_w f_{yt} \leq 0.35 \quad \text{Equation 2.12}$$

$$\rho_w = \frac{A_{sh}}{bs} \quad \text{Equation 2.13}$$

Where:

b = width of rectangular column section

μ_D = maximum local displacement ductility ratio of reinforced concrete member

α' = concrete shear stress adjustment factor

ρ_w = web reinforcement ratio

The concrete shear capacity, V_c , of sections within the plastic hinge region shall be determined using $\mu_D = 2$ for SDC B, $\mu_D = 3$ for SDC C, and Equation 2.14 for SDC D (§ 4.9).

$$\mu_D = 1 + \frac{\Delta_{pd}}{\Delta_{yi}} \quad \text{Equation 2.14}$$

Where:

Δ_{pd} = plastic displacement demand

Δ_{yi} = idealized yield displacement corresponding to the idealized yield curvature, ϕ_{yi}

The nominal shear reinforcement strength, V_s , provided by rectangular ties and stirrups shall be determined using Equation 2.15 (§ 8.6.3).

$$V_s = \frac{A_{sh} f_{yt} d}{s} \quad \text{Equation 2.15}$$

Where:

d = effective depth of section in the direction of loading measured from the compression face of the member to the centroid of the tension reinforcement.

To ensure yielding of the transverse reinforcement prior to crushing of the concrete, V_s shall not be taken to be greater than the shear reinforcement strength calculated using Equation 2.16 (§ 8.6.4).

$$V_s \leq 0.25 \sqrt{f'_c} A_e \quad \text{Equation 2.16}$$

The minimum amount of shear reinforcement, A_{sh} , is dependent upon the web reinforcement ratio, ρ_w . For SDC B, ρ_w must be greater than 0.002, and for SDC C and D, ρ_w must be greater than 0.004. ρ_w is determined using Equation 2.13.

The length of the plastic hinge region, L_{pr} , shall be taken as the larger of 1.5 times the gross cross-sectional column dimension in the direction of bending, the region of the column where the moment demand exceeds 75% of the plastic moment, or the analytical plastic hinge length, L_p , which is calculated using Equation 2.17 (§ 4.11.7).

$$L_p = 0.08L + 0.15 f_{ye} d_{bl} \geq 0.3 f_{ye} d_{bl} \quad \text{Equation 2.17}$$

Where:

L = length of column from point of maximum moment to point of zero moment

f_{ye} = expected yield strength of longitudinal column reinforcement = 68 ksi for Gr. 60 reinforcement (Table 8.4.2-1)

d_{bl} = nominal bar diameter of longitudinal column reinforcement

The maximum spacing for transverse reinforcement within the plastic hinge shall not exceed the smallest of one-fifth of the least dimension of the column cross section, six times the nominal diameter of the longitudinal reinforcement ($6d_b$), or 6 inches for single hoop reinforcement (§ 8.8.9). The volumetric ratio of lateral reinforcement required outside of the plastic hinge region shall be the same type and configuration and shall not be less than 50% of that determined for the plastic hinge region (§ 8.8.8). Additionally, details pertaining to crossties and continuously wound hoops are similar to those defined in ACI specifications.

2.2 Previous Studies

2.2.1 SCC Stress-Strain Relationship

Similar to other physical properties of SCC, the elastic modulus is highly dependent on the mixture constituents. Some studies have shown that the elastic modulus is lower for SCC when compared with CC of similar compressive strength (Bonen and Shah 2005; Khayat et al. 2001; Kumar et al. 2011); whereas, others have shown that the elastic modulus is very similar to that of CC (Gutzmer 2008), (Mortsell and Rodum 2001).

Experimental results regarding the stress-strain relationship of SCC and direct strain and ductility comparisons between SCC and CC were difficult to find in the literature. The stress-strain relationship is important in the design of reinforced concrete structures because it assesses the overall response of concrete under applied loads. The region of the stress-strain curve that is difficult to analyze is the descending portion of the curve, known as the “strain softening” region. Strain softening in concrete is defined as its loss of load-carrying capacity after sustaining its maximum load (Rilem 2000). Decrease in stress with increase in strain after concrete reaches its ultimate compressive strength is vital in estimating the ductility of a section. For a majority of the studies found in the literature, stress-strain characteristics were only measured until the compressive strength was obtained on the ascending portion of the stress-strain curve. Few studies have focused on the descending portion of the stress-strain curve for SCC. The journal articles noted below document two experiments that studied the complete stress-strain relationship of SCC.

Desnerck, De Schutter, and Taerwe (2012) studied the stress-strain relationship of both SCC and CC, including the strain-softening portion of the stress-strain curve. The researchers quantified the ductility of SCC from the toughness of the concrete, which they defined as the area under the complete stress-strain curve obtained from testing concrete in uniaxial compression. To balance out the influence of compressive strength on toughness, they compared the ratio of toughness to concrete compressive strength, which they defined as specific toughness. From their results, SCC showed higher strain at strength values compared with CC, which resulted in higher specific toughness. However, the specific toughness of the strain-softening portion of the stress-strain curve showed little difference between SCC and CC. Another observation noted from this experiment was that concrete with lower compressive strength had higher specific toughness. The researchers made the assumption that there is a tradeoff

between ductility and desired strength in a concrete section. Additionally, they concluded that the strain-softening behavior of concrete decreases as concrete age increases, which correlates to a decrease in ductility with age for both SCC and CC (Desnerck et al. 2012).

Kumar, Singh, and Bhargava (2011) investigated the stress-strain relationship of SCC under uniaxial compression. Experimental results showed that SCC had lower measured strain after the axial load dropped by 20% from the peak load in comparison with CC. From that, the researchers concluded that SCC mixtures were less ductile than comparable CC mixtures. Results also indicated that strain at strength in SCC increased as compressive strength increased. Additionally, a new stress-strain model for SCC mixtures was proposed based upon concrete compressive strength (Kumar et al. 2011).

2.2.2 Reinforced SCC Columns

While there have been many research studies conducted regarding SCC material properties, few have focused on the structural performance of SCC columns, and even fewer have investigated the structural performance of SCC columns under seismic loads.

Restrepo, Seible, Stephan, and Shoettler (2006) investigated the seismic performance of reinforced concrete bridge columns constructed with high performance steel and concrete. The objectives of the study were to compare the performance of a column reinforced with high strength steel to that of a column reinforced with conventional ASTM A 706 steel, and also to examine the effect that incorporating SCC in both columns had on their performance. In the study, two circular 3-ft. diameter cantilever bridge columns with 9.5-ft. shear spans were fabricated and tested under constant axial load and quasi-static reverse cyclic lateral loading. Axial load indices corresponded to 7.5% for both columns tested. Longitudinal reinforcement and transverse volumetric reinforcement ratios were 2.54% and 1.74%, respectively, for specimen 1, which contained ASTM A 706 reinforcement, and 1.27% and 0.85%, respectively, for specimen 2, which contained high performance steel reinforcement. Transverse steel reinforcement throughout each specimen consisted of butt-welded hoops. The specified SCC compressive strength was 8 ksi. Results indicated that specimen 1 reached a displacement ductility and drift of 5.8% and 5.8%, respectively, whereas specimen 2 reached a ductility and drift of 2.4% and 3.9%, respectively. The researchers reported that the use of SCC had no overall effect on column performance (Restrepo et al. 2006).

Said and Nehdi (2007) studied the seismic behavior of full-scale structural frame column-joint connections. The objective of the study was to compare the behavior of a beam-column joint constructed with SCC and subjected to reverse cyclic loading to a joint subjected to the same loading conditions but constructed with CC. specimen 1 was fabricated with CC that had a measured 28-day compressive strength of 50.9 MPa (7.38 ksi); specimen 2 was fabricated with SCC that had a measured 28-day compressive strength of 50.4 MPa (7.31 ksi). The specimens were the same size and had identical reinforcement; the columns contained longitudinal reinforcement ratios of 2.8% and the beams had ratios of 1.2%. The transverse reinforcement consisted of two 10-mm (.394 in.) diameter interlocking rectangular ties spaced at 80 mm (3.15 in.) throughout the plastic hinge regions of the column, and one rectangular tie at the same spacing throughout the beam plastic hinge. Loading procedures were identical for each specimen. The specimen columns were subjected to axial load indices of approximately 10.5%, and the beam ends were subjected to vertically applied quasi-static reverse cyclic loading, approximately 1.67 m. (5.48 ft.) from the column face. Results indicated that each specimen exhibited similar performance until a drift of approximately 4.5%, after which the load-carrying capacity of specimen 2 deteriorated rapidly. Overall, specimen 1 attained a displacement ductility and drift of 6.0% and 9.0%, respectively; whereas, specimen 2 attained a displacement ductility of 5.0 and a drift ratio of 7.9%. Additionally, joint energy dissipation of specimen 1, defined as the cumulative area between load-displacement curves, exceeded that of specimen 2 by 38%. Overall, the researchers concluded that SCC

beam-column joints may not have the same load-carrying capacity under extreme seismic conditions as CC joints. They believed that the reduction in coarse aggregate content in SCC reduced its contribution to shear resistance compared with CC. They recommended that more studies are needed to investigate the behavior of SCC in plastic hinge regions under seismic loads, with emphasis placed on the effect of varying coarse aggregate sizes and amounts (Said and Nehdi 2007).

Galano and Vignoli (2008) compared the performance of reinforced SCC and CC slender columns subjected to short-term eccentric axial loads. During the course of the study, 60 2000-mm (6.56 ft.) high column specimens with 100-mm by 100-mm (3.94 in. by 3.94 in.) cross sections were tested. Variables altered between specimens were the concrete type and strength (normal strength and high strength), longitudinal and transverse steel reinforcement ratios, and axial load eccentricity. Strain data and lateral deflections were measured at the column mid-heights while specimens were loaded under displacement control at various eccentricities. From the data, primary and secondary bending moments along with ductilities within the column's critical sections could be determined. Results showed that SCC slender columns constructed with normal and high strength concretes exhibited lower ultimate normalized strength in comparison with CC. The researchers defined column normalized strength as the peak axial load divided by the product of the concrete's 28-day compressive strength and the column's cross-sectional area. Normal strength SCC showed soft and ductile failure modes compared to CC, but no notable differences in behavior were observed between medium-to-high-strength SCC and CC. Soft and ductile failure was characterized by a gradually decreasing slope in the post-peak branch of the axial load versus the mid-height deflection relationship. They recommended that additional tests should be conducted on slender columns of both concrete types to determine the significance of changing single variables, such as longitudinal and transverse steel reinforcement ratios (Galano and Vignoli 2008).

Paultre, Khayat, Cusson, and Tremblay (2005) studied the structural performance of SCC in confined concrete columns subjected to concentric axial load. In the study, nine reinforced column specimens were cast with SCC and two with CC. In combination with research conducted by Cusson and Paultre (1994) and Paultre et al. (1996), seven other reinforced column specimens were added to the sample population compared in this study. Additionally, five SCC and CC column specimens were fabricated without steel reinforcement. Specimens were 1400-mm (4.59 ft.) high with 235-mm (9.25 in.) square cross sections. Reinforced specimens had longitudinal steel ratios of 3.6%, and transverse steel ratios between 4.8% and 4.9%. Confinement reinforcement consisted of both normal strength and high strength steel. All of the reinforced and three of the un-reinforced specimens were subjected to concentric monotonic axial loading until failure. Column ductility was defined by dividing the measured strain at a 50% drop from column compressive strength by the strain measured at the column compressive strength. The two remaining unreinforced specimens were sawed into three sections and had cylindrical cores removed from both column ends and at mid-height. The cored specimens were tested in uniaxial compression to obtain compressive strength and elastic modulus of the in-place concrete. Results indicated that SCC columns exhibited greater ductility and slightly lower maximum load carrying capacity compared with similarly reinforced CC columns. The researchers believed the increase in the ductility of SCC was attributed to its lower elastic modulus due to a higher paste volume and lower coarse aggregate content. Additionally, higher ductilities were achieved for columns that contained lower compressive strength SCC and CC. Results from cored specimens indicated that greater homogeneity and a more uniform distribution of in-place compressive strengths were obtained in SCC specimens compared with CC specimens. However, cored SCC cylinders developed lower in-place compressive strengths compared with control SCC test cylinders that were fabricated concurrent to the columns (Paultre et al. 2005).

Lin, Hwang, Lin, and Liu (2008) tested square reinforced SCC columns under concentric axial compression. In this study, 16 SCC and 16 CC columns were constructed with variable concrete compressive strengths, longitudinal and transverse steel reinforcement ratios, and transverse reinforcement strengths and arrangements. Specimens were 1400-mm (4.59 ft.) high with 300-mm (11.8 in.) square cross sections. The specimens were tested under monotonic axial load until failure. Ductility

was defined as the area beneath the stress-strain curve up to a 50% drop in stress from the column compressive strength and also defined from the slope of the descending portion of the stress-strain curve between the strain at strength and the strain at a 50% drop in strength. Test results showed that SCC had 15% higher stiffness and 32% higher ductility than CC. The researchers recommended that SCC mixtures should be designed with approximately the same amount of coarse aggregate as CC mixtures in order to improve the mechanical behavior of the hardened concrete (Lin et al. 2008).

Khairallah (2013) tested circular reinforced SCC columns under concentric axial compression. Twenty reinforced concrete specimens were tested in this study, 10 of which were fabricated with SCC and 10 with CC. Specimen geometry consisted of 150-mm diameter by 600-mm height (5.90 in. by 23.6 in.) columns, and longitudinal steel ratios of 3.5%. Transverse steel reinforcement entailed spiral steel hoops with confinement ratios of 1.6%. Three specimen groups were confined with carbon fiber reinforced polymer (CFRP), fiber reinforced polymer (FRP), and glass fiber reinforced polymer (GFRP) wraps applied on the outside of the cover concrete. Another specimen group had additional confinement steel hoops added, which resulted in a confinement ratio of 3.2%. The last specimen group had no additional confinement added. Specimens were tested under monotonic axial load until failure. Ductility of the specimens was defined by the area under the load-displacement curve up to a 25% drop from the peak load, divided by the area under the load-displacement curve up to the peak load. Results from the study showed that SCC had considerably higher ductility for each confinement technique used in comparison with CC (Khairallah 2013).

3. METHODOLOGY

3.1 Stress-Strain Relationship Study

This experimental study was performed to evaluate the fresh and hardened properties of SCC and CC mixtures that were developed for the column study specimens. Standard ASTM procedures were followed in order to evaluate properties of both concrete types. For this study, the SCC fresh properties of interest included air content, filling ability, passing ability, and visual stability index (VSI). CC fresh properties of interest included air content and slump. Hardened properties of interest for both SCC and CC focused on the concrete stress-strain relationship. Obtained measurements included compressive strength, strain at strength, ultimate strain, ductility, and elastic modulus.

3.1.1 Concrete Mixtures

One SCC and three CC mixtures were developed during the course of this study. Grace Construction Products provided the SCC mix design in addition to the chemical admixtures used for all concrete batches. The target compressive strength of the SCC mixture was 6,500 psi, and the target slump flow range was 22 – 25 inches. The main variables altered among SCC batches were curing duration and proportions of admixtures.

Various CC mixtures were batched and tested in order to achieve a compressive strength range corresponding to the strengths obtained for SCC mixtures. Additionally, a desired CC slump of approximately 4 inches was a design consideration in order to obtain concrete mixtures that could be placed and consolidated in columns with congested steel. Two mix designs were provided by the South Dakota Department of Transportation (SDDOT); these mixtures were identified as SDDOT Structural Concrete Class A45 and Class A50. The last mix was designed by a local concrete ready-mix plant (Winter, Inc., Brookings, South Dakota). This mixture was designed to give higher compressive strength compared with what was attainable with standard SDDOT mixtures. The higher strength was needed to match the strength of the SCC mixtures.

3.1.1.1 Mix Designs

A summary of mix designs for each concrete type is presented in 3.1 and Table 3.2. Designations SCC and CC throughout this report represent self-consolidating concrete and conventional concrete, respectively. Following concrete designation, label B_ represents the mix ID indicating the mix design source. For both SCC and CC, batches B1 and B2 were produced to test concrete fresh and hardened properties in order to find suitable designs to use in reinforced concrete columns. The remaining batches were produced and tested during the column study portion of the project. CC-B3 data are from test cylinders fabricated with the concrete used to cast the footings of the column test specimens. This concrete was SDDOT A45 Structural Concrete batched by GCC Ready-Mix in Brookings, South Dakota. CC-B4 and SCC-B3 data are from test cylinders fabricated with the concrete used to cast the columns and loading blocks of the column test specimens.

Table 3.1 Mix Design Matrix for CC

Mix ID	CC-B1	CC-B2	CC-B3	CC-B4
Mix Source	SDDOT A50	Winter, Inc.	SDDOT A45	SDDOT A50
Curing Duration (days)	0	28	3	7
w/cm	0.378	0.348	0.395	0.378
Type III Cement (lb/yd3)	572	625	524	572
Fly Ash (lb/yd3)	143	156	131	143
Water (lb/yd3)	270	272	259	270
Coarse Aggregate (lb/yd3)	1695	1637	1715	1695
Fine Aggregate (lb/yd3)	1130	1174	1165	1130
Air-Entrainment (Daravair® M) (oz/cwt)	0.7	0.8	Info. Not Available	0.7
Superplasticizer (ADVA® Cast 575) (oz/cwt)	1.0	2.3		1.0

Table 3.2 Mix Design Matrix for SCC

Mix ID	SCC-B1	SCC-B2	SCC-B3
Mix Source	Grace CP	Grace CP	Grace CP
Curing Duration (days)	0	28	7
w/cm	0.373	0.373	0.373
Type III Cement (lb/yd3)	525	525	525
Fly Ash (lb/yd3)	225	225	225
Water (lb/yd3)	280	280	280
Coarse Aggregate (lb/yd3)	1400	1400	1400
Fine Aggregate (lb/yd3)	1450	1450	1450
Air-Entrainment (Daravair® M) (oz/cwt)	0.8	0.6	0.6
Superplasticizer (ADVA® Cast 575) (oz/cwt)	3.0	3.1	3.1*

*Adjustments were made for each batch to attain desired SCC flowable properties.

3.1.1.2 Concrete Constituents

The cement used for all concrete mixtures was GCC Type III Portland Cement produced in Rapid City, South Dakota. Type III cement was specified for the SCC mixtures in order to add more fine particles into the concrete. Type III cement is finer than Type I/II cement. Finer cement powder helps improve the segregation resistance of SCC. For consistency, Type III cement was adopted for CC mixtures as well. The cement test data sheet can be found in Appendix A-1.

Following SDDOT requirements, the fly ash used for all concrete mixtures was Class F fly ash. The fly ash test data sheet can be found in Appendix A-2.

The aggregates used for all concrete mixtures were provided by local aggregate supplier, LG Everist, Inc., headquartered in Sioux Falls, South Dakota. For both concrete types, the same coarse and fine aggregates were used. The fine aggregate was 3/8 in. washed concrete sand that came from an LG Everist pit in Brookings. The coarse aggregates were 3/4 in. and 1/2 in. crushed Pink Sioux Quartzite from an LG Everist quarry in Dell Rapids, South Dakota. Aggregate quality reports were conducted by Midwest

Testing Laboratory, Inc. in Fargo, North Dakota on the aggregates during the year prior to this study. Aggregate quality reports as well as aggregate gradations can be found in Appendix A-3. Two chemical admixtures were added to both SCC and CC mixtures: air-entraining admixture (Daravair® M) and superplasticizer (ADVA® Cast 575). Daravair® M enabled the mixtures to follow SDDOT requirements of 5.0% to 7.5% entrained air in the fresh concrete. ADVA® Cast 575 superplasticizer was used to improve concrete workability for both SCC and CC applications. The admixture quantities were adjusted based on measured fresh concrete properties obtained from trial batches. Literature on the two admixtures can be found in Appendix B.

3.1.2 Mixing and Batching

Concrete for each batch was produced in a portable one-half-cubic-yard-capacity adjustable-tilt drum mixer, which was powered by an electric motor and had three interior paddles. Through trial and error, it was discovered that the concrete mixed most effectively when the mixer drum was in a nearly horizontal position. This limited batch sizes for the SCC mixtures to approximately 3.5 cubic feet in order to keep the concrete from spilling out of the mixer. Figure 3.1 shows SCC being discharged from the mixer.



Figure 3.1 Portable Concrete Mixer

SCC mixtures were prepared following a procedure recommended by Grace Construction Products. First, all concrete constituents were measured out separately. The air-entrainer was added to the water and the solution was mixed thoroughly. The interior walls of the mixer were sprayed down with water in order to prevent absorption of water from the concrete to the mixer drum. Next, the mixer was started and the dry concrete constituents were added and mixed until a uniform composition was apparent. As the mixer drum continued to rotate, the water solution was slowly added and mixed with the dry constituents. Once the concrete attained a homogeneous mixture, the mixer was shut off and the superplasticizer was added. After sitting for two minutes to let the mixture rest, the mixer was started again for an additional eight minutes. The eight-minute mixing period was found to be the ideal amount of time to allow the superplasticizer to fully disperse. Conventional concrete followed the same mixing procedures as SCC.

3.1.3 Curing Methods

Standard 6 in. x 12 in. cylindrical concrete test specimens were cast in plastic molds. Each mold was capped with a plastic cover and cured for 24 hours before removing the cover and stripping the mold. All

of the test cylinders were cured for 28 days before they were tested in uniaxial compression. Cured cylinders were stored in a room that had humidity and temperature control for the durations presented in Table 3.1 and Table 3.2.

3.1.4 Fresh Properties

After concrete batching, samples were taken out of the wheelbarrows following ASTM C172-10: “Practice for Sampling Freshly Mixed Concrete” (ASTM 2010a). However, unlike the ASTM standard, which calls for two or more samples to be taken from the middle of the batch, all of the concrete was used due to the small size of each batch.

3.1.4.1 Slump Flow Test

For SCC, the flowability was measured following ASTM C1611-09b: “Standard Test Method for Slump Flow of Self-Consolidating Concrete” (ASTM 2009a). This test is conducted in a manner similar to ASTM C143 “Standard Test Method for Slump of Hydraulic-Cement Concrete” (ASTM 2012a), which is used to evaluate fresh CC. However, in the slump flow test, the slump cone is inverted and typically filled in one lift of SCC, rather than three lifts, which is required with CC. Another difference between the slump test and the slump flow test is that the slump test requires rodding of the CC (25 times each lift), whereas the slump flow test requires no rodding of the SCC. After the SCC is added to the inverted slump cone, the cone is pulled upward to a height of 9 inches in three seconds. The slump flow test is shown in Figure 3.2.



Figure 3.2 Slump Flow Test

Two measurements are recorded during the slump flow test. One records the average total diameter of the spread taken in orthogonal directions across the flow. The average diameter, taken to the nearest ½ inch and termed the SCC measured slump flow, can be calculated using Equation 3.1. The slump flow is used to monitor consistency among different SCC batches of the same mix and also to quantify the unconfined flow potential. Typically, slump flows of 18 to 30 inches are specified, depending on the intended use of the concrete (ACI 2007).

$$SlumpFlow = (d_1 + d_2) / 2$$

Equation 3.1

Where:

d_1 = the largest diameter of the circular spread of the concrete

d_2 = diameter measured orthogonal to d_1

The other measurement recorded during the slump flow test is the time it takes for the slump flow to reach 20 inches in diameter, which is referred to as T_{20} . T_{20} is used to evaluate the viscosity of the mixture, and is recorded to the nearest 0.2 second. T_{20} recordings between three and five seconds are typical of successfully batched SCC (PCI 2003). Along with slump flow and T_{20} , the visual stability index (VSI) of SCC is also documented during the slump flow test. VSI is a test that evaluates if segregation is apparent in the SCC and assigns values from 0 – 3 to the mixture. A value of 0 indicates a highly stable mixture with no signs of segregation or bleeding. A value of 1 indicates a stable mixture with no signs of segregation but signs of bleeding as indicated by water sheen on the surface of the concrete. A value of 2 indicates an unstable mixture with a mortar halo extending outside of the slump flow less than ½ in., in addition to a pile of aggregate in the middle of the flow. A value of 3 indicates a highly unstable mixture that is clearly segregated, as indicated by a large aggregate pile in the middle of the slump flow and a mortar halo extending outside of the flow greater than ½ in. (ASTM 2009a). Mortar halos can be noted by the evidence of water around the outside circumference of the slump flow. One problem with the VSI assessment is that it is subjective. Therefore, VSI is most beneficial when it is performed by experienced individuals.

Concrete slump flow was measured for each batch produced in this study. T_{20} was timed concurrently with the slump flow, and VSI readings were documented following each test.

3.1.4.2 Passing Ability Test

Following the slump flow test, the SCC passing ability was measured in accordance with ASTM C1621-09b: “Standard Test Method for Passing Ability of Self-Consolidating Concrete by J-Ring” (ASTM 2009b). This test is similar to the slump flow test, but it adds a circular steel device known as a J-Ring around the perimeter of the inverted slump cone. This device is intended to represent steel reinforcement and the passing ability of the SCC through that reinforcement. This test and the J-Ring are shown in Figure 3.3. Other than the addition of the J-Ring, the test is run identically to the slump flow test. If the average diameters obtained from the slump flow and J-Ring tests differ by less than 1 inch, there is no apparent blocking. If the average diameters differ by more than 2 inches, there is noticeable to extreme blocking.



Figure 3.3 J-Ring Test

3.1.4.3 Other Fresh Tests

After testing the SCC flowability and passing ability, the air content was measured following ASTM C231-10: “Standard Test Method for Air Content of Freshly Mixed Concrete by the Pressure Method” (ASTM 2010b) using a vertical type B pressure air meter. One variation from the ASTM standard was that the SCC was not rodded while filling the pressure meter mold.

For CC, the first property tested was concrete slump following ASTM C143-12: “Standard Test Method for Slump of Hydraulic-Cement Concrete” (ASTM 2012a). Air content of the concrete was measured in accordance with ASTM C231-10 after testing concrete slump.

3.1.5 Hardened Properties

Standard 6 in. x 12 in. concrete cylinder specimens were cast for both SCC and CC. ASTM C1758–11: “Standard Practice for Fabricating Test Specimens with Self-Consolidating Concrete” (ASTM 2011) was followed for SCC specimens, and ASTM C192 –12: “Standard Practice for Making and Curing Concrete Test Specimens in the Laboratory” (ASTM 2012b) was followed for CC specimens. Differences between the two standards are the sample preparation technique; CC molds were filled in three lifts with specified rodding and tamping between lifts, whereas SCC molds were filled in one lift with no rodding or tamping.

3.1.5.1 Uniaxial Compression Test

After curing for 28 days, each concrete cylinder was tested in uniaxial compression. Prior to testing, specimen ends were capped with high-strength sulfur capping compound in order to provide full contact between specimen ends and machine loading platens. ASTM C617 -12: “Standard Practice for Capping Cylindrical Concrete Specimens” (ASTM 2012c) was followed for the cylinder capping process. An Instron 400RD hydraulic compression testing machine was used to test cylinders in uniaxial compression. To capture concrete strains under applied stresses, an Instron 8-in. averaging extensometer was clamped at the specimen mid-height to measure strain along the middle 8-in. segment of the specimen. Compression tests were generally conducted in accordance with ASTM C39–12: “Standard Test Method for Compressive Strength of Cylindrical Concrete Specimens” (ASTM 2012d), but were slightly modified to have the testing machine operate in displacement control rather than load control. Displacement-

controlled loading allows for capturing data past the peak load. The post-peak data are used to describe the descending portion of the stress-strain curve and determine the ultimate strain. A typical failure of a test specimen is shown in Figure 3.4. Specimens were considered to have failed after the axial load drops to 50% of the peak load.

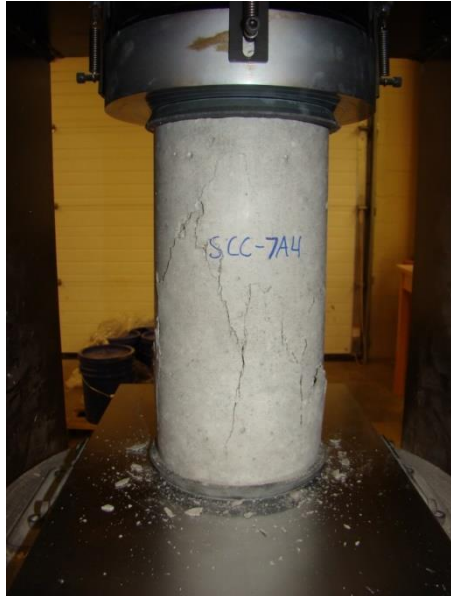


Figure 3.4 SCC Standard Cylinder Specimen at Failure

3.1.5.2 Stress-Strain Relationship

The stress-strain relationships were determined using measurements obtained from the compression testing machine load cell and the extensometer. The testing machine automatically calculated stress based on the load cell reading and the test cylinder diameter. The extensometer had a gage length of 8 inches, a range of ± 0.1 inch, and recorded strain readings to the nearest 10^{-6} in./in. Stress and strain values were recorded at a rate of 10 readings per second in order to capture the entire stress-strain relationship. Each test began with a soft-start zone in order to fully seat the specimen between the machine loading platens. After the soft-start, readings were recorded until stress had dropped 20% from the specimen compressive strength, f'_c . Following that point, the extensometer was removed to prevent it from being damaged, and the displacement of loading platens was recorded by the machine until stress had dropped 50% from f'_c . Only strain values obtained from the extensometer were used in the analysis of concrete hardened properties.

Two important properties of concrete investigated in this study included the strain at strength, ϵ_o , and the ultimate strain, ϵ_u . Strain at strength corresponds to the strain when the concrete reaches its compressive strength, f'_c . Ultimate strain corresponds to the strain when the concrete falls from f'_c by 15% to $0.85f'_c$. Concrete ductility, D , is defined as the ultimate strain divided by the strain at strength.

3.1.5.2.1 Concrete Elastic Modulus, E_c

The concrete elastic modulus was determined experimentally as the slope of the straight line extending between the origin and the point corresponding to $0.45f'_c$ on the stress-strain curve, in accordance with ACI R8.5.1 (2011).

The theoretical E_c was determined using Equation 3.2 in accordance with ACI 8.5.1 (2011).

$$E_c = 33w_c^{1.5} \sqrt{f'_c} \quad (psi) \quad \text{Equation 3.2}$$

Where:

w_c = concrete unit weight (pcf)

f'_c = concrete compressive strength (psi)

For normal weight concrete, the unit weight of concrete, w_c , can be taken as 145 pcf. Therefore, the concrete elastic modulus can be determined using Equation 3.3.

$$E_c = 57,000 \sqrt{f'_c} \quad (psi) \quad \text{Equation 3.3}$$

For this study, the concrete unit weight was not determined for every batch. For consistency, E_c was calculated based on Equation 3.3.

3.2 Column Study

Four 12-in. square bridge columns were designed, constructed, and tested in the J. Lohr Structures Laboratory at South Dakota State University for this study. Two parameters were varied: the type of concrete used, and the axial load level. Two of the columns were constructed with SCC and the other two with CC. Within each concrete group, an axial load index of 7.5% was applied to one column, while the other was subjected to 15% axial load index. Specimens subjected to 7.5% axial load index were labeled CC1 and SCC1, while specimens subjected to 15% axial load index were labeled CC2 and SCC2. Axial load index is defined as the axial load divided by the product of the concrete compressive strength and the gross cross-sectional area of the column. The selected axial loads are typical in bridge columns.

3.2.1 Design of Specimens

The test specimens were designed to represent approximately one-third scale models of bridge columns in double curvature. The column specimens were supported by rectangular footings, which transferred the applied axial load to the floor of the laboratory. The column specimens were fixed at the footing and free at the top where the lateral load was applied. The location of lateral load application represented the inflection point of a column with double curvature. A representation of the prototype column and the corresponding test column are shown in Figure 3.5.

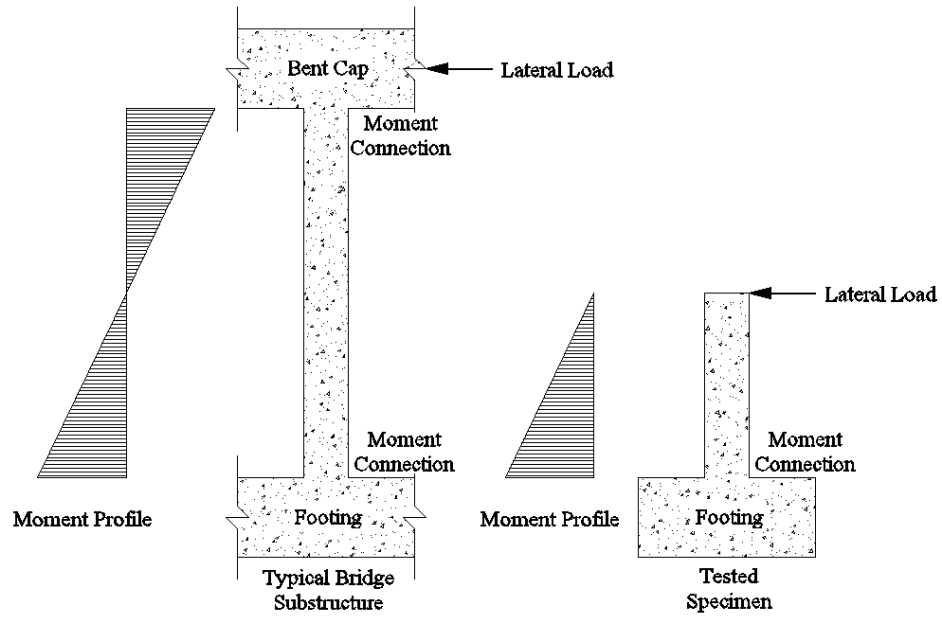
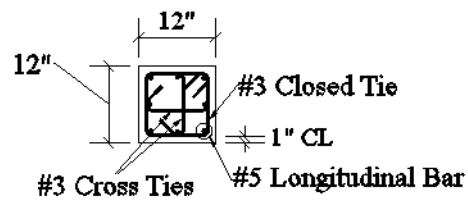
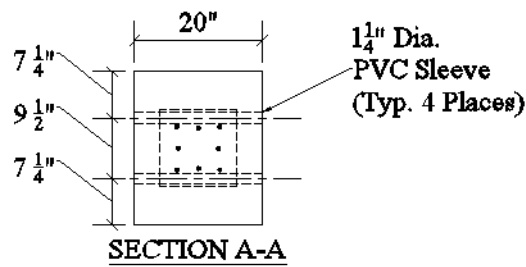
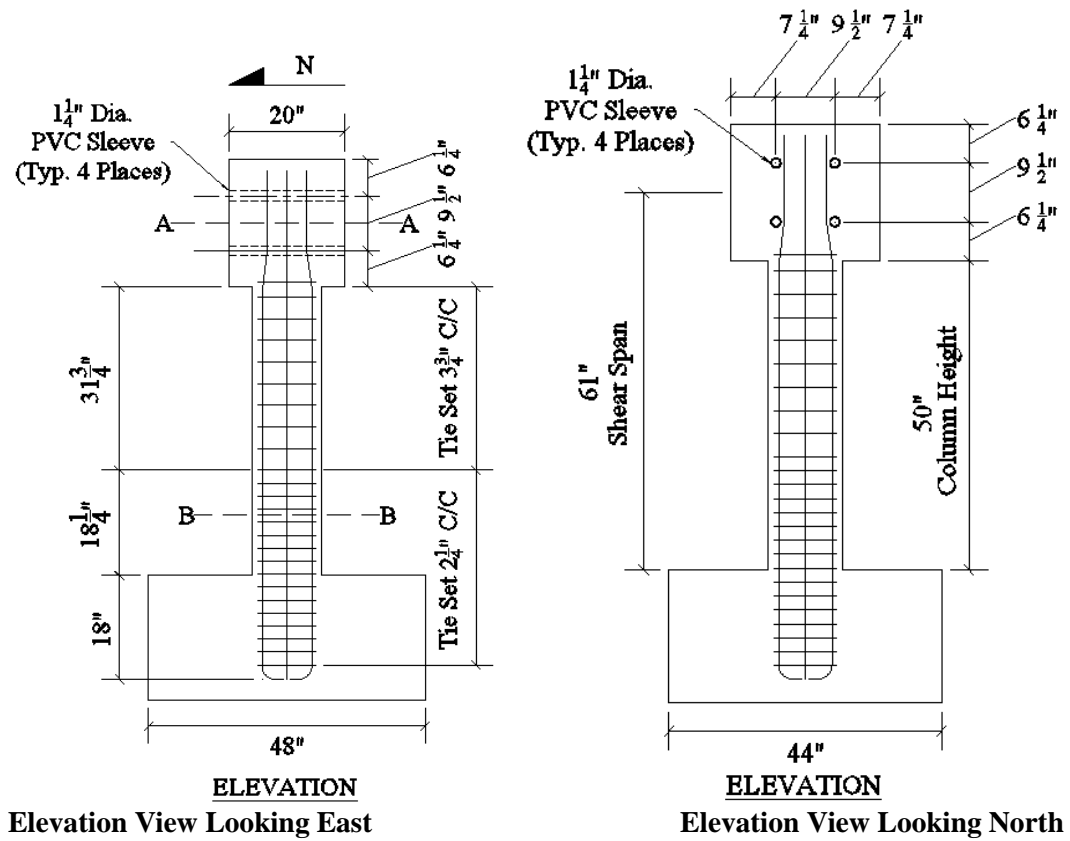


Figure 3.5 Prototype Column and Corresponding Test Column



Section View

Figure 3.6 Details of Column Specimens

3.2.1.1 Column Height

The test specimen column height was based on a target column aspect ratio (column height divided by column depth in the direction of applied lateral load) between four and five, and was also limited due to the constraints of the testing laboratory. A height of 50 inches was selected for the columns. With the addition of the concrete loading block at the top of the specimens, the shear span distance between the line of action of the applied lateral load and the top of the footing was 61 inches, resulting in an aspect ratio of 5.08.

3.2.1.2 Column Cross Section

The test specimens had identical longitudinal steel reinforcement. The column cross section was 12-in. square. The longitudinal reinforcement consisted of eight #5 bars resulting in a steel ratio, ρ_l , of 1.72%. The bars were placed equally along the four sides of the cross section, leading to identical flexural strengths in both directions. Figure 3.7 shows a column cross section with labeled longitudinal bars. Bar designation LB_ represents “Longitudinal Bar #_.”

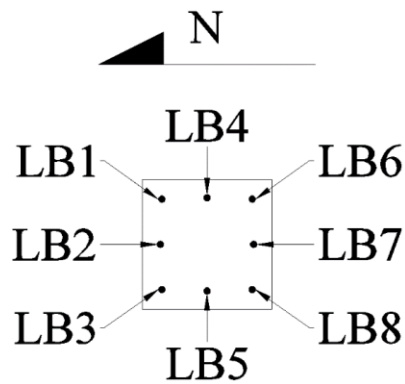


Figure 3.7 Longitudinal Bar Designations

Figure 3.8 depicts the column cross sections as seen from the top of the column reinforcement cage. Longitudinal bars, shown in purple, were bent inward toward the center of the cross section in the specimen loading block to allow passage of PVC pipe sleeves used to connect the actuator head to the loading block. The footing depth was adequate to develop the bars in tension; however, bar ends were bent inward at 90 degrees toward the center of the columns at the bottom of the footings for ease of construction. This bar termination followed ACI 318-§ 21.12.2.2 (ACI 2011) for fixed-end conditions of longitudinal bars with hooks and also aided in the specimen fabrication.

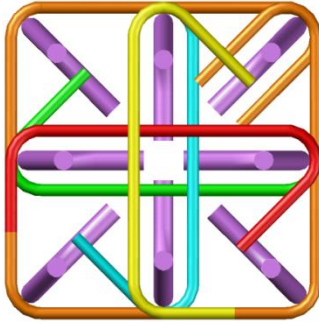


Figure 3.8 Reinforcement Cage Configuration at the Top of the Column

Above the column portion of the test specimens, concrete loading blocks were designed to transfer the applied axial and lateral loads to the columns. The block dimensions were 22-in. high by 20-in. deep (in the direction of lateral loading) by 24-in. wide. The geometry of the blocks was governed by testing constraints due to the required position of the PVC sleeves. Additionally, blocks were sized so the hydraulic actuator used to apply the lateral loads would be at mid-stroke. The block reinforcement consisted of three #6 bars oriented in both directions at the block top and bottom. The target concrete compressive strength in each column was 6,500 psi for both SCC and CC. Grade 60 steel was specified for all reinforcing steel.

3.2.1.3 Transverse Reinforcement

Transverse reinforcement was designed following the code provisions provided in the previous chapter. For simplicity of construction and uniformity in the column cross sections, reinforcement tie sets included a closed tie and cross-ties oriented in each direction, which allowed for engagement of every longitudinal bar. Both the closed tie and cross-ties were #3 bars following minimum code requirements. Based on this tie set, spacing throughout the column was determined. Throughout the potential plastic hinge region, calculations following ACI 318 (ACI 2011), AASHTO LRFD Bridge Design Specifications (AASHTO 2012), and AASHTO LRFD Seismic Bridge Design Specifications (AASHTO 2011) required a maximum tie set spacing of 2.25 inches. This resulted in $A_{sh}/s \cdot h_c$ of 0.015. Each code required this spacing regimen for the first 18 inches above the top of the footing. Transverse reinforcement with the same spacing extended 15 inches into the footing following the AASHTO § 5.10.11.4.3 (AASHTO 2011) connections provision. Outside of the plastic hinge region, the maximum spacing was governed by ACI 318-§ 21.6.4.5 (ACI 2011), which limits c/c spacing to six times the nominal diameter of the longitudinal reinforcement ($6d_b$) to prevent premature buckling of longitudinal bars. The resulting spacing outside of the plastic hinge region was 3.75 inches.

In Figure 3.8, the column longitudinal bars are depicted in purple, transverse closed ties are orange, and transverse cross-ties are red and yellow in one tie set, and green and blue in successive tie sets. The placement of the cross-ties was done such that the 90-degree ends were alternated between adjacent tie sets in accordance with ACI (ACI 2011) and AASHTO (AASHTO 2011; AASHTO 2012) specifications. Closed tie free ends terminated around a corner longitudinal bar with a 3-in. bar extension following the end of a 135-degree bend. ACI provisions (ACI 2011) define this bar termination as a *seismic hook*. Cross-ties terminated with a seismic hook at one end, and a 2¼-in. bar extension ($6d_b$) following a 90-degree bend at the other. Concrete cover was 1 inch outside of the closed ties. Scaled concrete cover was used to keep the ratio of confined to unconfined concrete as high as possible while still allowing passage of ¾-in. coarse aggregate in the SCC and CC mixtures during concrete placement.

Based on the designed transverse steel configurations, shear capacities of the columns were calculated and compared with expected shear demands. Procedures for determining shear strength of the columns varied between codes. Column shear strengths exceeded shear demands under anticipated loading conditions in this project.

3.2.1.4 Footing Design

The footings were designed to prevent both yielding of the flexural steel reinforcement and shear failure under the anticipated applied axial and lateral loads. All four footings were identically sized and reinforced. The target concrete compressive strength was 4,500 psi. The specified steel reinforcement was Grade 60. The footings were 48-in. long by 44-in. wide by 21½ -in. deep. Rocking of the footings under the anticipated lateral loads was prevented by two hold-down beams placed on top of the footings. Because of the hold-downs, reinforcement in the footings was designed for both positive and negative bending moments in the longitudinal and transverse directions. Flexural reinforcement included two identical cages at the top and bottom of the footings with bar hook extensions oriented toward each other. In both longitudinal and transverse directions, reinforcement consisted of six #6 bars. Bars terminated following a 90-degree bend with $12d_b$ (9 in.) bar extensions after the bend in accordance with ACI 318-§ 7.1.2 (ACI 2011). Six #4 vertical shear ties were positioned on both the north and south sides of the footing. Shear ties were added to the footings because the shear demand was relatively close to the nominal shear capacity of the concrete. The concrete cover was 2 inches on each face of the footing. Typical footing views are shown in Figure 3.9. A 3D representation of the complete test specimen reinforcement configuration is shown in Figure 3.10.

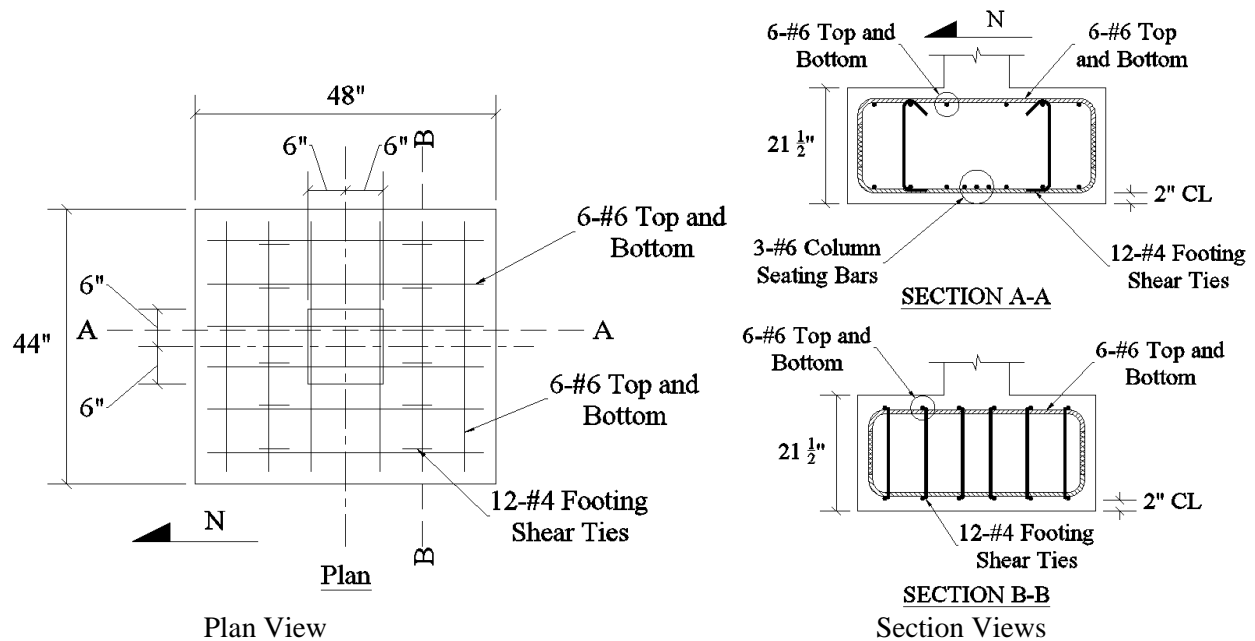


Figure 3.9 Footing Details

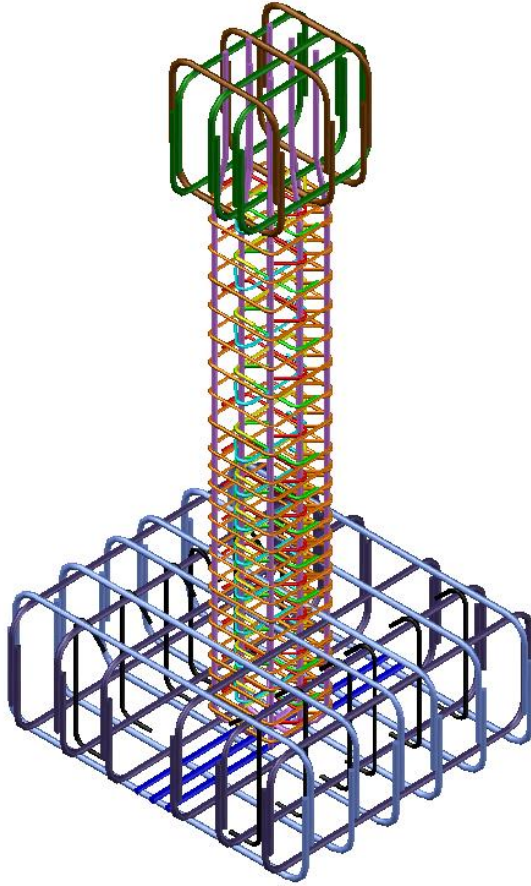


Figure 3.10 3-D Representation of Specimen Reinforcement

3.2.2 Instrumentation

To collect desired data during testing, specimens were instrumented with strain gages and load cells. All four specimens were instrumented identically. Each specimen used 27 strain gages and three load cells. Column specimens had strain gages applied to six longitudinal bars, three transverse closed ties, and three crossties. Instrumented longitudinal bars were located in exterior steel layers on the north and south sides of the column, perpendicular to the line of action of the applied lateral load, as seen in Figure 3.11. Corner column longitudinal bars had strain gages located at the column-footing interface, between the first and second tie sets above the footing, and between the second and third tie sets above the footing. Middle longitudinal bars on the north and south sides of the column had gages located in the footing at 12, 8, and 4 inches below the column-footing interface. These gages were needed to verify calculations for lateral deflection due to bond slip of the longitudinal reinforcement.

To measure strain in the confinement reinforcement within the potential plastic hinge region of the columns, three transverse reinforcement tie sets directly above the column-footing interface were gaged, as observed in Figure 3.11. Each closed tie had one gage located at the middle of its east and west legs, and each crosstie had a middle gage. Gaged closed tie and crosstie sides were parallel to the line of action of the applied lateral load.

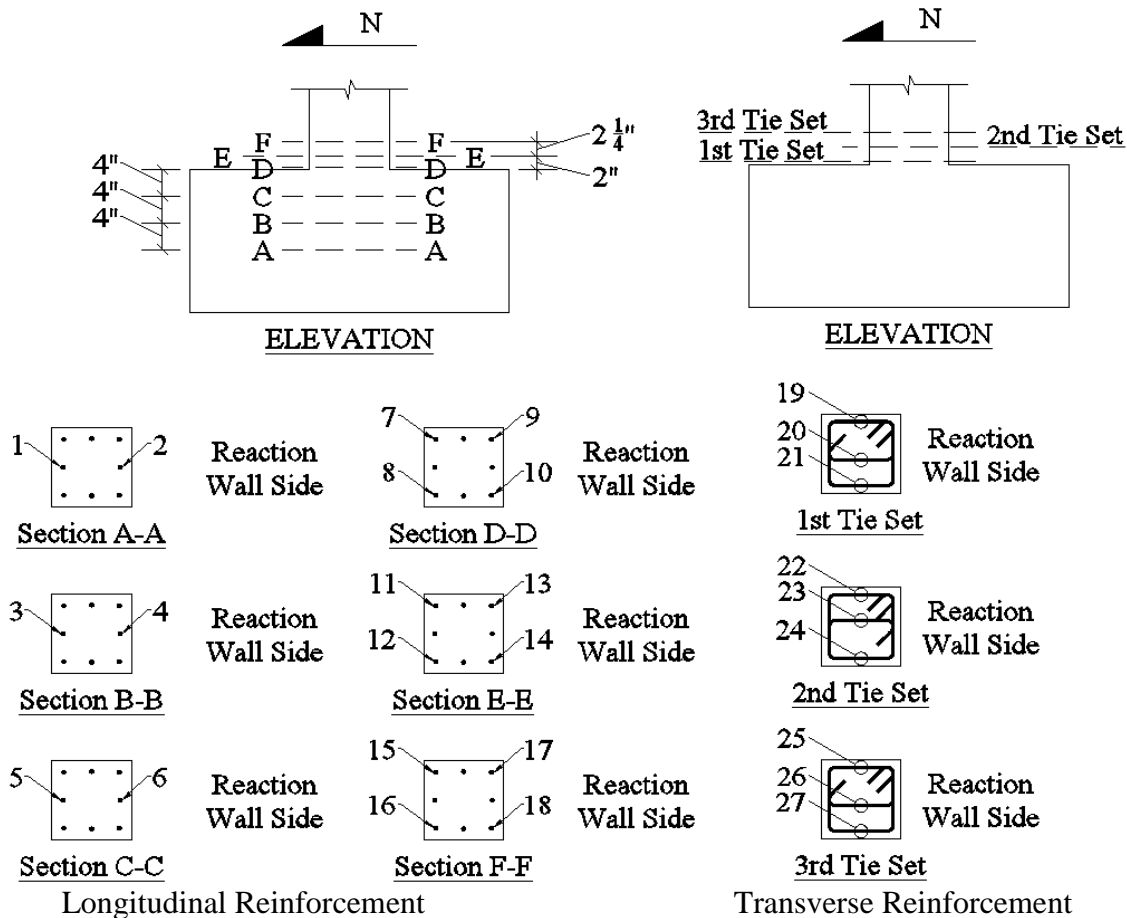


Figure 3.11 Locations of the Strain Gages

3.2.3 Construction

All four test specimens were built simultaneously in the structures lab. The footing reinforcement cages were fully constructed first, with the exclusion of the middle two longitudinal bars that would be placed after insertion of the column reinforcement cage. After gaging the column longitudinal and transverse bars, the column reinforcement cages were constructed. For each column, the longitudinal bars were laid down horizontally and the transverse closed ties were spaced about the bars at specified positions. After the longitudinal bars were oriented correctly and the closed ties were in position, the crossties were added and tied. A typical completed cage is shown in Figure 3.12.

The completed column reinforcement cages were then inserted into position inside the footing reinforcement cages, and the remaining footing longitudinal bars were inserted through the column reinforcement. Four galvanized steel wire lifting loops were centered on top of each footing and tied to the footing reinforcement cages to allow for column mobility using the structures lab crane. Completed column/footing cages were then placed into previously constructed footing forms, which were elevated on plywood and dimensional lumber joist-floors. The footing forms were sealed in order to protect the laboratory floor. Release oil was applied to all plywood surfaces inside the forms to make the removal process easier. Specimens constructed up to this point are shown in Figure 3.12.



(a) Column Steel Cage



(b) Completed Footing/Column Steel Cage

Figure 3.12 Steel Reinforcement Cage

Concrete for all four footings was provided by a local ready-mix plant. Each footing used the same CC mixture from one truck. The specified compressive strength, slump, and entrained air content were 4,500 psi, 4 inches, and 6%, respectively. Prior to placing concrete for the footings, the concrete slump and air content were measured, and five 6-in. by 12-in. concrete cylinders were sampled. The concrete in the footings was placed and vibrated in two 11-in. lifts. The footing surfaces were then troweled. Footings and test cylinders were cured for three days. After curing the footings, the column formwork was constructed on top of them. The column formwork was plumbed and the reinforcement cages were centered and held in place inside the formwork using wire ties.

After the column formwork was built, the loading block reinforcement cages were constructed on top of them. The loading block formwork was then built around these cages. Four 1¼-in. PVC pipe sleeves were placed horizontally through each loading block form and were parallel to the line of action of the applied lateral load. These sleeves would create a void in the concrete that would allow passage of threaded rods used to attach the actuator head to the loading block. Prior to pouring concrete for the specimens, four ½-in. diameter galvanized anchor bolts were attached vertically to plywood forms on top of the loading block formwork. The bolts had 9-in. embedment depths with 2-in. hooks at the end and 3-in. extensions above the top of the loading blocks. These bolts were used to attach the axial load application crossbeam to the loading blocks.

The column and loading block concrete was batched on two separate days. On the first day, the two CC specimens were placed. On the second day, the two SCC specimens were placed. Due to capacity limitations of the concrete mixer, seven batches of concrete were needed to provide the required amount to complete each specimen. Concrete was mixed and then transported to the top of the loading blocks using a one-yard concrete bucket attached to the laboratory crane. CC specimens were mechanically

vibrated in roughly 20-in. lifts. SCC specimens were not mechanically vibrated because they consolidated in the formwork under their own weight. There was minimal wait time between batches because the amount of time it took to complete mixing was approximately the same amount of time needed to place the concrete and consolidate it. Concrete was troweled at the top of the loading blocks around the formwork used for the anchor bolts. For each batch, two standard 6-in. by 12-in. concrete test cylinders were sampled; therefore, the total sample size of cylinders was 14 CC cylinders and 14 SCC cylinders. After concrete placement, the tops of the loading blocks were sealed with plastic to cure concrete for 24 hours before stripping the specimen formwork. After stripping the forms, the specimens were covered with burlap and cured for six additional days. The concrete test cylinders were subjected to similar curing conditions. The cylinders were cured for seven days and then stored in the lab under the same ambient conditions as the columns.

3.2.4 Material Properties

In order to assess the results, the concrete and steel reinforcement material properties were measured. The steel and concrete properties were needed to perform moment-curvature analysis of the columns, which was required to conduct the column tests and verify the results.

3.2.4.1 Hardened Concrete Properties

Concrete compressive strength and strain at strength were measured by testing standard concrete cylinders in uniaxial compression. At 28 days, five cylinders from the footings and one cylinder from each batch (seven of each concrete type) from the SCC and CC columns were tested.

Column testing occurred when the concrete age ranged from 68 to 76 days for CC and SCC, respectively. On the day of testing the first column in each concrete group, the remaining seven concrete test cylinders from that group were tested. Columns in each concrete group were tested 48 hours apart; therefore, the strength gain between the day the cylinders were tested and the day the columns were tested was considered negligible.

3.2.4.2 Reinforcing Steel Properties

Reinforcing steel properties were measured by testing the column transverse and longitudinal steel reinforcement in tension. For the transverse reinforcement, three #3 bars were tested. For the longitudinal reinforcement, three #5 bars were tested. Tensile testing was conducted using an MTS 370 Landmark testing machine. Steel strain was captured using an MTS contacting extensometer. Since the MTS Landmark System had a tension force capacity of 22 kips, the #5 bars had to be machined down (dog-boned) to a 0.35 in. diameter cross section in order to be tested up to failure. The #3 bars were tested in their original state.

3.2.5 Test Setup

Two stiffened W24x131 steel sections were anchored to the laboratory floor using twenty-four 1¼-in. diameter Grade 36 steel threaded rods. A 25-ton capacity laboratory crane was used to lift and place the test specimens between the steel sections. The specimens were elevated above the floor approximately ½ inch using joint expansion material, and then the columns were plumbed. To fully transfer the applied axial loads from the footings to the laboratory floor, a gypsum cement mixture (Plaster of Paris) was poured between the footing bottoms and the floor. Concurrently, this mixture was placed on top of the loading blocks in order to create a completely flat and level interface between the axial load application crossbeam and the loading blocks. The crossbeam was a stiffened W10x88 steel section that had 1 7/8-in.

diameter holes machined through both the top and bottom flanges and the web on each end of the beam. These holes allowed the passage of 1 3/8-in. diameter Dywidag® bars. After the gypsum mixture hardened sufficiently, the crossbeam was lowered onto the loading blocks. Anchor bolts protruding from the loading blocks extended through the bottom flange of the cross-beam through pre-drilled holes. Four 1/2-in. nuts were tightened onto the bolts, which fixed the crossbeam to the loading blocks.

To prevent the footings from sliding due to the anticipated reverse lateral loading, two W8x21 steel sections were bolted to the floor anchor beams on the north and south sides of the column footings, and were perpendicular to the line of action of the applied lateral load. Steel plates and composite shims were used to fill the gap between the footings and the beams. Rocking of the footings under the applied lateral loads was prevented by two steel W-Sections that were placed on top of the footings at the north and south ends, acting as hold-down beams. Each beam had two 1 1/2-in. diameter holes machined through the top and bottom flanges and the web on each beam end. These holes allowed passage of two 1 1/4-in. diameter Grade 36 steel threaded rods. Rods were screwed into a pre-welded plate and 1 1/4-in. nut anchors on the bottom side of the web of the floor anchor beams. They were tightened down on the top flange of the hold-down beams using 1 1/4-in. nuts. Graphical depictions of the test setup are shown in Figure 3.13 through Figure 3.15.

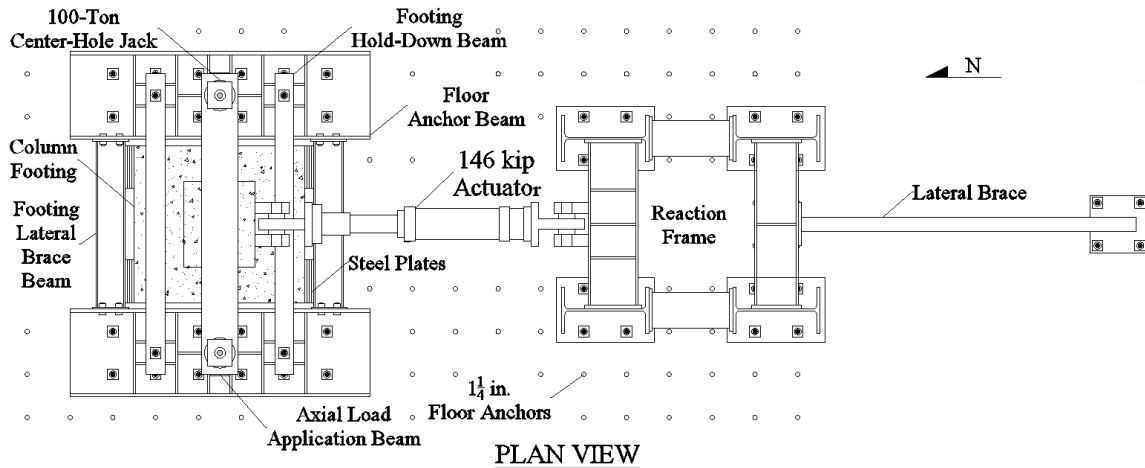


Figure 3.13 Plan View of Test Setup

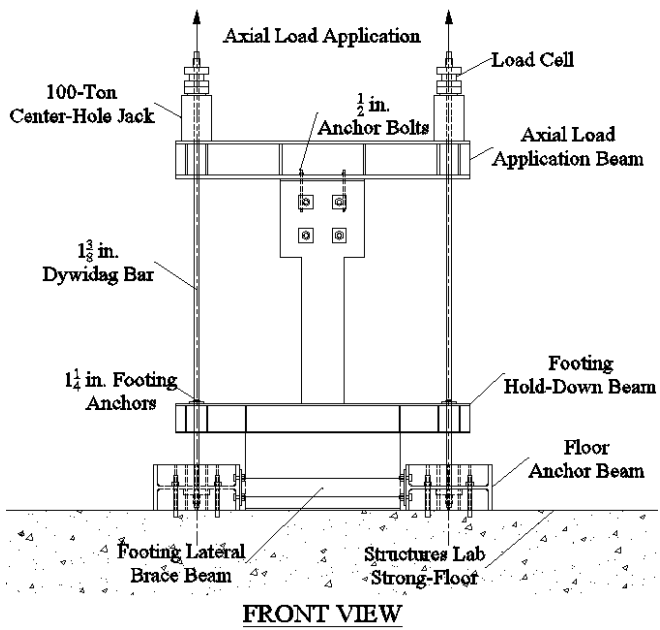
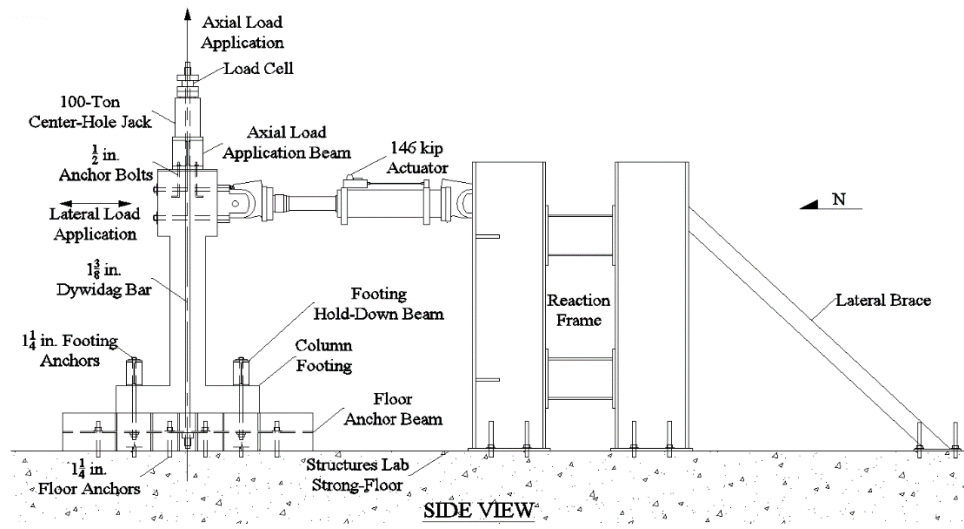


Figure 3.14 Elevation Views of Test Setup

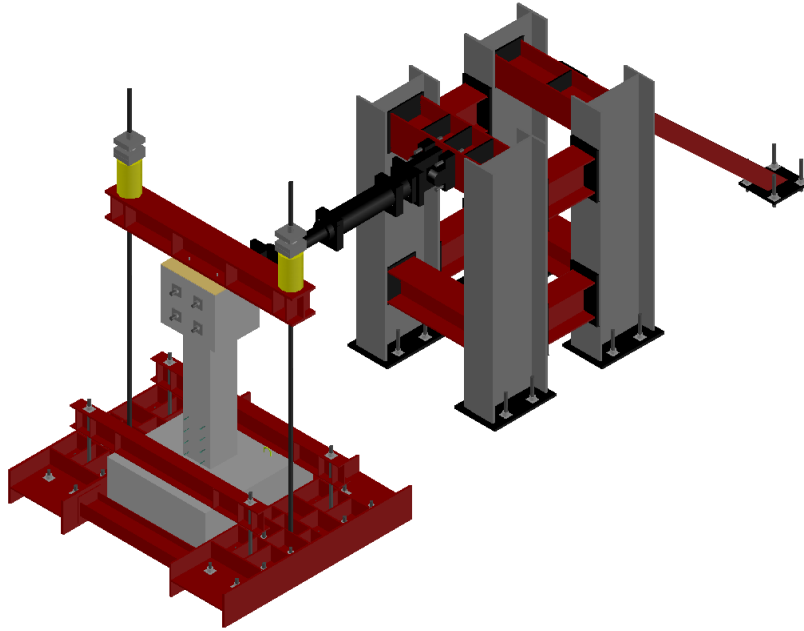


Figure 3.15 3-D View of Test Setup

Axial load was applied to the specimens using two 1 3/8-in. diameter Dywidag® bars. These bars extended vertically from anchors pre-welded on the bottom side of the webs of the floor anchor beams through 1-7/8-in. diameter machined holes in the axial load application crossbeam. Each bar was pre-stressed using two 100-ton-capacity Enerpac® Hollow Plunger Cylinders (center-hole jacks), which were connected in parallel to an Enerpac® electric hydraulic pump. Jacks were placed on opposite ends of the top flange of the cross-beam. A Dywidag® bar anchoring system was used above the jacks. Donut-style load cells (100-kip) were sandwiched between plates on top of the jack, below the anchoring system in order to monitor the axial load applied to the specimens. Jack cylinders could then be advanced, retracted, or held constant in order to maintain the specified axial load. Additionally, to minimize inconsistency in applied axial loads under a slight change in piston movement, two 1,000-psi pressure accumulators were hooked to the system between the hydraulic pump and the cylinders.

Lateral load was applied to the specimens using a 146-kip MTS hydraulic actuator. The actuator base was connected to a stiffened W14x90 cross-beam, which was fastened to a reaction frame. The actuator head was extended to the loading blocks on top of the columns. Four 1 1/4-in diameter B7 steel alloy threaded rods were passed through the loading blocks and actuator head, and were anchored on each end. At its initial position, the actuator was leveled and at mid-stroke. The maximum possible stroke for the actuator was ± 10 in. A picture of the test setup is shown in Figure 3.16.



Figure 3.16 Test Setup

The lateral displacement of the columns was measured along the centerline of the applied lateral load from the actuator. The actuator contained an LVDT that measures the displacement of its head. The applied lateral load was measured by the actuator load cell. Axial load applied to the column specimens by the center-hole jacks was measured by load cells sandwiched between the Dywidag® bar anchoring plates located above the jacks. Data measured by strain gages and load cells were recorded by a Micro-Measurements System 7000 Data Acquisition System.

3.2.6 Experimental Procedure

The experimental procedure was identical for the four column specimens. During testing, each column was subjected to lateral load reversals and constant axial loads that varied in amount among the test specimens, depending on the specified axial load indices.

Column specimens were tested after their concrete had cured for approximately 10 weeks. Prior to testing, moment-curvature analysis was performed to determine the section nominal moment capacity. For this study, moment-curvature relationships for each test specimen were computed using the computer program *RCMC v. 2.0* (Wehbe and Saiidi 2003). The idealized effective yield moment, $(M_y)_{eff}$, was taken as the section nominal moment capacity. $(M_y)_{eff}$ was determined by equating the area under the idealized moment-curvature relationship and the theoretical moment-curvature relationship determined from *RCMC*. The elastic region of the idealized moment-curvature relationship passed through the point of first yield of the tension longitudinal reinforcement, and the plastic region terminated at the ultimate section curvature, ϕ_u . An illustration of this is shown in Figure 3.17. The effective lateral yield force, $(F_y)_{eff}$, could be determined from $(M_y)_{eff}$ and the specimen shear span. $(F_y)_{eff}$ is the lateral force required to

develop $(M_y)_{eff.}$ at the column critical section. The column yield displacement, Δ_y , corresponded to the column displacement at $(F_y)_{eff.}$.

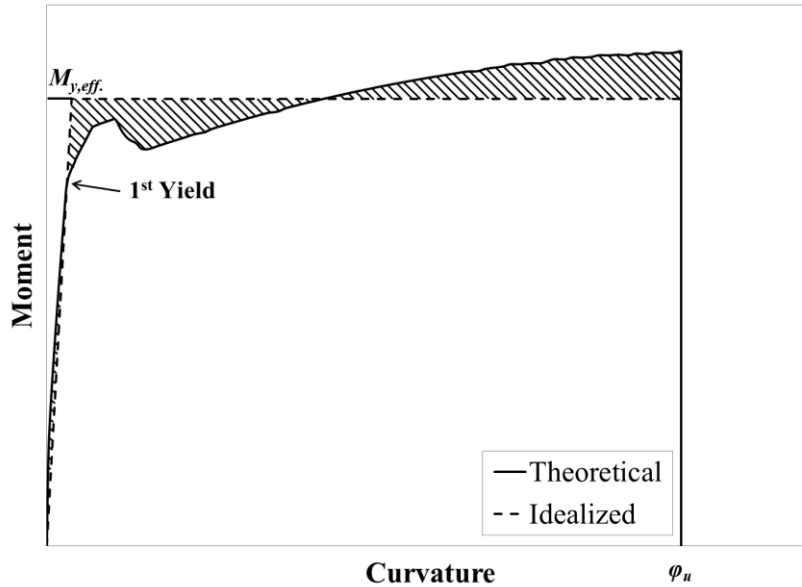


Figure 3.17 Typical Moment-Curvature of the Experimental R/C Cross Sections

On the day of testing, the predetermined axial load was applied to the specimens prior to the lateral load. The lateral load was applied by the hydraulic actuator. The lateral force was applied in monotonic load-control until $\pm 0.75(F_y)_{eff.}$. The specimens were then loaded in displacement control for the remainder of the test. Each specimen was subjected to the same testing procedure, with three complete push-pull cycles at each target load or displacement. Target loads and displacements represented $\pm 0.375(F_y)_{eff.}$, $\pm 0.75(F_y)_{eff.}$, and then successive displacement ductility, μ_{Δ} , levels of ± 1 , ± 2 , ± 3 , etc., until failure. During the tests, displacement ductility was taken with respect to the yield displacement at $(F_y)_{eff.}$. Specimen failure was defined when a longitudinal steel bar fractured or when the column lateral load carrying capacity reduced in successive cycles of the same displacement ductility level by more than 25%. Using lateral displacements recorded by the actuator, Δ_y was experimentally determined by averaging three positive and three negative displacements at $\pm 0.75(F_y)_{eff.}$, and dividing the displacement by 0.75. Once the yield displacement was determined, the actuator was switched to displacement control and cycled at successive μ_{Δ} levels, as stated previously.

Specimens CC1 and CC2 were tested prior to obtaining results for the reinforcing steel properties. Therefore, $(F_y)_{eff.}$ for specimens CC1 and CC2 was determined using nominal steel properties ($f_y = 60$ ksi, $E = 29,000$ ksi, $\epsilon_y = 0.00207$ in./in.), which were lower than the measured steel properties obtained from tensile testing ($f_y = 75$ ksi, $E = 30,000$ ksi, $\epsilon_y = 0.00245$ in./in.). This underestimated $(F_y)_{eff.}$ for specimens CC1 and CC2, and resulted in a Δ_y that occurred very close to the displacement at first yield of the tension longitudinal reinforcement. Typically, Δ_y would be larger than the displacement at first yield. Specimens SCC1 and SCC2 were tested after obtaining measured steel properties, so $(F_y)_{eff.}$ was higher. To ensure consistency between tests, the displacements at first yield of the longitudinal tension reinforcement were adopted as the reported yield displacement. Therefore, the reported displacement ductilities correspond to the displacement at first yield of the longitudinal tension reinforcement for each specimen. Consequently, the lateral load peaks did not necessarily correspond to a whole number displacement ductility.

3.2.6.1 Other Considerations

Each specimen was subjected to simultaneous axial compression and lateral load. In its un-deflected shape, the system of forces acting on the column is shown in Figure 3.18. For negligible lateral deflections, the axial compressive load, P , can be assumed vertical, and the bending moment, M , at the critical section would be determined using Equation 3.4.

$$M = F_{actuator} \cdot L \quad \text{Equation 3.4}$$

Where:

$F_{actuator}$ = lateral force applied by the hydraulic actuator and measured by the actuator load cell

L = shear span distance from the critical section to the line of action of the applied lateral load

At high lateral deflections, P becomes inclined and assumes an angle, α , to the vertical direction. Because of this, P develops a horizontal force component, P_H , which resists the lateral load applied by the actuator, $F_{actuator}$. Therefore, the net lateral load resisted by the column is not equal to $F_{actuator}$. Additionally, the vertical component of the axial load, P_V , contributes to the overall bending moment at the critical section due to the lateral deflection. This is known as the P - Δ effect. Figure 3.18 shows the geometry of the system of forces when lateral deflection is not negligible. The geometry is based on the test setup and the anchoring points of the Dywidag® bars close to the floor. The inclination of the actuator that accompanies the lateral deflection is neglected. Thus, $F_{actuator}$ is assumed horizontal at all times.

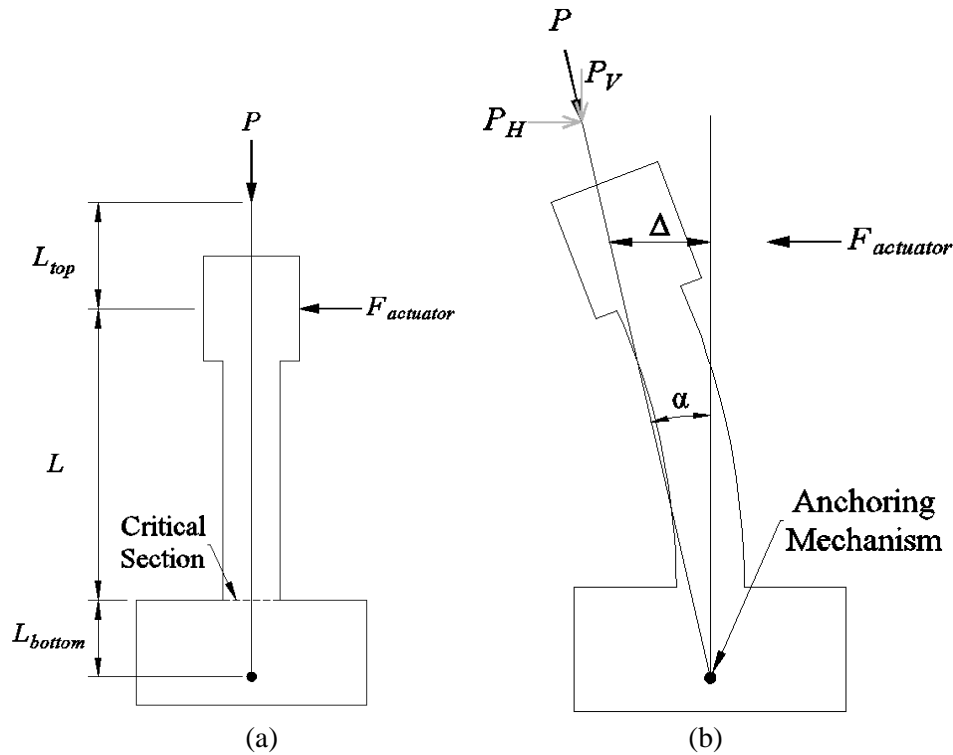


Figure 3.18 System of Forces Acting on the (a) Un-deflected Specimen, (b) Deflected Specimen

To present net lateral loads and to account for P-Δ effects, techniques developed by a collaboration of researchers and published by the Pacific Earthquake Engineering Research Center (PEER) were used (Berry et al. 2004). To calculate the net lateral load, F_H , resisted by the column, the horizontal component of the axial load, P_H , needed to be subtracted from $F_{actuator}$. Equation 3.5 through Equation 3.7 were used to calculate F_H .

$$\alpha = \tan^{-1} \left[\frac{\Delta \left(\frac{L + L_{top}}{L} \right)}{L + L_{bot} + L_{top}} \right] \quad \text{Equation 3.5}$$

$$P_H = P \cdot \sin \alpha \quad \text{Equation 3.6}$$

$$F_H = F_{actuator} - P_H \quad \text{Equation 3.7}$$

Where:

α = angle between the initial position of the column and the line of action of the applied axial load under lateral displacement, Δ

Δ = lateral displacement measured at the line of action of the applied lateral load

L = shear span distance from the critical section to the line of action of the applied lateral load

L_{top} = vertical distance between the line of action of the applied lateral load and the applied axial load

L_{bottom} = vertical distance between the critical section and the anchoring mechanism applying the axial load

To calculate the total moment, M_{total} , at the critical section due to the applied lateral loads and the P-Δ effect, Equation 3.8 was used. P_V represents the vertical component of P . The resultant effective lateral load, F_{eff} , could then be determined using Equation 3.9.

$$M_{base} = F_H \cdot L + P_V \cdot \Delta \cdot \left(\frac{L_{top} + L}{L} \right) \quad \text{Equation 3.8}$$

$$F_{eff} = \frac{M_{base}}{L} \quad \text{Equation 3.9}$$

Plots presented in the following chapter that contain the label “Lateral Load” on the y-axis represent the net lateral loads, F_H , resisted by the columns and not the lateral loads measured by the actuator load cell, $F_{actuator}$. Additionally, the first lateral load-displacement hysteresis plot shown for each specimen contains a best-fit line with the label “P-Δ.” This line shows the effect that P-Δ has on the reduction of the lateral load envelope. The second lateral load-displacement hysteresis plot shown for each specimen throughout the following chapter is plotted with the effective lateral load on the y-axis.

Specimens were marked with a square grid pattern in order to help identify locations of cracks and concrete deterioration. Successive grid lines were 4 inches apart; hence, the 12-in. wide and 50-in. high

columns were marked with three vertical lines and 12 horizontal lines on each face. Note that grids started at the bottom of the columns, so the top horizontal grid lines formed 4-in. by 2-in. rectangles with the loading blocks. During each test, cracks were marked when the column was at the maximum lateral deflection during a loading cycle. In the photos shown in the following chapter, blue and red lines on the columns identify cracks marked during push and pull excursions, respectively.

Selected lateral load-strain plots are provided for data obtained from longitudinal and transverse reinforcement in each specimen. One aspect to note is that the presented strains may exclude portions of the test if the strain gage malfunctioned during the test. If the malfunctioning gage became active later in the test, the data were not analyzed. In each plot, designations LB_ and SG_ represent longitudinal bar number and strain gage number, respectively. Labels C_ and H_ in the transverse reinforcement plots represent cross-ties and closed hoops, respectively. Numbers subsequent to the letters designate which tie set above the footing is represented, starting with number 1 closest to the footing.

3.2.7 Theoretical Analysis

Load-displacement response of the column specimens under monotonic lateral loads were computed analytically and compared to the experimental results.

Calculated deflections for the column specimens were based on three components: deflections due to flexure, reinforcement bond slip, and shear (Paulay and Priestley 1992). Total deflection is computed using Equation 3.10.

$$\Delta_t = \Delta_f + \Delta_s + \Delta_{sh} \quad \text{Equation 3.10}$$

Where:

Δ_f = flexural deflection

Δ_s = bond slip deflection

Δ_{sh} = shear deflection

3.2.7.1 Deflection Due to Flexure

In order to calculate lateral deflections due to flexural deformations, theoretical moment-curvature relationships for the column cross-section were developed. For this study, moment-curvature relationships for each test specimen were computed using a computer program *RCMC v. 2.0* (Wehbe and Saiidi 2003). *RCMC* was written in C++ and allows the user to input the reinforced concrete column section geometry, concrete unconfined and confined properties, and locations within the cross section, along with steel properties, quantities, and locations within the cross section. For a given axial load, the program iteratively calculates moment-curvature relationships up to section failure using equilibrium of forces and compatibility of strains.

In the program, for various strain levels at the cross section ends, strain profiles are determined such that they would result in equilibrium between the applied axial load and the internal forces in the steel and concrete. The section curvature is then found from this strain profile. The bending moment at the corresponding curvature is determined by summing the moment of the forces about the section's plastic centroidal axis. This process is repeated at incremental strains until the section fails. Section failure is defined by the program as the point representing crushing of the core concrete. If one or more steel layers

ruptured prior to crushing of the core concrete, the program would continue to run. However, in this study, failure was defined as either rupture of the outermost tension steel layer or crushing of the core concrete, whichever occurred first. Because of this, only moment-curvature output data obtained prior to either rupture of the outermost tension steel or crushing of the core concrete were analyzed.

In *RCMC*, multiple models are available to define the stress-strain relationships of steel and concrete. For this study, the models used are presented in Equation 3.11 through Equation 3.27. The stress-strain relationship of the steel was modeled using linear and parabolic profiles. The beginning linear portions of the stress-strain curve represented the steel elastic modulus up to the yield strain, and then from yield strain to the strain at the beginning of strain hardening. Following the linear regions, a non-linear parabolic strain hardening model was used to define the region between the strain at the beginning of strain hardening and the ultimate strain. The non-linear region is defined using Equation 3.11 (Priestley et al. 1996).

$$f_s = f_y \left[1.5 - 0.5 \left(\frac{\varepsilon_{su} - \varepsilon_s}{\varepsilon_{su} - \varepsilon_{sh}} \right)^2 \right] \quad \text{Equation 3.11}$$

Where:

f_s = strain in steel

f_y = steel yield stress

ε_s = stress in steel

ε_{su} = ultimate strain in steel

ε_{sh} = strain at beginning of strain hardening

Unconfined concrete in the sections was modeled using the Hognestad Model (Park and Paulay 1975), which is defined by Equation 3.12. This model exhibits an ascending parabolic stress-strain relationship up until the concrete compressive strength, f'_c , followed by a linear decrease of 15% in stress between the strain at strength and the ultimate strain. The ultimate strain was taken as 0.004 in./in. (Priestley et al. 1996).

$$f_c = f'_c \left[\frac{2\varepsilon_c}{\varepsilon_0} - \left(\frac{\varepsilon_c}{\varepsilon_0} \right)^2 \right] \quad \text{Equation 3.12}$$

Where:

f_c = concrete stress

f'_c = concrete compressive strength

ε_c = concrete strain

ε_0 = concrete strain at strength

Confined concrete was modeled using a fully parabolic stress-strain relationship, and defined using Equation 3.13 through Equation 3.26 (Mander et al. 1988).

$$f_{cc} = \frac{f'_{cc} xr}{r-1+x^r} \quad \text{Equation 3.13}$$

Where:

$$f'_{cc} = f'_c \left(-1.254 + 2.254 \sqrt{1 + \frac{7.94 f'_l}{f'_c}} - 2 \frac{f'_l}{f'_c} \right) \quad \text{Equation 3.14}$$

$$f'_l = \rho_s k_e f_{yh} \quad \text{Equation 3.15}$$

$$\rho_s = \rho_x + \rho_y \quad \text{Equation 3.16}$$

$$\rho_x = \frac{A_{sx}}{sb_c} \quad \text{Equation 3.17}$$

$$\rho_y = \frac{A_{sy}}{sd_c} \quad \text{Equation 3.18}$$

$$k_e = \frac{A_e}{A_{cc}} \quad \text{Equation 3.19}$$

$$A_e = \left(b_c d_c - \sum_{i=1}^n \frac{(w'_i)^2}{6} \right) \left(1 - \frac{s'}{2b_c} \right) \left(1 - \frac{s'}{2d_c} \right) \quad \text{Equation 3.20}$$

$$A_{cc} = A_c (1 - \rho_{cc}) \quad \text{Equation 3.21}$$

$$x = \frac{\varepsilon_c}{\varepsilon_{cc}} \quad \text{Equation 3.22}$$

$$\varepsilon_{cc} = 0.002 \left[1 + 5 \left(\frac{f'_{cc}}{f'_c} - 1 \right) \right] \quad \text{Equation 3.23}$$

$$r = \frac{E_c}{E_c - E_{sec}} \quad \text{Equation 3.24}$$

$$E_c = 57,000 \sqrt{f'_c} \quad \text{Equation 3.25}$$

$$E_{sec} = \frac{f'_{cc}}{\varepsilon_{cc}} \quad \text{Equation 3.26}$$

Variables in the above equations are defined as follows:

f_{cc} = confined concrete stress

f'_{cc} = compressive strength of confined concrete

f'_l = effective lateral confining stress on concrete

ρ_s = volumetric ratio of transverse confining steel

k_e = confinement effectiveness coefficient

f_{yh} = yield strength of transverse reinforcement

$\rho_{x,y}$ = volumetric ratio of transverse confining steel in the x and y directions, respectively

$A_{sx, sy}$ = total area of transverse bars running in the x and y directions, respectively

s = center-to-center spacing of transverse reinforcement

b_c = core dimension to centerline of perimeter hoop in x-direction

d_c = core dimension to centerline of perimeter hoop in y-direction

A_e = area of effectively confined concrete core

A_{cc} = area of confined concrete core

w'_i = i^{th} clear distance between adjacent longitudinal bars

s' = clear vertical spacing between hoop bars

A_c = area of core of section enclosed by the centerlines of the perimeter hoop

ρ_{cc} = ratio of area of longitudinal reinforcement to area of core of section

ε_c = confined concrete strain

ε_{cc} = confined concrete strain at strength

E_c = elastic modulus of concrete

E_{sec} = ratio of confined concrete compressive strength to confined concrete strain at strength

The final confined concrete property required for analysis using *RCMC* is the confined concrete ultimate strain, ε_{cu} , which was conservatively determined using Equation 3.27 (Paulay and Priestley 1992).

$$\varepsilon_{cu} = 0.004 + 1.4\rho_s f_{yh} \left(\frac{\varepsilon_{su}}{f_{cc}} \right) \quad \text{Equation 3.27}$$

Where:

ε_{su} = ultimate strain in steel

Using the measured concrete and steel properties, the confined concrete properties for each specimen were calculated using Equation 3.11 through Equation 3.27. The confinement steel amount changed depending on whether the section was inside or outside of the plastic hinge region. Moment-curvature analysis was performed for each test specimen based on the unconfined and confined concrete properties, the measured steel properties, and the applied axial loads at failure during column testing.

When a lateral load is applied to the free end of a cantilever column, the bending moment varies linearly from zero at the free end to maximum at the interface of the column and footing. Based upon moment-curvature analysis, a curvature profile along the column height was developed for each column. A typical curvature profile along the height of a column at its ultimate state is shown in Figure 3.19. In order to

estimate flexural deflection at the free end of the column, the moment of the area of the curvature profile along the column height must be taken about the top of the column. Equation 3.28 demonstrates how the moment-area theorem was applied in order to calculate the flexural deflection, Δ_f , at the top of the column. Based on a given lateral load, the area of the curvature profile was discretized into segments. The width of each segment was smaller if the section curvature surpassed the yield curvature. Typically, for a lateral load corresponding to first yield of the tension reinforcement, the area of the curvature profile was discretized into approximately 15 segments. For a lateral load corresponding to the ultimate state, the area was discretized into approximately 100 segments. The areas of each segment and the distances from the centroid of the areas to the top of the column were then determined. The moment of each area was then taken about the top of the column in order to calculate the flexural deflection.

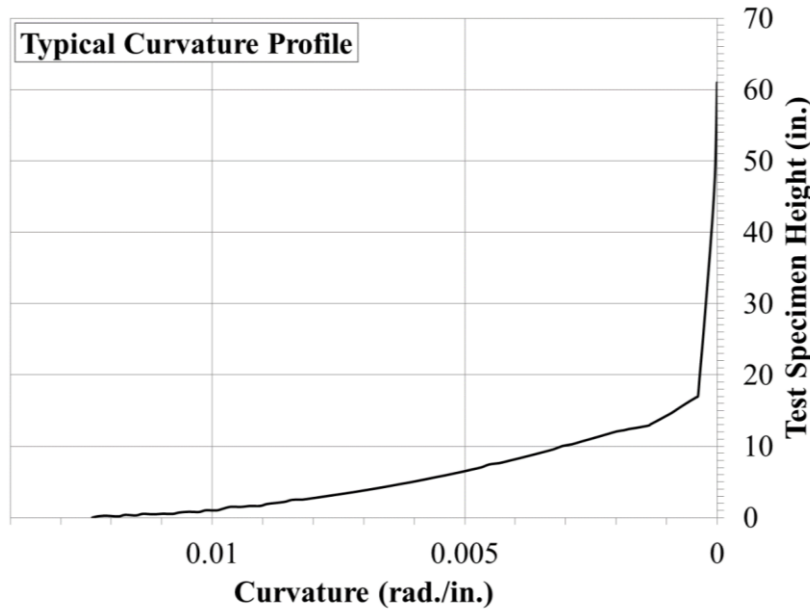


Figure 3.19 Typical Curvature along Column Height at the Ultimate State

$$\Delta_f = \int_0^l x \phi dx \quad \text{Equation 3.28}$$

Where:

x = distance from the top of the column

ϕ = curvature along the height of the column

l = column height

For each column specimen, moment-curvature analysis was performed and flexural deflections were calculated for nine successive lateral load cases. The flexural deflection was considered at the mid-height of the loading block (at the line of action of the applied lateral load). The distance between the line of action of the applied lateral load and the top of the column was 11 inches. This region would theoretically undergo rigid-body rotation and negligible curvature due to its high flexural stiffness compared with the column and the low bending moment. Since the moment and corresponding curvature values throughout this region were relatively low, the additional flexural deflection was insignificant.

3.2.7.2 Deflection Due to Shear

Deflections due to shear were calculated using a shear stiffness expression that was developed by Park and Paulay (1975). The expression takes into consideration reduction in shear stiffness due to shear cracking. Shear cracks are assumed to be at 45-degree angles along the member height. The expression is presented as Equation 3.29.

$$K_{v,45} = \frac{\rho_v}{1 + 4n\rho_v} E_s b_w d \quad \text{Equation 3.29}$$

Where:

$K_{v,45}$ = shear stiffness of an element with 45-degree cracks

E_s = elastic modulus of shear reinforcement

E_c = elastic modulus of concrete

b_w = section width perpendicular to the applied shear force

d = effective section depth parallel to the applied shear force

n = modular ratio, E_s/E_c

ρ_v = shear reinforcement ratio, A_v/sb_w

A_v = area of shear reinforcement in direction parallel to applied shear force

s = spacing of shear reinforcement tie sets along the member

Once the shear stiffness along the column height is determined, the stiffness, applied shear force, and shear span distance can be entered into Equation 3.30 in order to calculate the shear deflection of the cracked member.

$$\Delta_{sh} = \frac{VL}{K_{v,45}} \quad \text{Equation 3.30}$$

Where:

$K_{v,45}$ = shear stiffness of an element with 45-degree cracks

V = Applied Shear Force

L = Shear Span

When shear stiffness along the length of the column varies due to altered transverse reinforcement characteristics, which is common in most columns, Equation 3.31 can be used. In this study, transverse reinforcement tie sets were spaced at 2.25 inches throughout the potential plastic hinge region, and 3.75 inches elsewhere. Additionally, reinforcement characteristics and concrete geometry above the column in the loading block were considered because that region represents a portion of the shear span; however, shear deflection contribution in this region of the specimen was negligible.

$$\Delta_{sh} = \sum_{i=1}^{i=m} \left[\frac{L_i}{(K_{v,45})_i} \right] V$$

Equation 3.31

Where:

m = total number of column segments with different shear stiffness

L_i = length of segment i

$(K_{v,45})_i$ = stiffness of segment i

For each column specimen, shear deflection was calculated for nine successive lateral load cases using three stiffness segments introduced previously, and Equation 3.31. Calculated shear deflections were negligible compared with the other deflection components.

3.2.7.3 Deflection Due to Bond Slip

In order for a column section at the column-footing interface to completely develop its flexural capacity, the column's longitudinal reinforcement must be fully developed into the footing. Along the development length of the longitudinal reinforcement, stresses and corresponding strains in the steel produce a bar extension in relation to the surrounding concrete. This event is known as reinforcement bond slip. Bond slip causes a rigid body rotation at the column-footing interface. An illustration of this is shown in Figure 3.20, which displays bond slip rotation of test specimen CC1 at $\mu_D = +3$. Rotation at the column-footing interface produces lateral displacement at the top of the shear span. This displacement is referred to as bond slip deflection, Δ_s .

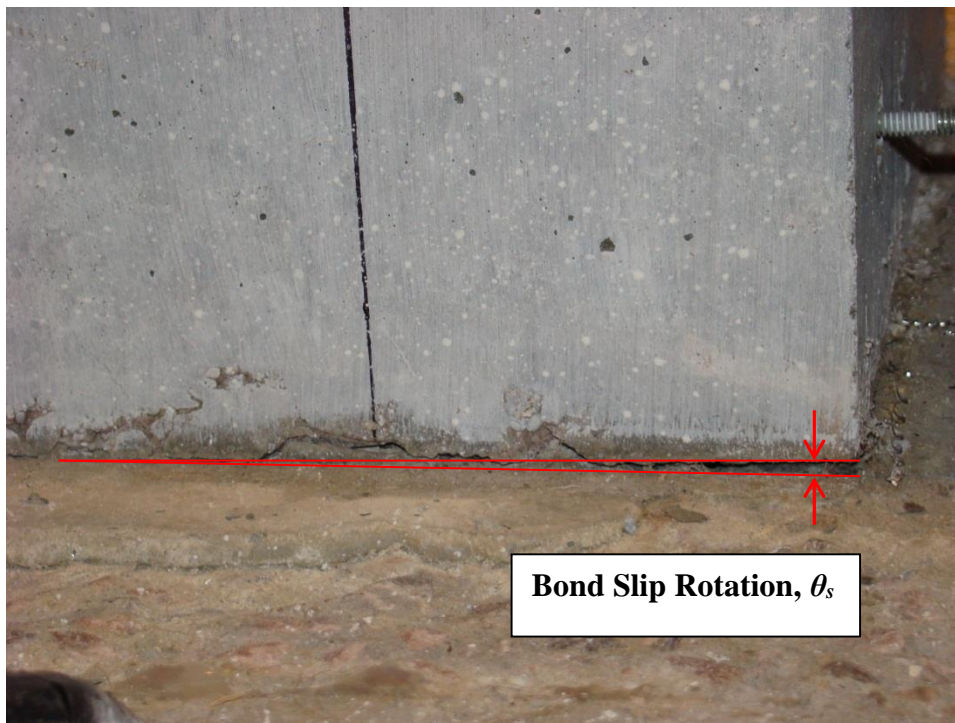


Figure 3.20 Typical Bond Slip Rotation of a Specimen

The bond slip deflection of the test specimens was calculated using a method developed by Wehbe et al. (1997). The method is based upon compatibility and equilibrium of the tensile longitudinal reinforcement, portrayed as stresses in Figure 3.21. The method assumes uniform bond stress along the length of the embedded bar in the column footing. Basic bond strength of the tensile bar was determined using Equation 3.32 (ACI 318 1963).

$$u = \frac{9.5\sqrt{f'_c}}{d_b} \leq 800 \text{ psi} \quad \text{Equation 3.32}$$

Where:

u = basic bond strength of tension bar

f'_c = compressive strength of the footing concrete

d_b = tension reinforcement bar diameter

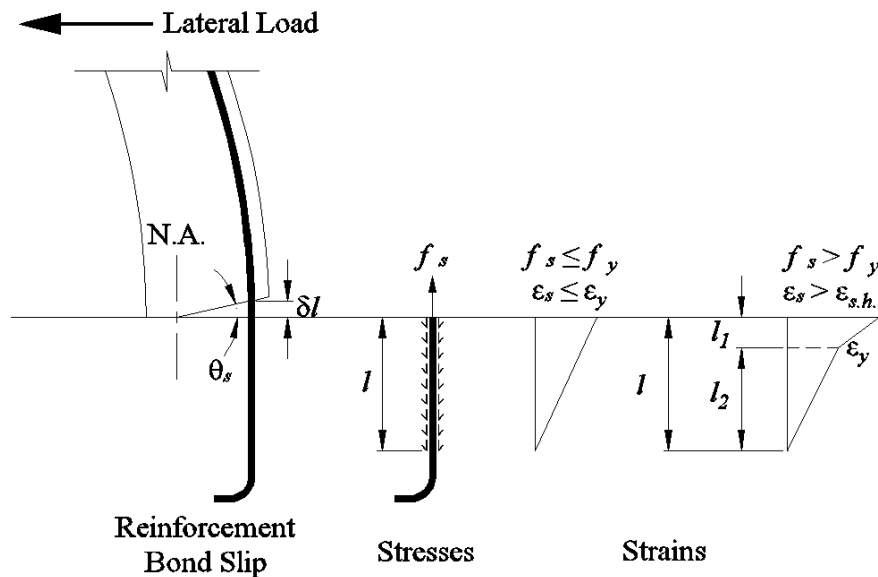


Figure 3.21 Bond Slip of Developed Bars

To develop the strain profile along the length of the embedded bar, moment-curvature analysis was used to determine the neutral axis depth and the strain in the outermost tension reinforcement at the column-footing interface. If the bar had reached strains less than or equal to the initial hardening strain, a linear strain profile was assumed. This is depicted as the left strain profile in Figure 3.21. With the strain profile of the outermost tension bars, the embedded length, l , could be determined using Equation 3.33. Once the embedded length was known, the longitudinal bar extension, δ_l , at the column-footing interface due to bond slip could be determined using Equation 3.34

$$l = \frac{f_s d_b}{4u} \quad \text{Equation 3.33}$$

Where: $f_s = E\epsilon_s < f_y$

$$\delta_l = \frac{\varepsilon_s l}{2} \quad \text{Equation 3.34}$$

If the outermost tension bars had entered the strain hardening region, then a bilinear strain profile was assumed, illustrated as the right strain profile in Figure 3.21. Total embedment length of the outermost tension reinforcement was split into two components, l_1 and l_2 . l_1 was the bar length of the outermost tension reinforcement in the strain hardening region, and l_2 was the bar length of the outermost tension reinforcement up to the strain hardening region. Development length components were calculated using Equation 3.35 and Equation 3.36.

$$l_1 = \frac{(f_s - f_y)d_b}{4u} \quad \text{Equation 3.35}$$

$$l_2 = \frac{f_y d_b}{4u} \quad \text{Equation 3.36}$$

Where:

f_s = stress in the outermost tension steel at column-footing interface

f_y = tension steel yield stress

Stress in the outermost tension steel at the column-footing interface, f_s , was calculated using Equation 3.37. This equation does not take into account stress and strain values recommended by Priestley et al. (1996), but rather uses known steel properties obtained from tensile testing. For this study, measured steel properties and ε_s values obtained from moment-curvature analysis were used to calculate f_s in each specimen for every load case. With both development length components, longitudinal bar extension could be determined using Equation 3.38.

$$f_s = f_y \left[\frac{f_{su}}{f_y} - \left(\frac{f_{su}}{f_y} - 1 \right) \left(\frac{\varepsilon_{su} - \varepsilon_s}{\varepsilon_{su} - \varepsilon_{sh}} \right)^2 \right] \quad \text{Equation 3.37}$$

$$\delta l = \frac{\varepsilon_y l_2}{2} + \frac{(\varepsilon_s + \varepsilon_y) l_1}{2} \quad \text{Equation 3.38}$$

Where:

ε_y = yield strain of tension steel

ε_s = strain in the outermost tension steel at column-footing interface

Once the longitudinal bar extension at the column-footing interface was determined based on strain in the outermost tension steel, bond slip rotation at the interface could be calculated knowing the depths of the neutral axis and the outermost tension steel layer. Longitudinal bar extension and bond slip rotation are depicted on the left side of Figure 3.21. The bond slip rotation calculation is presented as Equation 3.39.

$$\theta_s = \frac{\delta l}{d_{n.a.-ten.steel}} \quad \text{Equation 3.39}$$

Where:

θ_s = bond slip rotation

δl = additional bar extension due to bond slip

$d_{n.a.-ten.steel}$ = distance from neutral axis to centroid of the outermost tension steel

After bond slip rotation was calculated, the lateral deflection at the top column due to bond slip could be determined using Equation 3.40.

$$\Delta_s = \theta_s \cdot L \quad \text{Equation 3.40}$$

Where:

L = shear span

For each column specimen, bond slip deflection was calculated for nine lateral load cases. One item to note in the calculations presented is the upper limit of 800 psi provided by ACI in Equation 3.32. Using this limit, calculated embedment lengths for each test specimen at its ultimate state were greater than provided embedment lengths. Consequently, Equation 3.33 through Equation 3.40, used to calculate bond slip deflections, would be inapplicable. However, by disregarding the upper limit set by ACI, calculated embedment lengths were less than provided embedment lengths; this approach was utilized for the analysis in this study.

4. RESULTS AND DISCUSSIONS

4.1 Stress-Strain Relationship Study

4.1.1 Fresh Concrete Properties

The measured SCC fresh properties are shown in Table 4.1. Slump flows obtained for each batch all fell within acceptable ACI limits, as well as the target range presented in the previous chapter. All T_{20} readings fell between two and five seconds, indicating the mixture had a medium viscosity. Each mixture had a *VSI* rating of zero, which indicated a highly stable mixture with no visual signs of segregation or bleeding. Between batches, differences in diameters obtained from slump flow and J-Ring tests ranged from 1 inch – 1.5 inches, indicating minimal to noticeable blocking. All three SCC batches had air contents that fell in the acceptable SDDOT range.

A summary of recorded fresh properties for the CC batches is shown in Table 4.1. Slump measurements among the four batches ranged from 2.75 inch–4.25 inch, which fell close to the target of 4 inches. The air-content of each batch fell within SDDOT acceptable limits, barring CC-B2, which fell slightly below 5.0%.

Table 4.1 Measured Fresh Properties

Mix ID	CC-B1	CC-B2	CC-B3	CC-B4	SCC-B1	SCC-B2	SCC-B3
Slump (in.)	4.25	4.5	2.75	4.0	Not Applicable		
Slump Flow (in.)	Not Applicable				23.0	24.5	22.5
J-Ring (in.)					22.0	23.0	21.5
T_{20} (sec.)					2.8	2.7	3.0
Air Content (%)	6.0	4.4	5.0	6.0	7.2	6.8	5.0
Unit Weight (lb/ft ³)	143.3	147.2	-	-	141.0	142.1	-
Concrete Temperature (°F)	71	78	-	-	64	-	-

4.1.2 Hardened Properties

The measured stress-strain relationships for the SCC and CC mixtures are shown in Figure 4.1.

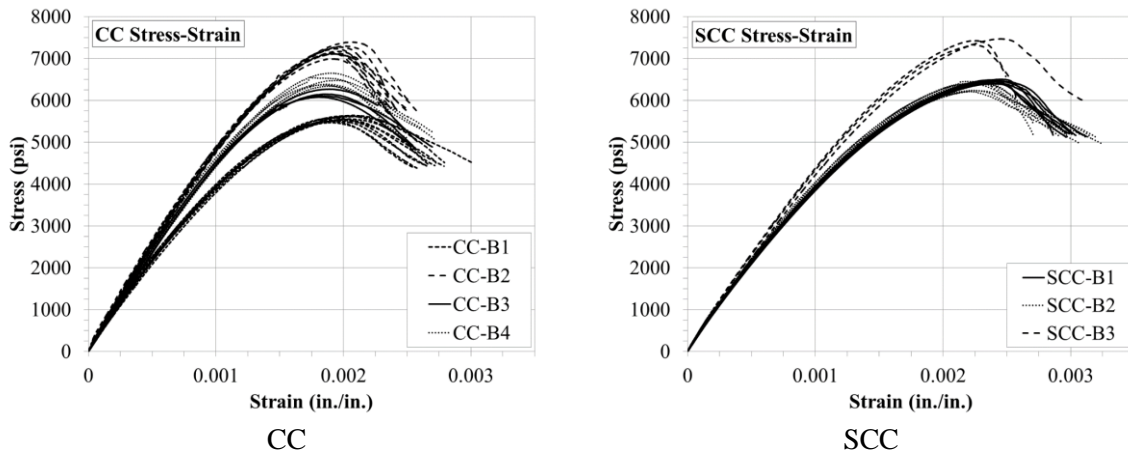


Figure 4.1 Measured Stress-Strain for the Conventional and SCC Mixes

As stated previously, three concrete compressive strength groups were compared in this study. These groups, identified as 1, 2, and 3, represent target compressive strengths of 6, 6.5, and 7 ksi, respectively. Actual measured compressive strengths for the SCC and CC groups are presented in Table 4.2.

Comparisons between the constitutive relationships of SCC and CC within each group are shown in Figure 4.2.

Table 4.2 Measured Compressive Strength

Compressive Strength Group	Measured Compressive Strength, f'_c (psi)			
	CC		SCC	
	Quantity of Specimens	Mean	Quantity of Specimens	Mean
1	4	6152	8	6345
2	6	6464	7	6459
3	10	7183	3	7413

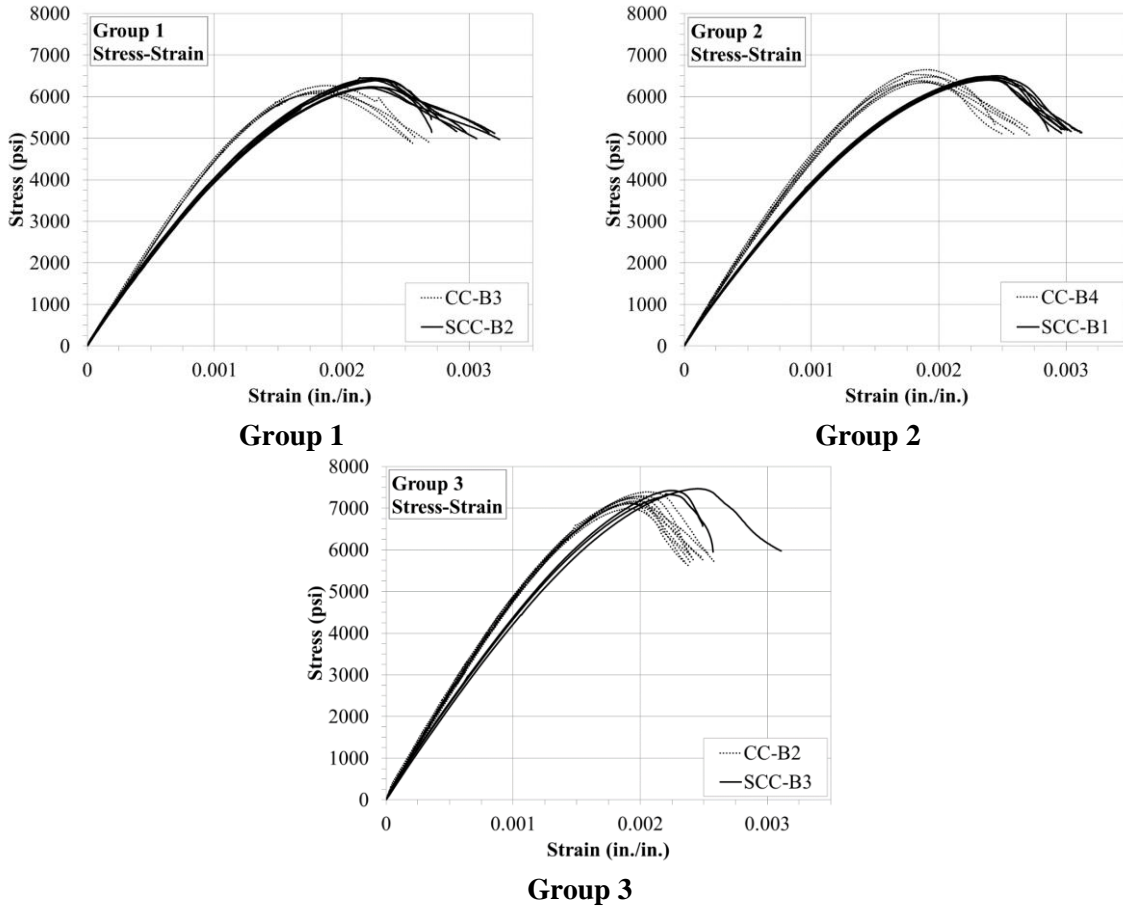


Figure 4.2 Comparison between SCC and CC Measured Stress-Strain Curves

The measured strain at strength and ultimate strain are presented in Table 4.3 and Table 4.4, respectively. The SCC mixtures consistently attained higher strain at strength and ultimate strain values compared with their respective CC mixtures. On average, the strain at strength of the SCC mixes varied from 117% to 129% of the strain at strength of the CC mixes, while the ultimate strain of the SCC mixes varied from 111% to 117% of the ultimate strain of the CC mixes.

Table 4.3 Measured Concrete Strain at Strength

Compressive Strength Group	Strain at Strength, ε_o (micro-strain)				Ratio of SCC to CC
	CC		SCC		
	Quantity of Specimens	Mean	Quantity of Specimens	Mean	
1	4	1841	8	2231	1.21
2	6	1865	7	2399	1.29
3	10	1956	3	2298	1.17

Table 4.4 Measured Concrete Ultimate Strain

Compressive Strength Group	Ultimate Strain, ε_u (micro-strain)				Ratio of SCC to CC
	CC		SCC		
	Quantity of Specimens	Mean	Quantity of Specimens	Mean	
1	4	2471	8	2855	1.16
2	6	2450	7	2866	1.17
3	10	2348	3	2609	1.11

Table 4.5 shows that SCC had slightly lower material ductility than CC for all three strength groups. This characteristic was visually observed while testing the specimens; the SCC cylinders degraded at a faster rate than their respective CC cylinders after reaching f'_c . The ductility of the SCC mixes varied from 90% to 96% of the ductility of the CC mixes. Additionally, the experimental results indicated that an increase in compressive strength caused a decrease in ductility for both SCC and CC.

Table 4.5 Measured Concrete Ductility

Compressive Strength Group	Ductility, $D = \varepsilon_u/\varepsilon_o$				Ratio of SCC to CC
	CC		SCC		
	Quantity of Specimens	Mean	Quantity of Specimens	Mean	
1	4	1.34	8	1.28	0.96
2	6	1.32	7	1.19	0.90
3	10	1.20	3	1.13	0.94

The measured elastic modulus (E_c) values for SCC and CC in each strength group are summarized in Table 4.6. The elastic modulus values of the SCC mixes were lower than those of the respective CC mixes. The elastic modulus of the SCC mixes varied from 85% to 89% of the elastic modulus of the CC mixes.

Table 4.6 Measured Concrete Elastic Modulus

Compressive Strength Group	Measured Elastic Modulus, E_c (ksi)				Ratio of SCC to CC
	CC		SCC		
	Quantity of Specimens	Mean	Quantity of Specimens	Mean	
1	4	4738	8	4209	0.89
2	6	4785	7	4079	0.85
3	10	5075	3	4450	0.88

Table 4.7 presents the measured and the theoretical elastic moduli (E_c) for the concrete mixes. The theoretical elastic modulus was determined using the ACI empirical equation (Equation 3.25). The measured CC elastic moduli varied between 101% and 106%, while the measured SCC elastic moduli varied between 0.89% and 0.93% of the values obtained from the ACI empirical equation.

Table 4.7 Comparison of Measured and Theoretical (ACI Empirical) Elastic Moduli

Mix ID	Measured Elastic Modulus, E_c (ksi)		Theoretical Elastic Modulus, E_c (ksi)	Ratio of Measured to Theoretical E_c
	Quantity of Specimens	Mean		
CC-B1	10	4292	4250	1.01
CC-B2	10	5075	4831	1.05
CC-B3	4	4738	4471	1.06
CC-B4	6	4785	4582	1.04
SCC-B1	7	4079	4581	0.89
SCC-B2	8	4209	4540	0.93
SCC-B3	3	4450	4908	0.91

Figure 4.3 shows a plot of the elastic moduli versus the square-root of the concrete strength. The solid radial line in the graph represents the ACI empirical equation for calculating the elastic modulus. Based on the mean of the measured values, the CC and SCC elastic moduli would be equal to $59,000\sqrt{f'_c}$ (psi) and $51,800\sqrt{f'_c}$ (psi), respectively. These values correspond to 1.036% and 0.909% of the ACI empirical elastic modulus.

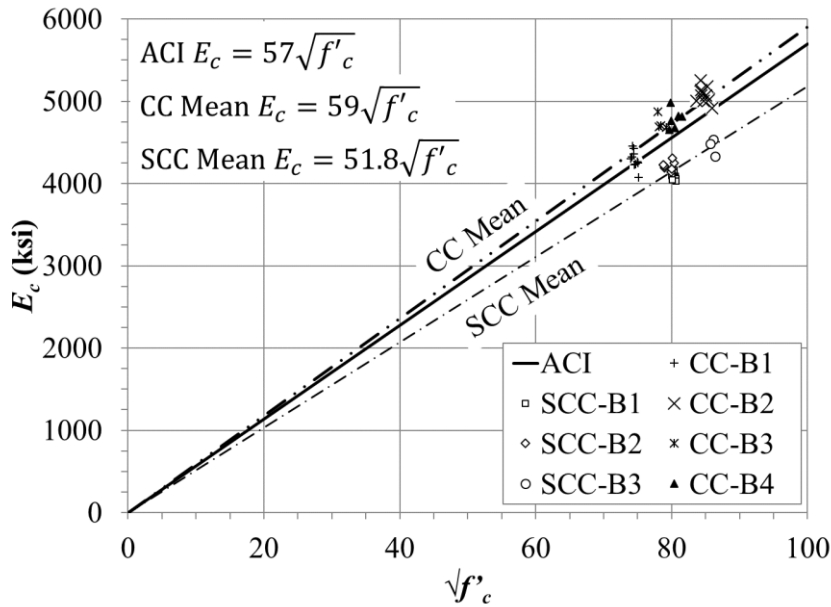


Figure 4.3 Theoretical (ACI Empirical) and Measured Elastic Moduli

4.2 Column Study

4.2.1 Material Properties

4.2.1.1 Fresh Concrete Properties

Fresh properties of the footing and column concrete on the batch date are presented in Table 4.8. Other fresh properties were not measured because the concrete mix designs were the same as those used for the stress-strain study.

Table 4.8 Fresh Concrete Properties of the Column Concrete

Concrete Type	Concrete Location	Concrete Slump (in.)	Concrete Slump Flow (in.)	Entrained Air (%)
CC	Column	4	-	6.0
SCC	Column	-	22.5	5.0
CC	Footing	3.75	-	6.5

4.2.1.2 Hardened Concrete Properties

The hardened concrete properties at 28 days and on the day of testing are shown in Table 4.9 and Figure 4.4.

Table 4.9 Hardened Concrete Properties of the Columns Concrete

Concrete Type	Concrete Location	At 28 Days		On Day of Testing	
		Concrete Compressive Strength, f'_c (psi)	Strain at Strength, ϵ_o (microstrain)	Concrete Compressive Strength, f'_c (psi)	Strain at Strength, ϵ_o (microstrain)
CC	Column	6450	1873	6830	1989
SCC	Column	7410	2298	8025	2432
CC	Footing	6150	1819	-	-

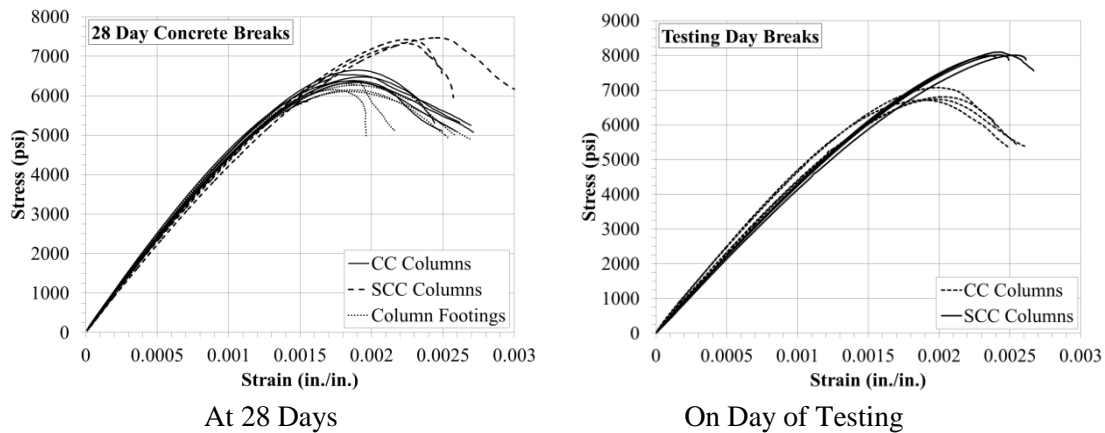


Figure 4.4 Measured Stress-Strain Relationship of the Column Concrete

4.2.1.3 Reinforcing Steel Properties

A summary of measured data is presented in Table 4.10, and stress-strain plots for both bar sizes are shown in Figure 4.5.

Table 4.10 Measured Steel Properties

Bar Size	At Yield		At Ultimate		Strain At Beginning of Strain Hardening	Elastic Modulus
	ϵ_y (millistrain)	f_y (ksi)	ϵ_u (millistrain)	f_u (ksi)	ϵ_{sh} (millistrain)	E_s (ksi)
#3	2.37	70.5	118.9	108.8	8.62	29784
#5	2.45	74.9	97.9	122.2	4.97	30625

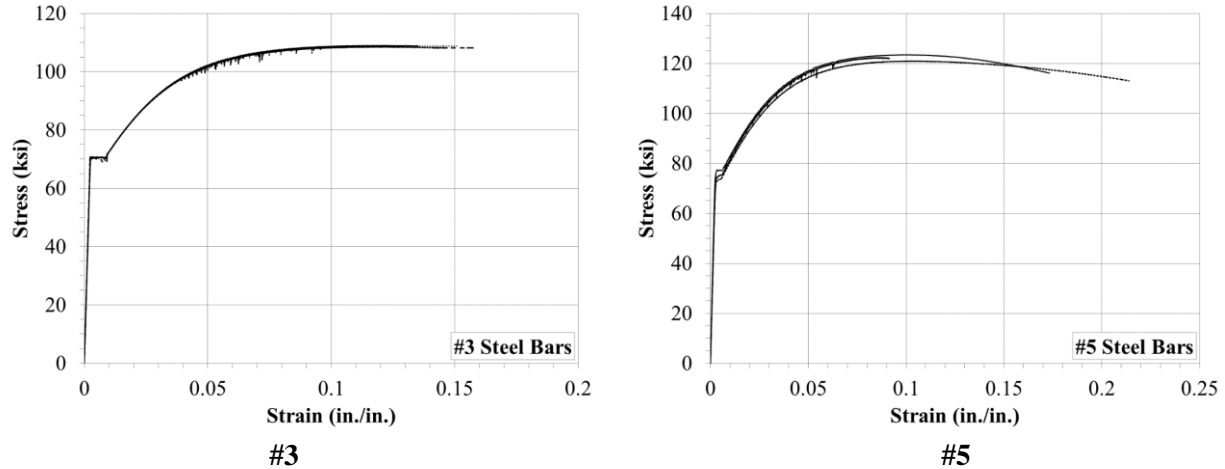


Figure 4.5 Measured Stress-Strain Relationship of Steel Bars

4.2.2 Testing Results

In each test, the specimen was subjected to the specified axial load before lateral loads were applied. During low-drift excursions, the applied axial load was close to the target axial load. Under high drifts, the applied axial load had a tendency to increase in value as a result of the additional stretching of the Dywidag® bars. To account for this, the hydraulic pressures of the center-hole jacks were manually adjusted to lower the axial loads at zero actuator displacement between lateral load excursions. This procedure allowed for the target axial load to be attained at the peak displacement. The manual adjustment resulted in a range of axial loads applied to each specimen. Axial load ranges are presented throughout this chapter. The target axial loads and the average axial loads measured at each full lateral excursion are presented in Table 4.11. Additional measurements taken at full excursions throughout each test are provided in Appendix C. The lateral load was cycled to target load levels prior to the yield displacement and to target displacement levels after the yield displacement. In general, three loading cycles were performed at each target level.

Table 4.11 Target and Measured Axial Load Information

Specimen	Concrete Compressive Strength, f'_c (psi)	Target Axial Load Index (%)	Target Axial Load (kips)	Average Experimental Axial Load Index (%)	Average Experimental Axial Load (kips)
CC1	6830	7.5	73.8	8.8	86.5
CC2		15.0	147.5	15.3	150.6
SCC1	8025	7.5	86.7	8.1	94.1
SCC2		15.0	173.3	14.6	169.1

4.2.2.1 Specimen CC1

Specimen CC1 was subjected to axial loads of 78.4 kips at first yield and 86.3 kips at ultimate. Throughout the test, applied axial loads ranged from 55.3 kips to 105.0 kips. Measured lateral and axial loads applied at each full push-pull excursion during the test are provided in Appendix C-1. Some

experimental measurement plots obtained for this specimen are presented in this section; the remaining plots can be found in Appendix D-1.

4.2.2.1.1 Lateral Displacement

Applied lateral load history for specimen CC1 is shown in Figure 4.6. The deviation in the loading pattern after the third loading cycle was the result of the planned loading sequence being interrupted to check a malfunction in the data acquisition system. This deviation had no consequences on the performance of the specimen because it happened at low-load levels. Issues with the system were resolved, and the specimen was re-loaded at low displacement ductility levels. At a lateral load of 11.69 kips in the push direction, two flexural cracks were found at 6 inches and 11 inches above the column-footing interface on the column south face. The measured displacement and lateral load at first yield of the longitudinal reinforcement was 0.47 inches and 14.60 kips, respectively.

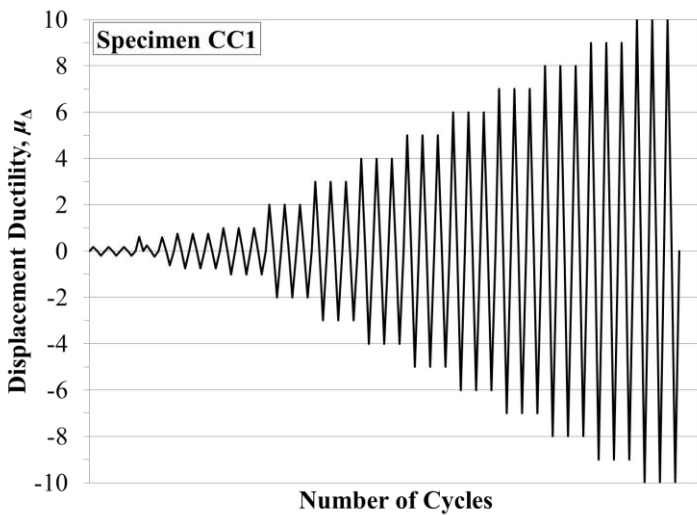


Figure 4.6 Lateral Load History for Specimen CC1

The measured lateral load-displacement hysteretic response is presented in Figure 4.7. The two vertical axes shown in the figure represent the applied lateral load and the applied lateral load normalized with respect to the measured yield force, F/F_y . The two horizontal axes represent the measured displacement along the centerline of the actuator and the column drift percentage. Displacement ductility, μ_{Δ} , is displayed along the horizontal axis with respect to the measured displacement at first yield. The P - Δ effect on the reduction of the lateral load envelope is also reflected in the plot. The measured effective lateral load-displacement hysteretic response is presented in Figure 4.7.

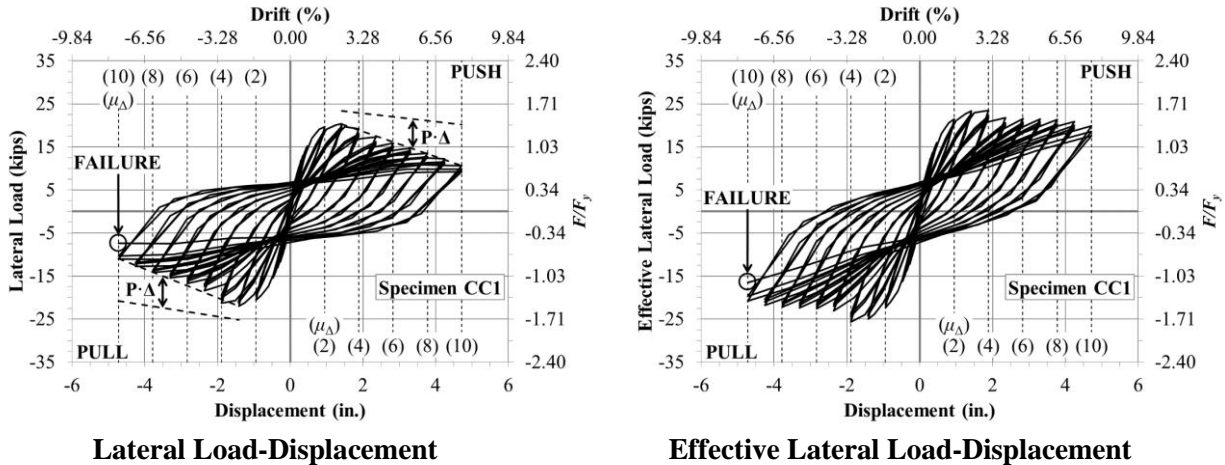


Figure 4.7 Measured Load-Displacement for Specimen CC1

At displacement ductility, μ_{Δ} , level of ± 1 , the specimen load-displacement response was almost linear. A noticeable drop in stiffness was not easily identifiable until $\mu_{\Delta} = \pm 2$. During the first cycle at $\mu_{\Delta} = \pm 3$, spalling of the concrete cover between the base of the column and approximately 3 inches above the base occurred on the north side of the column during the push excursion, and the south side of the column during the pull excursion. The peak lateral load attained by the specimen occurred during the first cycle at $\mu_{\Delta} = \pm 3$ in both push and pull directions. Lateral loads of 20.4 kips in the push direction and 22.0 kips in the pull direction were attained. Successive displacement ductility levels resulted in an increased rate of spalling of concrete cover and reduction in the applied lateral load. At $\mu_{\Delta} = \pm 5$ and $\mu_{\Delta} = \pm 6$, the footing concrete near the base of the column cracked at the surface and lifted up on the tension side. Crack penetration was limited to a depth of less than 1/4 inch and extended out from the column face approximately 4 inches. At $\mu_{\Delta} = \pm 8$, the closed hoop of the first tie set above the footing was completely uncovered, exposing the column southwest corner longitudinal bar, LB8, above it.

During the first cycle at $\mu_{\Delta} = \pm 10$, corner longitudinal bars LB3 and LB8 on the west side of the column started to buckle between the first and second tie sets above the footing. Also, on the first excursion in the pull direction, the 90-degree hook on the first north-south cross-tie above the footing began to open, and the middle south longitudinal bar, LB7, started to buckle outward. On the third pull excursion at this μ_{Δ} level, a “popping” noise was heard. However, the specimen did not show significant strength degradation, and no physical evidence of bar fracture was observed on any of the exposed longitudinal bars. Because of this, the specimen was subjected to a full excursion at $\mu_{\Delta} = +11$. Upon full actuator displacement, two additional “popping” noises were heard, and it was visually observed that LB7 had ruptured. After removing strain gage protection from longitudinal bars above the footing, additional ruptures were observed in both LB3 and LB8. Also, upon inspection of the lateral load-displacement hysteresis, strength degradation during the third excursion of $\mu_{\Delta} = -10$ was apparent. Therefore, specimen failure was defined after LB3 ruptured at a displacement ductility of 10.0 and a corresponding drift of 7.74%. At the end of the test, spalled column concrete cover extended from the base of the column to approximately 5–7 inches above the base. Figure 4.8 presents pictures of specimen CC1 at successive μ_{Δ} levels throughout the test.

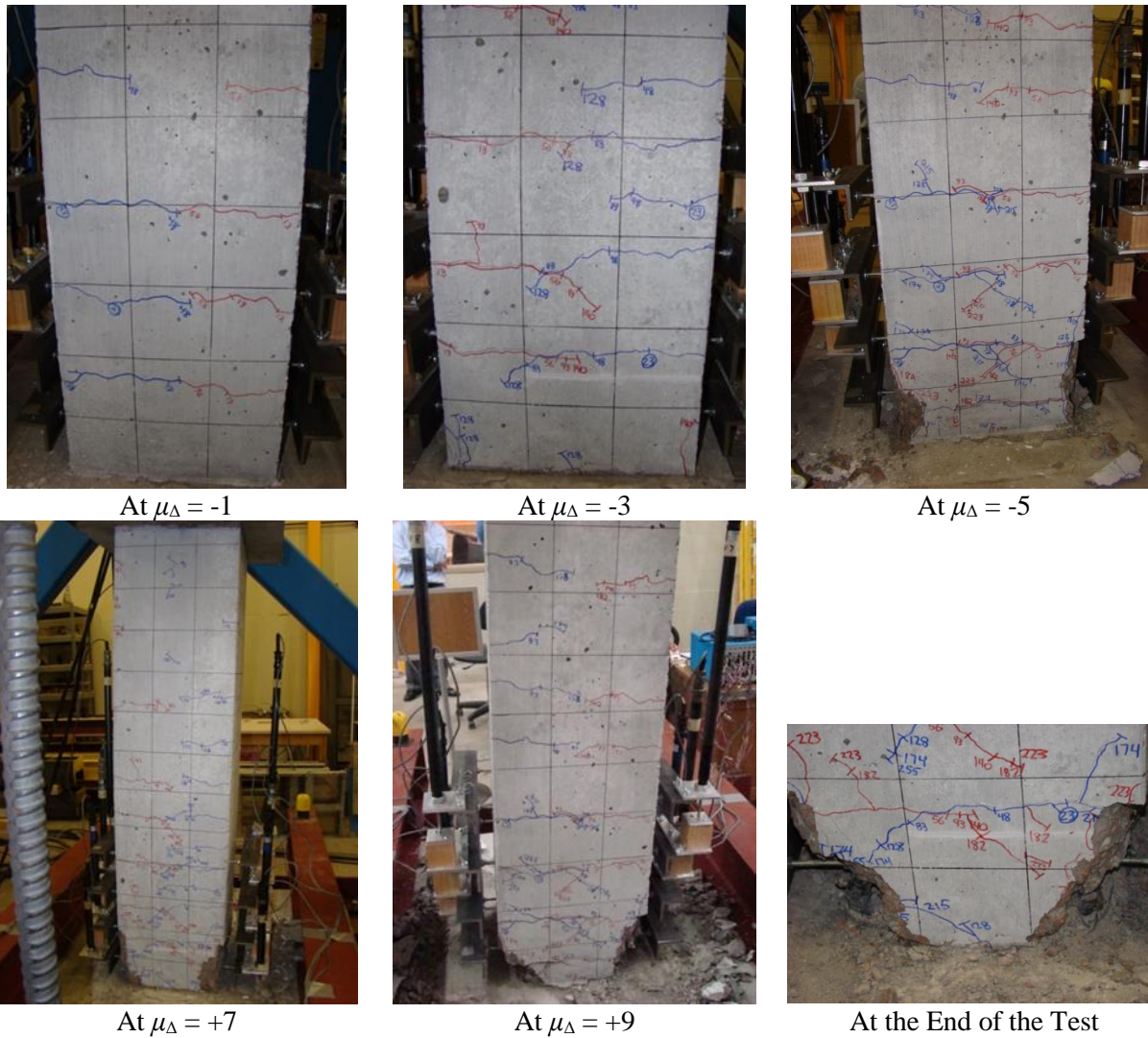


Figure 4.8 Visual Inspection of Specimen CC1 (1st Excursion)

4.2.2.1.2 Reinforcing Steel Strain

Figure 4.9 presents measured lateral load-strain relationships of LB7 at sections 12, 8, and 4 inches below the column-footing interface. The plots show that strains surpassed the steel yield point in both tension and compression for all three sections within the column footing. SG6, located 4 inches below the column-footing interface on this bar, measured strains multiple magnitudes past the steel yield point, as seen in Figure 4.9. Strain penetration into the footing led to bond slip of steel reinforcing bars, and consequently, additional lateral deflection in the column due to bond slip rotation at the column-footing interface.

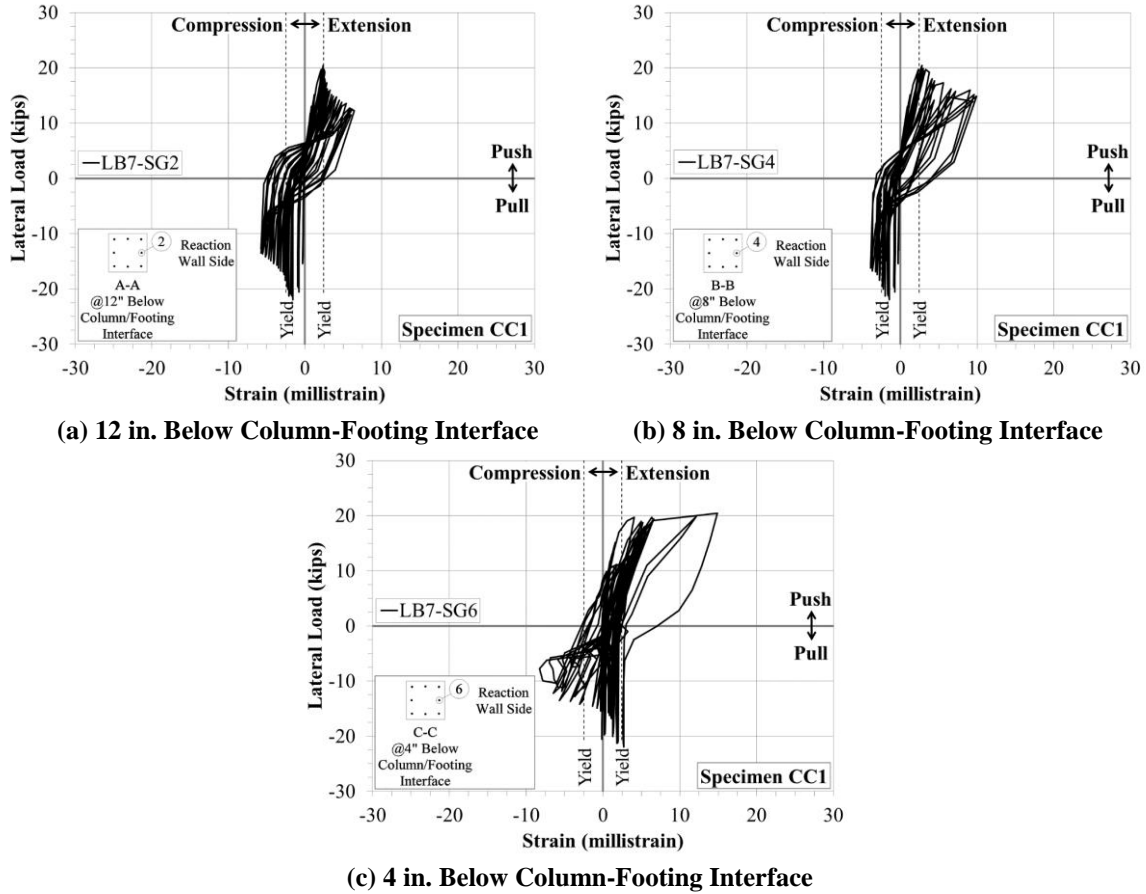


Figure 4.9 Measured Lateral Load-Strain in Longitudinal Steel below Column-Footing Interface of Specimen CC1

Figure 4.10 presents measured lateral load-strain readings for LB3. As stated previously, this was the first bar to rupture during the test. The data presented in this figure are from strain gages located at the column-footing interface, between the first and second transverse reinforcement tie sets, and between the second and third tie sets, respectively. The first strain gage above the footing, SG8, reached the steel yield strain first. SG8 and the second gage above the footing, SG12, recorded comparable strain values before both gages went offline at $\mu_{\Delta} \pm 7$. The third gage above the footing, SG16, went offline at $\mu_{\Delta} = \pm 4$.

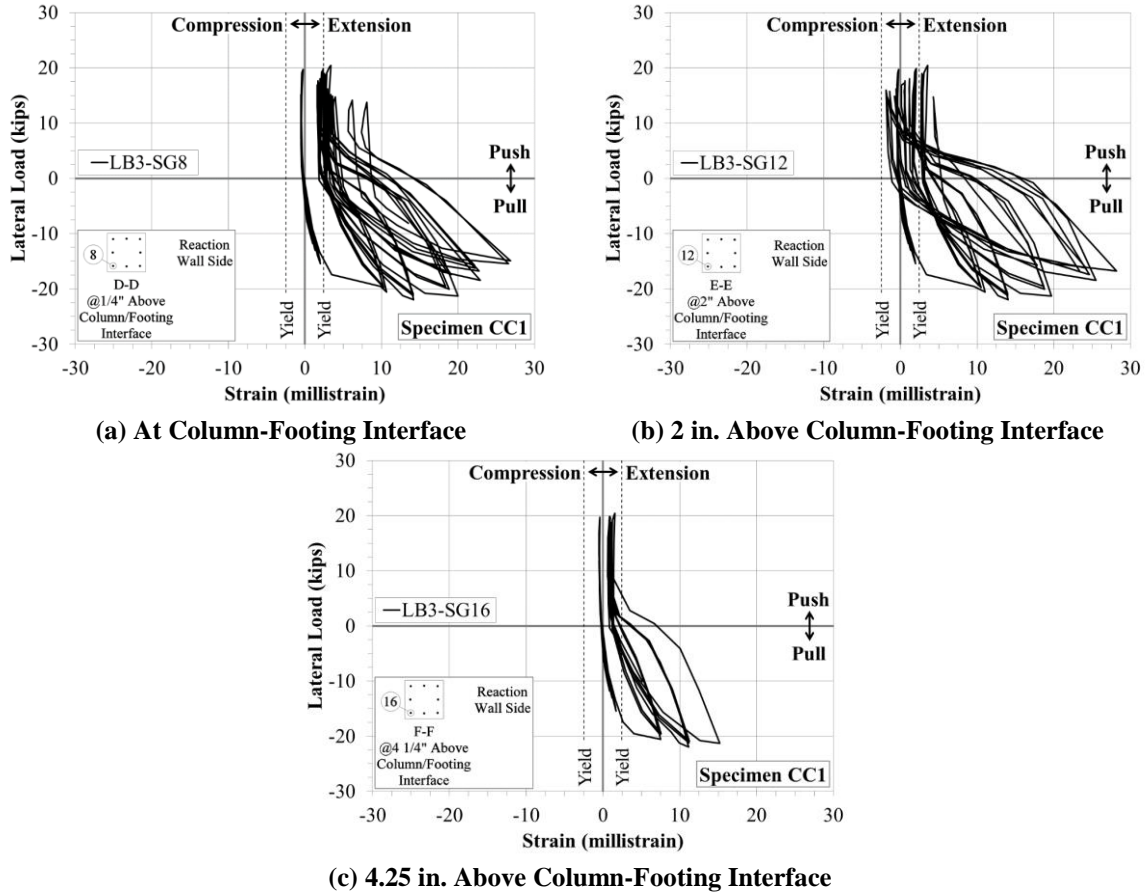


Figure 4.10 Measured Lateral Load-Strain in Longitudinal Steel of at and Above Column-Footing Interface of Specimen CCI

Transverse reinforcement in the column plastic hinge region did not yield prior to rupture of the longitudinal reinforcement. Lateral load-strain response plots of gages located on the first three transverse reinforcement tie sets above the footing are shown in Figure 4.11. The plots indicate that strain in the transverse reinforcement increased as distance from the footing increased.

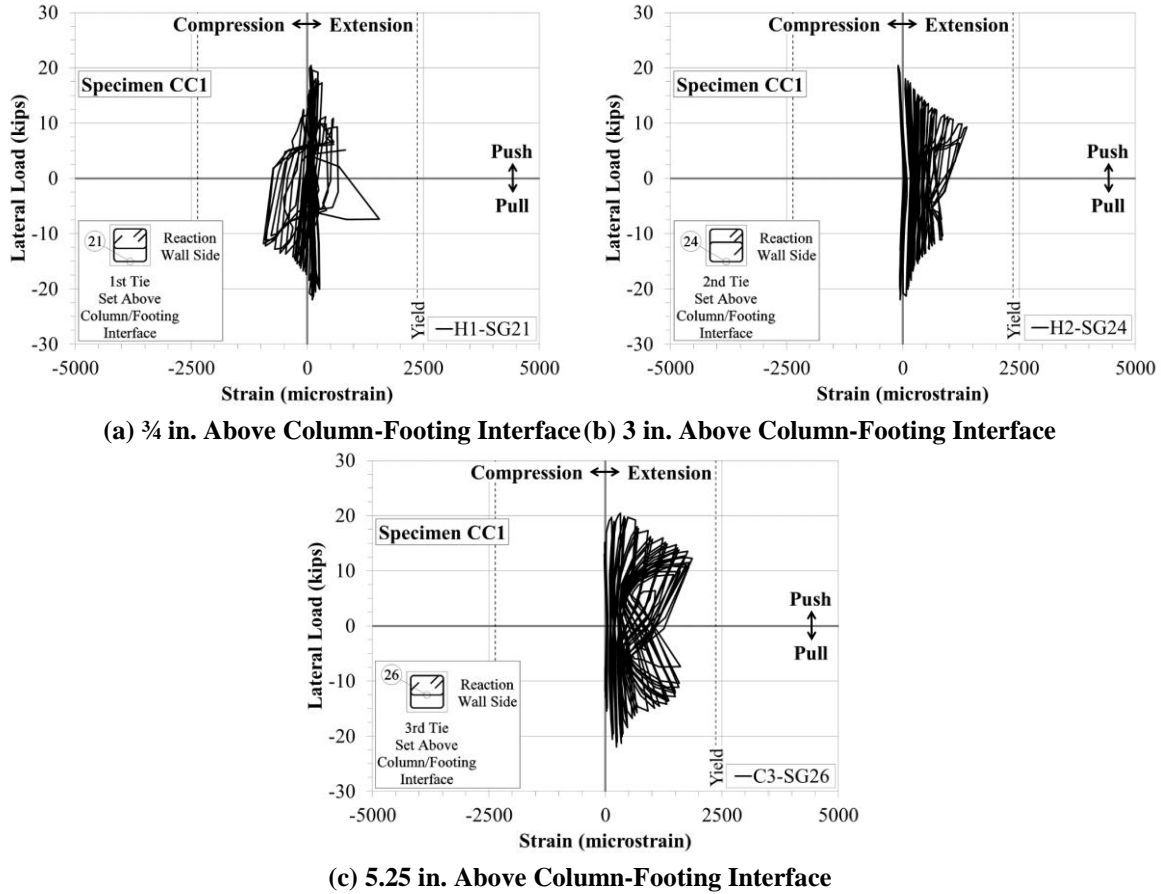


Figure 4.11 Measured Lateral Load-Strain in Transverse Steel of Specimen CC1

4.2.2.2 Specimen CC2

Specimen CC2 was subjected to axial loads of 147.4 kips at first yield and 148.0 kips at ultimate. Throughout the test, applied axial loads ranged from 121.5 kips to 164.2 kips. Measured lateral and axial loads applied at each full push-pull excursion during the test are provided in Appendix C-2. Some experimental measurement plots obtained for this specimen are presented in this section; the remaining plots can be found in Appendix D-2.

4.2.2.2.1 Lateral Displacement

Applied lateral load history for specimen CC2 is shown in Figure 4.12. From the plot, an irregularity is apparent in the seventh loading cycle. This cycle was intended to signify $\mu_{\Delta} = \pm 1$; however, measured strain data from longitudinal steel in the plastic hinge region indicated that none of the bars had yielded by this point. Because of this, the displacement in the next push excursion was increased at slight increments until the first strain gage indicated a bar had yielded. This was taken as the yield displacement during the test. At a lateral load of 11.69 kips in the pull direction, a flexural crack was located at 11 inches above the column-footing interface on the north side of the column. The measured displacement and load at first yield of longitudinal reinforcement was 0.54 inches and 20.13 kips, respectively. Measured lateral load-displacement and measured effective lateral load-displacement hysteretic responses are presented in Figure 4.13.

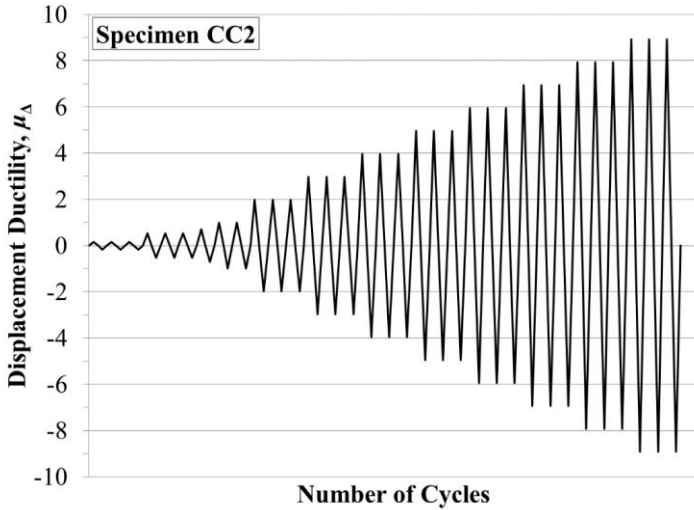


Figure 4.12 Lateral Load History for Specimen CC2

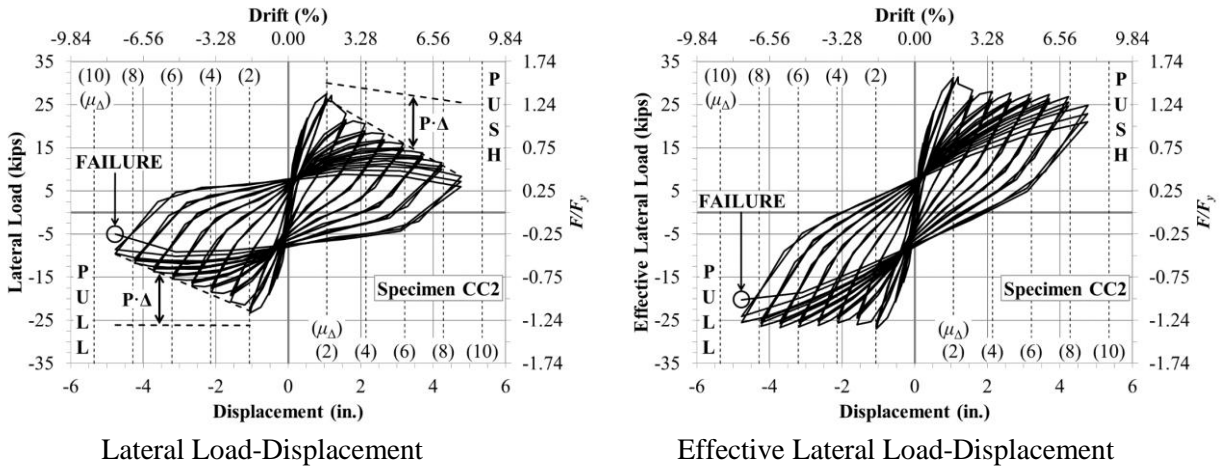


Figure 4.13 Measured Load-Displacement for Specimen CC2

Similar to specimen CC1, load-displacement response of specimen CC2 was fairly linear until a noticeable drop in stiffness between $\mu_{\Delta} = \pm 1$ and ± 2 . During the first excursion at $\mu_{\Delta} = +2$, crushing of column concrete cover at approximately 6 inches above the footing was observed in the northwest corner of the column. The first cycle at $\mu_{\Delta} = \pm 2$ also signified the peak lateral loads attained by the specimen. Applied lateral loads of 27.6 kips in the push direction and 23.4 kips in the pull direction were attained by the specimen. Discrepancies between maximum measured lateral loads were attributed to the scaled column reinforcement cage located slightly off-center toward the south-side of the column. As with specimen CC1, successive displacement ductility levels after reaching the peak lateral load resulted in an increased rate of spalling of concrete cover and reduction in applied lateral load. Compared with specimen CC1, concrete spalling and drop in lateral load were more abrupt. This was believed to be due to the higher axial loads applied to specimen CC2. At $\mu_{\Delta} = \pm 5$, the closed hoop of the third tie set above the footing became exposed on the column north side. At $\mu_{\Delta} = \pm 6$, the closed hoop of the second tie set above the footing and the southwest corner longitudinal bar, LB8, became exposed between the second and third tie sets above the footing. By $\mu_{\Delta} = \pm 8$, the first three closed hoops above the footing were nearly fully exposed on both north and south sides of the column.

During the first excursion at $\mu_{\Delta} = +9$, the 90-degree hook on the second north-south crosstie above the footing began to open and the middle longitudinal bar on the column north side, LB2, began to buckle outward. During the first excursion at $\mu_{\Delta} = -9$, the 90-degree hook on the first north-south crosstie above the footing began to open, and the middle longitudinal bar on the column south side, LB7, began to buckle outward. On the third pull excursion at this μ_{Δ} level, a “popping” noise was heard, and significant strength degradation was recognized on the lateral load-displacement plot. Upon inspection, a fracture was found on LB2 directly above the first tie set. Therefore, specimen failure was defined at a displacement ductility of 8.9 and corresponding drift of 7.82%. At the end of the test, spalled column cover concrete extended from the base of the column to approximately 9 to 12 inches above the base on both north and south sides of the column. Figure 4.14 presents pictures of specimen CC2 at successive μ_{Δ} levels throughout the test.

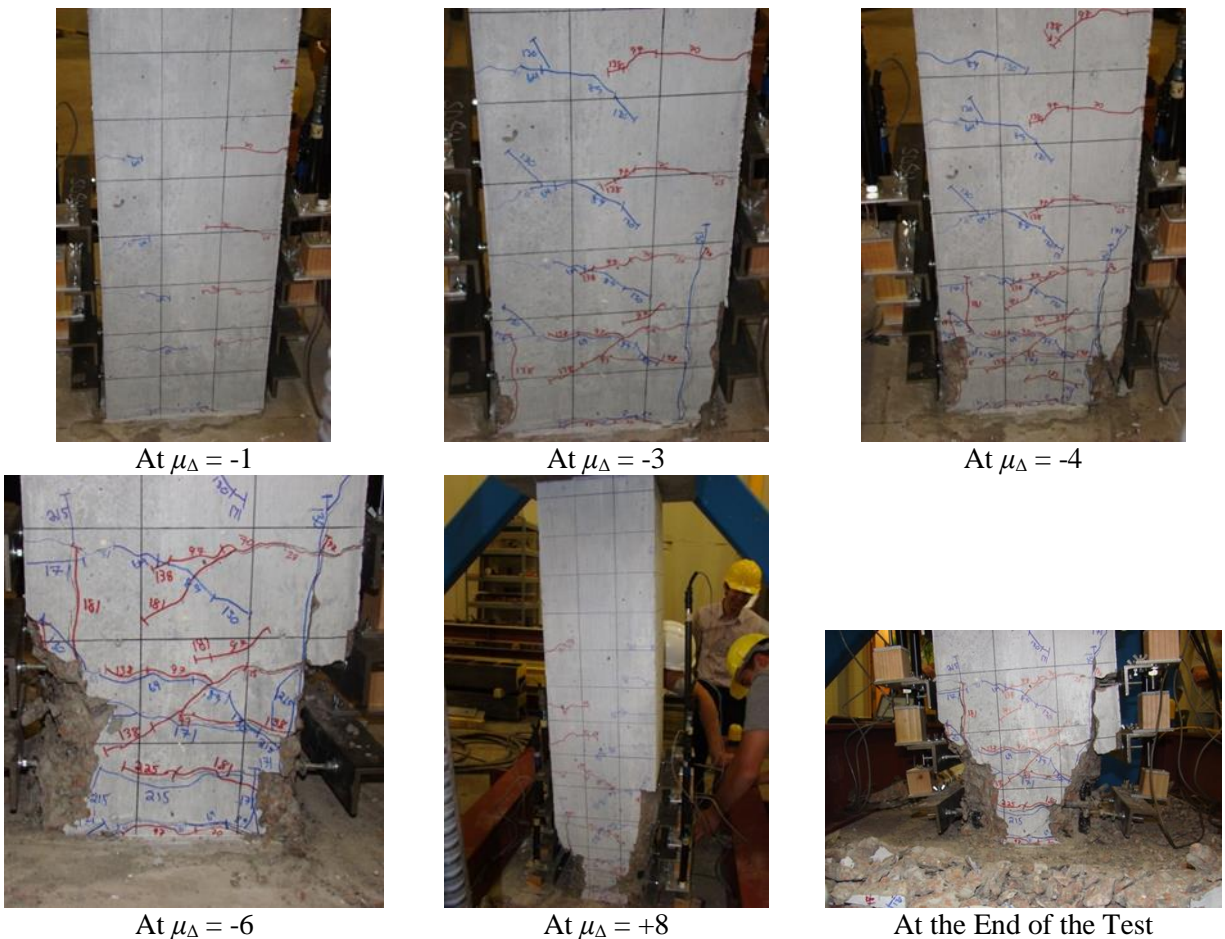


Figure 4.14 Visual Inspection of Specimen CC2 (1st Excursion)

4.2.2.2 Reinforcing Steel Strain

Measured lateral load-strain relationships of LB2 at sections 12, 8, and 4 inches below the column-footing interface are presented in Figure 4.15. The plots show strains surpassing the steel yield point in both tension and compression for the bottom two sections in the column footing, and in tension exclusively for the top section in the column footing. The top gage, SG5, recorded strains nearly eight magnitudes past the yield point, as seen in Figure 4.15. As stated previously, this longitudinal bar was the first to rupture during the test.

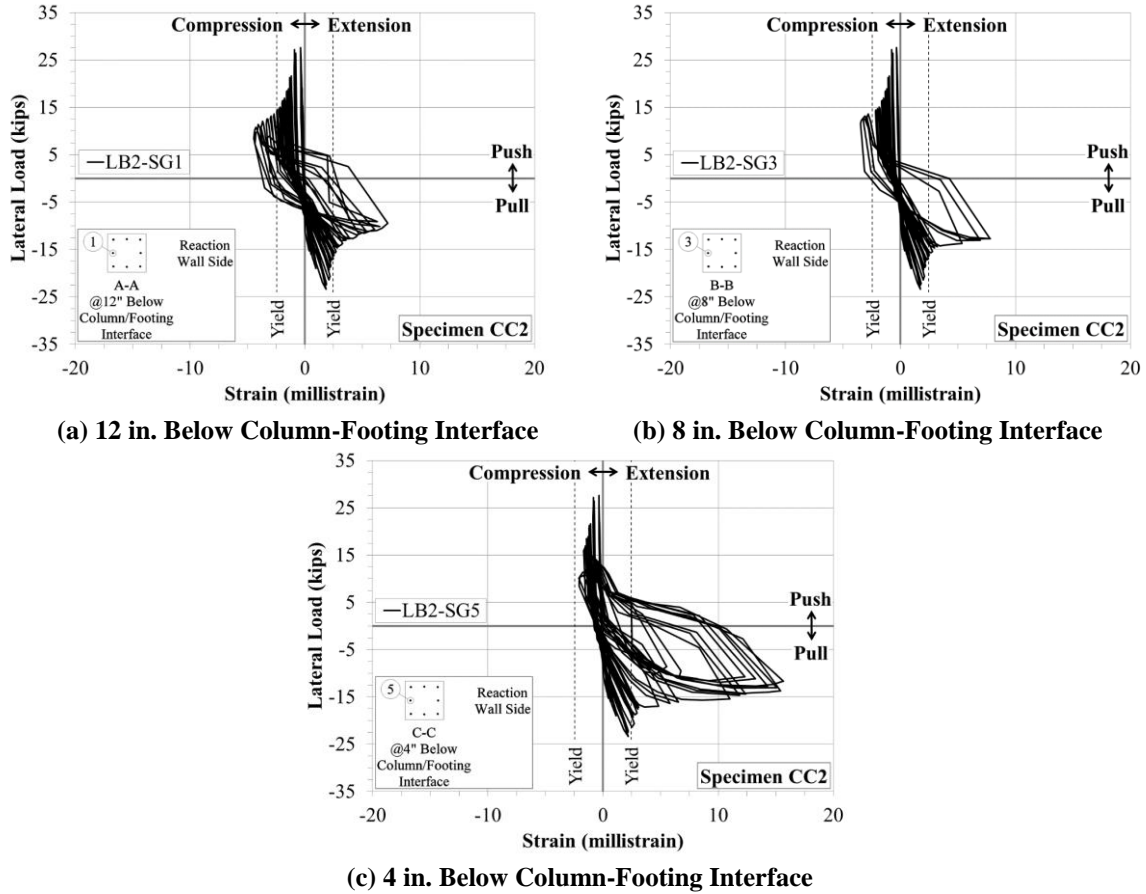


Figure 4.15 Measured Lateral Load-Strain in Longitudinal Steel below Column-Footing Interface of Specimen CC2

Measured lateral load-strain readings for the northeast corner longitudinal bar, LB1, are presented in Figure 4.16. The data presented in this figure are from strain gages located at the column-footing interface, between the first and second transverse reinforcement tie sets, and between the second and third tie sets, respectively. Gages on this bar measured an increase in strain with an increase in distance from the footing. The top gage, SG15, was the first of the three to reach the steel yield strain. It also recorded the highest strains before going offline at $\mu_{\Delta} = \pm 5$. The middle gage, SG11, also went offline at $\mu_{\Delta} = \pm 5$, and the bottom gage, SG7, lasted until $\mu_{\Delta} = \pm 7$.

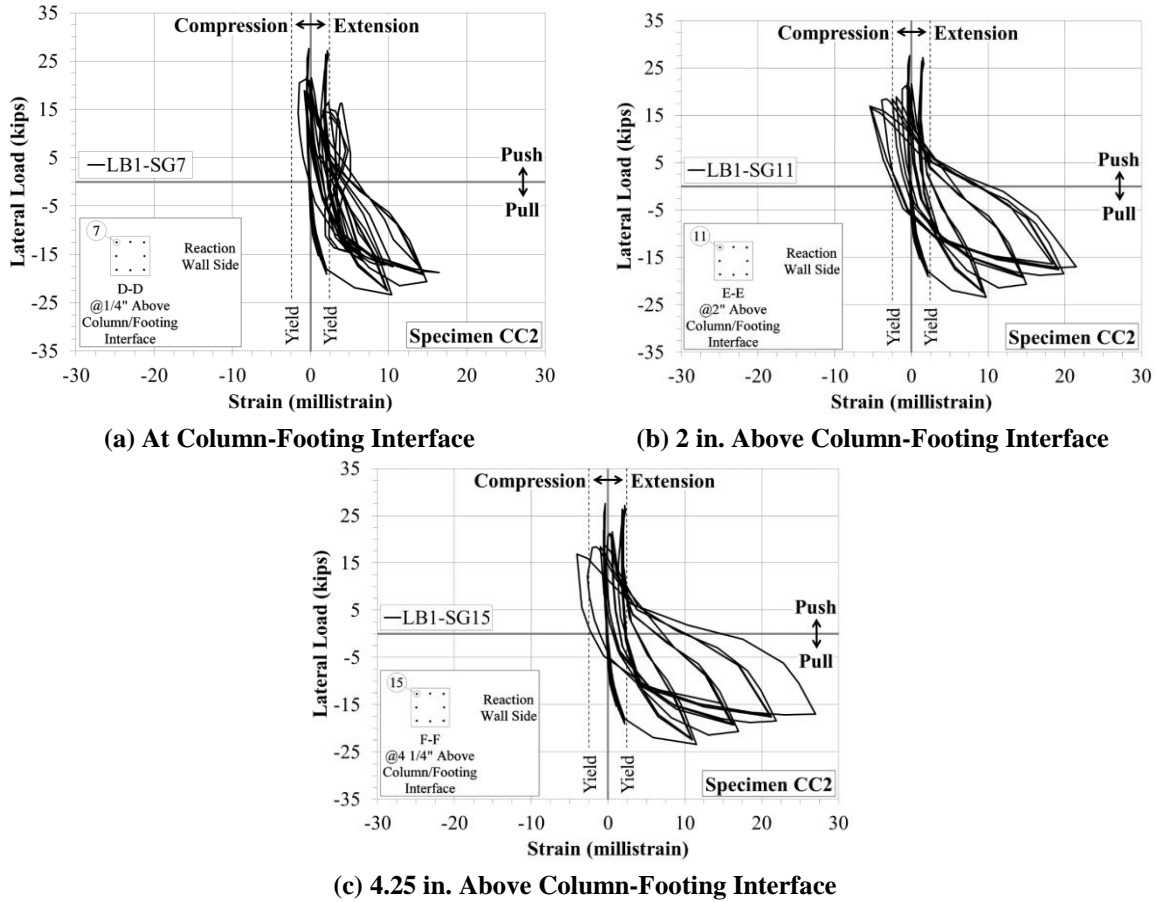


Figure 4.16 Measured Lateral Load-Strain in Longitudinal Steel of at and Above Column-Footing Interface of Specimen CC2

Transverse reinforcement in the column plastic hinge region reached strain values high enough to yield the steel in both the second (H2) and third (H3) tie sets above the footing. Lateral load-strain response plots of gages located on the first three transverse reinforcement tie sets above the footing are shown in Figure 4.17. The plots indicate that strain in the transverse reinforcement increased as distance from the footing increased.

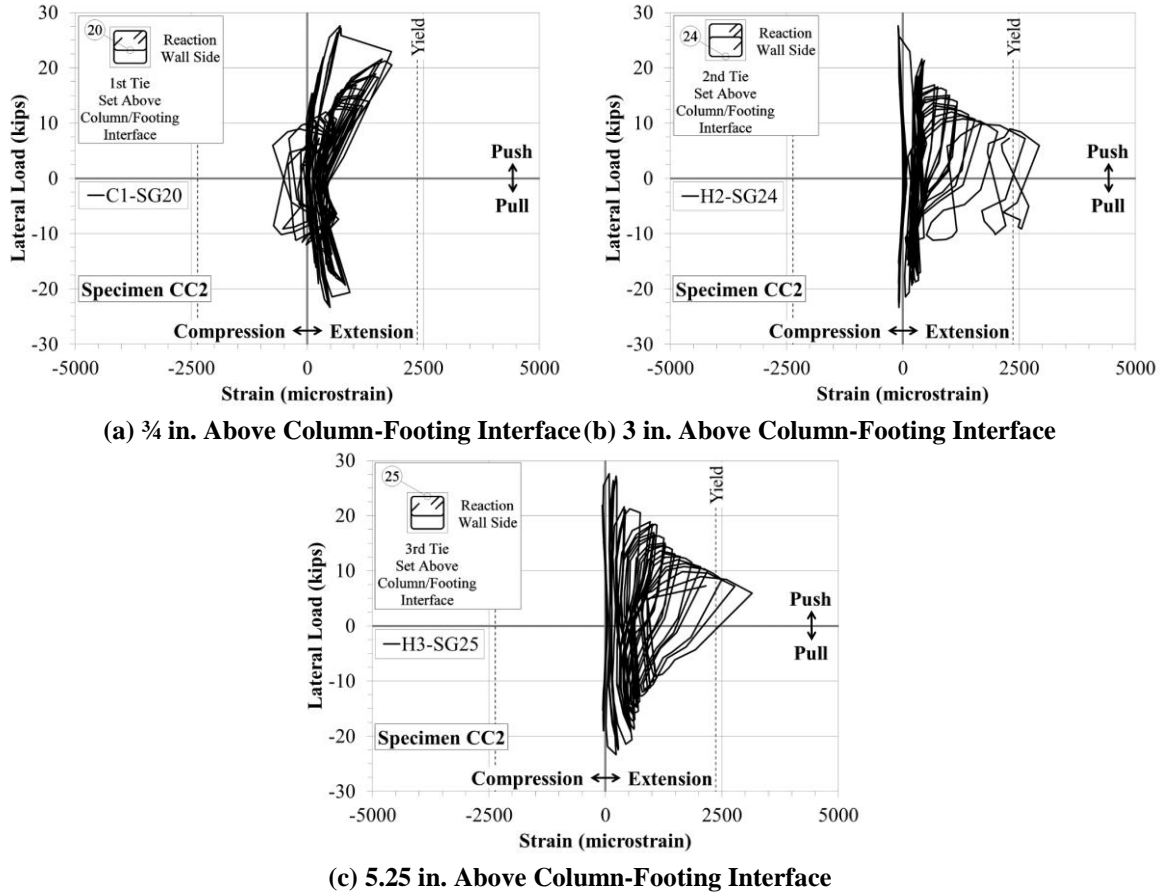


Figure 4.17 Measured Lateral Load-Strain in Transverse Steel of Specimen CC2

4.2.2.3 Specimen SCC1

Specimen SCC1 was subjected to axial loads of 84.1 kips at first yield and 99.1 kips at ultimate. Throughout the test, applied axial loads ranged from 61.7 kips to 109.1 kips. Measured lateral and axial loads applied at each full push-pull excursion during the test are provided in Appendix C-3. Selected experimental measurement plots obtained for this specimen are presented in this section; the remaining plots can be found in Appendix D-3.

4.2.2.3.1 Lateral Displacement

Applied lateral load history for specimen SCC1 is shown in Figure 4.18. At a lateral load of 11.71 kips in the push direction, four flexural cracks were located between 8 and 22 inches above the column-footing interface on the south column face. At a lateral load of 13.64 kips in the pull direction, three flexural cracks were located between 7 and 16 inches above the column-footing interface on the north column face. Measured displacement and load at first yield of longitudinal reinforcement was 0.54 inches and 15.77 kips, respectively.

In Figure 4.18, an observation to note is the difference in the applied lateral load history of specimen SCC1 compared with that of specimen CC1. As stated in the previous chapter, specimen SCC1 had a higher effective lateral yield force, $(F_y)_{eff.}$, compared with specimen CC1. Therefore, the displacement corresponding to $(F_y)_{eff.}$ was much higher for specimen SCC1 than for specimen CC1, which subjected specimen SCC1 to fewer loading cycles before failure. Due to the displacement at $(F_y)_{eff.}$ exceeding the

displacement at first yield, μ_{Δ} increments of ± 1 during the test correspond to reported increments of ± 1.37 . Measured lateral load-displacement and measured effective lateral load-displacement hysteretic responses are presented in Figure 4.19.

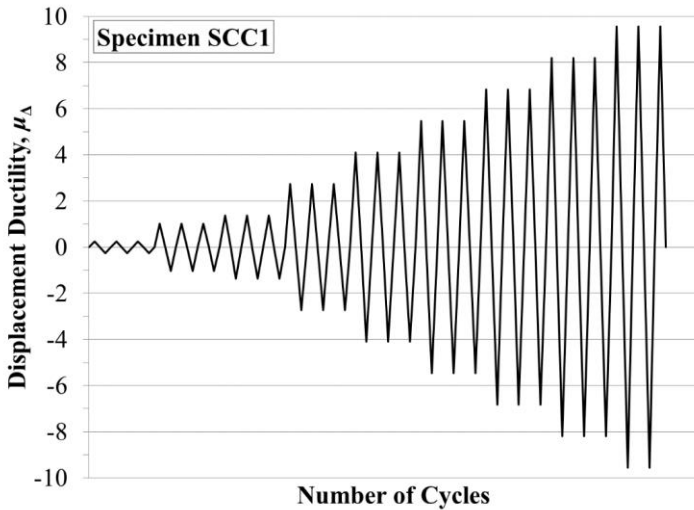


Figure 4.18 Lateral Load History for Specimen SCC1

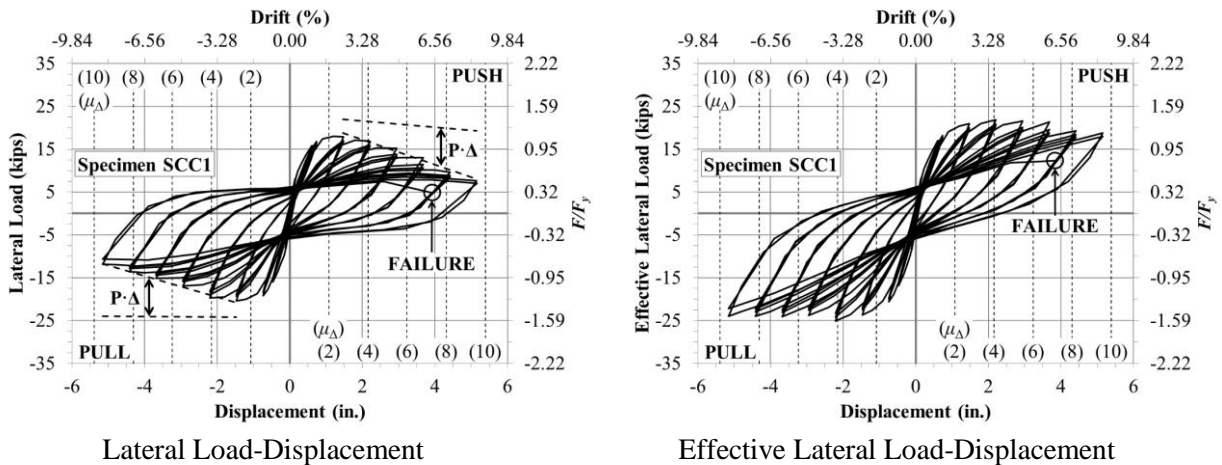


Figure 4.19 Measured Load-Displacement for Specimen SCC1

Similar to specimens CC1 and CC2, the load-displacement response of specimen SCC1 was almost linear until a noticeable drop in stiffness between $\mu_{\Delta} = \pm 1.4$ and $\mu_{\Delta} = \pm 2.7$. During the first loading cycle at $\mu_{\Delta} = \pm 2.7$, crushing of column concrete cover between the column-footing interface and approximately 4 inches above the interface was observed on the column north side during the push excursion, and the column south side during the pull excursion. The first loading cycle at $\mu_{\Delta} = \pm 2.7$ also represented peak lateral loads attained by the specimen. The specimen reached an applied lateral load of 18.0 kips in the push direction, and 20.5 kips in the pull direction. As with specimen CC2, differences between the maximum attained lateral loads were attributed to the scaled column reinforcement cage being slightly off-centered in the column cross section. The reinforcement cage in specimen SCC1 was off-centered toward the column north side. Following $\mu_{\Delta} = \pm 2.7$, additional spalling of concrete cover and reduction in applied lateral load occurred. At $\mu_{\Delta} = \pm 5.5$, the closed hoop of the first transverse reinforcement tie set above the footing became exposed on the north side of the column. During the first excursion at $\mu_{\Delta} = -8.2$,

the northeast and southwest corner longitudinal bars, LB1 and LB8, became exposed between the first and second tie sets above the footing.

By the end of the first excursion at $\mu_{\Delta} = -9.6$, the northwest corner column longitudinal bar, LB3, became visible between the first and second tie sets above the footing. Subsequent cycles at $\mu_{\Delta} = \pm 9.6$ caused LB3 to start to buckle between the first and second tie sets above the footing. On the third pull excursion at $\mu_{\Delta} = -9.6$, a “popping” noise was heard, and significant flexural strength degradation was documented. The bar fracture was not physically located, but a researcher present during the test visually observed LB8 spasm simultaneously with the “pop” noise that was heard. Therefore, it was assumed that the fracture of LB8 caused failure at a displacement ductility of 9.6 and a corresponding drift of 8.45%. Failure was affirmed after removing strain gage protection from LB8. At the end of the test, spalled column concrete cover extended from the base of the column to approximately 3 to 6 inches above the base on the north and south sides of the column. Figures 4.20 shows pictures of specimen SCC1 at successive μ_{Δ} levels throughout the test.

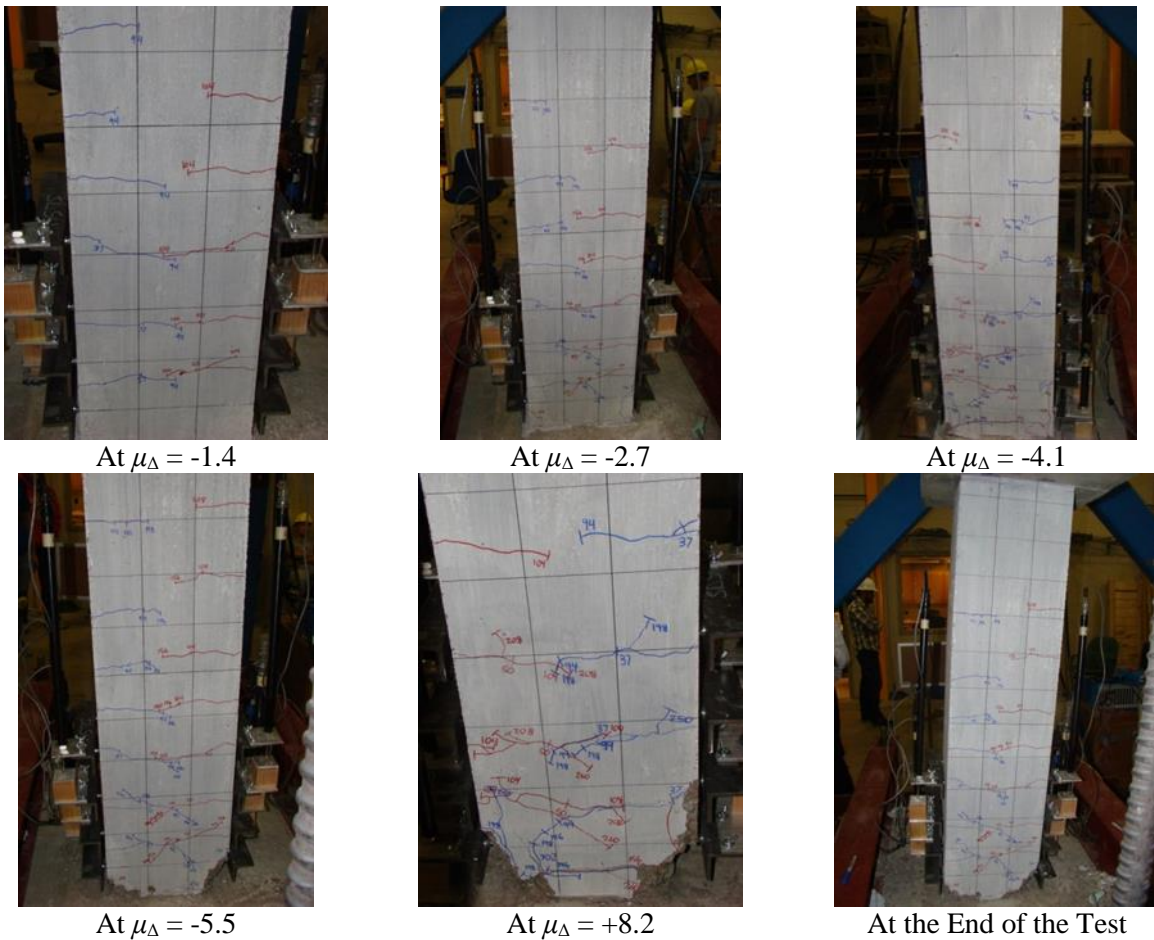


Figure 4.20 Visual Inspection of Specimen SCC1 (1st Excursion)

4.2.2.3.2 Reinforcing Steel Strain

Figure 4.21 shows measured lateral load-strain relationships of the middle longitudinal bar on the column north side, LB2, at sections 12, 8, and 4 inches below the column-footing interface. The bottom strain gage, SG1, went offline as early as $\mu_{\Delta} = \pm 1.4$, so presented values are not very representative of column response. Both gages SG3 and SG5, located at sections 8 and 4 inches below the column-footing

interface, went well past the steel yield point, as observed in Figure 4.21. SG3 lasted until the first pull cycle at $\mu_{\Delta} = -9.6$. SG5 still attained higher strains, even though it went offline at $\mu_{\Delta} = \pm 5.5$.

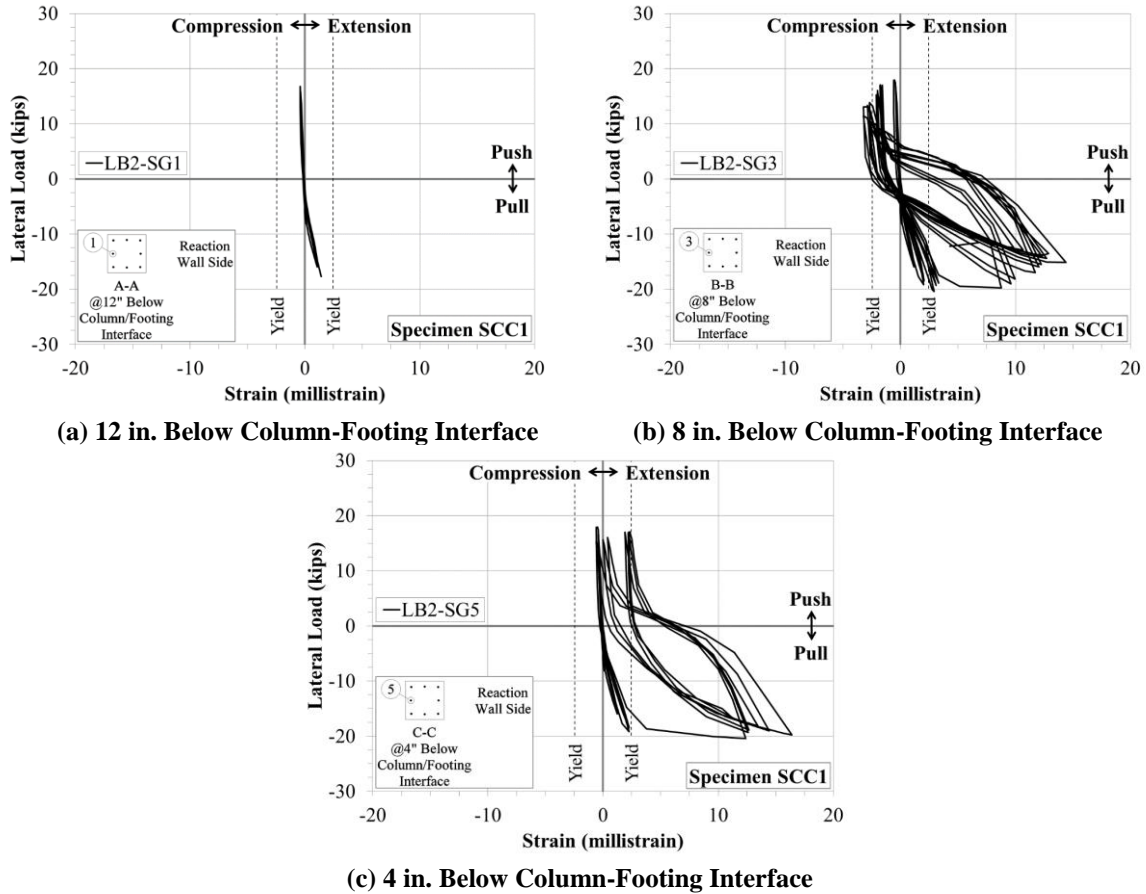


Figure 4.21 Measured Lateral Load-Strain in Longitudinal Steel below Column-Footing Interface of Specimen SCC1

Figure 4.22 displays the lateral load-strain readings for the southeast corner longitudinal bar, LB6. Strain gages provided in these figures were located at the column-footing interface, between the first and second transverse reinforcement tie sets, and between the second and third tie sets, respectively. The bottom gage, SG9, recorded strains for the longest duration before going offline at $\mu_{\Delta} = \pm 8.2$. The middle gage, SG13, reached the largest strains before going offline, despite the fact that it only recorded until $\mu_{\Delta} = \pm 5.5$. The top gage, SG17, reached the steel yield strain first. It also recorded higher strains at equivalent lateral loads in comparison with SG9 and SG13 before it went offline at $\mu_{\Delta} = \pm 4.1$.

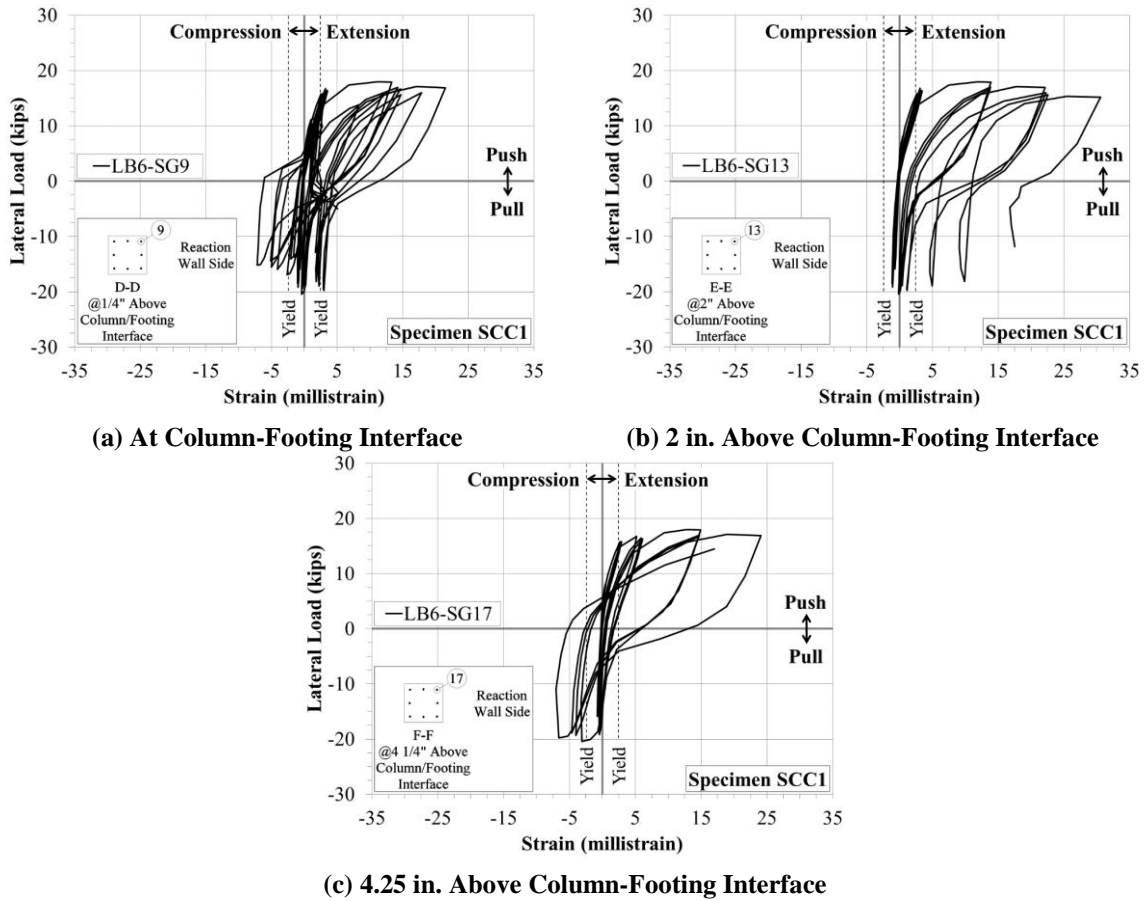


Figure 4.22 Measured Lateral Load-Strain in Longitudinal Steel of at and Above Column-Footing Interface of Specimen SCC1

Similar to specimen CC1, the transverse reinforcement in the column plastic hinge region of specimen SCC1 reached fairly high strain values but did not yield prior to rupture of longitudinal reinforcement. Lateral load-strain response plots of gages located on the first three transverse reinforcement tie sets above the footing are shown in Figure 4.23. The plots indicate that strains in the transverse reinforcement increased as distance from the footing increased.

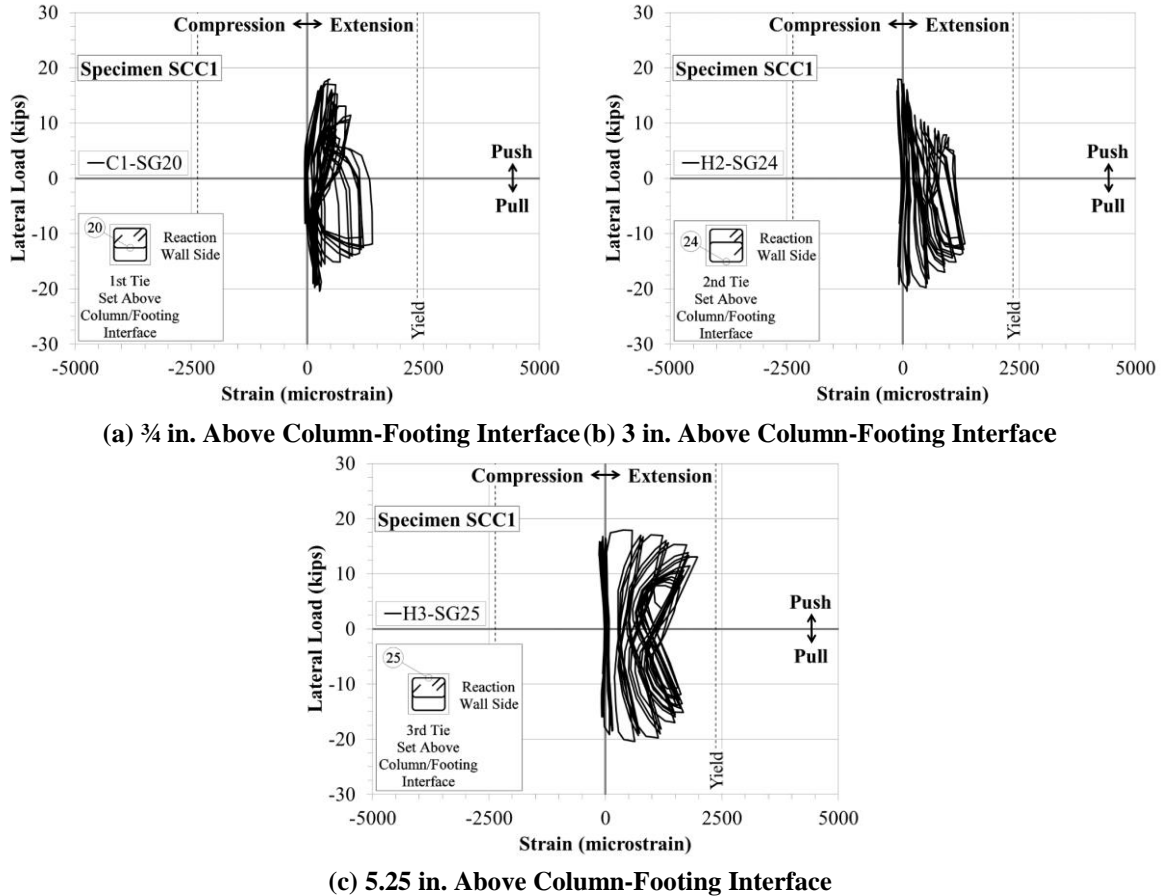


Figure 4.23 Measured Lateral Load-Strain in Transverse Steel of Specimen SCC1

4.2.2.4 Specimen SCC2

Specimen SCC2 was subjected to axial loads of 172.4 kips at first yield and 172.2 kips at ultimate. Applied axial loads throughout the test ranged from 130.0 kips to 189.4 kips. Measured axial and lateral loads applied at each full push-pull excursion throughout the test can be found in Appendix C-4. Particular experimental measurement plots obtained for this specimen are presented in this section; the remaining plots are located in Appendix D-4.

Specimen SCC2 differs from previously tested specimens due to its final fabricated state. After placing concrete in each column and curing the concrete for the specified amount of time, the column formwork was removed. Upon removal of the formwork for specimen SCC2, voids in the concrete cover throughout the potential plastic hinge region on each column face near the footing were evident. The surface voids were believed to be a result of the time delay between batching and placing the concrete into the bottom of the column of specimen SCC2. Due to that delay, the SCC became less flowable than it had been directly after batching; therefore, the concrete did not fully consolidate in the bottom lift of the column. An illustration of these surface flaws is shown in Figure 4.24. Upon inspection of the defects, it was not believed that the voids extended into the column core; thus, the voids were grouted and the column was tested as is.



Figure 4.24 Specimen SCC2 Plastic Hinge Region Concrete Defects (Looking North)

4.2.2.4.1 Lateral Displacement

Applied lateral load history for specimen SCC2 is shown in Figure 4.25. Similar to previously tested specimens, the first flexural cracks occurred in the column when it was subjected to its first push-pull cycle at $\pm 0.75(F_y)_{eff}$. At a lateral load of 13.52 kips in the push direction, a flexural crack was found at the column-footing interface on the south face of the column. At a lateral load of 11.46 kips in the pull direction, a flexural crack was located at the column-footing interface on the opposite column face.

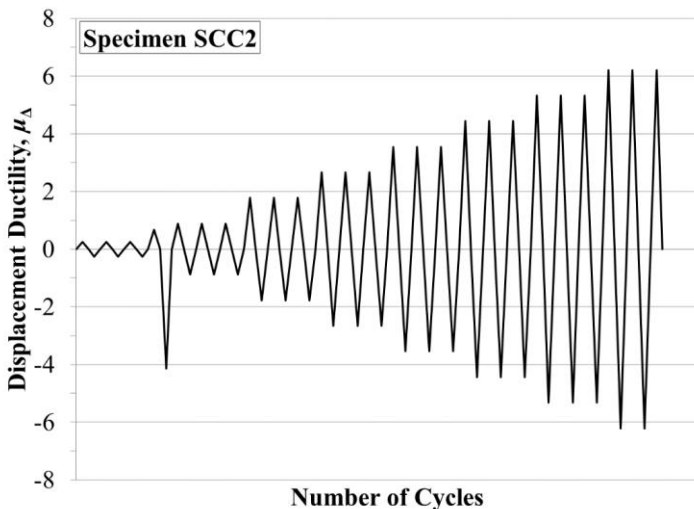


Figure 4.25 Lateral Load History for Specimen SCC2

From Figure 4.25, an observation to note is the large jump in the fourth cycle pull excursion. At this point in the test, the actuator was still in load-control, with a target load of $\pm 0.75(F_y)_{eff}$. Specimen SCC2 was loaded to a full push excursion of $+0.75(F_y)_{eff}$, but when loading switched to the pull direction with a target load of $-0.75(F_y)_{eff}$, the column never reached the target load and it deflected substantially before the emergency stop button for the actuator was engaged. When the hydraulic actuator is operated in load control, it will “search” for a target load by extending or retracting its piston until the target load is reached. If the specimen does not resist enough to meet the target load, the actuator will continue to

extend or retract until it is manually stopped or it runs out of piston stroke. During this event, measurements were not documented when the specimen was at its maximum displacement, because once the emergency stop is enabled, the load is released by the actuator. However, the research team present during the test recalled the displacement reaching approximately 2.4 inches from visual observation of computer monitors displaying measurement values. This estimated displacement corresponds to $\mu_{\Delta} = -4.1$. The region of the test corresponding to the loading incident is represented by the dashed line with diamond markers in the plotted lateral load-displacement and effective lateral load-displacement responses shown in Figure 4.26.

One reason the column may not have reached the desired load in the pull direction was because of premature crushing of column concrete cover as a result of surface defects in the plastic hinge region. Another possible explanation was attributed to the column reinforcement cage located slightly off-center to the south within the column cross section, which would reduce its flexural capacity in the pull direction. Since the specimen was not subjected to three push-pull cycles at $\pm 0.75(F_y)_{eff}$, the corresponding displacement at $(F_y)_{eff}$ was not interpolated using six measured displacement values as previous specimens were. Therefore, the push displacement recorded at $+0.75(F_y)_{eff}$ was used to extrapolate the corresponding displacement at $(F_y)_{eff}$. The extrapolated displacement value was slightly less than the average measured displacement at first yield of the longitudinal steel obtained from strain gage data. The difference is shown in Figure 4.26. Therefore, μ_{Δ} increments of ± 1 during the test correspond to reported increments of ± 0.9 . Measured displacement and load at first yield of longitudinal reinforcement was 0.58 inches and 20.58 kips, respectively.

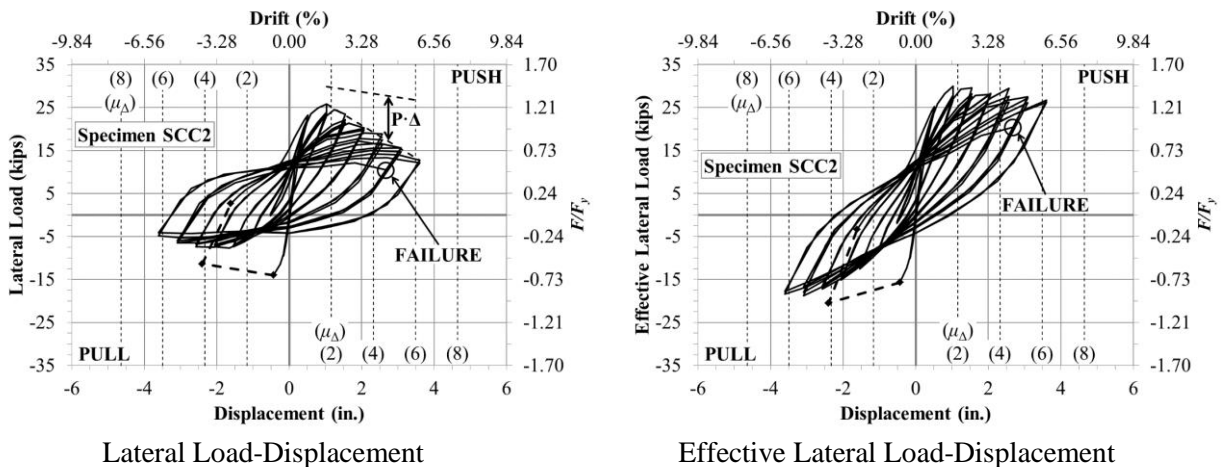


Figure 4.26 Measured Lateral Load-Displacement for Specimen SCC2

Prior to the loading incident, the lateral load-displacement response of specimen SCC2 was fairly linear. After the loading incident, residual stresses remained in longitudinal bars and caused the lateral load-displacement relationship to shift up, as seen in Figure 4.26. Bars on the north side of the column saw substantial plastic deformation and experienced strains well past the steel yield strain. Since loading was applied to the specimen at a rapid pace, flexural cracks were not marked.

After the loading incident, the specimen was returned to zero lateral displacement, and the actuator switched to displacement control for the remainder of the test. After this point, loading continued in successive cycles starting at $\mu_{\Delta} = \pm 0.9$. At $\mu_{\Delta} = +1.8$, five flexural cracks appeared from 7 to 26 inches above the footing on the column south side. Signs of crushing of the column concrete cover were also noted within the bottom 4 inches above the footing on the column north side. The first excursion at this displacement ductility level also represented the peak lateral load attained by the specimen in the push

direction. This peak load was 25.8 kips. Because of the loading incident, the peak lateral load attained in the pull direction was not recorded.

Successive displacement ductility levels following $\mu_{\Delta} = \pm 1.8$ resulted in additional spalling of concrete cover and reduction in applied lateral load. Due to increased axial loads applied to specimen SCC2 compared with specimen SCC1, a substantial drop in the applied lateral load after the peak load had been reached is apparent. At $\mu_{\Delta} = +2.7$, the southwest corner longitudinal bar, LB8, became exposed between the first and second tie sets above the footing. At $\mu_{\Delta} = -3.6$, the southeast corner longitudinal bar, LB6, became exposed between the first and second tie sets above the footing. At $\mu_{\Delta} = -5.3$, the northwest corner longitudinal bar, LB3, became exposed between the same tie sets. At $\mu_{\Delta} = +6.2$, spalling of column concrete cover extended higher up the column in the southwest corner, exposing LB8 between the second and third tie set above the footing. LB3, LB6, and LB8 all appeared to be in the beginning stages of buckling under subsequent cycles at $\mu_{\Delta} = \pm 6.2$. On the third push excursion at this displacement ductility, a “pop” sound was heard; thus, strain gage protection was removed from the column corner longitudinal bars, and it was found that LB8 had ruptured. Therefore, failure was defined at a displacement ductility of 6.2 and a corresponding drift of 5.92%. By the end of the test, column concrete cover had spalled from the base of the column to approximately 2 to 3 inches above the base on the north and south sides of the column, and as far as 14 inches in the column corners. Figure 4.27 presents pictures of specimen SCC2 at various μ_{Δ} levels throughout the test.

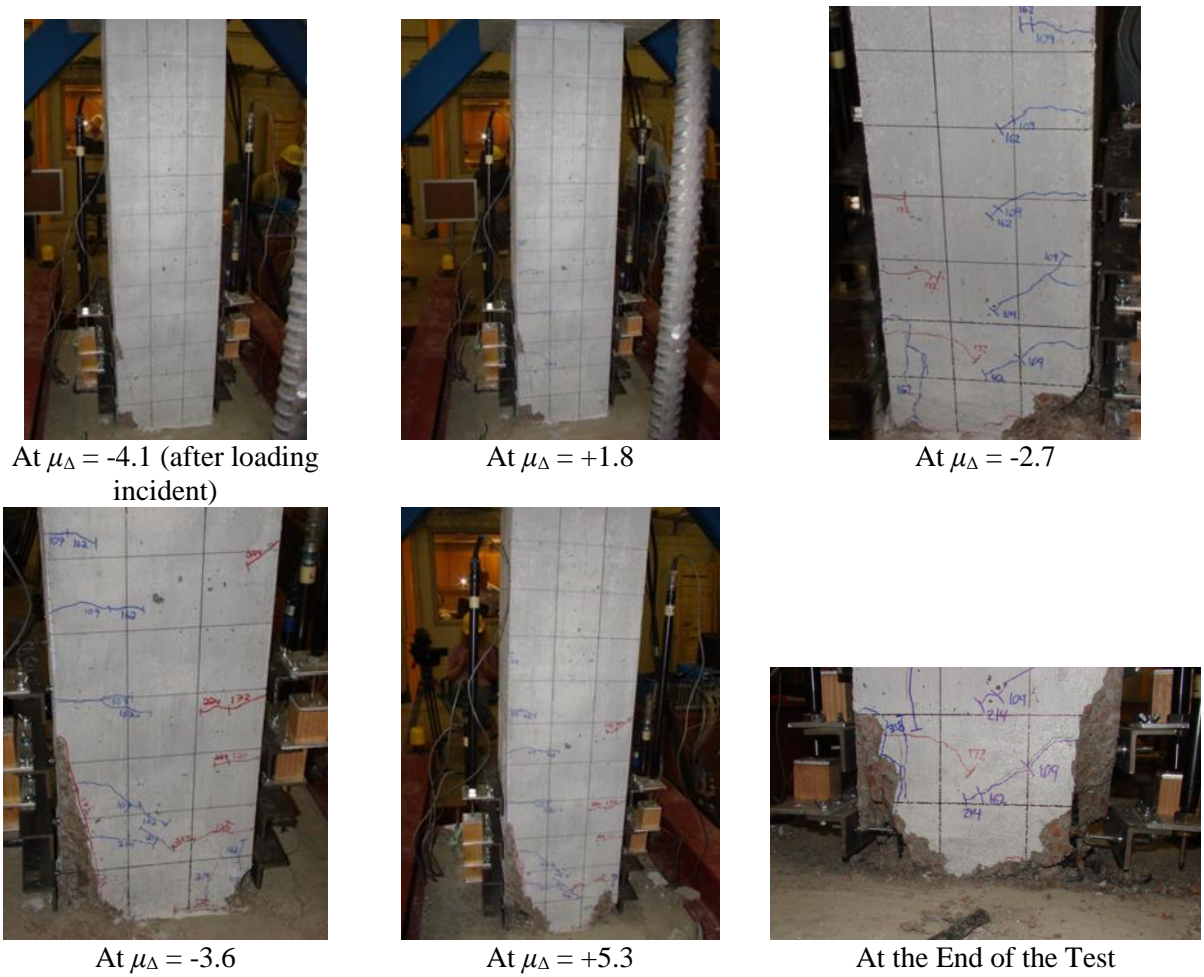


Figure 4.27 Visual Inspection of Specimen SCC2 (1st Excursion)

4.2.2.4.2 Reinforcing Steel Strain

Measured lateral load-strain relationships for the middle longitudinal bar on the south side of the column, LB7, at sections 12, 8, and 4 inches below the top of the footing are presented in Figure 4.28. From the figure, tensile and compressive strains past the steel yield point were measured for all three sections. Upon inspection of the plots, one can see where the loading incident happened from the linear region where the pull lateral load reached a maximum value followed by an upward shift in loads. As expected, an increase in strain between the bottom gage, SG2, and the middle gage, SG4, was measured at corresponding loads as the steel became closer to the column-footing interface. The top gage, SG6, reached very high compressive strains during pull cycles starting at $\mu_{\Delta} = -4.4$. This gage went offline during the second loading cycle at $\mu_{\Delta} = -6.2$.

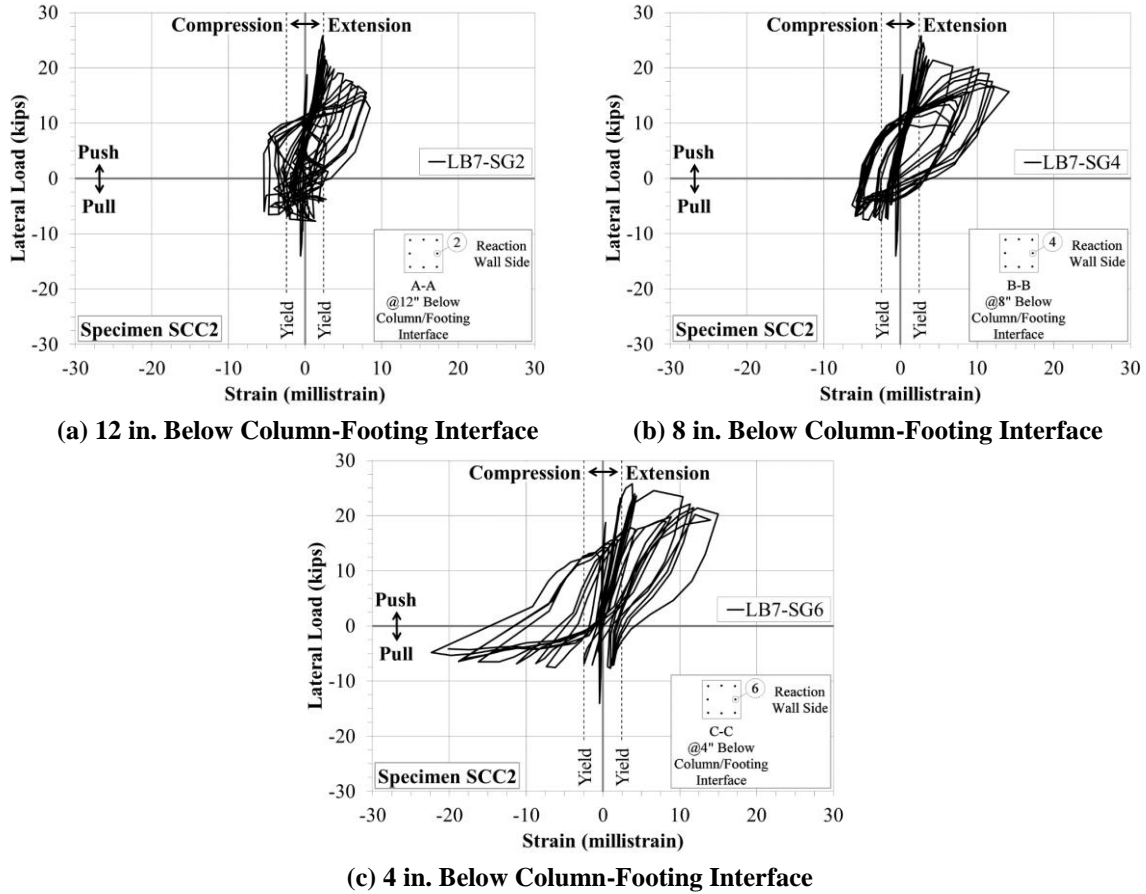


Figure 4.28 Measured Lateral Load-Strain in Longitudinal Steel below Column-Footing Interface of Specimen SCC2

Figure 4.29 displays the measured lateral load-strain relationship of LB3 at locations within the first 4 ¼ inches above the column-footing interface. The first gage above the interface, SG8, was the first gage on this bar to measure the steel yield strain, and it also recorded the highest tensile strains before going offline at $\mu_{\Delta} = \pm 3.5$. SG12, located between the first and second transverse reinforcement tie sets, recorded extensive tensile and compressive strains, with strains shifted more toward compression than tension. This gage went offline at $\mu_{\Delta} = \pm 4.4$. The gage farthest from the interface, SG16, measured nearly parallel tensile and compressive strains for corresponding push-pull cycles before going offline at $\mu_{\Delta} = \pm 5.3$.

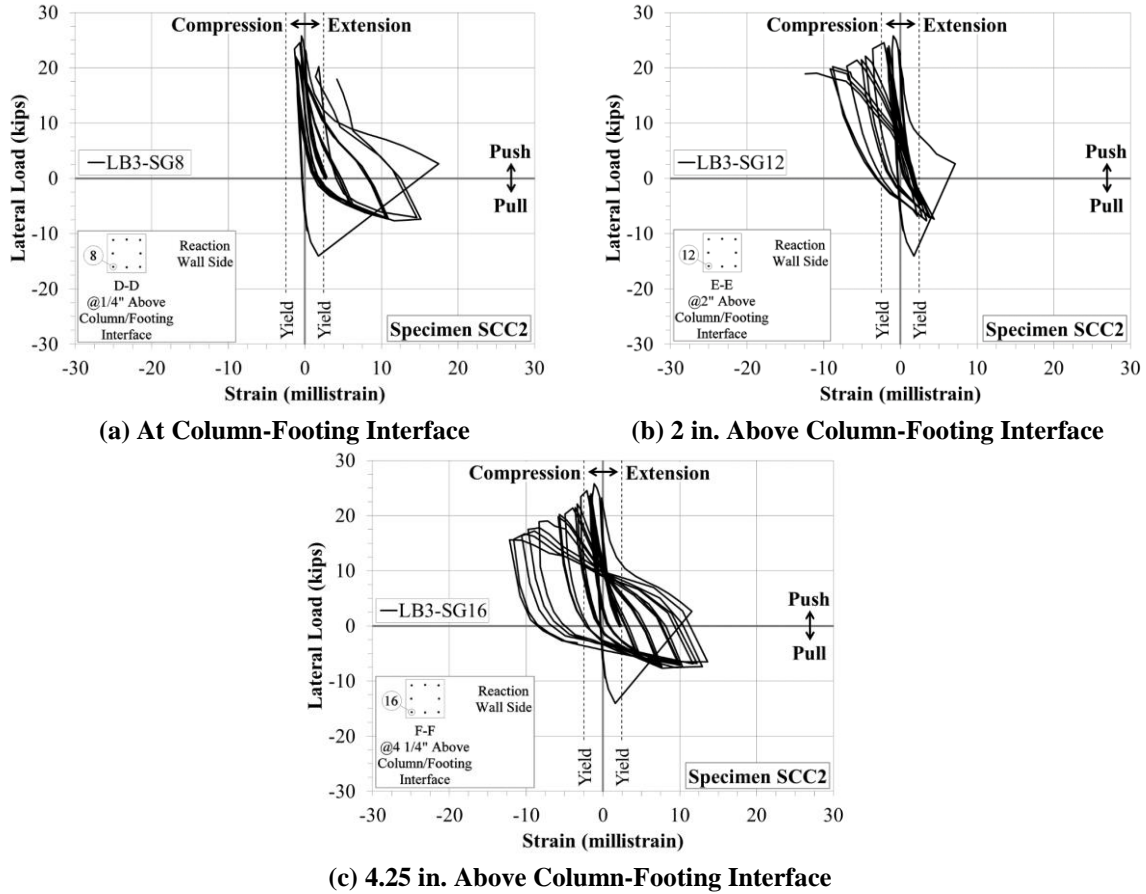
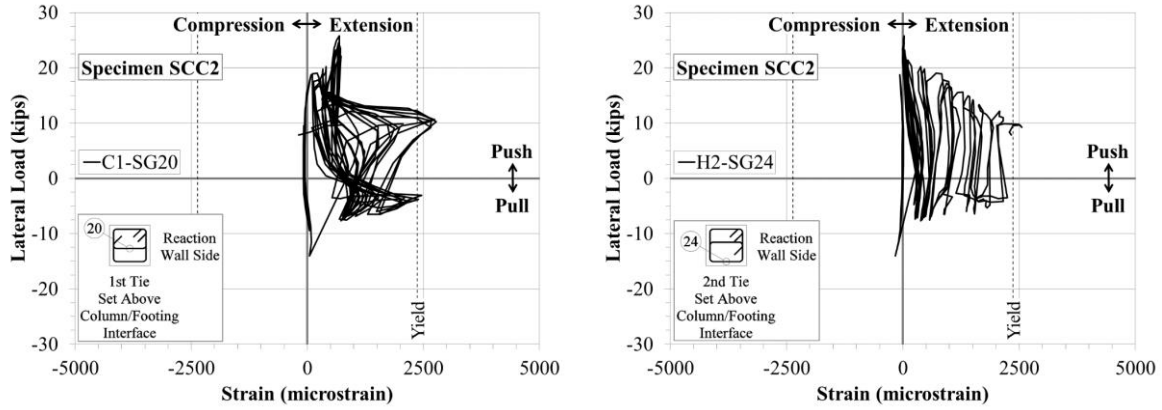
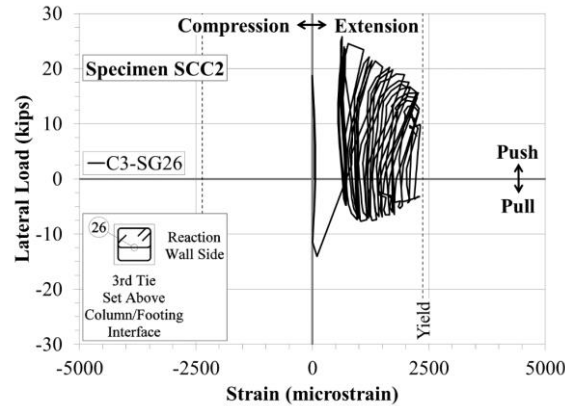


Figure 4.29 Measured Lateral Load-Strain in Longitudinal Steel of at and Above Column-Footing Interface of Specimen SCC2

Measured lateral load-strain relationships for the first three transverse reinforcement tie sets above the footing are presented in Figure 4.30. Both the first north-south cross-tie, C1, and the second closed hoop, H2, above the footing surpassed the steel yield strain. The third north-south cross-tie above the footing, C3, nearly yielded. As with the gaged longitudinal bars in the footing, the location of the loading incident is easily identifiable from the plots. There was a linear lateral load-strain relationship at very low strains followed by an increase in strain. Unlike previous specimens, SCC2 recorded the highest strains in the transverse reinforcement closer to the footing, although differences in strain values are slight.



(a) $\frac{3}{4}$ in. Above Column-Footing Interface (b) 3 in. Above Column-Footing Interface



(c) 5.25 in. Above Column-Footing Interface

Figure 4.30 Measured Lateral Load-Strain in Transverse Steel of Specimen SCC2

4.2.3 Remarks and Observations

The lateral load-displacement relationships presented in Figure 4.7, Figure 4.13, Figure 4.19, and Figure 4.26 show that all four specimens displayed wide and stable hysteresis loops, which are suggestive of ductile flexural response (Priestley et al. 1996). Measured lateral load-displacement and effective lateral load displacement response envelopes for each specimen are shown in Figure 4.31. The measured peak net and effective lateral loads recorded at successive displacement ductility levels during the tests produced the backbone of the envelopes in the figure.

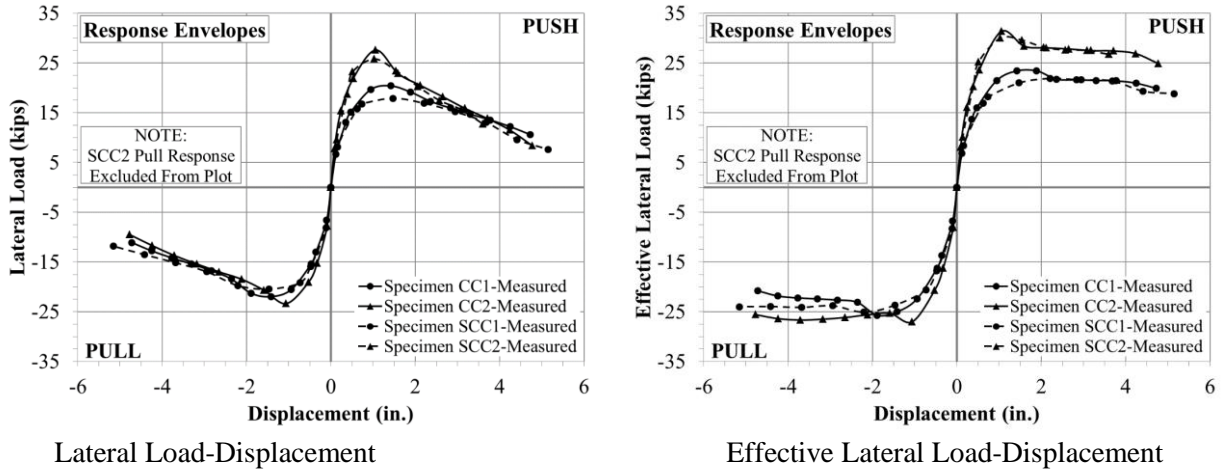


Figure 4.31 Response Envelopes

Table 4.12 presents a summary of experimental results obtained for all four specimens. The measured lateral force at first yield, $F_{y,meas}$, corresponds to the force required to yield the outermost tension steel bars. Experimentally, $F_{y,meas}$ was determined using strain gage data from longitudinal bars at the critical column section. The lateral forces corresponding to the first bar yield in tension for the push and pull excursions were recorded. $F_{y,meas}$ was determined as the average of the push and pull yield forces. Similarly, the displacement at first yield, Δ_y , was determined as the average of the displacements at first yield in the push and pull excursions. The ultimate displacement, Δ_u , was considered as the maximum lateral displacement achieved by the specimen prior to failure. Failure of each specimen was initiated by buckling of the outermost longitudinal compression bars. One or more of the buckled bars ruptured in tension during either the second or third loading cycle at Δ_u due to low-cycle fatigue.

The displacement ductility, μ_Δ , attained by the column corresponds to Δ_u divided by Δ_y . The corresponding drift ratio, expressed as a percentage, represents Δ_u divided by the specimen shear span, which was 61 inches for this study. The last column in Table 4.12 represents the energy absorbed by each specimen during testing. Absorbed energy for each specimen was determined by taking the summation of the area within each lateral load-displacement response hysteresis, provided in Figure 4.7, Figure 4.13, Figure 4.19, and Figure 4.26. Summation of the absorbed energy was terminated at a specimen displacement of zero prior to the final push or pull excursion that caused failure.

Table 4.12 Summary of Experimental Results

Specimen	Axial Load Ratio @ Ultimate $P/(f'_c A_g)$	Measured Force @ First Yield, $(F_y)_{meas}$ (kips)	Measured Displacements				Energy Absorbed (kip-in.)
			Δ_y (in.)	Δ_u (in.)	μ_Δ	Drift Ratio (%)	
CC1	0.09	14.60	0.472	4.72	10.00	7.74	1365
CC2	0.15	20.13	0.535	4.77	8.91	7.82	1424
SCC1	0.09	15.77	0.539	5.15	9.56	8.45	1045
SCC2	0.15	20.58	0.581	3.61	6.21	5.91	792

For both concrete groups, as axial load increased, measured Δ_y increased. Additionally, specimens subjected to higher axial loads were able to attain higher flexural capacities as well as higher lateral loads prior to yielding of longitudinal reinforcement. Direct evaluation between concrete types shows that specimen CC1 attained a higher μ_Δ than specimen SCC1, but a lower drift, with ratios between CC and SCC of 1.05 and 0.92, respectively. Specimen CC1 was subjected to more lateral loading cycles than specimen SCC1, which made the difference in absorbed energy. The absorbed energy ratio of specimen CC1 to specimen SCC1 was 1.31. Specimen SCC2 could not be directly compared to specimen CC2 due to the irregular load path that specimen SCC2 undertook because of the loading incident. Specimen SCC2 was subjected to inelastic deformation early on in the test, but was still able to undergo successive loading cycles and attain a drift of nearly 6%.

All four specimens experienced extensive concrete deterioration in the plastic hinge region at and directly above the column-footing interface on the north and south sides of the column. Between axial load groups, the distance from the footing where the concrete cover spalled increased as axial load increased. Spalling on specimens CC1 and SCC1 extended from the top of the footing to approximately 3 to 7 inches above the footing, whereas spalling on specimens CC2 and SCC2 extended up the column corners approximately 14 inches. Excluding specimen SCC2, strains in the confinement steel generally were lower near the column-footing interface and became higher as the distance from the footing increased. For specimens CC1 and SCC1, confinement steel in the plastic hinge region did not yield prior to fracture of the longitudinal reinforcement, whereas, in specimens CC2 and SCC2, the steel yielded at all three instrumented sections. Additionally, as μ_Δ increased, strain in the transverse steel increased even though the applied lateral load decreased. This was attributed to the increased contribution from the transverse reinforcement as the concrete in the section deteriorated. Also, all longitudinal bar fractures in each specimen were not located at the column-footing interface, but rather, were located between the first and second transverse reinforcement tie sets, approximately 1 to 2 inches above the interface.

4.2.4 Analytical Results

4.2.4.1 Calculated Deflections

Figure 4.32 shows the analytical lateral load-deflection envelopes for the four column specimens. Table 4.13 and Table 4.14 show tabulated results for each load step. Load step 5 for each specimen represents the total deflection at first yield in the outermost tension steel layer, while load step 9 represents total deflection directly prior to specimen failure. The analysis showed that failure of the specimens that were subjected to the lower axial load (CC1 and SCC1) was initiated by tension steel rupture, while failure of the specimens that were subjected to the higher axial load (CC2 and SCC2) was initiated by crushing of the core concrete.

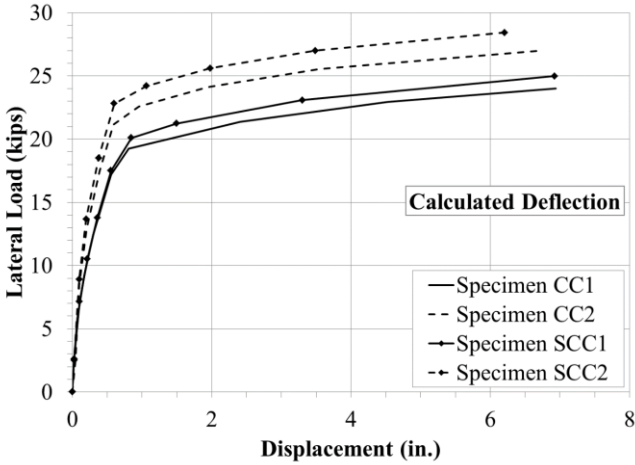


Figure 4.32 Analytical Lateral Load-Deflection Envelopes

Table 4.13 Analytical Lateral Deflections for Group 1 Specimens

Specimen	Load Number	Lateral Load (kips)	Flexural Deflection (in.)	Bond Slip Deflection (in.)	Shear Deflection (in.)	Total Deflection (in.)
CC1	1	2.58	0.021	0.000	0.005	0.03
	2	5.81	0.061	0.002	0.012	0.07
	3	9.20	0.143	0.014	0.019	0.17
	4	12.39	0.241	0.042	0.026	0.30
	5*	17.21	0.408	0.116	0.036	0.55
	6	19.26	0.579	0.131	0.039	0.81
	7	21.36	1.730	0.635	0.045	2.41
	8	22.96	3.079	1.403	0.048	4.53
	9**	24.02	4.400	2.490	0.050	6.94
SCC1	1	2.60	0.021	0.000	0.005	0.03
	2	7.16	0.084	0.004	0.015	0.10
	3	10.53	0.173	0.021	0.022	0.22
	4	13.76	0.274	0.054	0.029	0.36
	5*	17.50	0.401	0.115	0.037	0.55
	6	20.10	0.473	0.113	0.041	0.85
	7	21.23	1.080	0.369	0.044	1.49
	8	23.08	2.286	0.968	0.048	3.30
	9**	24.97	4.344	2.531	0.052	6.93

*First Yield of the Outermost Tension Steel

**Rupture of the Outermost Tension Steel

Table 4.14 Analytical Lateral Deflections for Group 2 Specimens

Specimen	Load Number	Lateral Load (kips)	Flexural Deflection (in.)	Bond Slip Deflection (in.)	Shear Deflection (in.)	Total Deflection (in.)
CC2	1	2.50	0.041	0.000	0.005	0.05
	2	8.46	0.078	0.001	0.018	0.10
	3	12.89	0.162	0.016	0.027	0.20
	4	17.46	0.292	0.061	0.037	0.39
	5*	21.14	0.418	0.130	0.044	0.59
	6	22.56	0.688	0.222	0.047	0.96
	7	24.11	1.376	0.520	0.050	1.95
	8	25.53	2.369	1.125	0.053	3.55
	9**	27.00	4.025	2.661	0.056	6.74
SCC2	1	2.51	0.021	0.000	0.005	0.03
	2	8.91	0.078	0.001	0.019	0.10
	3	13.67	0.158	0.013	0.029	0.20
	4	18.50	0.284	0.057	0.039	0.38
	5*	22.80	0.422	0.132	0.048	0.60
	6	24.19	0.761	0.252	0.051	1.06
	7	25.61	1.389	0.539	0.054	1.98
	8	27.00	2.320	1.116	0.057	3.49
	9**	28.42	3.777	2.369	0.060	6.20

*First Yield of the Outermost Tension Steel

**Crushing of the Core Concrete

Table 4.15 presents each deflection component as a percentage of total deflection. As expected, flexural deflections had the highest contribution at first yield of the outermost tension reinforcement and at ultimate state for each specimen. At first yield, flexural contribution was greatest, and ranged from 70.2% to 73.7% of the total deflections for each specimen. At ultimate state, flexural contribution dropped slightly, and ranged from 59.7% to 63.4% of the total deflections for each specimen.

Contrary to flexural deflections, bond slip deflections had higher contribution to the total deflections at ultimate state than at first yield. For each specimen, deflections at first yield fell between 20.9% and 21.9%, and at ultimate state ranged from 35.9% to 39.5%. Shear deflections had relatively minor impacts on overall deflections. This can be attributed to the high amount of shear reinforcement provided throughout each specimen. Shear deflections were most prevalent at first yield, accounting for between 6.5% and 7.9% of the total deflections. At ultimate state, shear contribution was negligible, accounting for less than 1.0% of total deflections for each specimen.

Table 4.15 Calculated Deflections due to Flexure, Bond Slip, and Shear

Specimen	Loading Stage	Contribution to Total Deflection (%)		
		Flexure	Bond Slip	Shear
CC1	1st Yield	73.7	20.9	6.50
	Ultimate	63.4	35.9	0.72
SCC1	1st Yield	72.5	20.9	6.62
	Ultimate	62.7	36.5	0.75
CC2	1st Yield	70.6	21.9	7.48
	Ultimate	59.7	39.5	0.84
SCC2	1st Yield	70.2	21.9	7.95
	Ultimate	60.9	38.2	0.96

4.2.4.2 Comparison between Experimental and Analytical Results

Table 4.16 presents a summary of the analytical (calculated) and experimental (measured) lateral deflections. Displacements at first yield of the outermost tension reinforcement and at ultimate state are presented along with displacement ductility and drift ratios for each specimen. The measured and calculated deflections at first yield were reasonably close. The differences between measured and calculated deflections at the ultimate state were more noticeable. Direct comparisons between the measured and calculated values are provided in Table 4.17. Figure 4.33 shows calculated lateral load-deflection response envelopes for each specimen. Measured envelope backbones are based on peak lateral loads recorded at successive displacement ductility levels during testing. The calculated load-deflection relationships do not include P - Δ effects. For the sake of comparing experimental and analytical results, the experimental results were adjusted for the P - Δ effects and plotted in Figure 4.33.

Table 4.16 Comparison between Experimental and Analytical Displacements

Specimen	Measured Displacements				Calculated Displacements			
	Δ_y (in.)	Δ_u (in.)	μ_Δ	Drift Ratio (%)	Δ_y (in.)	Δ_u (in.)	μ_Δ	Drift Ratio (%)
CC1	0.472	4.72	10.0	7.7	0.554	6.94	12.5	11.4
CC2	0.535	4.77	8.9	7.8	0.591	6.74	11.4	11.1
SCC1	0.539	5.15	9.6	8.4	0.554	6.93	12.5	11.4
SCC2	0.581	3.61	6.2	5.9	0.601	6.20	10.3	10.2

Table 4.17 Ratios of Experimental to Analytical Displacements

Specimen	Ratio: Measured to Calculated			
	Δ_y	Δ_u	μ_Δ	Drift
CC1	0.85	0.68	0.80	0.68
CC2	0.91	0.71	0.78	0.71
SCC1	0.97	0.74	0.76	0.74
SCC2	0.97	0.58	0.60	0.58

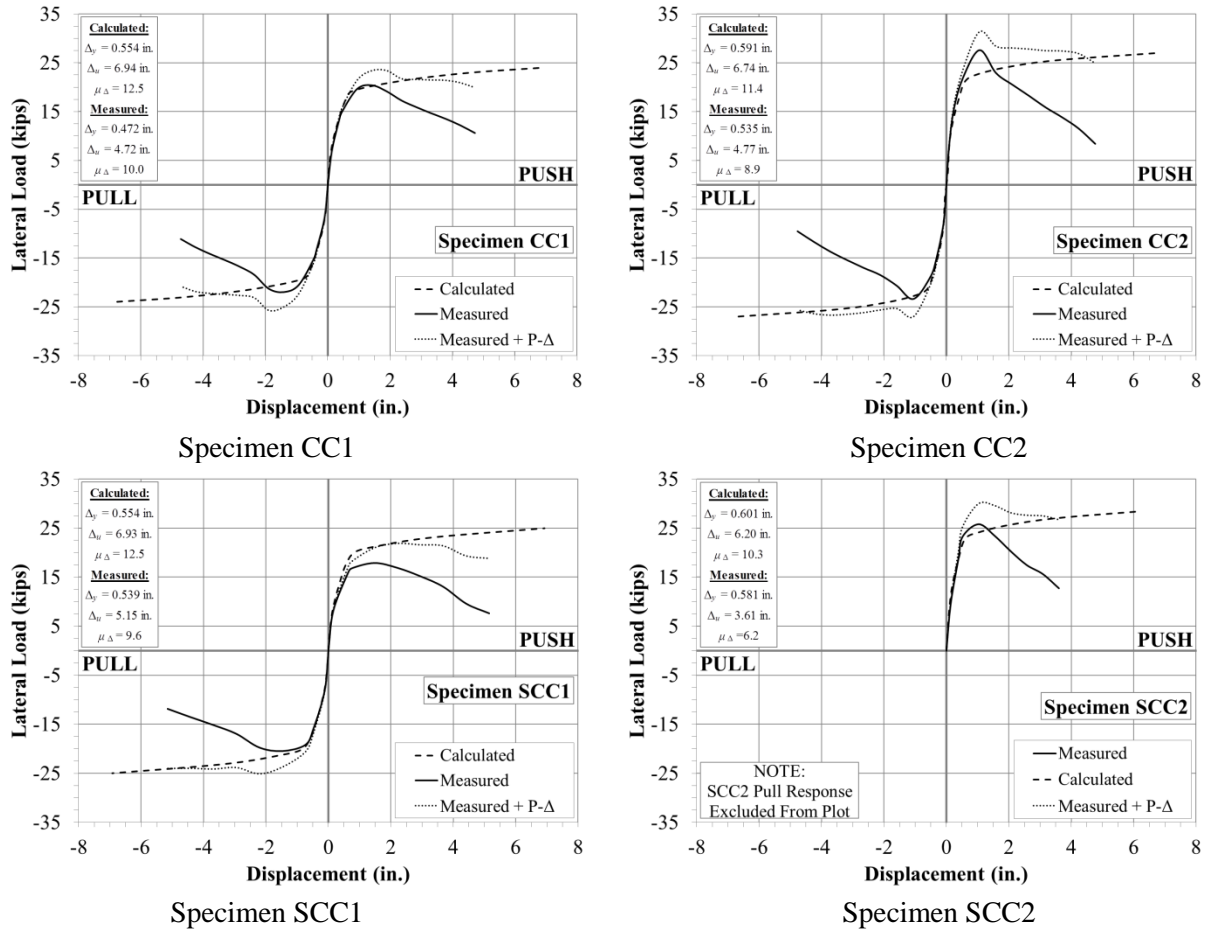


Figure 4.33 Experimental and Analytical Response Envelopes

One explanation for the discrepancy between calculated and measured results is that the analytical study assumes monotonic loading and does not account for low-cycle fatigue of the longitudinal reinforcement. Under cyclic loading, the low-cycle fatigue results in strength degradation and premature rupture of the longitudinal reinforcement. Another source for the difference between calculated and measured deflections is the calculated bond slip deflection. Bond slip deflections may have been overestimated since the calculations do not take into account longitudinal bar buckling and the associated reduction in strength. With the reduction in strength, the actual tensile strains in the outermost tensile bars may have been lower than those obtained by analysis. Therefore, the overestimated strains lead to increased bond slip bar elongation and consequently to greater bond slip rotation.

5. SUMMARY, FINDINGS, AND CONCLUSIONS

5.1 Summary

The study presented in this report was conducted to 1) compare the stress-strain relationship of SCC to CC and 2) compare the seismic performance of reinforced SCC bridge columns to CC bridge columns. This study involved multiple tasks used to assess the structural performance of SCC bridge columns under seismic loads and included a literature review, experimental evaluation of concrete mixtures, experimental testing of reinforced concrete bridge columns under combined axial loading and lateral load reversals, and analytical evaluation of reinforced concrete bridge columns to validate experimental results.

The experimental evaluation of concrete mixtures included developing and batching multiple CC and SCC mixtures with compressive strengths of approximately 6, 6.5, and 7 ksi. Fresh concrete properties were measured and standard 6-in. by 12-in. cylinders were cast, cured, and tested in uniaxial compression. Hardened concrete properties were measured, with particular emphasis placed on the stress-strain relationship of the concrete.

The experimental evaluation of reinforced concrete bridge columns included designing, fabricating, instrumenting, and testing four 12-in. square bridge column specimens at the Lohr Structures Laboratory at South Dakota State University. Specimen size was based upon constraints of the testing laboratory. The steel reinforcement configurations were identical and followed minimum code requirements of ACI and AASHTO. Two of the specimens were constructed with SCC and two were constructed with CC. Within each concrete group, the main variable between the two specimens was the applied axial load. One specimen was subjected to an axial load of approximately $0.075f'_cA_g$ while the other specimen was subjected to an axial load of approximately $0.15f'_cA_g$, where f'_c is the concrete compressive strength and A_g is the gross cross-sectional area of the column. The applied axial load is representative of the gravity load range normally seen in bridge columns. Lateral load reversals were applied to the specimens at successively increasing displacements until failure. The specimens were instrumented with surface mounted strain gages on longitudinal and transverse steel reinforcement at various locations throughout the column to measure strain in the reinforcement. Also, multiple load cells were used to measure applied loads.

The following findings and conclusions are based on the experimental tests carried out in this study.

5.2 Findings

The following findings are based on the experimental tests carried out in this study.

5.2.1 SCC Stress-Strain Relationship

- At compressive strengths of 6, 6.5, and 7 ksi, the strain at strength for the SCC mix was 21%, 29%, and 17%, respectively, higher than that of the CC mix.
- At compressive strengths of 6, 6.5, and 7 ksi, the ultimate strain for SCC mixes was 16%, 17%, and 11%, respectively, higher than that of the CC mix.
- At compressive strengths of 6, 6.5, and 7 ksi, the ductility of the SCC mix was 4%, 10%, and 6%, respectively, lower than that of the CC mix.

- At compressive strengths of 6, 6.5, and 7 ksi, the elastic modulus for the SCC mix was 11%, 15%, and 12%, respectively, lower than that of the CC mix.
- On average, the elastic modulus for the conventional mixes was 3.6% while the elastic modulus for the SCC mixes was 9.1% lower than the value obtained from the ACI empirical equation.

5.2.2 Column Performance

- Due to construction defects, the results of specimen SCC2 were biased and, therefore, should not be used for comparing the performance of CC and SCC columns.
- The measured displacement ductility was 10.0, 8.9, 9.6, and 6.2 for specimens CC1, CC2, SCC1, and SCC2. Comparison of CC1 and SCC1 results indicate that the SCC column attained 11% lower ductility than the CC column.
- The measured column drifts were 7.7%, 7.8%, 8.5%, and 5.9% for specimens CC1, CC2, SCC1, and SCC2. Comparison of CC1 and SCC1 results indicate that the SCC column attained 10% higher drift than the CC column.
- Under lateral load reversals, the energy absorbed by the column was 1365 kip-in., 1424 kip-in., 1045 kip-in., and 792 kip-in. for specimens CC1, CC2, SCC1, and SCC2, respectively. The energy absorbed by specimen SCC1 was 30.5% less than that absorbed by specimen CC1.
- Specimens CC1 and SCC1, which were subjected to the lower axial load, failed due to rupture of outermost tension steel; while specimen SCC2, which was subjected to a higher axial load, failed due to crushing of concrete core.
- No extensive shear cracking was observed in any of the column specimens. Comparison of the strain readings taken from the shear reinforcement showed no significant difference between the SCC and the CC specimens.
- The analytical solution slightly overestimated the measured lateral displacement of the column specimens.

5.3 Conclusions

Based on the results of this study, the following conclusions can be drawn.

- For the same concrete strength, the strain at strength and ultimate strain of SCC are higher than those of CC.
- For the same concrete strength, the ductility of SCC is lower than that of CC.
- For the same concrete strength, the elastic modulus of SCC is lower than that of CC.
- The ACI empirical equation for determining the concrete elastic modulus overestimates the elastic modulus of SCC.
- For the same axial load, the displacement ductility of CC columns is higher than that of SCC columns, while the drift ratio of SCC columns is higher than that of CC columns.
- Under cyclic lateral loading with increasing amplitude, the energy absorbed before failure by CC columns is higher than that of SCC columns.
- The seismic performance of SCC bridge columns is adequate and is comparable to CC columns.
- SCC can be used for constructing bridge columns in high seismic regions.

6. REFERENCES

- American Concrete Institute (ACI) Committee 237 (2007). "Self-Consolidating Concrete," ACI 237R-07, ACI, Farmington Hills, MI.
- American Concrete Institute (ACI) Committee 318 (1963). "ACI Standard Building Code Requirements for Reinforced Concrete," ACI 318-63, ACI, Detroit, MI.
- American Concrete Institute (ACI) Committee 318 (2011). "Building Code Requirements for Structural Concrete and Commentary," ACI 318-11, ACI, Farmington Hills, MI.
- American Association of State Highway and Transportation Officials (AASHTO) (2011). "Guide Specifications for LRFD Seismic Bridge Design," Second Edition, AASHTO, Washington, DC.
- American Association of State Highway and Transportation Officials (AASHTO) (2012). "AASHTO LRFD Bridge Design Specifications," Sixth Edition, AASHTO, Washington, DC.
- ASTM Standard C172 (2010a). "Practice for Sampling Freshly Mixed Concrete," ASTM International, West Conshohocken, PA, 2010, DOI: 10.1520/C0172_C0172M-10, www.astm.org.
- ASTM Standard C1611 (2009a). "Standard Test Method for Slump Flow of Self-Consolidating Concrete," ASTM International, West Conshohocken, PA, 2009, DOI: 10.1520/C1611_C1611M-09B, www.astm.org.
- ASTM Standard C1621 (2009b). "Standard Test Method for Passing Ability of Self-Consolidating Concrete by J-Ring," ASTM International, West Conshohocken, PA, 2009, DOI: 10.1520/C1621_C1621M-09B, www.astm.org.
- ASTM Standard C231 (2010b). "Standard Test Method for Air Content of Freshly Mixed Concrete by the Pressure Method," ASTM International, West Conshohocken, PA, 2010, DOI: 10.1520/C0231_C0231M-10, www.astm.org.
- ASTM Standard C143 (2012a). "Standard Test Method for Slump of Hydraulic-Cement Concrete," ASTM International, West Conshohocken, PA, 2012, DOI: 10.1520/C0143_C0143M-12, www.astm.org.
- ASTM Standard C1758 (2011). "Standard Practice for Fabricating Test Specimens with Self-Consolidating Concrete," ASTM International, West Conshohocken, PA, 2011, DOI: 10.1520/C1758_C1758M-11, www.astm.org.
- ASTM Standard C192 (2012b). "Standard Practice for Making and Curing Concrete Test Specimens in the Laboratory," ASTM International, West Conshohocken, PA, 2012, DOI: 10.1520/C0192_C0192M-12, www.astm.org.
- ASTM Standard C617 (2012c). "Standard Practice for Capping Cylindrical Concrete Specimens," ASTM International, West Conshohocken, PA, 2012, DOI: 10.1520/C0617_C0617M-12, www.astm.org.
- ASTM Standard C39 (2012d). "Standard Test Method for Compressive Strength of Cylindrical Concrete Specimens," ASTM International, West Conshohocken, PA, 2012, DOI: 10.1520/C0039_C0039M-12, www.astm.org.
- Berry, M., Parrish, M., Eberhard, M. (2004). *PEER Structural Performance Database – User’s Manual v. 1.0*, University of California, Berkeley, Pacific Earthquake Engineering Research Center, Berkeley, CA.
- Bonen, D., Shah, S. (2005). "Fresh and Hardened Properties of Self-Consolidating Concrete." *Progress in Structural Engineering and Materials*, 7(1): 14-26.
- Cusson, D., Paultre, P. (1994). "High-Strength Concrete Columns Confined by Rectangular Ties," *ASCE Journal of Structural Engineering* 120(3): 783-804.

- Desnerck, P., De Schutter, G., Taerwe, L. (2012). "Stress-Strain Behaviour of Self-Compacting Concretes Containing Limestone Fillers." *Structural Concrete*, 13(2): 95-101.
- Galano, L., Vignoli, A. (2008). "Strength and Ductility of HSC and SCC Slender Columns Subjected to Short-Term Eccentric Load." *ACI Structural Journal*, 105(3), 259-269.
- Goodier, C. I. (2003). "Development of Self-Compacting Concrete." *Proceedings of the Institution of Civil Engineers: Structures and Buildings*, 156(4), 405-414.
- Gutzmer, Z. D. (2008). "High Performance Concrete in Bridge Applications." MS Thesis, South Dakota State University, Brookings, SD, 313 pp.
- Khairallah, F. (2013). "Mechanical Behavior of Confined Self-Compacting Reinforced Concrete Circular Columns Under Concentric Axial Loading." *Ain Shams Engineering Journal*, 4(4), 641-649.
- Khayat, K., Paultre, P., Tremblay, S. (2001). "Structural Performance and In-Place Properties of Self-Consolidating Concrete Used for Casting Highly Reinforced Columns." *ACI Materials Journal*, 98(5), 371-378.
- Kumar, R., Singh, B., Bhargava, P. (2011). "Flexural Capacity Predictions of Self-Compacting Concrete Beams Using Stress-Strain Relationship in Axial Compression." *Magazine of Concrete Research* 63(1): 49-59.
- Lin, C., Hwang, C., Lin, S., Liu, C. (2008). "Self-Consolidating Concrete Columns Under Concentric Compression." *ACI Structural Journal*, 105(4), 425-432.
- Mander, J. B., Priestley, M.J.N., Park, R. (1988). "Theoretical Stress-Strain Model for Confined Concrete." *Journal of Structural Engineering*, 114: 1804-1826.
- Mortsell, E., Rodum, E. (2001). "Mechanical and Durability Aspects of SCC for Road Structures," *Proceedings of the Second International Symposium on SCC*, pp. 459 – 468.
- Okamura, H., and Ouchi, M. (1998). "Self-Compacting High Performance Concrete." *Progress in Structural Engineering and Materials*, 1(4), 378-383.
- Park, R., Paulay, T. (1975). *Reinforced Concrete Structures*, John Wiley and Sons, Inc., New York, NY.
- Paulay, T., Priestley, M.J.N. (1992). *Seismic Design of Reinforced Concrete and Masonry Buildings*, John Wiley and Sons, Inc., New York, NY.
- Paultre, P., Khayat, K., Cusson, D., Tremblay, S. (2005). "Structural Performance of Self-Consolidating Concrete Used in Confined Concrete Columns." *ACI Structural Journal*, 102(4), 560-568.
- Paultre, P., Khayat, K.H., Langlois, Y., Trudel, A., Cusson, D. (1996). "Structural Performance of Some Special Concretes," *4th Int. Symposium on Utilization of High-Strength/High-Performance Concrete*, Paris, France. pp. 787-796.
- Precast/Prestressed Concrete Institute (PCI) (2003). "Interim Guidelines for the Use of Self-Consolidating Concrete in Precast/Prestressed Concrete Institute Member Plants," PCI Interim SCC Guidelines TR-6-03, PCI, Chicago, IL.
- Priestley, M.J.N., Seible, F., Calvi, G.M. (1996). *Seismic Design and Retrofit of Bridges*, John Wiley and Sons, Inc., New York, NY.
- Restrepo, J., Seible, F., Stephan, B., Shoettler, M. (2006). "Seismic Testing of Bridge Columns Incorporating High-Performance Materials." *ACI Structural Journal*, 103(4), 496-504.
- Rilem Technical Committee 148-SCC (2000). "Test Method for Measurement of the Strain-Softening Behaviour of Concrete under Uniaxial Compression." *Materials and Structures* 33(6) 347-51.



Said, A., Nehdi, M. (2007). "Behaviour of Reinforced Self-Consolidating Concrete Frames." *Proceedings of the Institution of Civil Engineers: Structures and Buildings 160*, Issue SB2, 95-104.

Wehbe, N., Saiidi, M. (2003). *User's Manual for RCMC v. 2.0: A Computer Program for Moment-Curvature Analysis of Confined and Unconfined Reinforced Concrete Sections*, University of Nevada, Reno, Center for Civil Engineering Earthquake Research, Reno, NV.

Wehbe, N., Saiidi, M., Sanders, D. (1997). *Effects of Confinement and Flares on the Seismic Performance of Reinforced Concrete Bridge Columns*, University of Nevada, Reno, Center for Civil Engineering Earthquake Research, Reno, NV.

APPENDIX A. CONCRETE CONSTITUENT TEST DATA

A-1. GCC Type III Cement Data Sheet

	GCC of America 130 Rampart Way, Ste. 205 Denver, CO 80230 Sales (303) 739-5900 Customer Service (800) CALL GCC																																																																																																																																		
Plant: Rapid City 501 N. Saint Onge Street Rapid City, SD 57702 Contact: Victor Gonzalez Phone: (605) 721-7042	Cement Type: Type III, Low Alkali, Type GU, Type HE Report Date: 9/26/2012 Production Period: 8/23/2012 to 9/11/2012 Average of the last 5 silos produced																																																																																																																																		
STANDARD REQUIREMENTS ASTM C 150 -12/AASHTO M 85-09/ASTM C1157-11-GU/HE																																																																																																																																			
CHEMICAL	PHYSICAL																																																																																																																																		
<table border="1" style="width: 100%; border-collapse: collapse;"> <thead> <tr> <th style="width: 40%;">Item</th> <th style="width: 20%;">Spec. Limit</th> <th style="width: 40%;">Test Result</th> </tr> </thead> <tbody> <tr><td>SiO₂ (%)</td><td>A</td><td>20.9</td></tr> <tr><td>Al₂O₃ (%)</td><td>A</td><td>4.6</td></tr> <tr><td>Fe₂O₃ (%)</td><td>A</td><td>3.4</td></tr> <tr><td>CaO (%)</td><td>A</td><td>64.4</td></tr> <tr><td>MgO (%)</td><td>6.0 max.</td><td>1.2</td></tr> <tr><td>SO₃ (%)</td><td>3.5 max.</td><td>3.1</td></tr> <tr><td>Ignition Loss (%)</td><td>3.0 max.</td><td>1.1</td></tr> <tr><td>Na₂O (%)</td><td>A</td><td>0.13</td></tr> <tr><td>K₂O (%)</td><td>A</td><td>0.59</td></tr> <tr><td>Equivalent Alkalies (%)</td><td>B</td><td>0.52</td></tr> <tr><td>Insoluble Residue (%)</td><td>0.75 max.</td><td>0.37</td></tr> <tr><td>Potential Compounds (%)</td><td></td><td></td></tr> <tr><td>C₂S</td><td>A</td><td>59</td></tr> <tr><td>C₃S</td><td>A</td><td>16</td></tr> <tr><td>C₃A</td><td>15 max</td><td>6</td></tr> <tr><td>C₄AF</td><td>A</td><td>10</td></tr> </tbody> </table>	Item	Spec. Limit	Test Result	SiO ₂ (%)	A	20.9	Al ₂ O ₃ (%)	A	4.6	Fe ₂ O ₃ (%)	A	3.4	CaO (%)	A	64.4	MgO (%)	6.0 max.	1.2	SO ₃ (%)	3.5 max.	3.1	Ignition Loss (%)	3.0 max.	1.1	Na ₂ O (%)	A	0.13	K ₂ O (%)	A	0.59	Equivalent Alkalies (%)	B	0.52	Insoluble Residue (%)	0.75 max.	0.37	Potential Compounds (%)			C ₂ S	A	59	C ₃ S	A	16	C ₃ A	15 max	6	C ₄ AF	A	10	<table border="1" style="width: 100%; border-collapse: collapse;"> <thead> <tr> <th style="width: 30%;">Item</th> <th style="width: 15%;">ASTM C1157 Spec. Limit Type GU</th> <th style="width: 15%;">ASTM C1157 Spec. Limit Type HE</th> <th style="width: 15%;">ASTM C 150 Limit Type III</th> <th style="width: 25%;">Test Result</th> </tr> </thead> <tbody> <tr><td>Air content (volume %)</td><td>B</td><td>B</td><td>12 max</td><td>7</td></tr> <tr><td>Blaine fineness (m²/kg)</td><td>B</td><td>B</td><td>A</td><td>576</td></tr> <tr><td>Fineness by 325 sieve %</td><td>B</td><td>B</td><td>A</td><td>98</td></tr> <tr><td>Autoclave expansion (%)</td><td>0.80 max.</td><td>0.80 max.</td><td>0.80 max.</td><td>-0.06</td></tr> <tr><td>False set (%)</td><td>A</td><td>A</td><td>50 min.</td><td>75</td></tr> <tr><td>Compressive strength</td><td></td><td></td><td></td><td></td></tr> <tr><td>1 day, Min, MPa (psi)</td><td>A</td><td>12 (1740)</td><td>12 (1740)</td><td>29.2 (4233)</td></tr> <tr><td>3 day, Min, MPa (psi)</td><td>13 (1890)</td><td>24 (3480)</td><td>24 (3480)</td><td>39.8 (5771)</td></tr> <tr><td>7 day, Min, MPa (psi)</td><td>20 (2900)</td><td>A</td><td>A</td><td>47.5 (6885)</td></tr> <tr><td>28 day, Min, MPa (psi)</td><td>28 (4060)</td><td>A</td><td>A</td><td>51.6 (7487)</td></tr> <tr><td>Time of setting, Vicat</td><td></td><td></td><td></td><td></td></tr> <tr><td>Initial: Not less than</td><td>45</td><td>45</td><td>45</td><td rowspan="2">116</td></tr> <tr><td>Not more than</td><td>420</td><td>420</td><td>375</td></tr> <tr><td>Expansion ASTM C 1038</td><td></td><td></td><td></td><td style="text-align: center;">2012 Average</td></tr> <tr><td>14-Day, % Max.</td><td>0.020</td><td>0.020</td><td>A</td><td>0.003</td></tr> </tbody> </table>	Item	ASTM C1157 Spec. Limit Type GU	ASTM C1157 Spec. Limit Type HE	ASTM C 150 Limit Type III	Test Result	Air content (volume %)	B	B	12 max	7	Blaine fineness (m ² /kg)	B	B	A	576	Fineness by 325 sieve %	B	B	A	98	Autoclave expansion (%)	0.80 max.	0.80 max.	0.80 max.	-0.06	False set (%)	A	A	50 min.	75	Compressive strength					1 day, Min, MPa (psi)	A	12 (1740)	12 (1740)	29.2 (4233)	3 day, Min, MPa (psi)	13 (1890)	24 (3480)	24 (3480)	39.8 (5771)	7 day, Min, MPa (psi)	20 (2900)	A	A	47.5 (6885)	28 day, Min, MPa (psi)	28 (4060)	A	A	51.6 (7487)	Time of setting, Vicat					Initial: Not less than	45	45	45	116	Not more than	420	420	375	Expansion ASTM C 1038				2012 Average	14-Day, % Max.	0.020	0.020	A	0.003
Item	Spec. Limit	Test Result																																																																																																																																	
SiO ₂ (%)	A	20.9																																																																																																																																	
Al ₂ O ₃ (%)	A	4.6																																																																																																																																	
Fe ₂ O ₃ (%)	A	3.4																																																																																																																																	
CaO (%)	A	64.4																																																																																																																																	
MgO (%)	6.0 max.	1.2																																																																																																																																	
SO ₃ (%)	3.5 max.	3.1																																																																																																																																	
Ignition Loss (%)	3.0 max.	1.1																																																																																																																																	
Na ₂ O (%)	A	0.13																																																																																																																																	
K ₂ O (%)	A	0.59																																																																																																																																	
Equivalent Alkalies (%)	B	0.52																																																																																																																																	
Insoluble Residue (%)	0.75 max.	0.37																																																																																																																																	
Potential Compounds (%)																																																																																																																																			
C ₂ S	A	59																																																																																																																																	
C ₃ S	A	16																																																																																																																																	
C ₃ A	15 max	6																																																																																																																																	
C ₄ AF	A	10																																																																																																																																	
Item	ASTM C1157 Spec. Limit Type GU	ASTM C1157 Spec. Limit Type HE	ASTM C 150 Limit Type III	Test Result																																																																																																																															
Air content (volume %)	B	B	12 max	7																																																																																																																															
Blaine fineness (m ² /kg)	B	B	A	576																																																																																																																															
Fineness by 325 sieve %	B	B	A	98																																																																																																																															
Autoclave expansion (%)	0.80 max.	0.80 max.	0.80 max.	-0.06																																																																																																																															
False set (%)	A	A	50 min.	75																																																																																																																															
Compressive strength																																																																																																																																			
1 day, Min, MPa (psi)	A	12 (1740)	12 (1740)	29.2 (4233)																																																																																																																															
3 day, Min, MPa (psi)	13 (1890)	24 (3480)	24 (3480)	39.8 (5771)																																																																																																																															
7 day, Min, MPa (psi)	20 (2900)	A	A	47.5 (6885)																																																																																																																															
28 day, Min, MPa (psi)	28 (4060)	A	A	51.6 (7487)																																																																																																																															
Time of setting, Vicat																																																																																																																																			
Initial: Not less than	45	45	45	116																																																																																																																															
Not more than	420	420	375																																																																																																																																
Expansion ASTM C 1038				2012 Average																																																																																																																															
14-Day, % Max.	0.020	0.020	A	0.003																																																																																																																															
<p>A Not applicable .</p> <p>B Limit not specified by purchaser. Test result provided for information only.</p>																																																																																																																																			
GCC OF AMERICA PORTLAND CEMENT IS WARRANTED TO CONFORM AT THE TIME OF SHIPMENT WITH ASTM C-150/AASHTO 85/ASTM C 1157-GU/C 1157-HE. NO OTHER WARRANTY IS MADE OR IMPLIED. HAVING NO CONTROL OVER THE USE OF ITS CEMENTS, GCC OF AMERICA DOES NOT GUARANTEE FINISHED WORK. GCC IS NOT RESPONSIBLE FOR ANY ADDITIVES NOT STATED IN THE CERTIFICATE OF COMPLIANCE.																																																																																																																																			
We certify that the above described cement, at the time of shipment, meets the chemical and physical requirements of ASTM C 150-12, ASTM C1157-11 Type GU, ASTM C 1157-11 Type HE and AASHTO M 85-09																																																																																																																																			
Signature: 	Title: Quality Control Manager or Chemist																																																																																																																																		

A-2. Coal Creek Class F Fly Ash Data Sheet




Adding Value to Energy™

ASTM C618 / AASHTO M 295 Testing of Coal Creek Fly Ash

Sample Type:	3200-ton	Report Date:	4/25/2011
Sample Date:	3/4 - 3/10/11	MTRF ID	486CC
Sample ID:			

Chemical Analysis		ASTM / AASHTO Limits		ASTM Test Method
		Class F	Class C	
Silicon Dioxide (SiO ₂)	<u>49.79</u> %			
Aluminum Oxide (Al ₂ O ₃)	<u>15.30</u> %			
Iron Oxide (Fe ₂ O ₃)	<u>6.38</u> %			
Sum of Constituents	<u>71.47</u> %	70.0% min	50.0% min	D4326
Sulfur Trioxide (SO ₃)	<u>0.69</u> %	5.0% max	5.0% max	D4326
Calcium Oxide (CaO)	<u>14.82</u> %			D4326
Moisture	<u>0.03</u> %	3.0% max	3.0% max	C311
Loss on Ignition (AASHTO M 295 req.)	<u>0.04</u> %	6.0% max 5.0% max	6.0% max 5.0% max	C311
Available Alkalies, as Na ₂ O (AASHTO M 295 req.)	<u>1.53</u> %	1.5% max	1.5% max	C311
Physical Analysis				
Fineness, % retained on #325	<u>21.85</u> %	34% max	34% max	C311, C430
Strength Activity Index - 7 or 28 day requirement				C311, C109
7 day, % of control	<u>94</u> %	75% min	75% min	
28 day, % of control	<u>82</u> %	75% min	75% min	
Water Requirement, % control	<u>92</u> %	105% max	105% max	
Autoclave Soundness	<u>-0.01</u> %	0.8% max	0.8% max	C311, C151
True Particle Density	<u>2.50</u>			

Headwaters Resources certifies that pursuant to current ASTM C618 protocol for testing, the test data listed herein was generated by applicable ASTM methods and meets the requirements of ASTM C618 for Class F fly ash.


Bobby Bergman
MTRF Manager



Materials Testing & Research Facility
2650 Old State Highway 113
Taylorsville, Georgia 30178
P: 770.684.0102
F: 770.684.5114
www.headwaters.com

A-3. Aggregate Testing Data

A-3.1 Aggregate Gradations



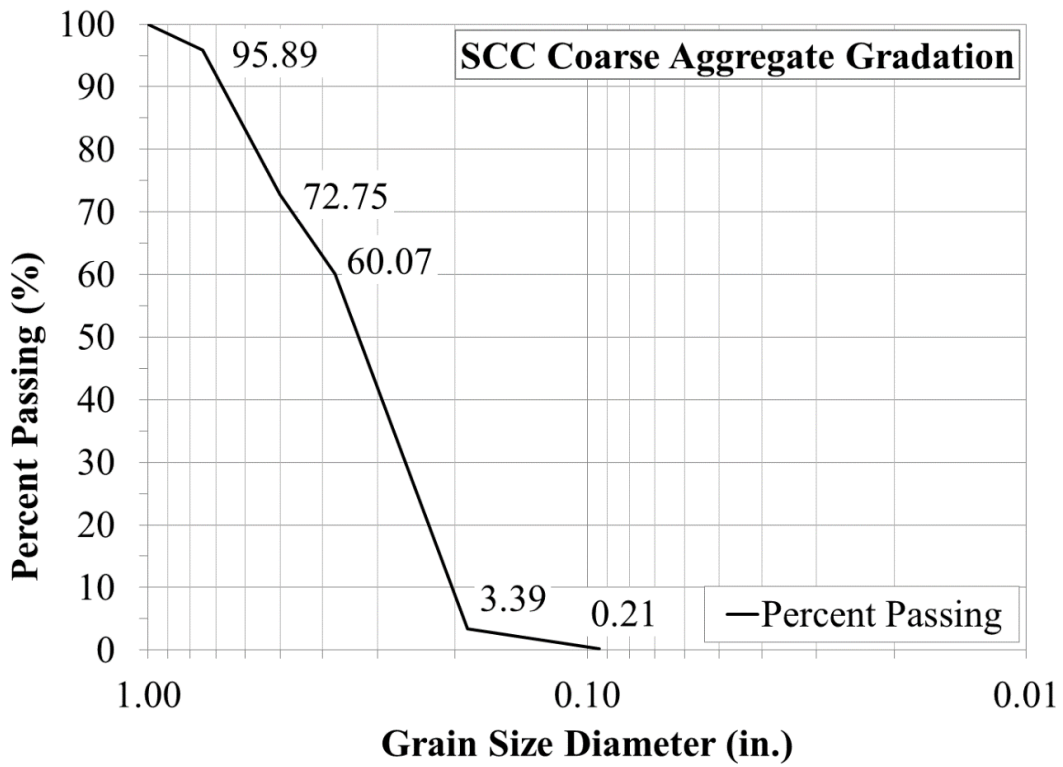
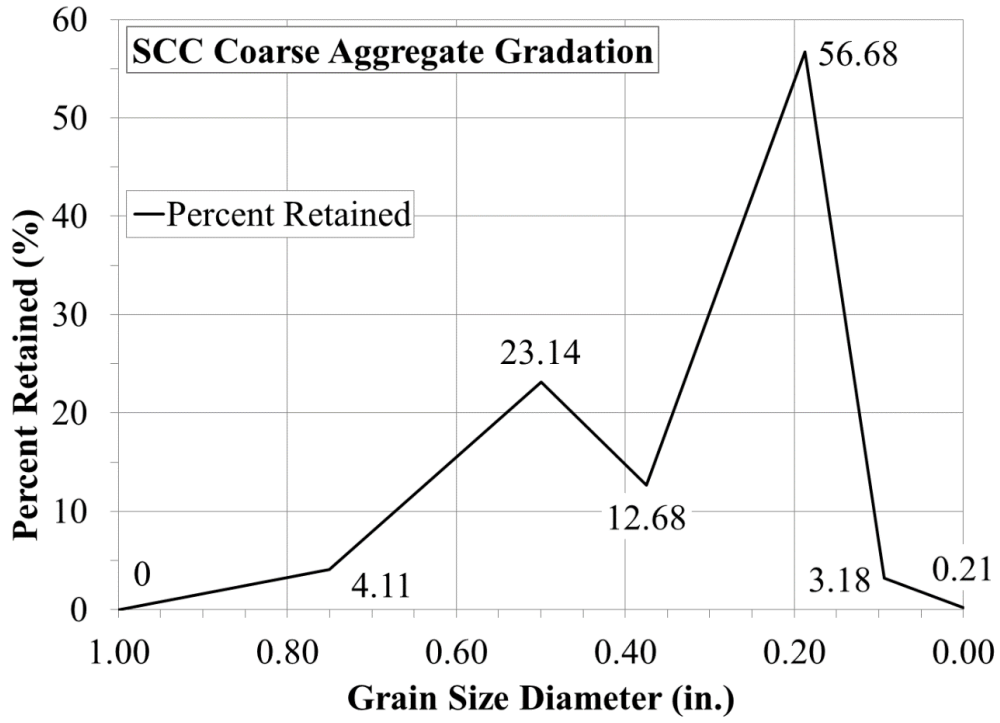
Source:	Project:				Date:
see below	Research Project at SDSU				10/2/12
	036 1" x #4 Quartzite Dells West	057 3/8" x #8 Quartzite Dells West	043 3/4" x #4 Quartzite Dells East	054 1/2" x #4 Quartzite Dells East	077 ASTM Conc Sand Brookings
Sieve	% Passing	% Passing	% Passing	% Passing	% Passing
4"					
2 1/2 "					
2"					
1 1/2"	100.0				
1"	100.0				
3/4"	77.0		100.0	100.0	
1/2"	30.0		57.0	99.0	
3/8"	12.0	96.0	24.0	80.0	100.0
1/4"		53.0			
# 4	1.1	25.0	1.8	8.3	99.0
#8	0.7	1.1	0.6	0.7	84.0
# 16	0.6	0.5	0.5	0.3	64.0
# 30	0.5	0.4	0.4	0.2	38.0
# 40		0.4			24.0
# 50	0.4	0.4			12.0
# 100		0.3			2.7
# 200	0.1	0.2	0.1	0.1	0.6

Remarks:
The above gradations are base on 2012 production averages.
The actual gradations may vary from what is listed above.

ASTM C136 - 06 Standard Test Method for Sieve Analysis of Fine and Coarse Aggregates

Sieve Analysis Performed on SCC Coarse Aggregate (3/4", 1/2") Tested Together in Correct Concrete Mixture Proportions

Sieve ID	Sieve Opening (in)	Sieve Weight (lbs)	Total Sieve + Aggregate Weight (lbs.)	Total Aggregate Weight (lbs.)	Percent Retained (%)	Percent Passing (%)
1"	1.00			0.000	0	100
3/4"	0.75	1.240	1.99	0.575	4.11	95.89
1/2"	0.50	1.085	1.59	3.240	23.14	72.75
3/8"	0.375	1.250	1.63	1.775	12.68	60.07
#4	0.187	1.135	1.32	7.935	56.68	3.39
#8	0.094	0.870	0.96	0.445	3.18	0.21
Pan		0.625	0.63	0.030	0.21	
Total Weight (lbs.)				14.0		



A-3.2 Fine Aggregate Data Sheet

AGGREGATE QUALITY REPORT

Report Number: M1121019.0006

Service Date: 11/30/11

Report Date: 02/10/12

Task: Brookings Pit



4102 7th Ave. N.
 Fargo, ND 58108-3042
 701-282-9633

Client

L.G. Everist, Inc.
 Attn: Jeff Darner
 P.O. Box 5829
 Sioux Falls, SD 57117-5829

Project

Plant Tests 2012 - L.G. Everist, Inc.
 300 S. Philips Ave., Suite 200
 Sioux Falls, SD

Project Number: M1121019

Sample Source:

L.G. Everist, Inc., Brookings, South Dakota, Brookings County,
 Township 110 North, Range 49 West, Section 31, South 1/2

Sample Description:

3/8" Minus Washed Sand

Date Submitted:

November 30, 2011

Test Results:

ASTM C 33
SPECIFICATIONS

Clay Lumps & Friable Particles (AASHTO T 112) #4-#16	0.1%	
Lightweight Particles (AASHTO T 113) Using 2.0 Sp. Gr. Zinc Chloride Solution	0.5%	
Using 1.95 Sp. Gr. Zinc Chloride Solution	0.4%	
Coal and Lignite (ASTM C 33)	0.0%	
Materials Finer than 75-µm (No. 200 Sieve) (ASTM C 117)	0.4%	3.0 Max.
Magnesium Sulfate Soundness (ASTM C 88)		
3/8"-#4 (1) ^a	13.5%	
#4-#8 (16) ^a	13.5%	
#8-#16 (20) ^a	9.6%	
#16-#30 (26) ^a	7.3%	
#30-#50 (27) ^a	4.9%	
Composite Blend ^a	7.4%	15.0 Max.
Bulk Density ("Unit Weight") and Voids in Aggregate (ASTM C 29)		
Loose Oven-Dry Bulk Density	104.4 lbs./ft. ³	
Loose Oven-Dry Void Content	35.9%	
Rodded Oven-Dry Bulk Density	110.5 lbs./ft. ³	
Rodded Oven-Dry Void Content	32.2%	
Relative Density, (Specific Gravity) & Absorption of Fine Aggregate (ASTM C 128)		
Bulk Oven-Dry Relative Density	2.611	
Saturated-Surface Dry Relative Density	2.645	
Apparent Relative Density	2.703	
Absorption	1.30%	
Uncompacted Void Content (Fine Aggregate Angularity)(ASTM C 1252)		
Test Method A - Standard Gradation	40.2%	

The tests were performed in general accordance with applicable ASTM, AASHTO, or DOT test methods. This report is exclusively for the use of the client indicated above and shall not be reproduced except in full without the written consent of our company. Test results transmitted herein are only applicable to the actual samples tested at the location(s) referenced and are not necessarily indicative of the properties of other apparently similar or identical materials.

AF0001, 9-28-10, Rev.1

Page 1 of 2

A-3.3 Coarse Aggregate Data Sheet

COARSE AGGREGATE QUALITY REPORT



Report Number: M1111001.0010
Service Date: 10/07/11
Report Date: 12/22/11 Revision 1 - Added Freeze-Thaw Results
Task: KCMMB West Quarry

4102 7th Ave. N.
 Fargo, ND 58108-3042
 701-282-9633

Client	Project
L.G. Everist, Inc. Attn: Jeff Damer P.O. Box 5829 Sioux Falls, SD 57117-5829	Plant Tests 2011-L.G. Everist, Inc. (Rural Route) 300 S. Philips Ave., Suite 200 Sioux Falls, SD
Project Number: M1111001	

TESTS OF COARSE AGGREGATE

SAMPLE SOURCE:	East Quarry, Dell Rapids, South Dakota, Mimihaha County Southwest ¼, Section 10, Township 104 North, Range 49 West.	
SAMPLE DESCRIPTION:	Size No. 67, 3/4" #4 Quarry Aggregate, Tracking #7148	
DATE SUBMITTED:	October 7, 2011	
TEST RESULTS:	2011 KCMMB CONCRETE MATERIAL SPECIFICATION KDOT Special Provision 07-04001	
Soundness of Aggregates by Freezing & Thawing (AASHTO T 103-C)		
Procedure A – Total Immersion, 50 cycles, 0.5% Methyl Alcohol and Water Solution		
¾" - #3/8"	0.0	1.0% Max.
3/8" - #4	0.2	2.0% Max.
Relative Density, (Specific Gravity) & Absorption of Coarse Aggregate (ASTM C 127)		
Bulk Oven-Dry Relative Density	2.631	
Saturated Surface-Dry Relative Density	2.638	
Apparent Relative Density	2.650	
Absorption	0.27%	0.5% Max.
Lightweight Particles (ASTM C 123)		
Using 2.0 Sp. Gr. Zinc Chloride Solution	0.0%	0.5% Max.
Clay Lumps & Friable Particles (ASTM C 142)		
¾" - 3/8"	0.0%	0.3% Max.
3/8" - #4"	0.0%	0.3% Max.
Coal and Lignite (ASTM C 33)	0.0%	0.05% Max.
Materials Finer than 75-µm (No. 200 Sieve) (ASTM C 117)	0.2%	0.5% Max.
Sum of all Deleterious	0.0%	1.0% Max.
Magnesium Sulfate Soundness (ASTM C88)		
¾" - 3/8"	0.29%	0.5% Max.
3/8" - #4	0.50%	4.0% Max.
Los Angeles Abrasion Loss of Small-Size Coarse Aggregate (ASTM C 131)		
Grading B (3/4" - 3/8")	18.7%	28% Max.

The tests were performed in general accordance with applicable ASTM, AASHTO, or DOT test methods. This report is exclusively for the use of the client indicated above and shall not be reproduced except in full without the written consent of our company. Test results transmitted herein are only applicable to the actual samples tested at the location(s) referenced and are not necessarily indicative of the properties of other apparently similar or identical materials.

COARSE AGGREGATE QUALITY REPORT



Report Number: M1111001.0010

Service Date: 10/07/11

Report Date: 12/22/11 Revision 1 - Added Freeze-Thaw Results

Task: KCMMB West Quarry

4102 7th Ave. N.

Fargo, ND 58108-3042

701-282-9633

Client

L.G. Everist, Inc.
Attn: Jeff Damer
P.O. Box 5829
Sioux Falls, SD 57117-5829

Project

Plant Tests 2011-L.G. Everist, Inc. (Rural Route)
300 S. Philips Ave., Suite 200
Sioux Falls, SD

Project Number: M1111001

TESTS OF COARSE AGGREGATE

Flat or Elongated Particles (ASTM D 4791)

3:1 Ratio 0.2%

Bulk Density ("Unit Weight") and Voids in Aggregate (ASTM C 29)

Loose Oven-Dry Bulk Density 87.2 lbs./ft.³

Loose Oven-Dry Void Content 46.9%

Rodded Oven-Dry Bulk Density 97.4 lbs./ft.³

Rodded Oven-Dry Void Content 40.7%

Services:

Midwest Testing Laboratory, Inc. Rep.:

Reported To:

Contractor:

Report Distribution:

(1) L.G. Everist, Inc., Emailed

Reviewed By:

Gregory A. Johnson

The tests were performed in general accordance with applicable ASTM, AASHTO, or DOT test methods. This report is exclusively for the use of the client indicated above and shall not be reproduced except in full without the written consent of our company. Test results transmitted herein are only applicable to the actual samples tested at the location(s) referenced and are not necessarily indicative of the properties of other apparently similar or identical materials.

A-4 Steel Reinforcement Mill Certificates

Stock Usage Report

For dates: 09-14-12 - 09-13-13, Full Lengths & Rems, Used only, Sorted by Job
(Wt/Cost of rems are deducted)

Page # 1

Property of Egger Steel Company

<<< Filter Set >>>

09-13-13 09:14:48

Quan Notes	Type & Size	Area	Grade Heat Cert	Length	Weigh Date	PO Number Recvd/Delivery Note	Sequence Used On Job	Date Used	Supplier Unit Cost	Cost Category
---------------	-------------	------	--------------------	--------	---------------	----------------------------------	-------------------------	-----------	-----------------------	------------------

Filters:
Material Category: Received
Material Category: On Order
Types: Rebar
Reserved for JobStkjoblist: 13014D

Job# 13014D

18	RE 3		A615-GR60 JW12102979	40' 0"	270# 04-23-12	PO-10027 602692		06-06-13		13014D
1	RE 3		A615-GR60 JW12102979	24' 0"	9# 01-15-13	2012IA-02012 602692		05-22-13		13014D
1	RE 3		A615-GR60 JW12102979	8' 0"	3# 03-18-13	PO-10027 602692		05-22-13		13014D
3	RE 3		A615-GR60 JW12102979	4' 0"	4# 10-12-12	2012IA-02012 602692		05-22-13		13014D
2	RE 4		A615-GR60 62130426	60' 0"	80# 03-05-13	PO-10909 332456		05-22-13		13014D
1	RE 4		A615-GR60 62130426	16' 0"	10# 05-22-13	PO-10909 332456		05-22-13		13014D
1	RE 4		A615-GR60 L80589	7' 0"	4# 01-15-13	PO-10714 7257		05-22-13		13014D
2 Rm	RE 4		A615-GR60 62130426	20' 0"	26# 05-22-13	PO-10909 332456		07-18-13		13014D
6	RE 5		A615-GR60 KN12101572	60' 0"	375# 06-12-12	PO-10145 246180		05-22-13		13014D

This report was generated by FabTral MRP software. For product information, call (541) 485-4719 or visit www.fabtral.com

Stock Usage Report

For dates: 09-14-12 - 09-13-13, Full Lengths & Rems, Used only, Sorted by Job
(Wt/Cost of rems are deducted)

Page # 2

Property of Egger Steel Company

<<< Filter Set >>>

09-13-13 09:14:48

Quan Notes	Type & Size	Area	Grade Heat Cert	Length	Weigh Date	PO Number Recvd/Delivery Note	Sequence Used On Job	Date Used	Supplier Unit Cost	Cost Category
---------------	-------------	------	--------------------	--------	---------------	----------------------------------	-------------------------	-----------	-----------------------	------------------

1 Rm	RE 5		A615-GR60 KN12101572	53' 0"	55# 05-22-13	PO-10145 246180		06-06-13		13014D
13	RE 6		A615-GR60 KN1110482201	60' 0"	1,171# 06-07-12	PO-10164 002107		05-22-13		13014D
7	RE 6		A615-GR60 KN1110482301	5' 0"	52# 03-15-13	PO-10163 002106		05-22-13		13014D
1 Rm	RE 6		A615-GR60 KN1110482201	50' 0"	75# 05-22-13	PO-10164 002107				13014D
1 Rm	RE 6		A615-GR60 KN1110482201	3' 0"	4# 05-22-13	PO-10164 002107				13014D

53		1,936.00 LF	1,820#
----	--	-------------	--------

Total		1,936.00 LF	1,820#
53			

SOLD ADELPHIA METALS I LLC
411 MAIN ST E
TO: NEW PRAGUE, MN 56071-

NUCOR
NUCOR CORPORATION
NUCOR STEEL TEXAS

CERTIFIED MILL TEST REPORT

Page: 1

SHIP ADELPHIA METALS-CUST PU
N/A
TO: JEWETT, TX 75846-

Ship from:
Nucor Steel - Texas
8812 Hwy 79 W
JEWETT, TX 75846
800-527-6445

Date: 18-Apr-2012
B.L. Number: 602692
Load Number: 211478

Material Safety Data Sheets are available at www.nucorbar.com or by contacting your inside sales representative.

NMAG-08 January 1, 2012

LOT # HEAT #	DESCRIPTION	PHYSICAL TESTS					CHEMICAL TESTS												
		YIELD P.S.I.	TENSILE P.S.I.	ELONG % IN 8"	BEND	WT% DEF	C	Ni	Mn	Cr	P	Mo	S	V	Si	Cb	Cu	Sn	C.E.
PO# => 803585																			
JW1210297901	Nucor Steel - Texas	71,600	107,300	14.0%			.40	.91	.012	.052	.12	.28	.58						
JW12102979	10#3 Rebar 40' A615M GR 420 (Gr60) ASTM A615/A615M-09b GR 60[420] AASHTO M31-07	494MPa	740MPa				.14	.15	.045	.003	.001								
PO# => 803585																			
JW1210298001	Nucor Steel - Texas	78,200	108,600	14.0%			.38	.93	.010	.046	.12	.28	.56						
JW12102980	10#3 Rebar 40' A615M GR 420 (Gr60) ASTM A615/A615M-09b GR 60[420] AASHTO M31-07	539MPa	749MPa				.13	.12	.038	.004	.002								

I hereby certify that the material described herein has been manufactured in accordance with the specifications and standards listed above and that it satisfies those requirements.
1.) Yield tests were not performed on this material.
2.) Melted and Manufactured in the United States.
3.) Mercury, Radium, or Alpha source materials in any form have not been used in the production of this material.

QUALITY ASSURANCE: Nathan Stewart

SOLD ADELPHIA METALS I LLC
411 MAIN ST E
TO: NEW PRAGUE, MN 56071-

NUCOR
NUCOR STEEL KANKAKEE, INC.

CERTIFIED MILL TEST REPORT

Page: 1

SHIP ADELPHIA METALS - RAIL
TO: C/O CENTRAL MISSOURI RELOAD
6680 ST JOHN
TRACK 701 & 714
KANSAS CITY, MO 64120-

Ship from:
Nucor Steel Kankakee, Inc.
One Nucor Way
Bourbonnais, IL 60914
815-937-3131

Date: 24-May-2012
B.L. Number: 442852
Load Number: 223836

Material Safety Data Sheets are available at www.nucorbar.com or by contacting your inside sales representative.

NMAG-08 January 1, 2012

LOT # HEAT #	DESCRIPTION	PHYSICAL TESTS					CHEMICAL TESTS												
		YIELD P.S.I.	TENSILE P.S.I.	ELONG % IN 8"	BEND	WT% DEF	C	Ni	Mn	Cr	P	Mo	S	V	Si	Cb	Cu	Sn	C.E.
PO# => 804154																			
KN1210152401	Nucor Steel - Kankakee Inc	69,647	101,836	14.9%	OK	-4.1%	.36	1.00	.012	.049	.22	.34	.56						
KN12101524	16#5 Rebar 60' A615M GR 420 (Gr60) ASTM A615/A615M-12 GR 60[420] AASHTO M31-07 Melted 03/27/12 Rolled 03/29/12	480MPa	702MPa				.033	.24	.13	.070	.007	.002							
PO# => 804154																			
KN1210152501	Nucor Steel - Kankakee Inc	67,580	97,873	13.8%	OK	-2.9%	.34	1.02	.012	.046	.22	.31	.54						
KN12101525	16#5 Rebar 60' A615M GR 420 (Gr60) ASTM A615/A615M-12 GR 60[420] AASHTO M31-07 Melted 03/28/12 Rolled 03/29/12	466MPa	675MPa				.033	.27	.13	.079	.013	.002							
PO# => 804154																			
KN1210157201	Nucor Steel - Kankakee Inc	66,300	98,538	14.1%	OK	-2.7%	.36	1.04	.014	.047	.19	.39	.57						
KN12101572	16#5 Rebar 60' A615M GR 420 (Gr60) ASTM A615/A615M-12 GR 60[420] AASHTO M31-07 Melted 03/29/12 Rolled 03/31/12	457MPa	679MPa				.035	.24	.15	.071	.008	.002							
PO# => 804154																			
KN1210157401	Nucor Steel - Kankakee Inc	67,237	101,335	15.5%	OK	-3.4%	.36	1.01	.013	.046	.23	.32	.56						
KN12101574	16#5 Rebar 60' A615M GR 420 (Gr60) ASTM A615/A615M-12 GR 60[420] AASHTO M31-07 Melted 03/29/12 Rolled 03/31/12	464MPa	699MPa				.035	.23	.13	.070	.008	.002							

I hereby certify that the material described herein has been manufactured in accordance with the specifications and standards listed above and that it satisfies those requirements.
1.) Yield tests were not performed on this material.
2.) Melted and Manufactured in the United States.
3.) Mercury, Radium, or Alpha source materials in any form have not been used in the production of this material.

QUALITY ASSURANCE: Scott Laurenti

APPENDIX B: ADMIXTURE LITERATURE

B-1. Superplasticizer - ADVA® Cast 575

Grace Concrete Products

GRACE

ADVA® CAST 575

High-range water-reducing admixture

ASTM C494 Type A and F, and ASTM C1017 Type I

Product Description



ADVA® Cast 575 is a high efficiency, low addition rate polycarboxylate-based high-range water reducer designed for the production of a wide range of concrete mixes, from conventional to Self-Consolidating Concrete. It is designed to impart extreme workability without segregation to the concrete.

ADVA Cast 575 meets the requirements of ASTM C494 as a Type A and F, and ASTM C1017 Type I plasticizing.

ADVA Cast 575 is supplied as a ready-to-use liquid that weighs approximately 8.9 lbs/gal (1.1 kg/L). ADVA Cast 575 does not contain intentionally added chlorides.

Uses

ADVA Cast 575 is a plant-added superplasticizer that is formulated to impart improved workability to the concrete and to achieve high early compressive strength as required by the precast industry. ADVA Cast 575 can be used for the production of Self-Consolidating Concrete (SCC) in precast/prestressed applications and may be used in conventional concrete production.

ADVA Cast 575 may be used in low water-cementitious ratio applications where concrete stability and improved tolerance to concrete material variability are required.

ADVA Cast 575 may be used to produce concrete with very low water/cementitious ratios while maintaining normal levels of workability.

Addition Rates

ADVA Cast 575 is an easy to dispense liquid admixture. Dosage rates can be adjusted to meet a wide spectrum of concrete performance requirements. Addition rates for ADVA Cast 575 can vary from 2 to 10 fl oz/100 lbs (130 to 650 mL/100 kg) with the type of application, but will typically range from 3 to 6 fl oz/100 lbs (200 to 390 mL/100 kg) of cementitious. Should conditions require using more than the recommended addition rate, please consult your Grace representative.

Mix proportions, cementitious content, aggregate gradations and ambient conditions will affect ADVA Cast 575 dosage requirements. If materials or conditions require using more than the recommended addition rates, or when developing mix designs for Self-Consolidating Concrete please consult your Grace representative for more information and assistance.

Product Advantages

- Excellent dosage efficiency, moisture control and air control
- Superior air entrainment control
- Enhanced concrete cohesiveness with low viscosity for rapid placement
- Superior finish on cast surfaces
- Enhanced strength development



Compatibility with Other Admixtures and Batch Sequencing

ADVA Cast 575 is compatible with most Grace admixtures as long as they are added separately to the concrete mix. However, ADVA products are not recommended for use in concrete containing naphthalene-based admixtures including Daracem® 19 and Daracem 100, and melamine-based admixtures including Daracem ML 330 and Daracem 65. In general, it is recommended that ADVA Cast 575 be added to the concrete mix near the end of the batch sequence for optimum performance. Different sequencing may be used if local testing shows better performance. Please see Grace Technical Bulletin TB-0110, *Admixture Dispenser Discharge Line Location and Sequencing for Concrete Batching Operations* for further recommendations. ADVA Cast 575 should not come in contact with any other admixture before or during batching, even if diluted in mix water.

Pretesting of the concrete mix should be performed before use and as conditions and materials change in order to assure compatibility with other admixtures, and to optimize dosage rates, addition times in the batch sequencing and concrete performance. For concrete that requires air entrainment, the use of an ASTM C260 air-entraining agent (such as Daravair® or Darex® product lines) is recommended to provide suitable air void parameters for freeze-thaw resistance. Please consult your Grace representative for guidance.

Packaging & Handling

ADVA Cast 575 is a light blue liquid available in bulk, delivered by metered trucks, in 275 gal (1040 L) totes, and 55 gal (210 L) drums. ADVA Cast 575 will freeze at approximately 32°F (0°C) but will return to full functionality after thawing and thorough mechanical agitation.

Dispensing Equipment

A complete line of accurate, automatic dispensing equipment is available.

ADVA Cast 575 ASTM C494 Type F High-Range Water Reducer Test Data

	US Units		Metric	
	Control	ADVA Cast 575	Control	ADVA Cast 575
Cement (pcy) (kg/m ³)	517	517	307	307
Coarse aggregate (pcy) (kg/m ³)	1944	1944	1153	1153
Fine aggregate (pcy) (kg/m ³)	1144	1214	679	720
Water (pcy) (kg/m ³)	248	211	147	125
w/cm	0.48	0.41	0.48	0.41
Slump (inches) (mm)	3.5	3.25	89	83
Plastic air (%)	5.4	5.5	5.4	5.5
Compressive strength				
1 day (psi) (MPa)	1460	2050	10.1	14.1
7 day (psi) (MPa)	4380	6040	30.2	41.6
28 day (psi) (MPa)	5570	7270	38.4	50.1
Initial set time (hr:min)	4:56	3:57	4:56	3:57
Length change 28 day (%)	-0.027	-0.029	-0.027	-0.029
Freeze-thaw resistance (RDME %)	in progress	in progress	in progress	in progress

www.graceconstruction.com

North American Customer Service: 1-877-4AD-MIX1 (1-877-423-6491)

ADVA, the ADVA logo, Daracem, Daravair and Darex are registered trademarks of W. R. Grace & Co.-Conn.

We hope the information here will be helpful. It is based on data and knowledge considered to be true and accurate and is offered for the users' consideration, investigation and verification, but we do not warrant the results to be obtained. Please read all statements, recommendations or suggestions in conjunction with our conditions of sale, which apply to all goods supplied by us. No statement, recommendation or suggestion is intended for any use which would infringe any patent or copyright. W. R. Grace & Co.-Conn., 62 Whittemore Avenue, Cambridge, MA 02140. In Canada, Grace Canada, Inc., 294 Clements Road, West, Ajax, Ontario, Canada L1S 3C6.

This product may be covered by patents or patents pending.
DCAC-34D Printed in U.S.A. 9/11

Copyright 2011. W. R. Grace & Co.-Conn.
FA/PDF

GRACE

B-2. Air Entrainer – Daravair® M

Grace Concrete Products

GRACE

DARAVAIR® 1000 Air-entraining admixture

ASTM C260

Product Description

Daravair® 1000 is a liquid air-entraining admixture that provides freeze-thaw resistance, yield control, and finishability performance across the full range of concrete mix designs. Daravair 1000 is a clean, light-orange product designed to generate specification-quality air systems. Based on a high-grade saponified rosin formulation, Daravair 1000 is chemically similar to vinsol-based products, but with increased purity and supply dependability. Daravair 1000 weighs approximately 8.5 lbs/gal (1.02 kg/L). Daravair 1000 does not contain intentionally added chloride.

Uses

Daravair 1000 air-entraining admixture may be used wherever the purposeful entrainment of air is required by concrete specifications. Formulated to perform across the entire spectrum of production mixes, Daravair 1000 generates quality, freeze-thaw resistant air systems in concrete conditions that include the following:

- Low slump
- Paving
- Central mix
- Extruded slip form
- Mixes containing hot water and accelerators
- Precast

Product Advantages

- Rapid air build suitable for short mix cycles
- Can be used in wide spectrum of mix designs

- High cement factor
- Fly ash and slag
- Superplasticizers
- Manufactured sands

Performance

Air is incorporated into the concrete by the mechanics of mixing and stabilized into millions of discrete semi-microscopic bubbles in the presence of a specifically designed air-entraining admixture such as Daravair 1000. These air bubbles act much like flexible ball bearings increasing the mobility, or plasticity and workability of the concrete. This can permit a reduction in mixing water with no loss of slump. Placeability is improved. Bleeding, plastic shrinkage and segregation are minimized.

Through the purposeful entrainment of air, Daravair 1000 markedly increases the durability of concrete to severe exposures particularly to freezing and thawing. It has also demonstrated a remarkable ability to impart resistance to the action of frost and de-icing salts as well as sulfate, sea and alkaline waters.



Addition Rates

There is no standard addition rate for Daravair 1000. The amount to be used will depend upon the amount of air required for job conditions, usually in the range of 4 to 8%. Typical factors which might influence the amount of air-entraining admixture required are temperature, cement, sand gradation, and the use of extra fine materials such as fly ash and microsilica. Typical Daravair 1000 addition rates range from ½ to 3 fl oz/100 lbs (30 to 200 mL/100 kg) of cement. Pretesting of concrete should be performed to confirm dosage rates required to achieve desired concrete performance.

The air-entraining capacity of Daravair 1000 is usually increased when other concrete admixtures are contained in the concrete, particularly water-reducing admixtures and water-reducing retarders. This may allow up to ⅔ reduction in the amount of Daravair 1000 required.

Mix Adjustment

Entrained air will increase the volume of the concrete making it necessary to adjust the mix proportions to maintain the cement factor and yield. This may be accomplished by a reduction in water requirement and aggregate content.

Compatibility with Other Admixtures and Batch Sequencing

Daravair 1000 is compatible with most Grace admixtures as long as they are added separately to the concrete mix. In general, it is recommended that Daravair 1000 be added to the concrete mix near the beginning of the batch sequence for optimum performance, preferably by “dribbling” on the sand. Different sequencing may be used if local testing shows better performance. Please see Grace

Technical Bulletin TB-0110, *Admixture Dispenser Discharge Line Location and Sequencing for Concrete Batching Operations* for further recommendations. Daravair 1000 should not be added directly to heated water.

Pretesting of the concrete mix should be performed before use, and as conditions and materials change in order to assure compatibility, and to optimize dosage rates, addition times in the batch sequencing and concrete performance. Please consult your Grace representative for guidance.

Packaging & Handling

Daravair 1000 is available in bulk, delivered by metered tank trucks and in 55 gal (210 L) drums. **Daravair 1000 will freeze at about 30°F (-1°C) but its air-entraining properties are completely restored by thawing and thorough mechanical agitation.**

Dispensing Equipment

A complete line of accurate automatic dispensing equipment is available. These dispensers can be located to discharge into the water line, the mixer, or on the sand.

Specifications

Concrete shall be air entrained concrete, containing 4 to 8% entrained air. The air contents in the concrete shall be determined by the pressure method (ASTM Designation C231) or volumetric method (ASTM Designation C173). The air-entraining admixture shall be a completely neutralized rosin solution, such as Daravair 1000, as manufactured by Grace Construction Products, or equal, and comply with *Standard Specification for Air-Entraining Admixtures* (ASTM Designation C260). The air-entraining admixture shall be added at the concrete mixer or batching plant at approximately ½ to 3 fl oz/100 lbs (30 to 200 mL/100 kg) of cement, or in such quantities as to give the specified air contents.

www.graceconstruction.com

North American Customer Service: 1-877-4AD-MIX1 (1-877-423-6491)

Daravair is a registered trademark of W. R. Grace & Co.—Conn.

We hope the information here will be helpful. It is based on data and knowledge considered to be true and accurate and is offered for the users' consideration, investigation and verification, but we do not warrant the results to be obtained. Please read all statements, recommendations or suggestions in conjunction with our conditions of sale, which apply to all goods supplied by us. No statement, recommendation or suggestion is intended for any use which would infringe any patent or copyright. W. R. Grace & Co.—Conn., 62 Whittemore Avenue, Cambridge, MA 02140. In Canada, Grace Canada, Inc., 294 Clements Road, West, Ajax, Ontario, Canada L1S 3C8.

This product may be covered by patents or patents pending.
AIR-7G Printed in U.S.A. 5/09

Copyright 2007. W. R. Grace & Co.—Conn.
FA/LV11M

GRACE

APPENDIX C: MEASURED COLUMN RESPONSE

C-1. Specimen CC1

Load Number	Applied Lateral Load (kips)	Applied Axial Load (kips)	Ratio to Target Axial Load	Measured Displacement (in.)	Displacement Ductility Range ($\pm\mu_{\Delta}$)	Cycle Number
8	6.61	73.0	0.99	0.09	±0.19	1
11	-6.63	73.0	0.99	-0.09		2
13	6.63	72.5	0.98	0.09		3
15	-6.64	73.0	0.99	-0.09		1
17	6.66	73.0	0.99	0.09		1
19	-6.65	72.5	0.98	-0.09		1
23	11.69	75.3	1.02	0.29	+0.62	1
29	6.64	73.86	1.00	0.12	+0.26	1
31	-6.61	73.39	0.99	-0.10	±0.62	1
33	11.78	75.72	1.03	0.29		1
39	-11.76	75.26	1.02	-0.28		1
44	13.02	76.66	1.04	0.34	±0.75	1
50	-13.03	76.19	1.03	-0.34		2
55	13.07	76.66	1.04	0.36		3
59	-13.04	76.66	1.04	-0.35		1
63	13.04	76.66	1.04	0.36		2
67	-12.98	76.66	1.04	-0.36	±1.0	1
74	15.17	78.51	1.06	0.47		2
82	-15.43	78.51	1.06	-0.47		3
88	14.85	78.06	1.06	0.47		1
94	-14.93	78.51	1.06	-0.47		2
98	14.76	78.06	1.06	0.47	±1.0	3
102	-14.85	78.51	1.06	-0.47		1

Table Continued on Following Page...

...Table Continued

Load Number	Applied Lateral Load (kips)	Applied Axial Load (kips)	Ratio to Target Axial Load	Measured Displacement (in.)	Displacement Ductility Range ($\pm\mu_{\Delta}$)	Cycle Number
109	19.67	86.41	1.17	0.94	±2.0	1
119	-20.57	87.34	1.18	-0.94		2
127	18.96	86.41	1.17	0.94		3
133	-19.73	86.88	1.18	-0.94		
139	18.73	85.95	1.17	0.95		
145	-19.54	86.88	1.18	-0.94		
154	20.40	95.25	1.29	1.42	±3.0	1
166	-21.96	96.64	1.31	-1.42		2
175	19.81	94.32	1.28	1.42		3
181	-21.20	96.18	1.30	-1.42		
187	19.39	94.32	1.28	1.42		
193	-20.95	96.18	1.30	-1.42		
200	19.15	101.29	1.37	1.89	±4.0	1
208	-21.30	105.00	1.42	-1.89		2
215	18.01	98.96	1.34	1.89		3
221	-20.07	102.22	1.39	-1.89		
228	17.62	98.03	1.33	1.89		
234	-19.55	101.75	1.38	-1.89		
241	17.29	84.57	1.15	2.36	±5.0	1
249	-18.42	89.21	1.21	-2.36		2
256	16.18	84.11	1.14	2.36		3
262	-17.41	87.35	1.18	-2.36		
268	15.72	83.18	1.13	2.36		
274	-16.93	86.42	1.17	-2.36		
281	15.94	89.68	1.22	2.83	±6.0	1
289	-16.75	93.39	1.27	-2.83		2
296	15.13	87.36	1.18	2.83		3
302	-16.25	91.07	1.23	-2.83		
308	14.86	86.43	1.17	2.84		
314	-15.76	90.14	1.22	-2.83		

Table Continued on Following Page...

...Table Continued

Load Number	Applied Lateral Load (kips)	Applied Axial Load (kips)	Ratio to Target Axial Load	Measured Displacement (in.)	Displacement Ductility Range ($\pm\mu_{\Delta}$)	Cycle Number
321	14.70	92.01	1.25	3.31	±7.0	1
329	-15.41	95.25	1.29	-3.31		2
336	14.15	90.15	1.22	3.30		3
342	-14.91	92.92	1.26	-3.30		
348	13.75	88.29	1.20	3.30		
354	-14.59	91.54	1.24	-3.30		
361	13.54	93.40	1.27	3.78	±8.0	1
369	-14.16	95.72	1.30	-3.78		2
376	12.73	90.15	1.22	3.78		3
382	-13.70	93.86	1.27	-3.78		
388	12.59	88.76	1.20	3.78		
394	-13.50	92.46	1.25	-3.78		
402	12.20	92.02	1.25	4.25	±9.0	1
410	-12.77	95.72	1.30	-4.25		2
417	11.50	89.23	1.21	4.25		3
423	-12.20	92.93	1.26	-4.25		
429	11.15	87.37	1.18	4.25		
435	-11.87	90.61	1.23	-4.25		
442	10.62	88.30	1.20	4.72	±10.0	1
450	-11.09	92.01	1.25	-4.72		2
457	9.84	83.66	1.13	4.72		3
463	-10.40	88.29	1.20	-4.72		
469	9.28	79.02	1.07	4.72		
475	-7.41	86.41	1.17	-4.72		
	Maximum	105.0	1.42			
	Minimum	72.5	0.98			
	Average	86.5	1.17			

NOTE: Push Excursions are Shaded in Gray, Pull Excursions are Not Shaded

C-2. Specimen CC2

Load Number	Applied Lateral Load (kips)	Applied Axial Load (kips)	Ratio to Target Axial Load	Measured Displacement (in.)	Displacement Ductility Range ($\pm\mu\Delta$)	Cycle Number
5	7.75	140.09	0.95	0.09	±0.16	1
9	-7.76	139.62	0.95	-0.09		2
12	7.78	140.09	0.95	0.08		3
14	-7.74	139.16	0.94	-0.09		
16	7.78	139.16	0.94	0.08		
18	-7.75	139.16	0.94	-0.09		
21	15.39	140.09	0.95	0.23	+0.52	1
28	-15.27	140.09	0.95	-0.31		2
33	15.38	139.16	0.94	0.24		3
37	-15.20	139.16	0.94	-0.33		
41	15.36	138.70	0.94	0.24		
45	-15.18	139.16	0.94	-0.34		
51	19.01	140.56	0.95	0.37	±0.70	1
59	-16.09	139.16	0.94	-0.37		
64	21.92	142.87	0.97	0.53	±1.0	1
70	-19.05	140.54	0.95	-0.53		2
76	21.46	141.94	0.96	0.53		
82	-18.48	140.09	0.95	-0.53		
89	27.59	159.56	1.08	1.06	±2.0	1
97	-23.37	154.46	1.05	-1.06		2
104	26.38	157.71	1.07	1.06		3
110	-22.47	152.60	1.03	-1.06		
116	26.13	157.26	1.07	1.06		
122	-22.21	152.60	1.03	-1.06		
130	22.90	154.46	1.05	1.59	±3.0	1
137	-20.66	149.83	1.02	-1.59		2
144	21.57	152.61	1.03	1.59		3
150	-19.30	147.04	1.00	-1.59		
156	21.00	151.68	1.03	1.59		
162	-18.96	146.58	0.99	-1.59		

Table Continued on Following Page...

...Table Continued

Load Number	Applied Lateral Load (kips)	Applied Axial Load (kips)	Ratio to Target Axial Load	Measured Displacement (in.)	Displacement Ductility Range ($\pm\mu\Delta$)	Cycle Number
169	20.50	159.57	1.08	2.12	±4.0	1
179	-18.46	151.70	1.03	-2.12		2
187	18.91	156.33	1.06	2.12		3
193	-17.55	150.30	1.02	-2.12		1
199	18.43	154.94	1.05	2.12		2
205	-17.23	149.37	1.01	-2.12		3
213	18.22	162.37	1.10	2.65	±5.0	1
223	-17.00	154.94	1.05	-2.65		2
231	16.92	159.12	1.08	2.65		3
237	-16.36	152.15	1.03	-2.65		1
243	16.52	157.73	1.07	2.65		2
249	-16.10	152.15	1.03	-2.65		3
257	15.87	163.77	1.11	3.18	±6.0	1
266	-15.41	156.34	1.06	-3.18		2
273	15.01	160.98	1.09	3.18		3
279	-14.71	154.48	1.05	-3.18		1
285	14.67	160.05	1.08	3.18		2
291	-14.39	153.09	1.04	-3.18		3
299	13.83	164.24	1.11	3.71	±7.0	1
308	-13.71	156.81	1.06	-3.71		2
315	13.01	161.91	1.10	3.71		3
321	-13.03	154.95	1.05	-3.71		1
327	12.60	159.59	1.08	3.71		2
333	-12.70	153.09	1.04	-3.71		3
341	11.52	162.38	1.10	4.24	±8.0	1
350	-11.70	155.42	1.05	-4.24		2
357	10.67	158.21	1.07	4.24		3
363	-11.19	152.64	1.03	-4.24		1
369	10.04	155.42	1.05	4.24		2
375	-10.72	151.25	1.03	-4.24		3

Table Continued on Following Page...

...Table Continued

Load Number	Applied Lateral Load (kips)	Applied Axial Load (kips)	Ratio to Target Axial Load	Measured Displacement (in.)	Displacement Ductility Range ($\pm\mu_{\Delta}$)	Cycle Number
383	8.41	154.96	1.05	4.77	±9.0	1
392	-9.50	151.25	1.03	-4.77		
399	7.14	148.93	1.01	4.77		2
405	-8.59	146.62	0.99	-4.77		
411	5.95	142.44	0.97	4.77		3
417	-5.04	143.85	0.98	-4.77		
	Maximum	164.2	1.11			
	Minimum	138.7	0.94			
	Average	150.6	1.02			

NOTE: Push Excursions are Shaded in Gray, Pull Excursions are Not Shaded

C-3. Specimen SCC1

Load Number	Corrected Lateral Load (kips)	Applied Axial Load (kips)	Ratio to Target Axial Load	Measured Displacement (in.)	Displacement Ductility Range ($\pm\mu\Delta$)	Cycle Number
7	8.10	81.24	0.94	0.15	±0.25	1
14	-8.12	80.77	0.93	-0.12		2
19	8.10	80.31	0.93	0.16		3
23	-8.12	80.77	0.93	-0.12		
27	8.10	80.31	0.93	0.16		
31	-8.12	80.31	0.93	-0.12		
39	15.80	84.49	0.97	0.61	±1.0	1
51	-15.92	84.49	0.97	-0.47		2
61	15.76	84.03	0.97	0.62		3
69	-15.90	84.02	0.97	-0.48		
77	15.78	83.56	0.96	0.63		
85	-15.89	84.02	0.97	-0.49		
94	16.77	84.96	0.98	0.74	±1.4	1
104	-19.18	86.80	1.00	-0.74		2
113	16.45	83.56	0.96	0.74		3
121	-18.54	85.87	0.99	-0.74		
129	16.27	83.56	0.96	0.74		
137	-18.36	85.87	0.99	-0.74		
146	17.89	94.23	1.09	1.47	±2.7	1
156	-20.45	98.83	1.14	-1.47		2
165	16.98	91.90	1.06	1.47		3
173	-19.31	96.98	1.12	-1.47		
181	16.67	90.97	1.05	1.47		
189	-18.89	96.05	1.11	-1.47		
198	16.91	101.18	1.17	2.21	±4.1	1
208	-19.75	108.58	1.25	-2.21		2
217	16.01	99.33	1.15	2.21		3
224	-19.00	105.79	1.22	-2.21		
232	15.61	98.40	1.14	2.21		
240	-18.18	104.41	1.20	-2.21		

Table Continued on Following Page...

...Table Continued

Load Number	Corrected Lateral Load (kips)	Applied Axial Load (kips)	Ratio to Target Axial Load	Measured Displacement (in.)	Displacement Ductility Range ($\pm\mu_{\Delta}$)	Cycle Number
249	15.19	97.47	1.12	2.94	±5.5	1
259	-16.95	104.41	1.20	-2.94		2
268	13.81	95.61	1.10	2.95		3
276	-15.98	101.62	1.17	-2.94		
284	13.32	94.69	1.09	2.95		
292	-15.51	100.23	1.16	-2.95		
301	13.04	101.65	1.17	3.68	±6.8	1
311	-15.16	109.05	1.26	-3.68		2
320	11.41	99.80	1.15	3.68		3
328	-14.45	105.35	1.22	-3.68		
336	10.60	99.34	1.15	3.68		
344	-14.04	103.49	1.19	-3.68		
354	9.59	98.87	1.14	4.42	±8.2	1
365	-13.54	105.82	1.22	-4.42		2
374	8.87	96.55	1.11	4.42		3
382	-12.88	103.03	1.19	-4.42		
390	8.44	94.70	1.09	4.42		
398	-12.48	100.24	1.16	-4.42		
408	7.63	97.48	1.12	5.15	±9.6	1
420	-11.84	105.83	1.22	-5.15		2
430	7.08	94.70	1.09	5.15		3
438	-10.68	100.73	1.16	-5.15		
446	3.83	92.39	1.07	5.15		
	Maximum	109.0	1.26			
	Minimum	80.3	0.93			
	Average	94.1	1.09			

NOTE: Push Excursions are Shaded in Gray, Pull Excursions are Not Shaded

C-4. Specimen SCC2

Load Number	Applied Lateral Load (kips)	Applied Axial Load (kips)	Ratio to Target Axial Load	Measured Displacement (in.)	Displacement Ductility Range ($\pm\mu_{\Delta}$)	Cycle Number
7	9.52	173.2	1.00	0.14	±0.26	1
13	-9.45	172.2	0.99	-0.16		2
19	9.53	172.2	0.99	0.14		3
25	-9.46	171.8	0.99	-0.17		
31	9.53	171.8	0.99	0.14		
37	-9.48	171.3	0.99	-0.17		
47	18.75	174.1	1.00	0.39	+0.66	1
58	-14.03	170.8	0.99	-0.44	-0.75	1
59	2.62	165.7	0.96	-1.62	-2.8	1
71	23.22	174.6	1.01	0.52	±0.9	1
77	0.22	163.0	0.94	-0.52		2
83	22.58	173.6	1.00	0.52		3
89	-0.06	163.0	0.94	-0.52		
95	22.35	173.6	1.00	0.52		
101	-0.12	162.0	0.93	-0.52		
109	25.80	182.5	1.05	1.03	±1.8	1
120	-4.64	150.4	0.87	-1.03		2
129	23.92	171.3	0.99	1.03		3
137	-4.74	150.0	0.87	-1.03		
145	23.55	170.4	0.98	1.03		
153	-4.73	149.0	0.86	-1.03		
162	23.44	178.7	1.03	1.55	±2.7	1
172	-7.40	149.0	0.86	-1.55		2
181	22.14	176.4	1.02	1.55		3
189	-7.20	148.1	0.85	-1.55		
197	21.47	175.5	1.01	1.55		
205	-7.12	147.2	0.85	-1.55		

Table Continued on Following Page...

...Table Continued

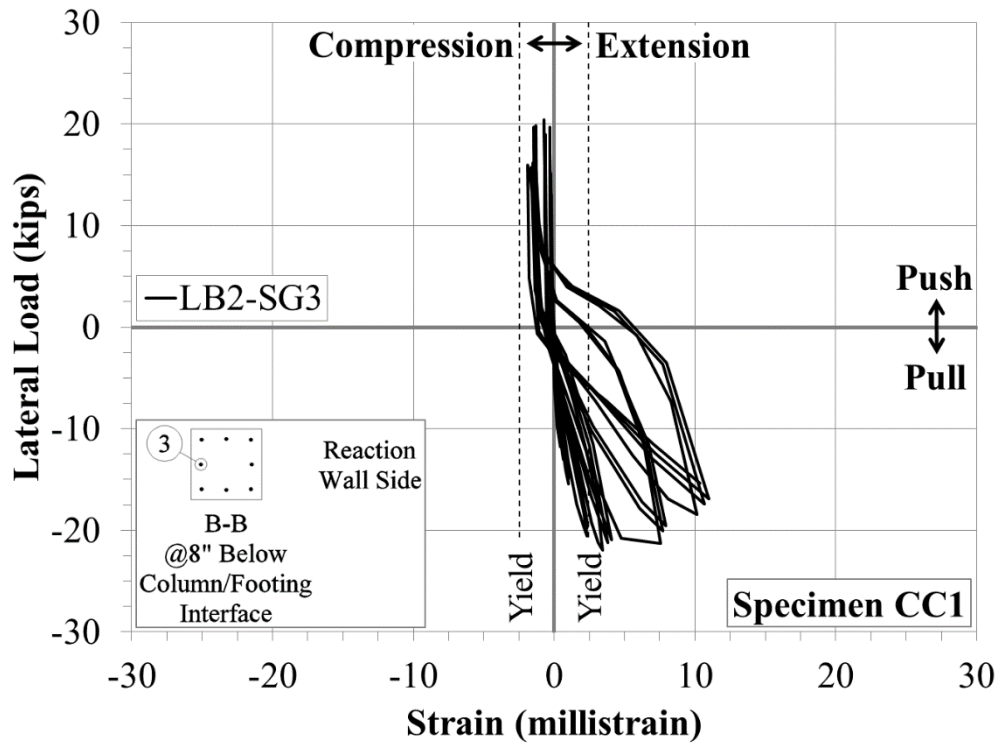
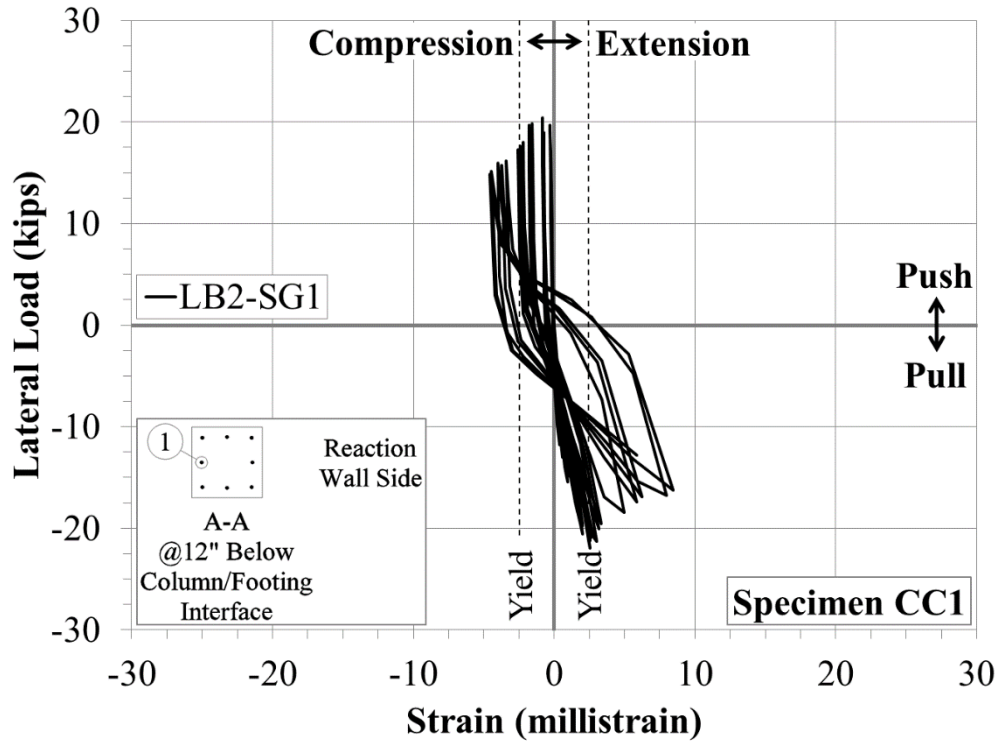
Load Number	Applied Lateral Load (kips)	Applied Axial Load (kips)	Ratio to Target Axial Load	Measured Displacement (in.)	Displacement Ductility Range ($\pm\mu_{\Delta}$)	Cycle Number
214	20.28	170.8	0.99	2.06	±3.6	1
224	-7.36	169.4	0.98	-2.06		2
232	20.17	177.3	1.02	2.06		3
240	-7.06	172.7	1.00	-2.06		
248	19.74	182.9	1.06	2.06		
256	-6.87	172.6	1.00	-2.06		
265	18.91	183.8	1.06	2.57	±4.4	1
275	-7.38	171.3	0.99	-2.57		2
284	17.46	177.3	1.02	2.57		3
292	-6.77	170.3	0.98	-2.57		
300	16.34	171.7	0.99	2.57		
308	-6.85	174.1	1.00	-2.57		
317	15.63	172.2	0.99	3.09	±5.3	1
327	-6.53	177.7	1.03	-3.09		2
336	15.56	168.5	0.97	3.09		3
344	-6.00	174.0	1.00	-3.09		
352	14.72	165.3	0.95	3.09		
360	-6.47	149.0	0.86	-3.09		
369	12.73	174.1	1.00	3.61	±6.2	1
379	-4.83	168.0	0.97	-3.61		2
388	12.16	175.0	1.01	3.61		3
396	-4.14	169.4	0.98	-3.60		
403	10.42	166.2	0.96	2.70		
	Maximum	183.8	1.06			
	Minimum	147.2	0.85			
	Average	169.1	0.98			

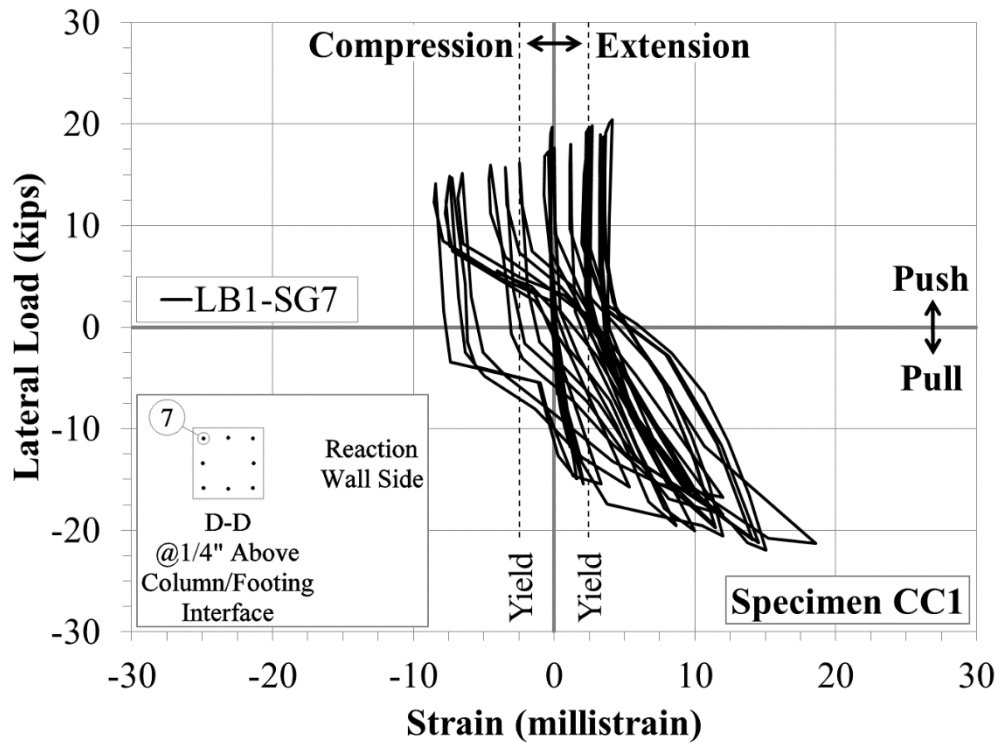
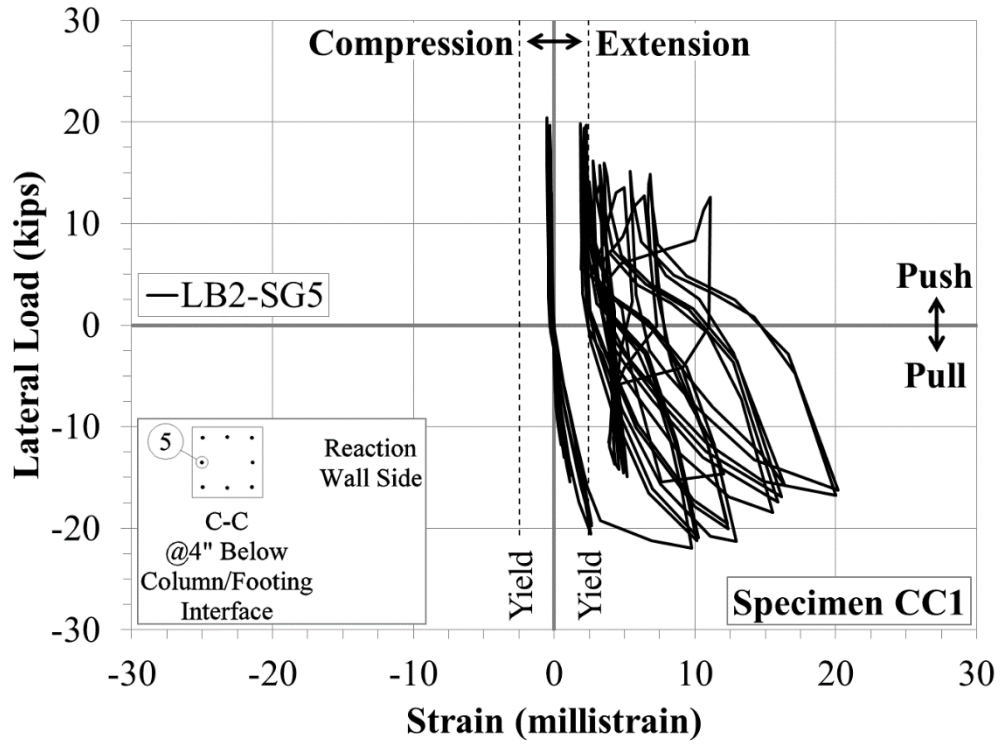
NOTE: Push Excursions are Shaded in Gray, Pull Excursions are Not Shaded

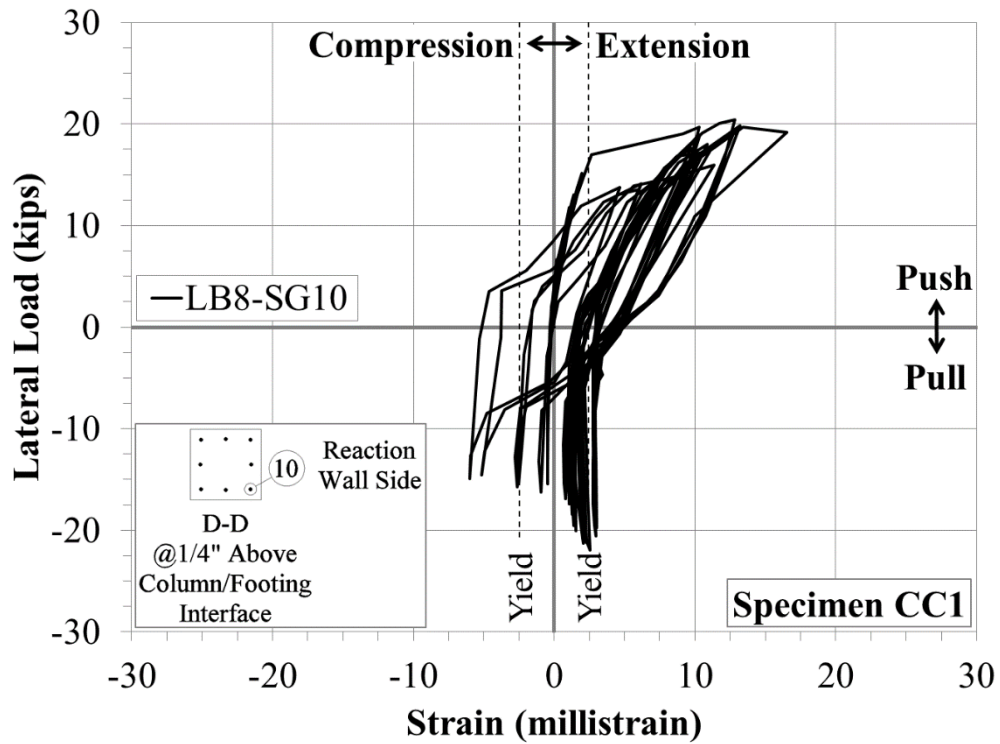
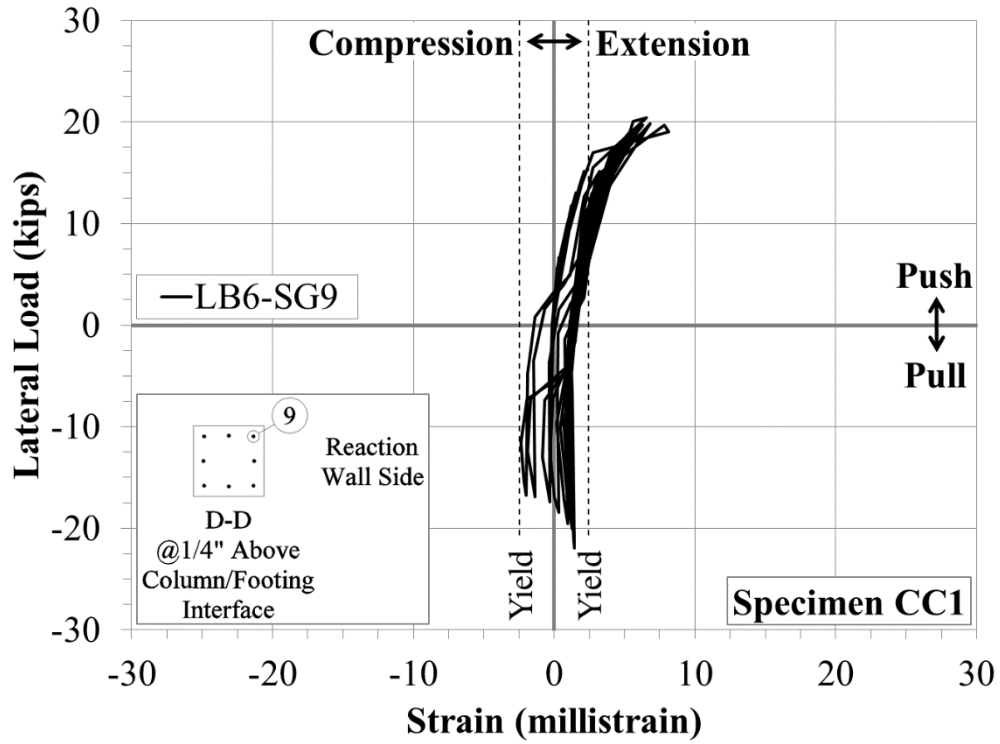
APPENDIX D: PLOTS OF EXPERIMENTAL MEASUREMENTS

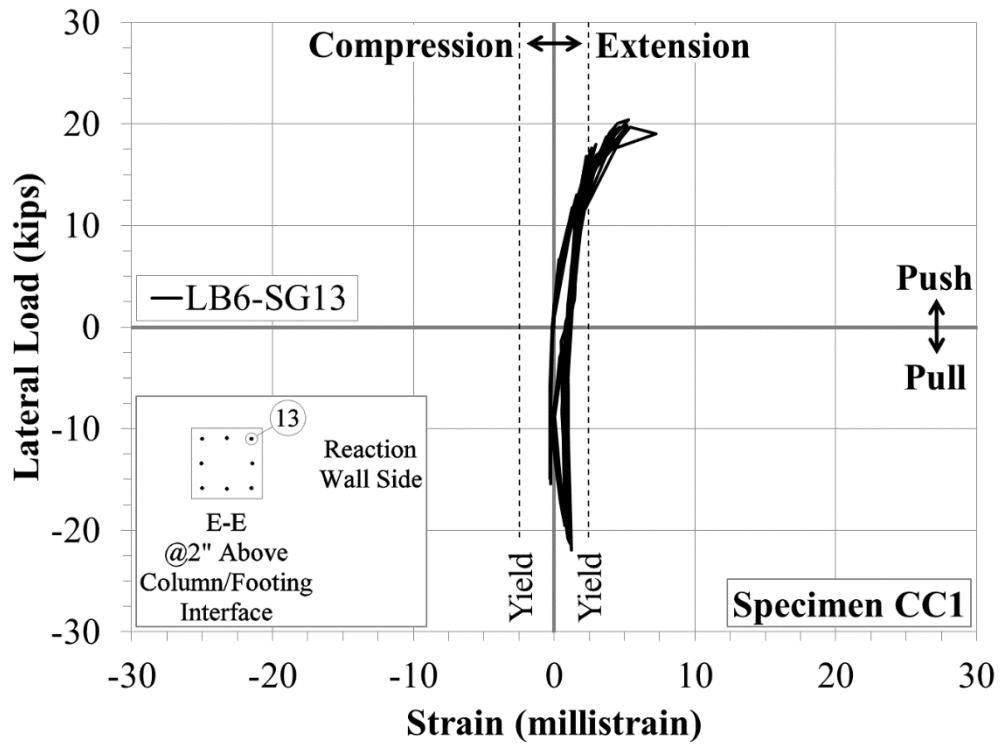
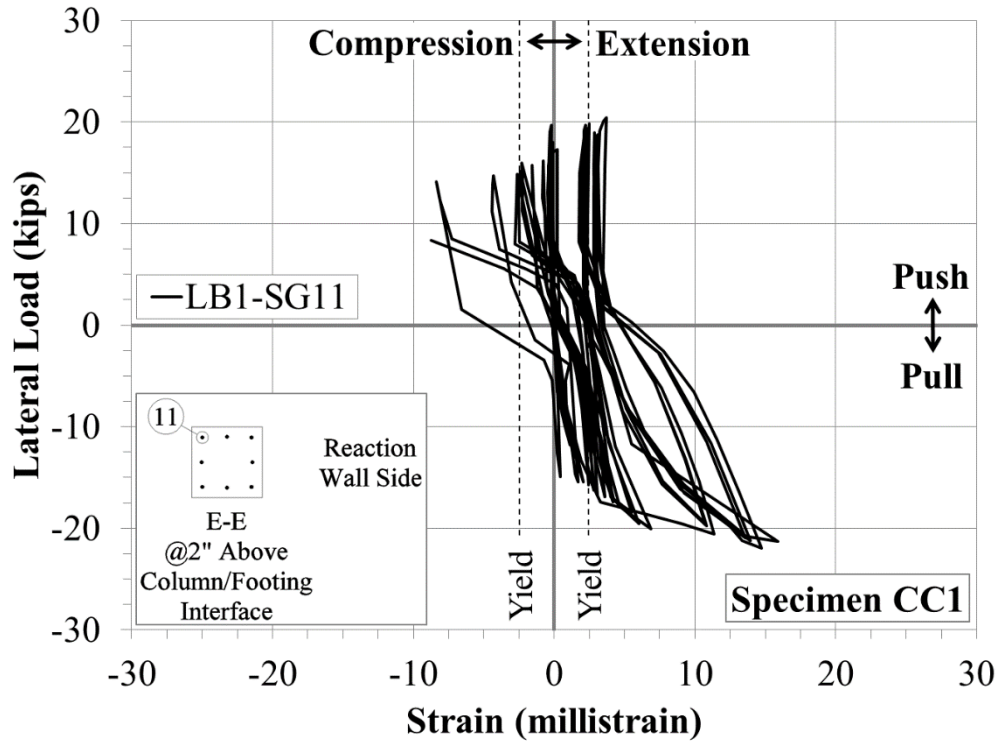
Appendix D provides plots of experimental measurements obtained during testing that were not presented in the body. Plots contain measured lateral load-strain data collected from longitudinal and transverse steel reinforcement. Data shown in the plots were cut off when the strain gages went off-line or were damaged during testing.

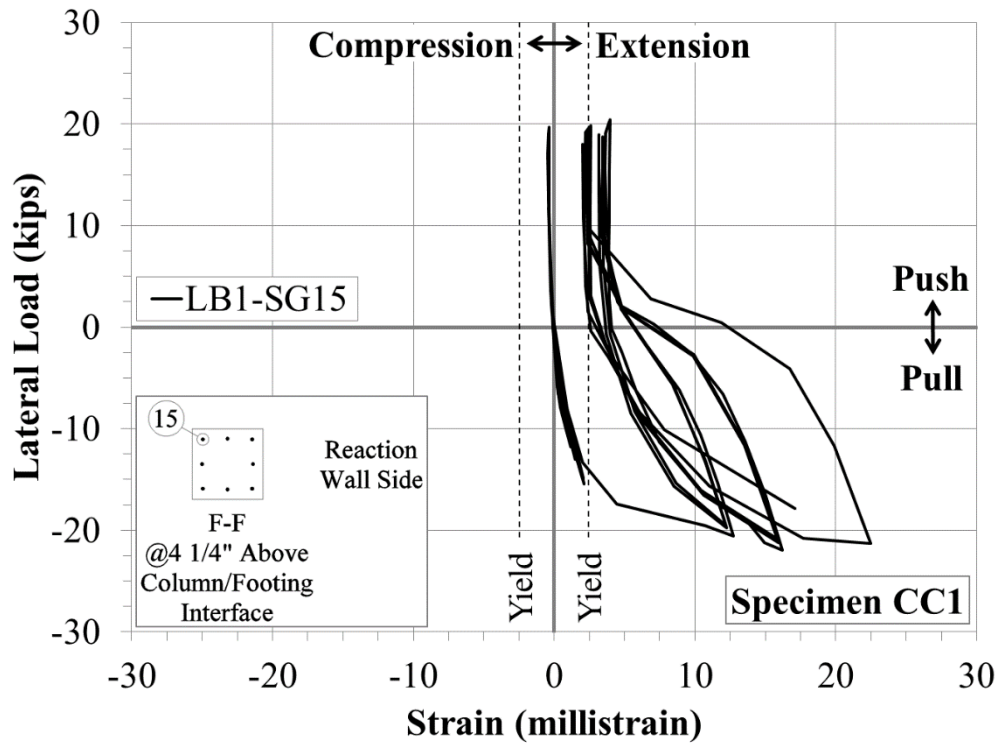
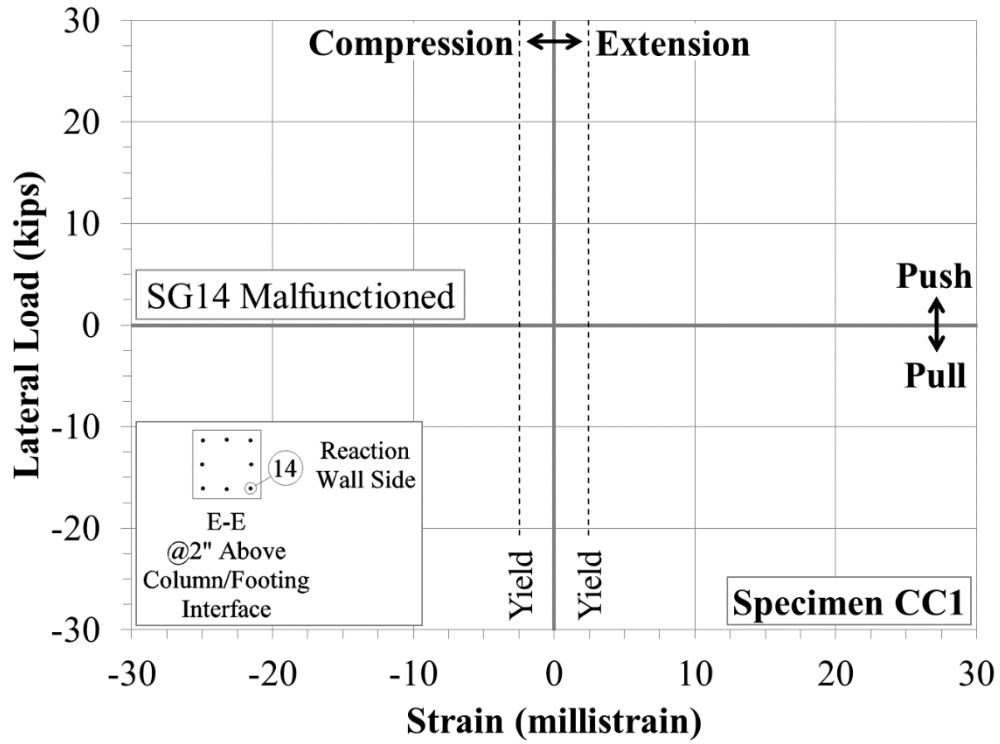
D-1. Specimen CC1

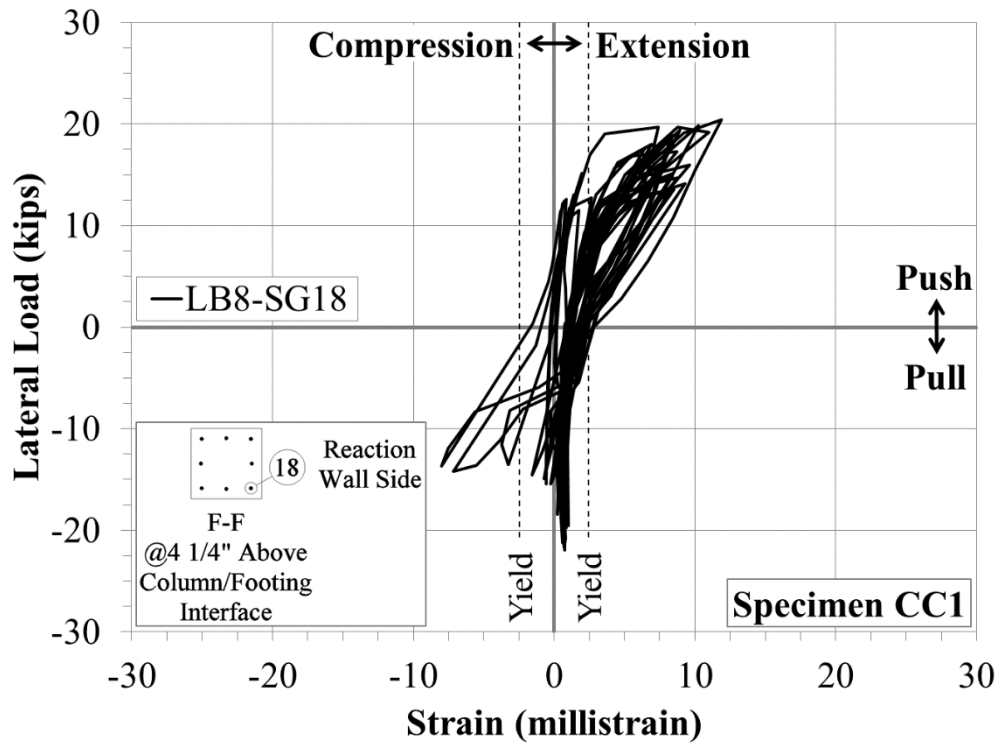
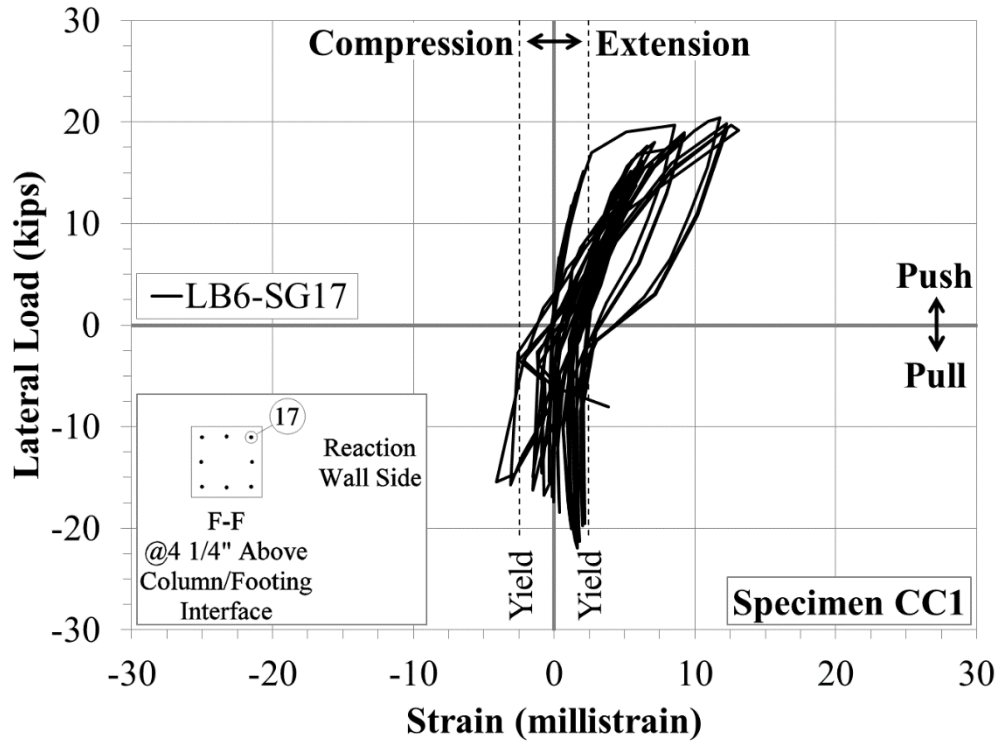


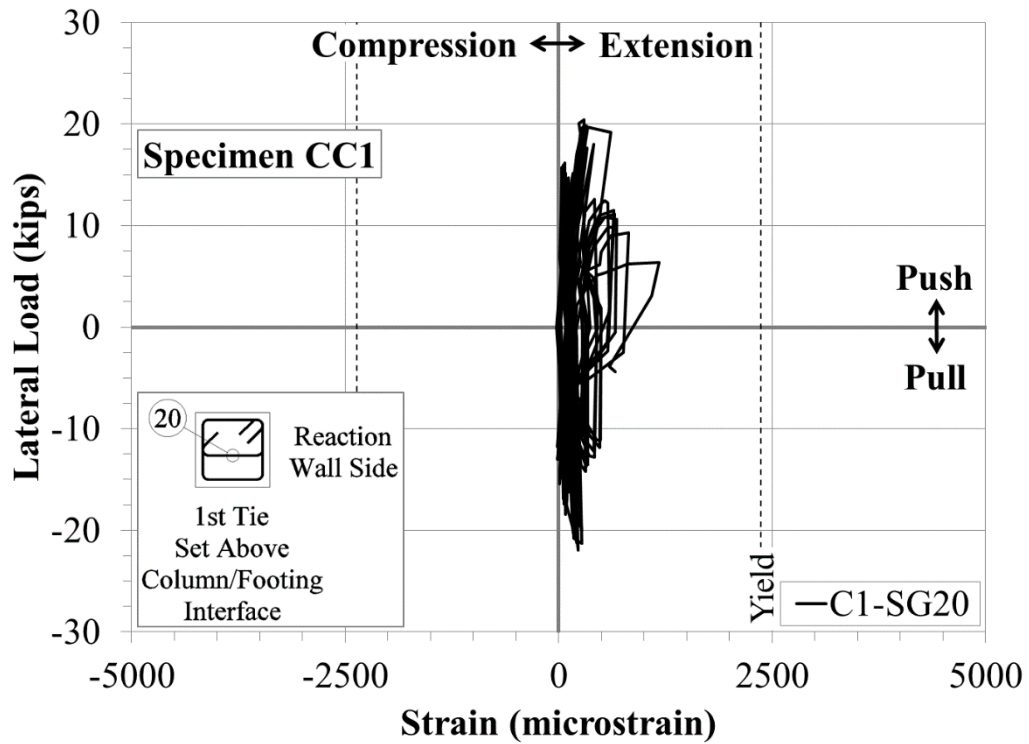
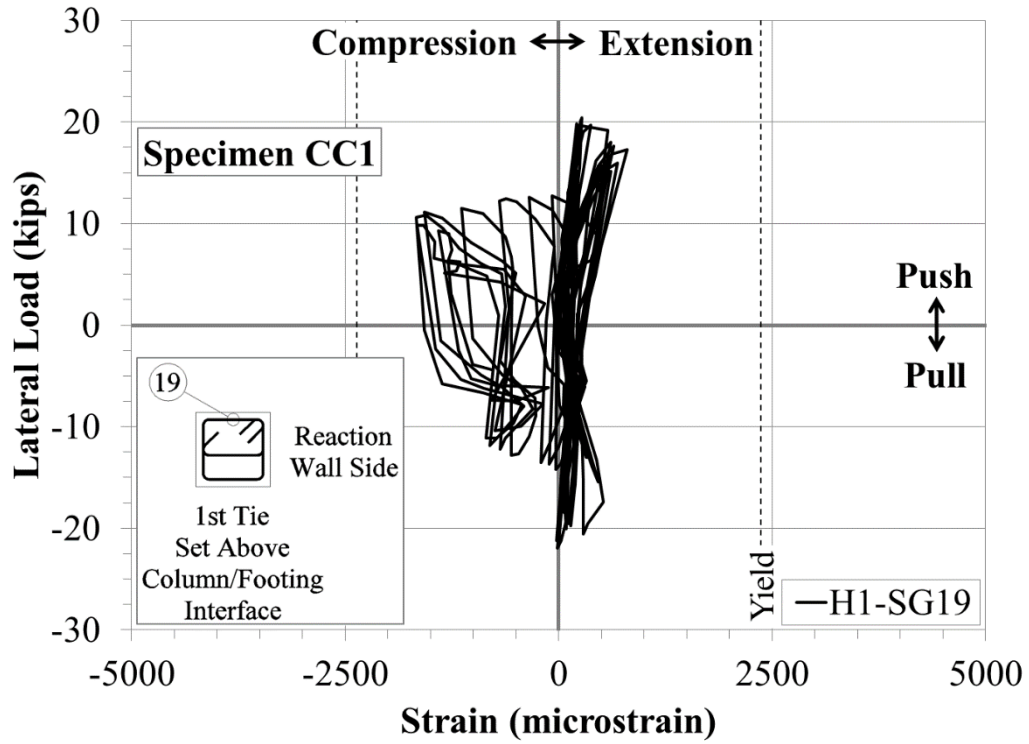


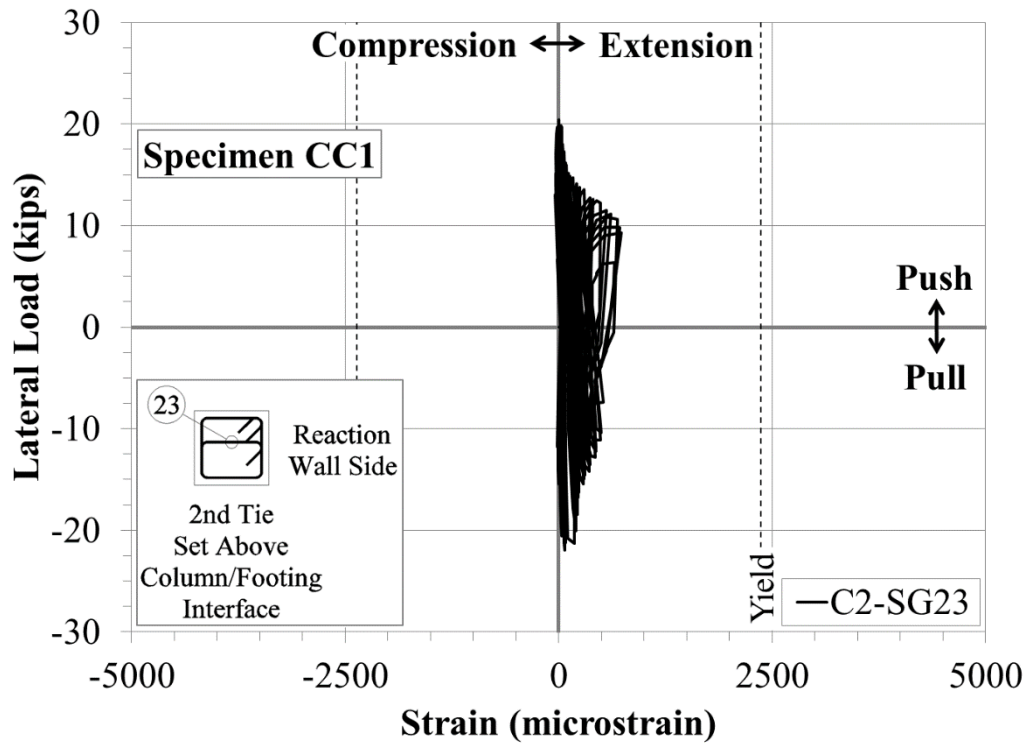
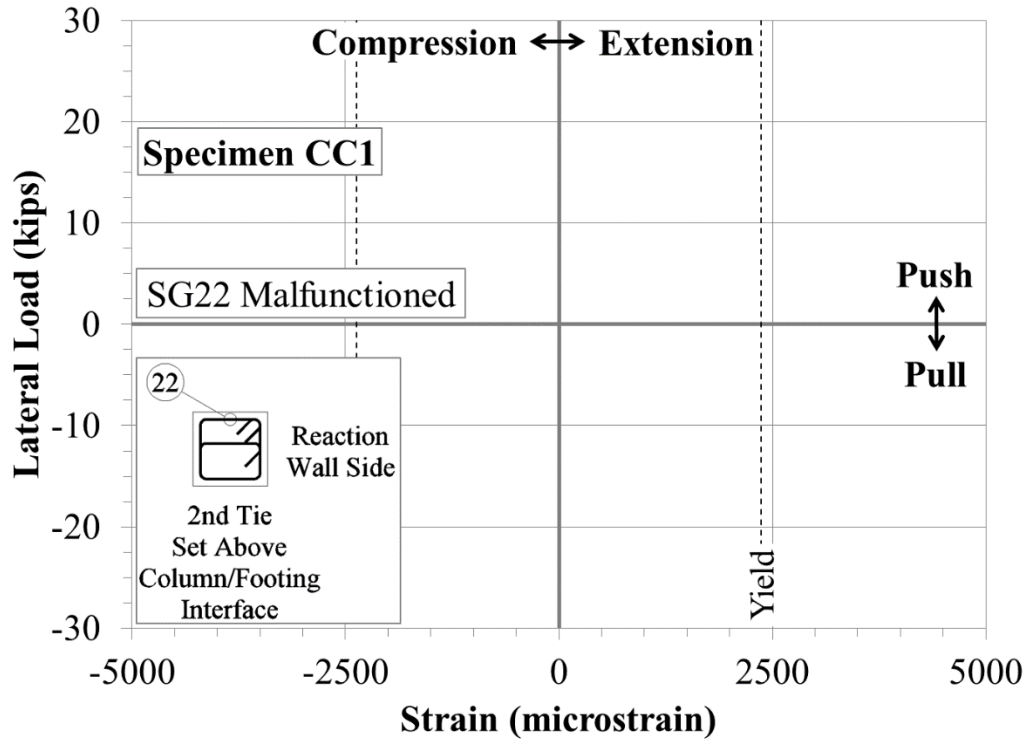


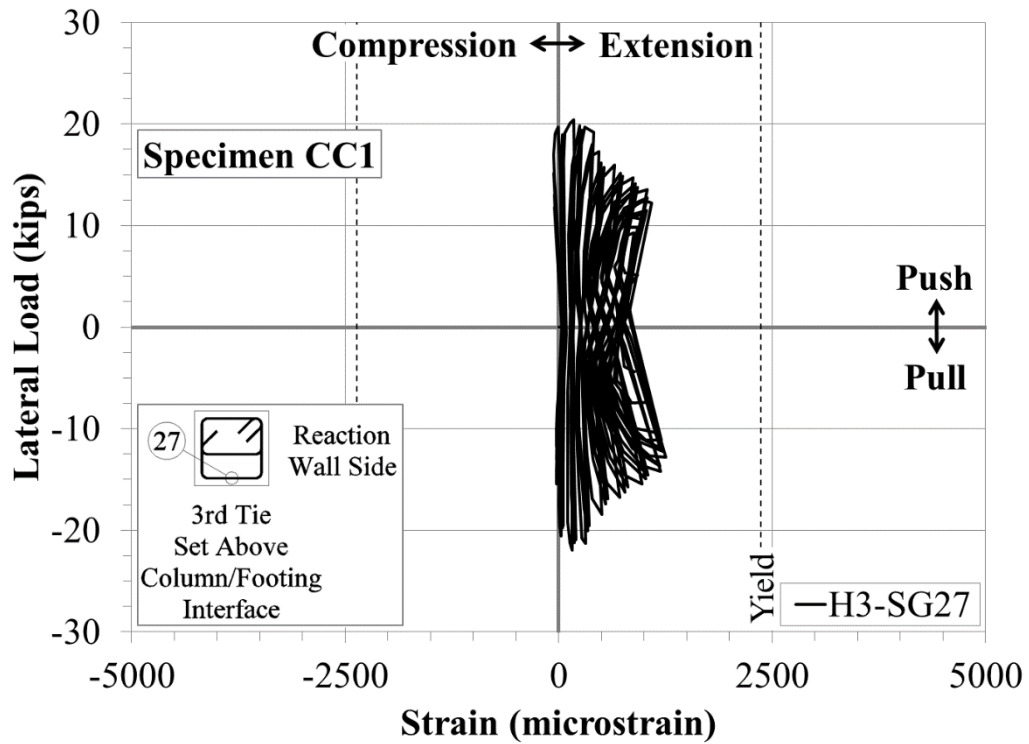
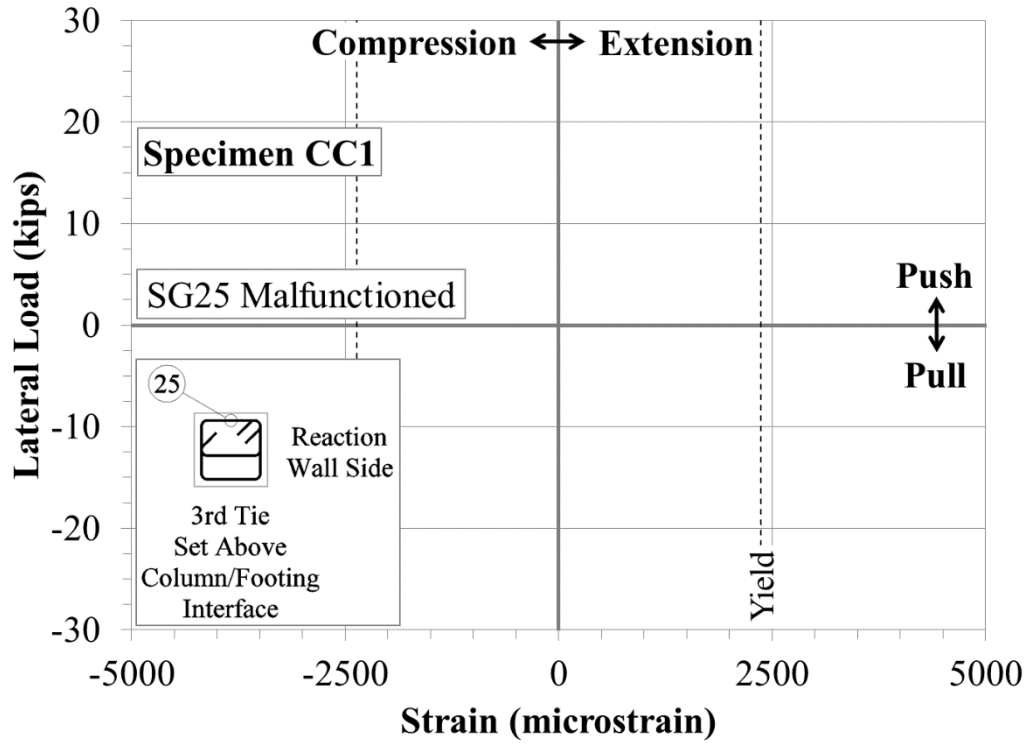




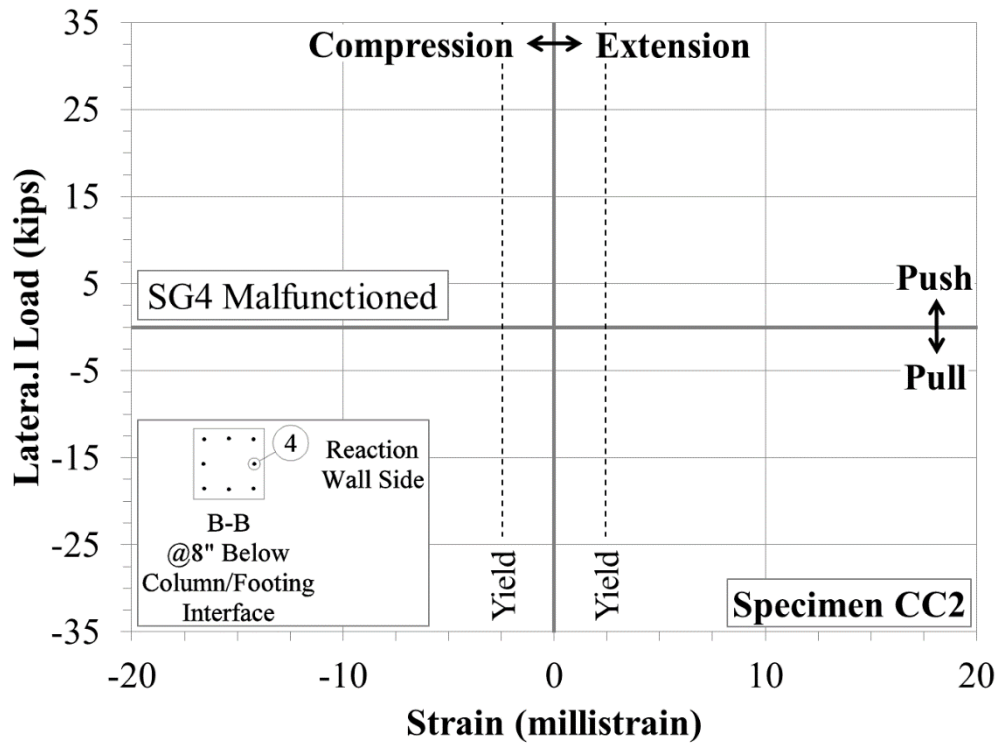
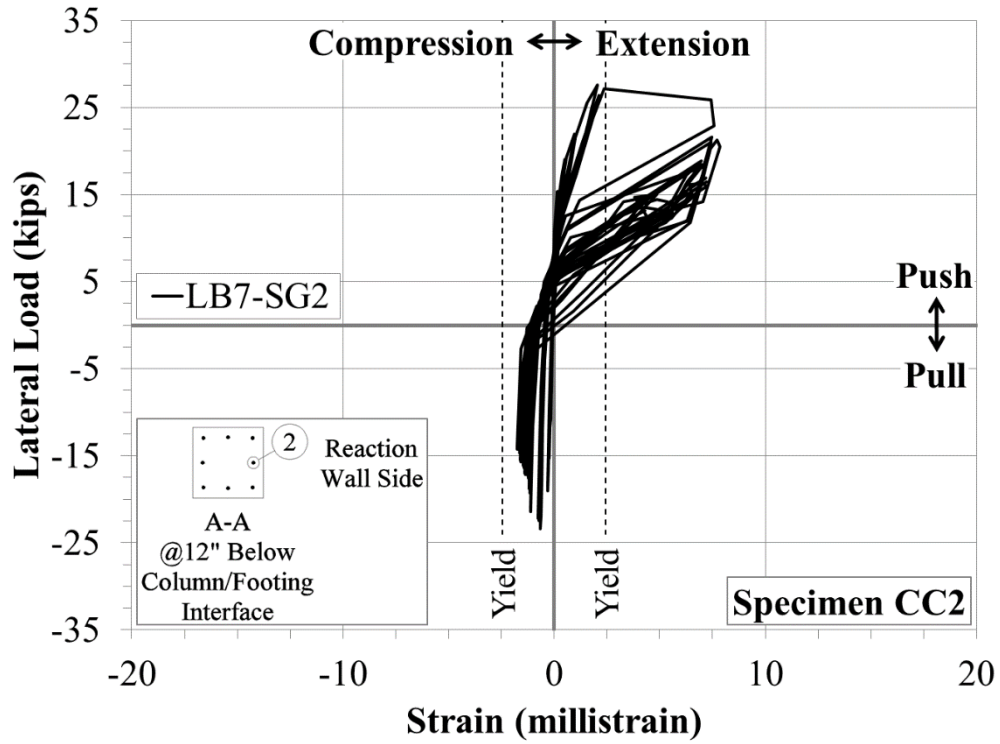


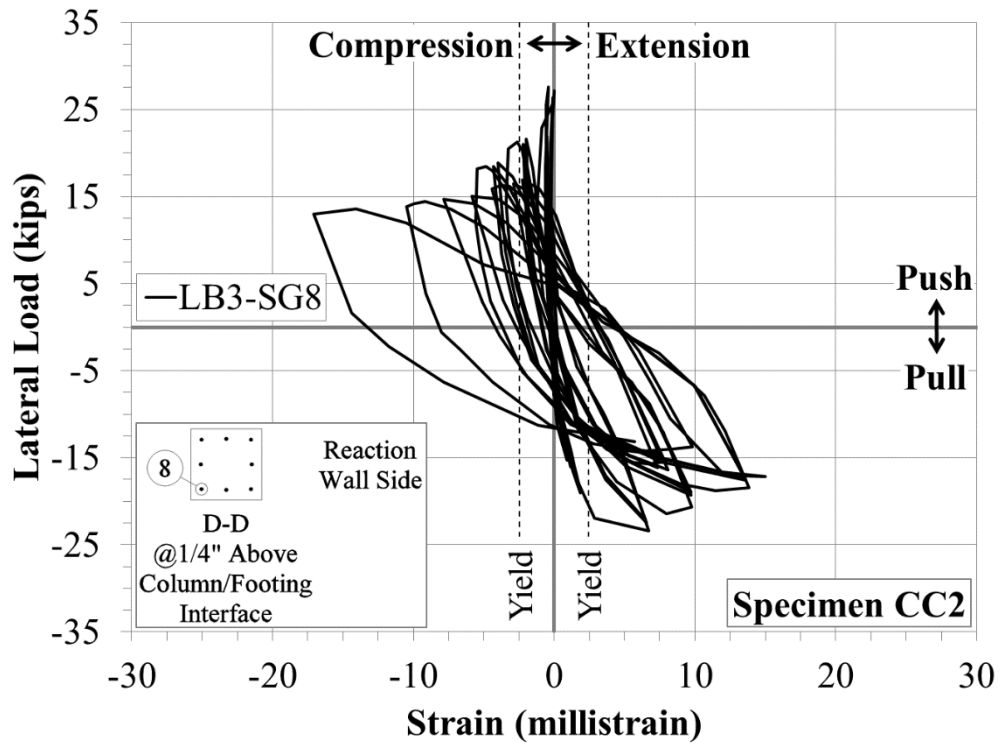
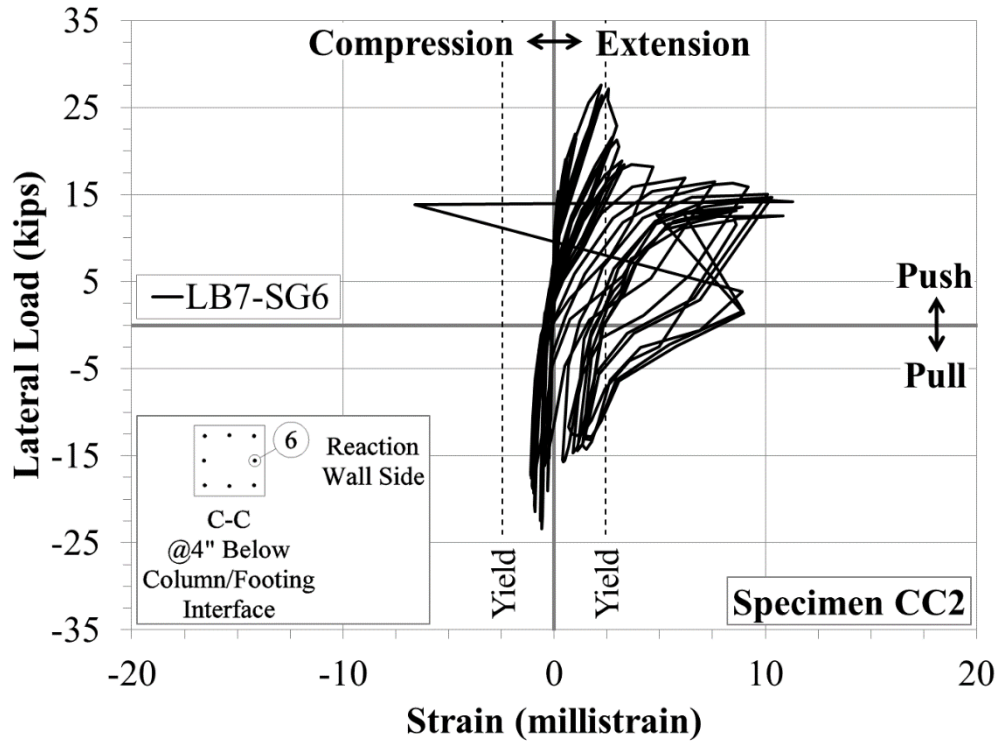


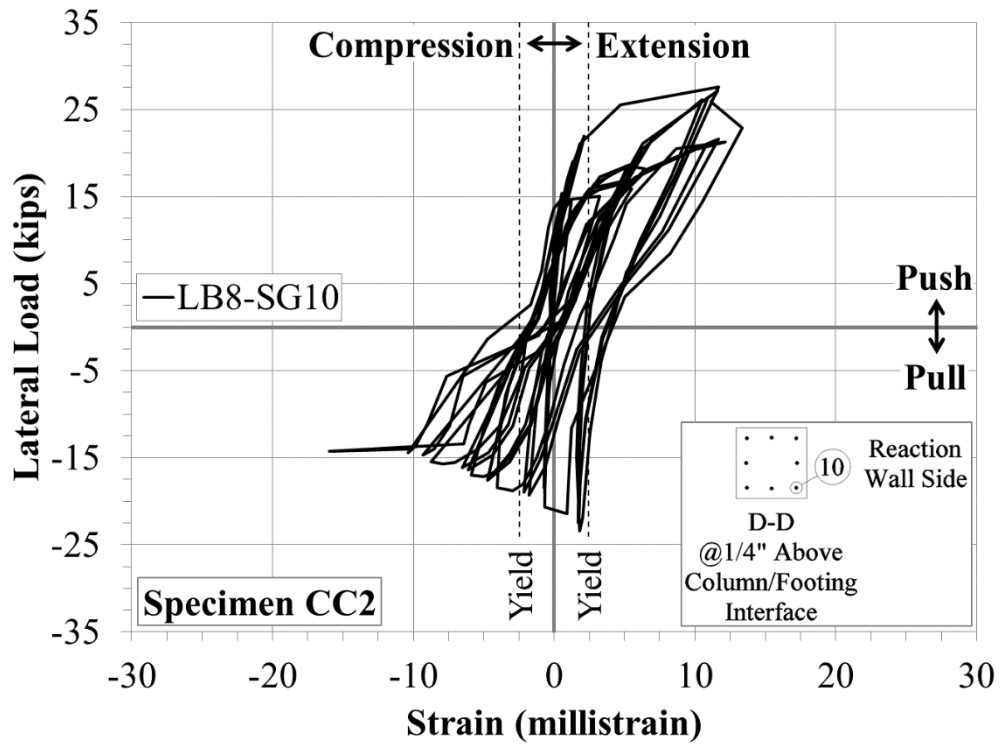
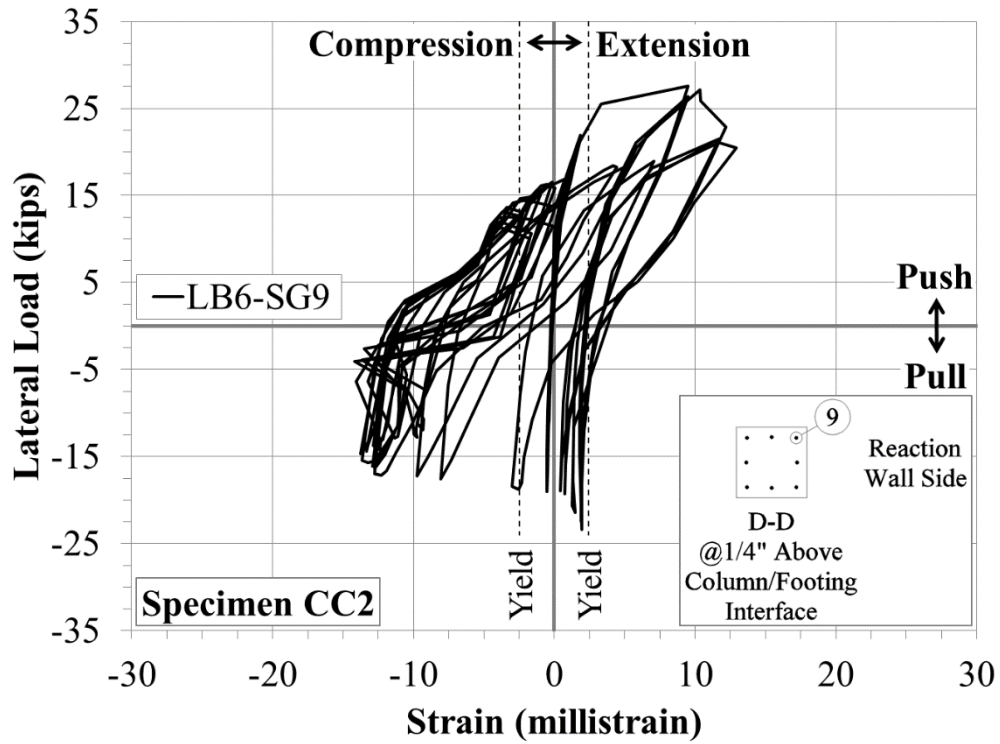


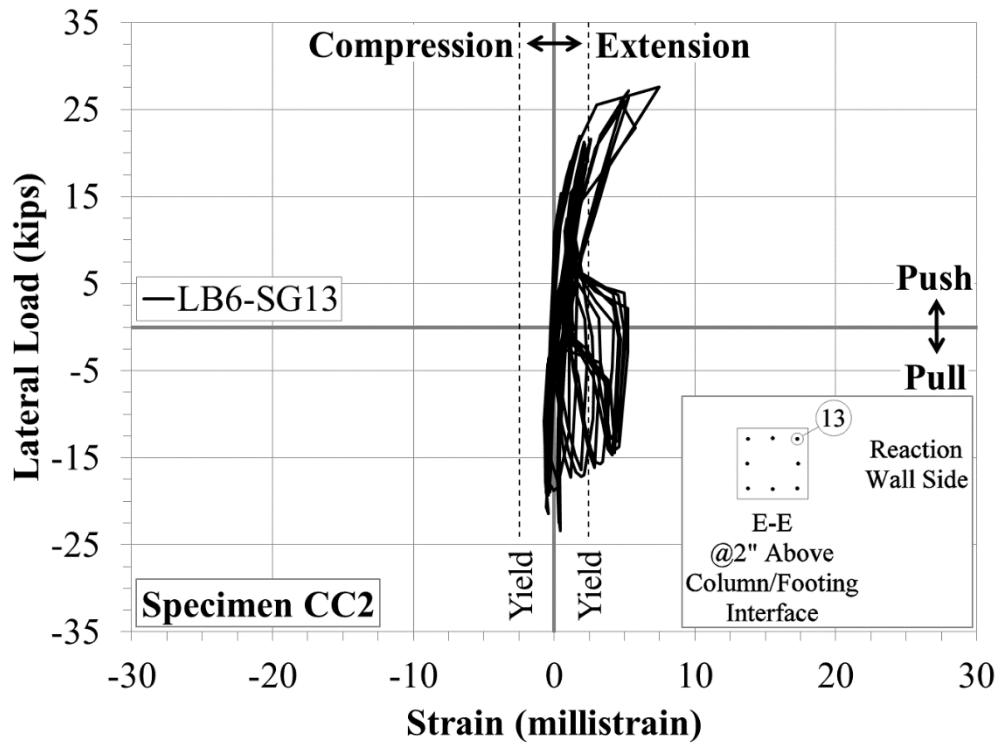
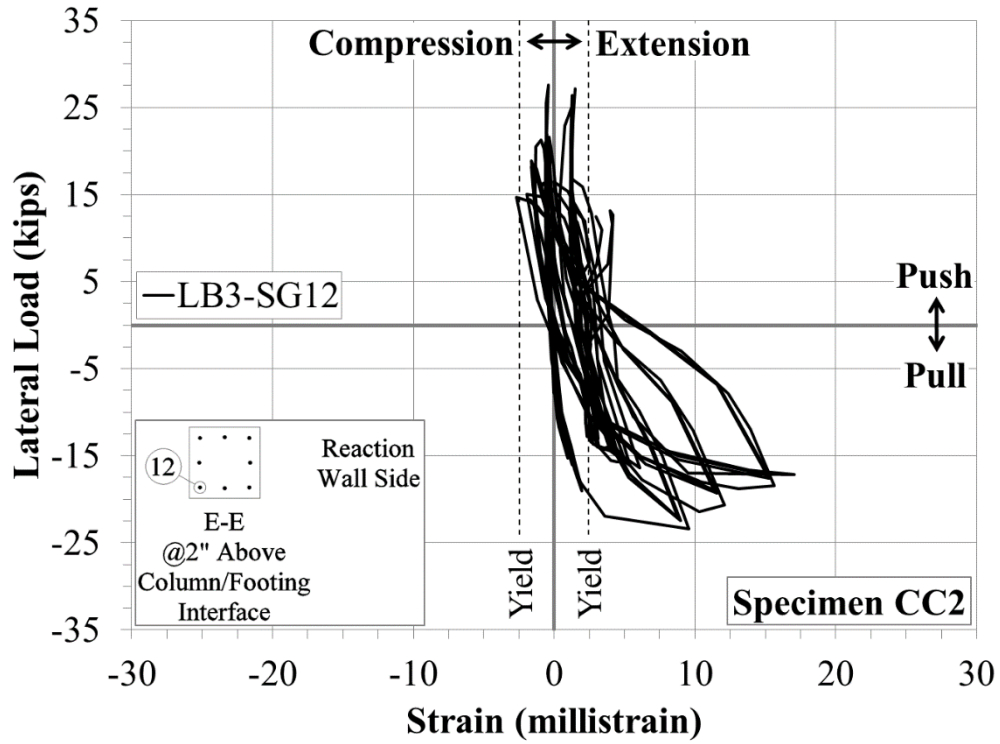


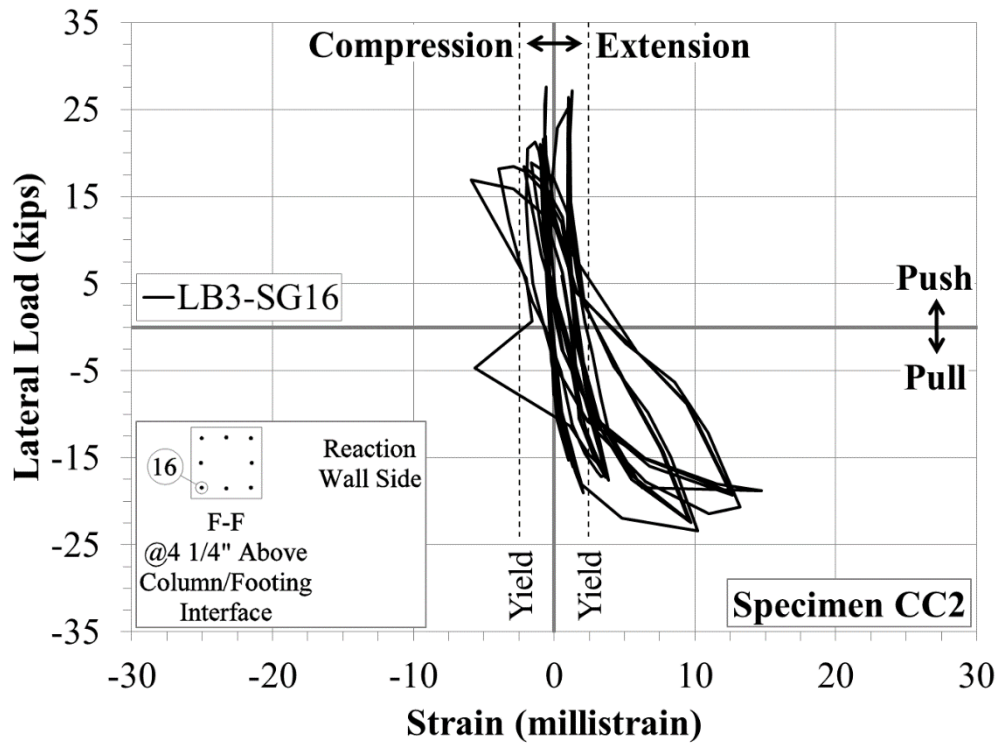
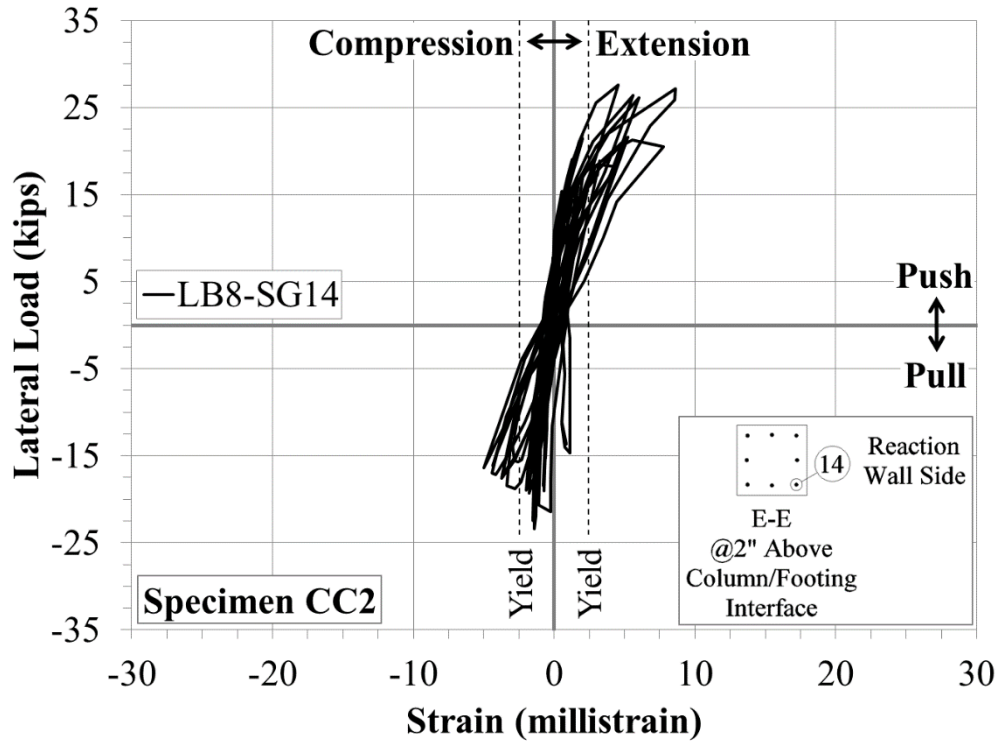
D-2: Specimen CC2

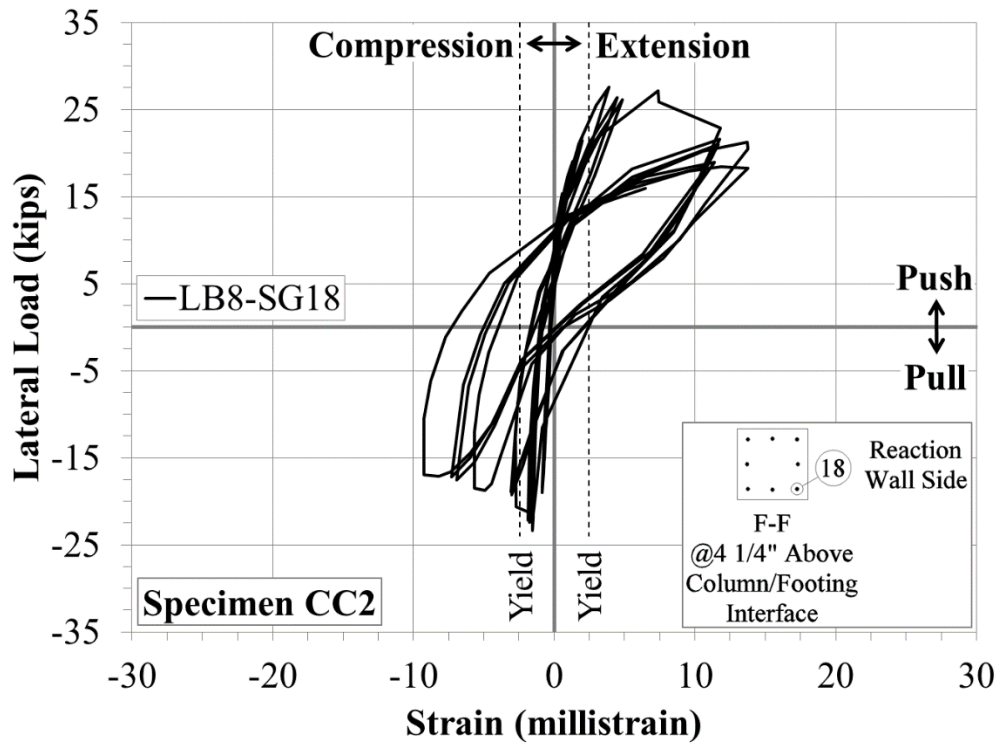
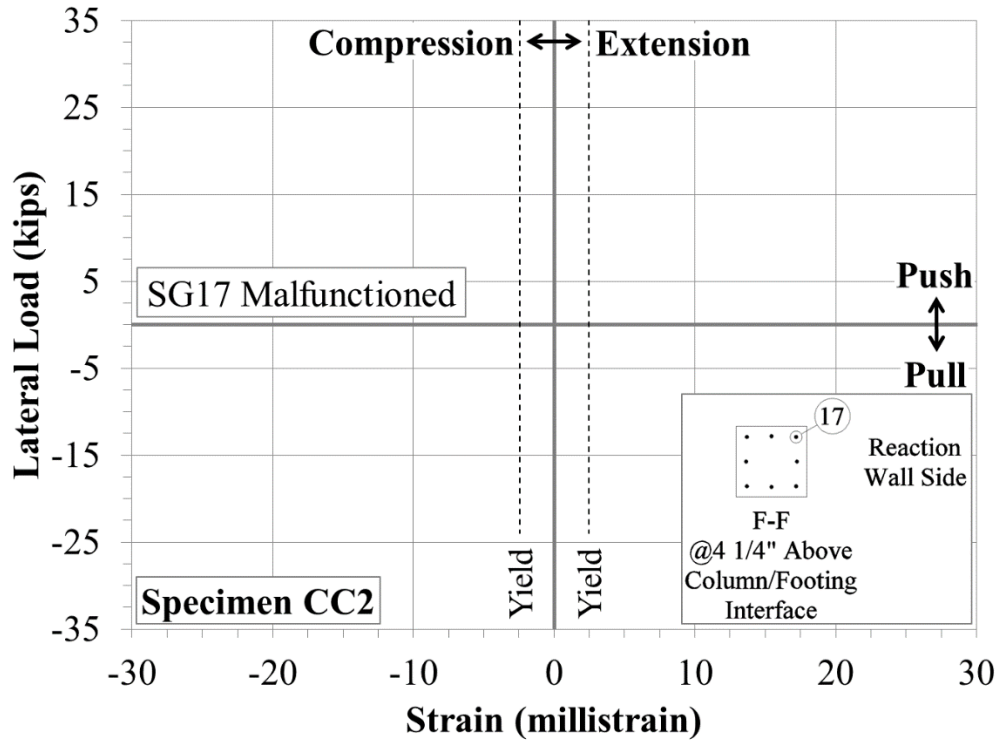


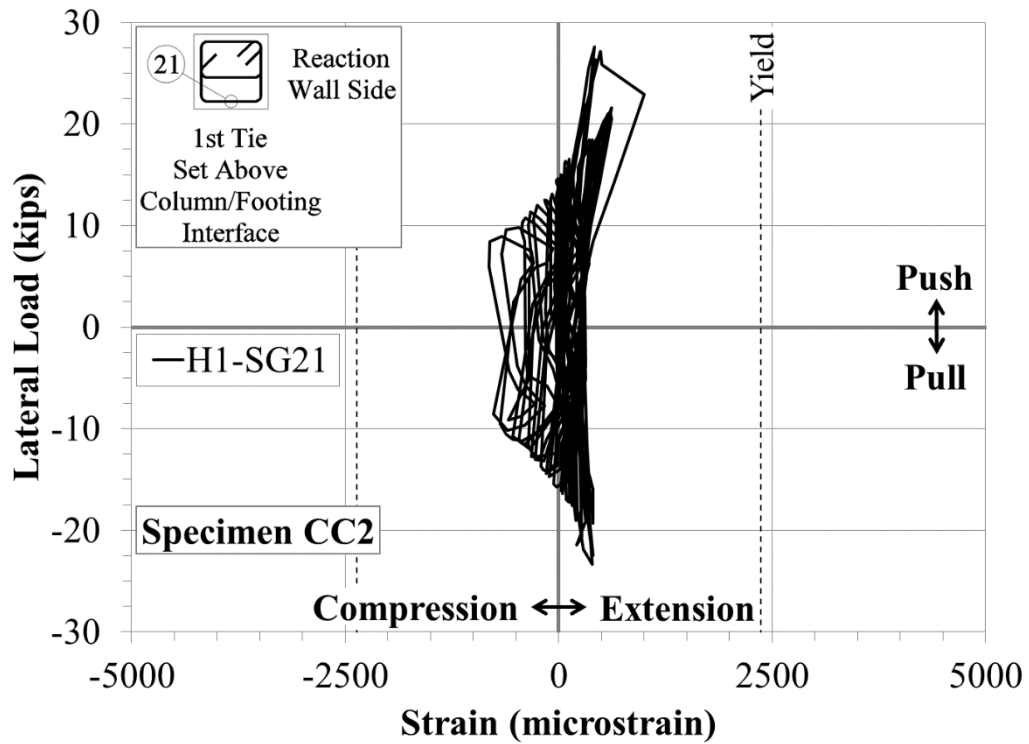
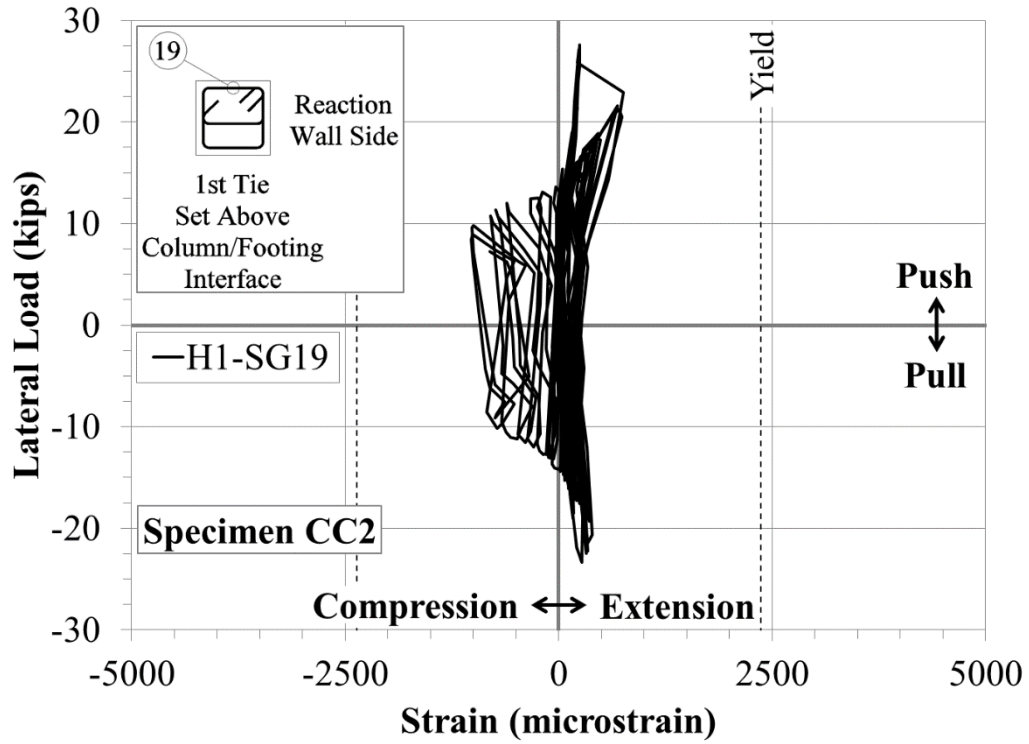


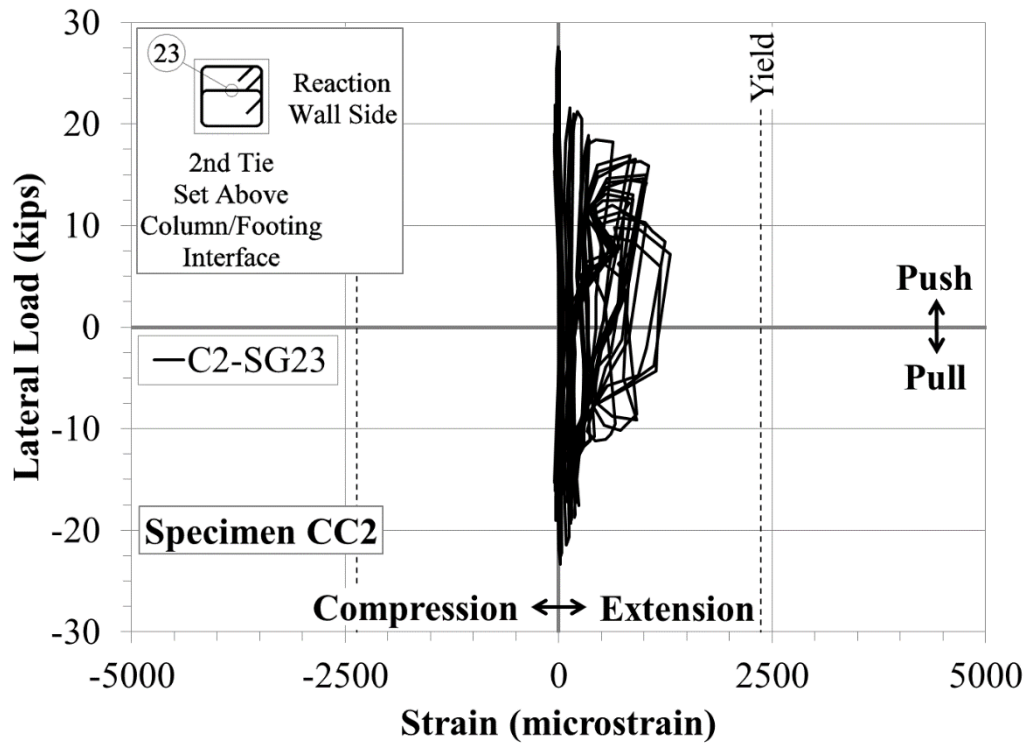
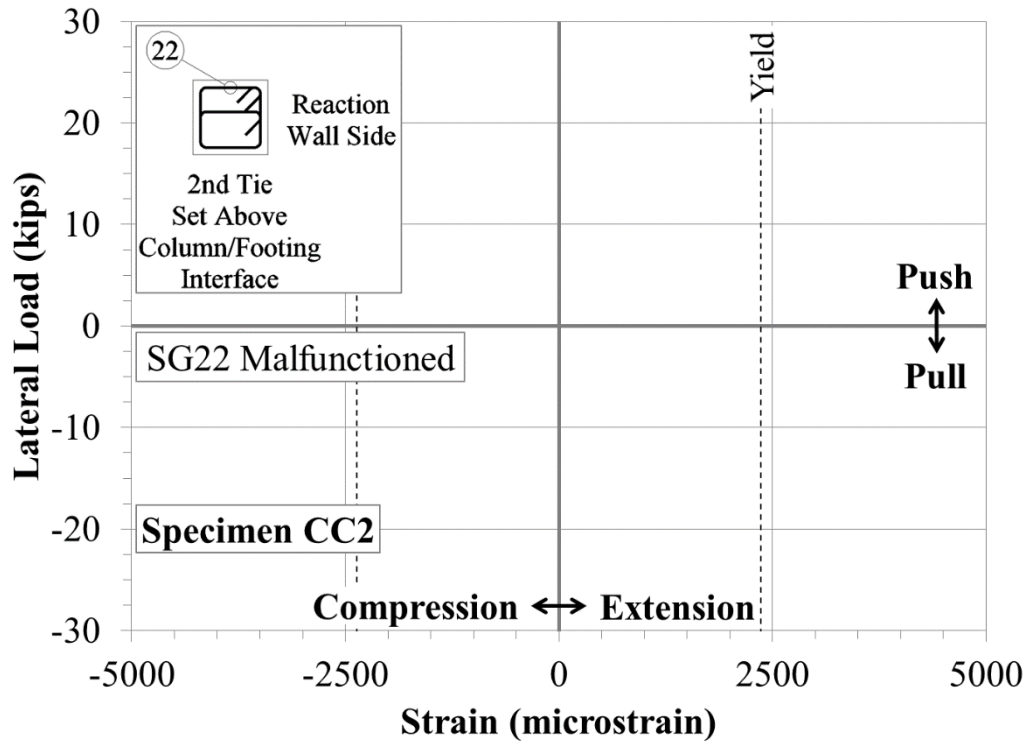


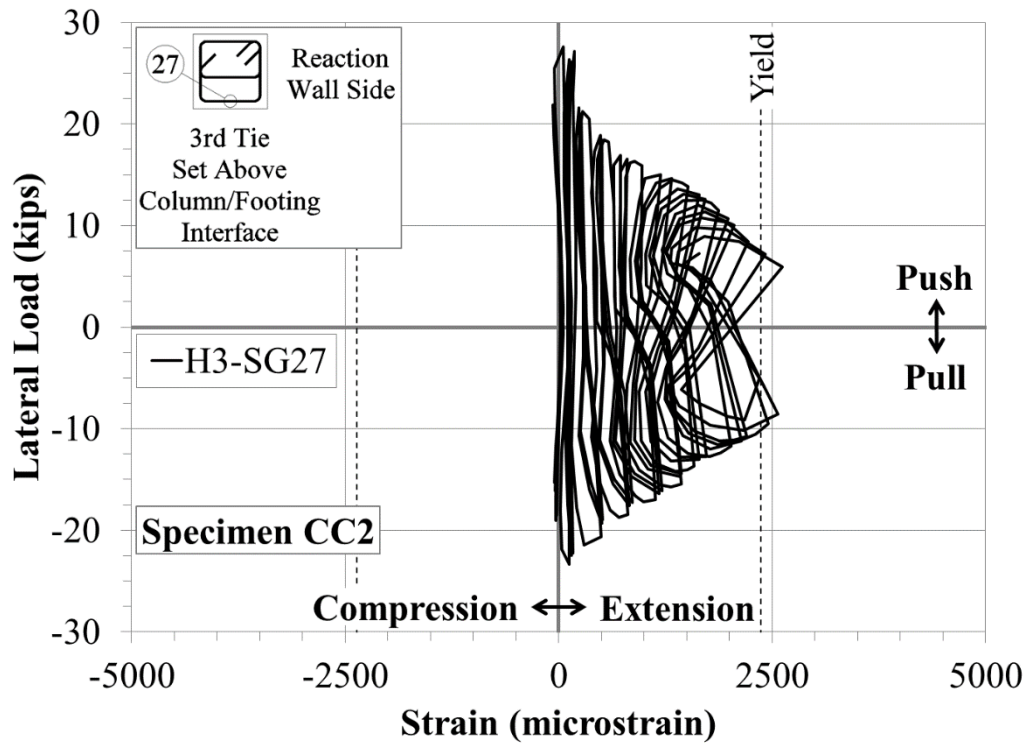
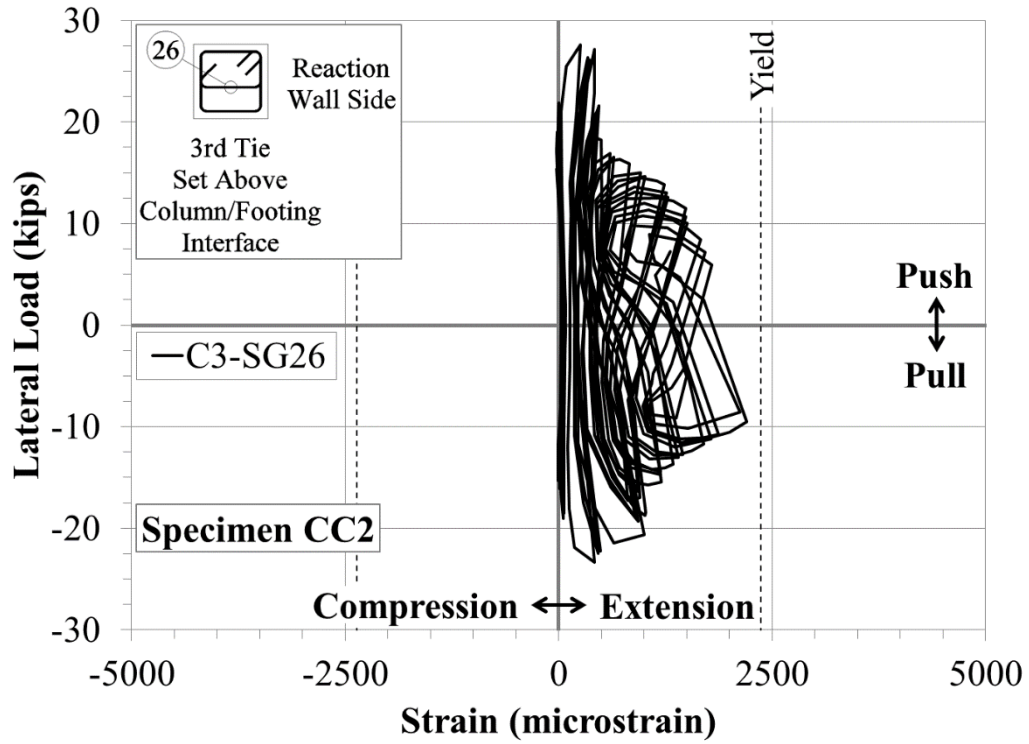




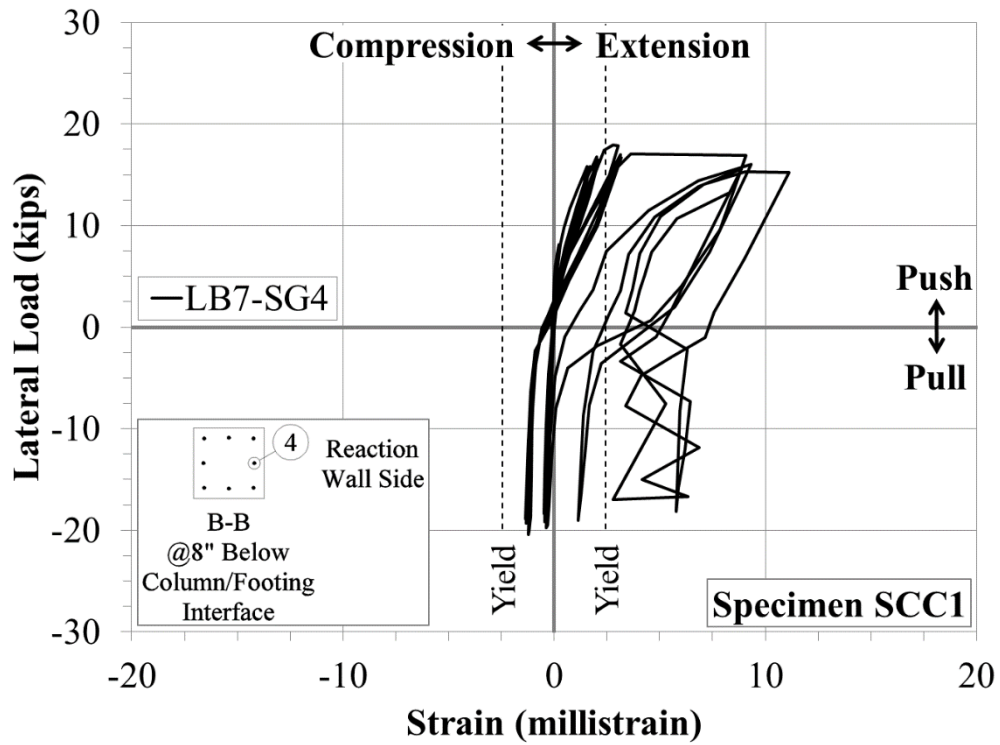
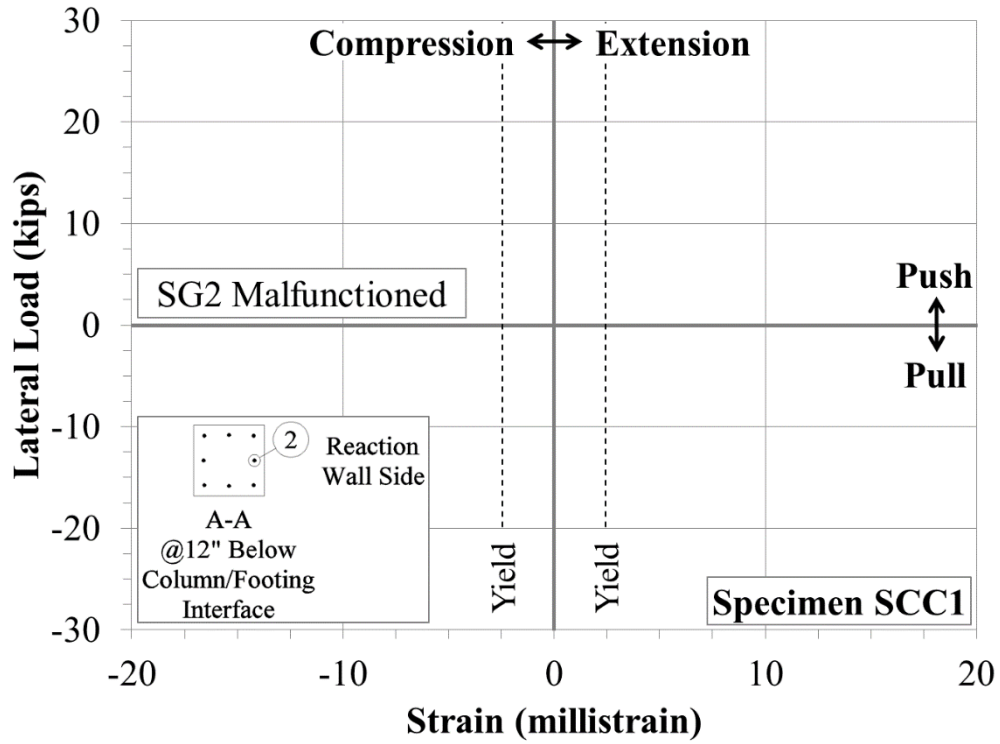


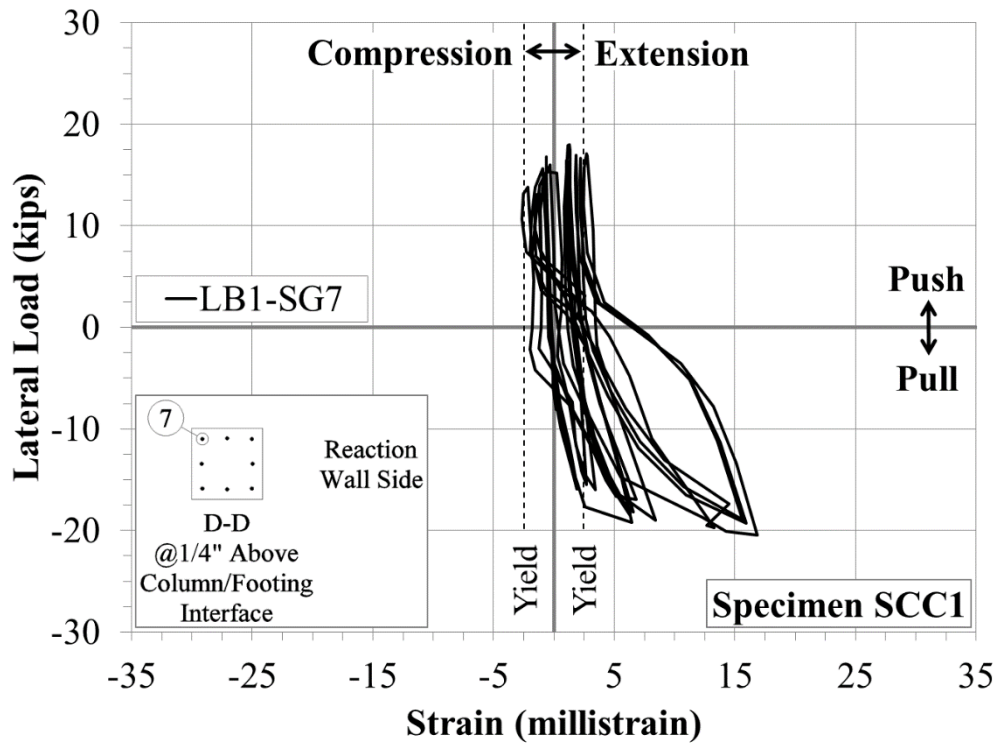
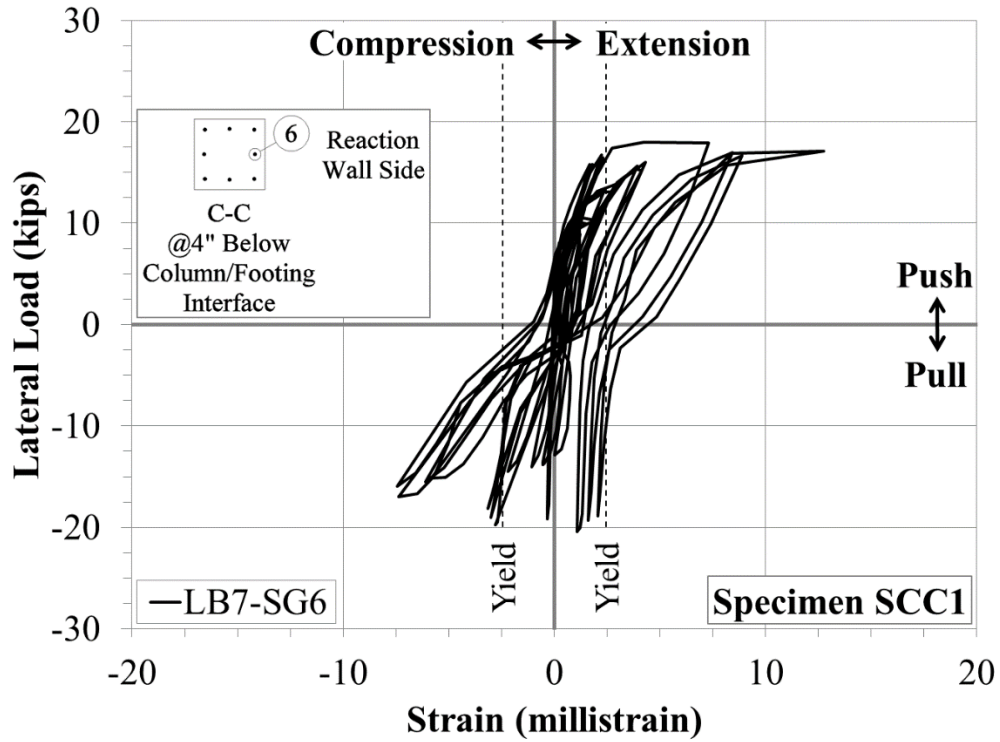


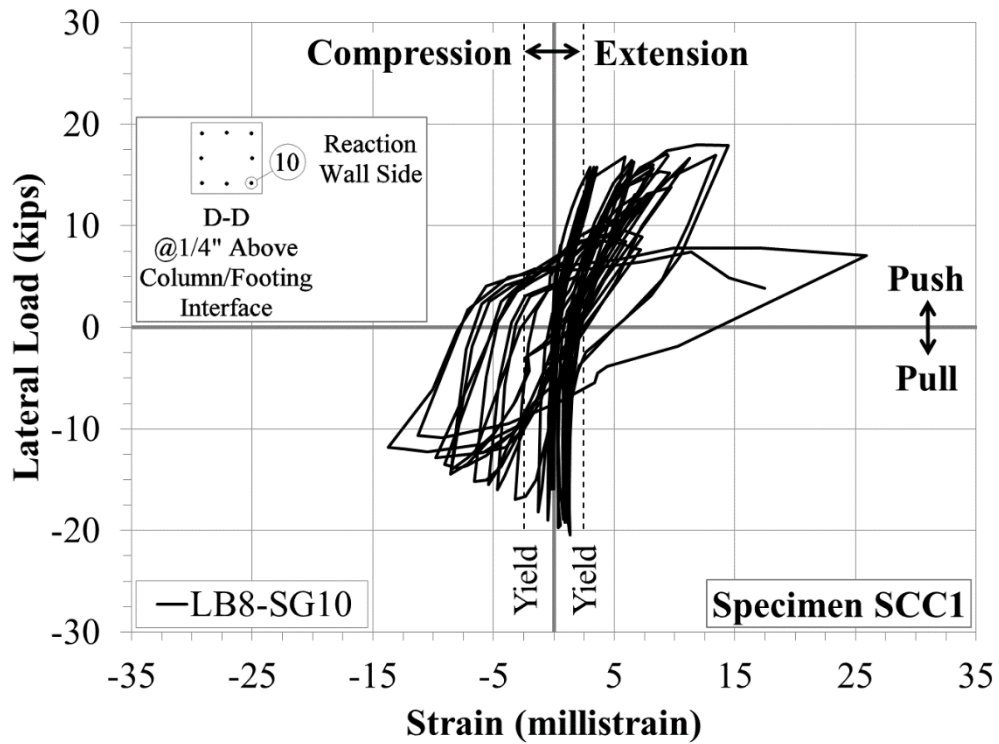
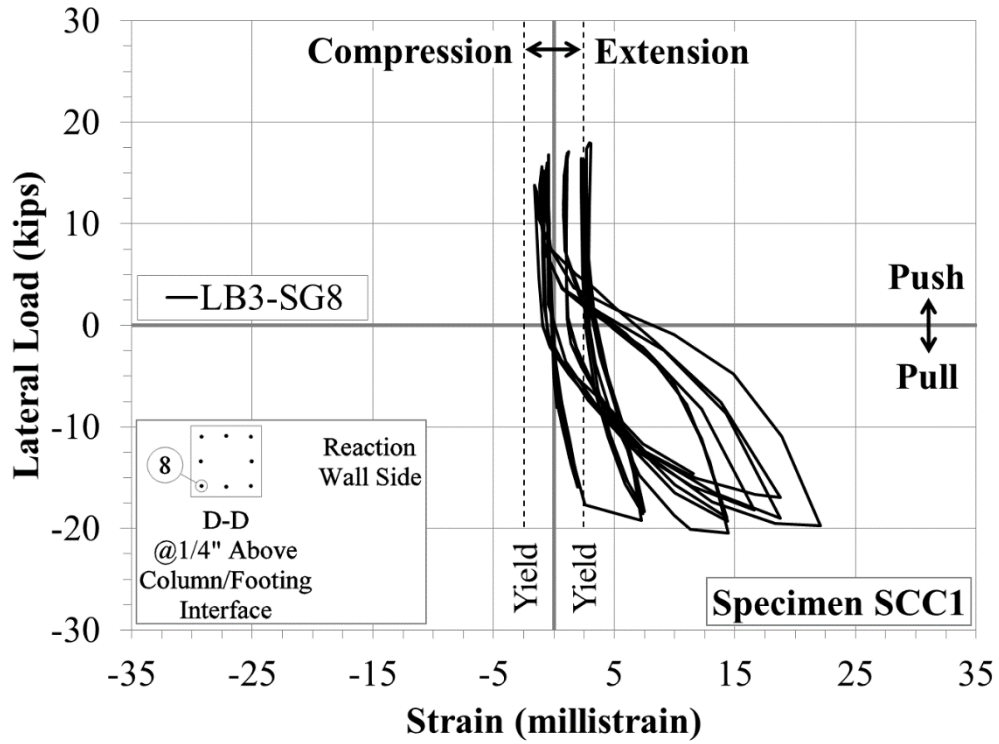


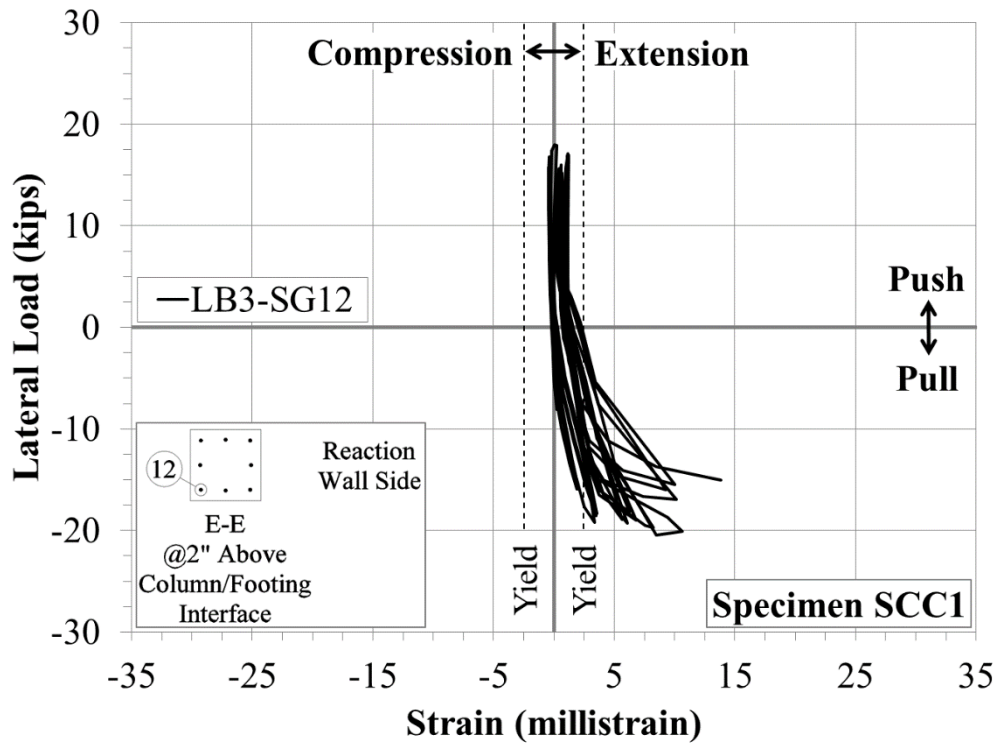
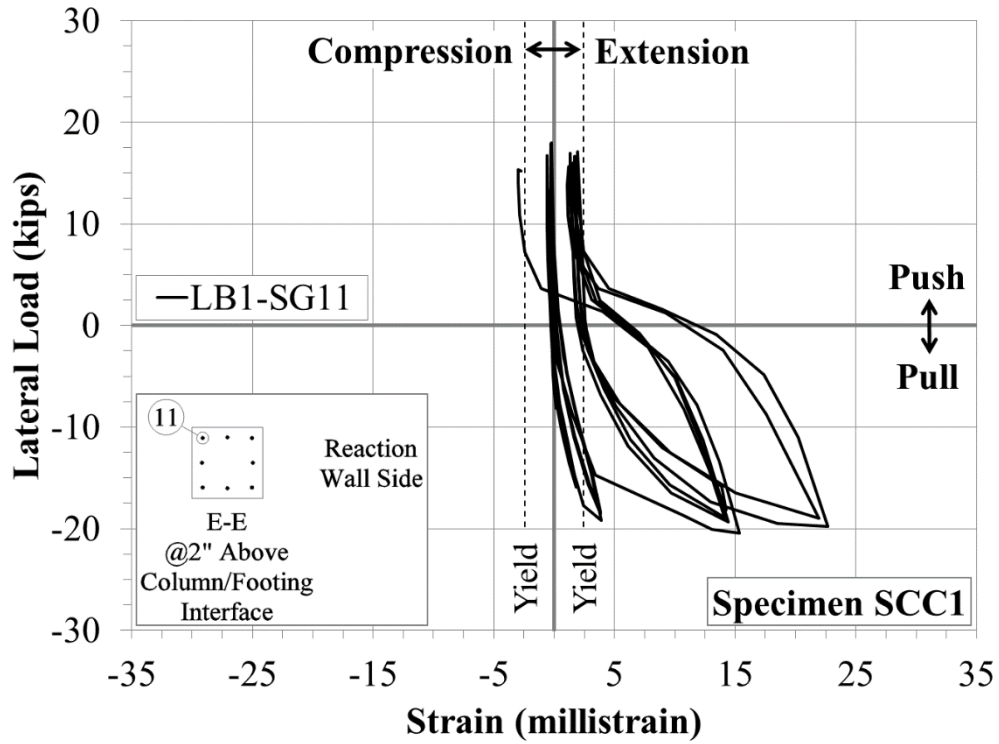


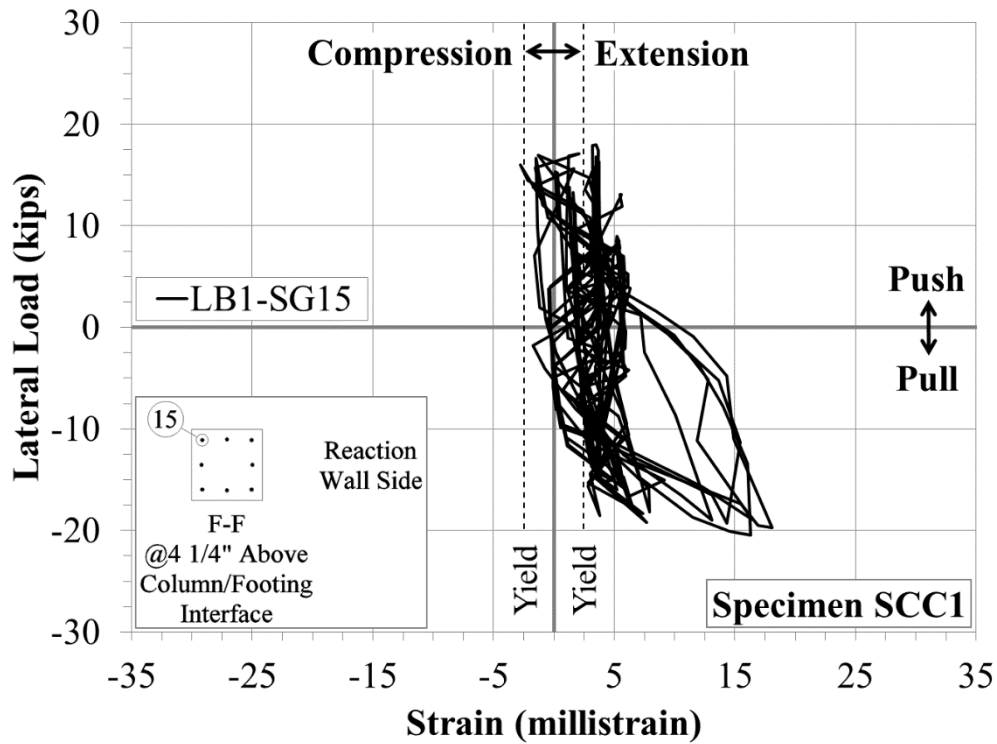
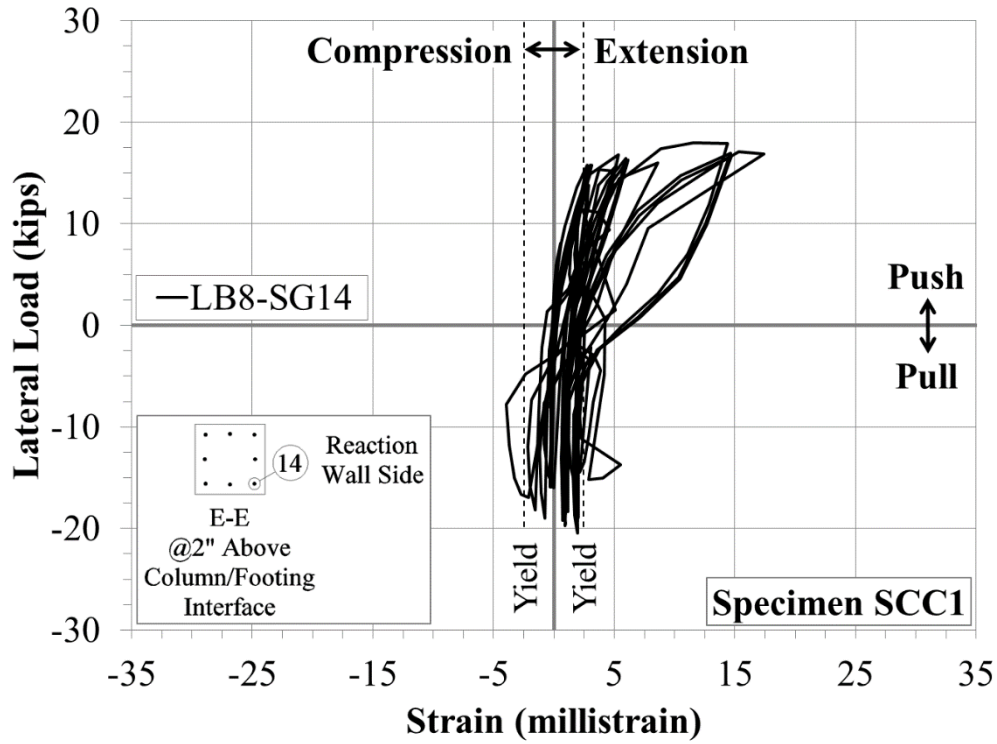
D-3: Specimen SCC1

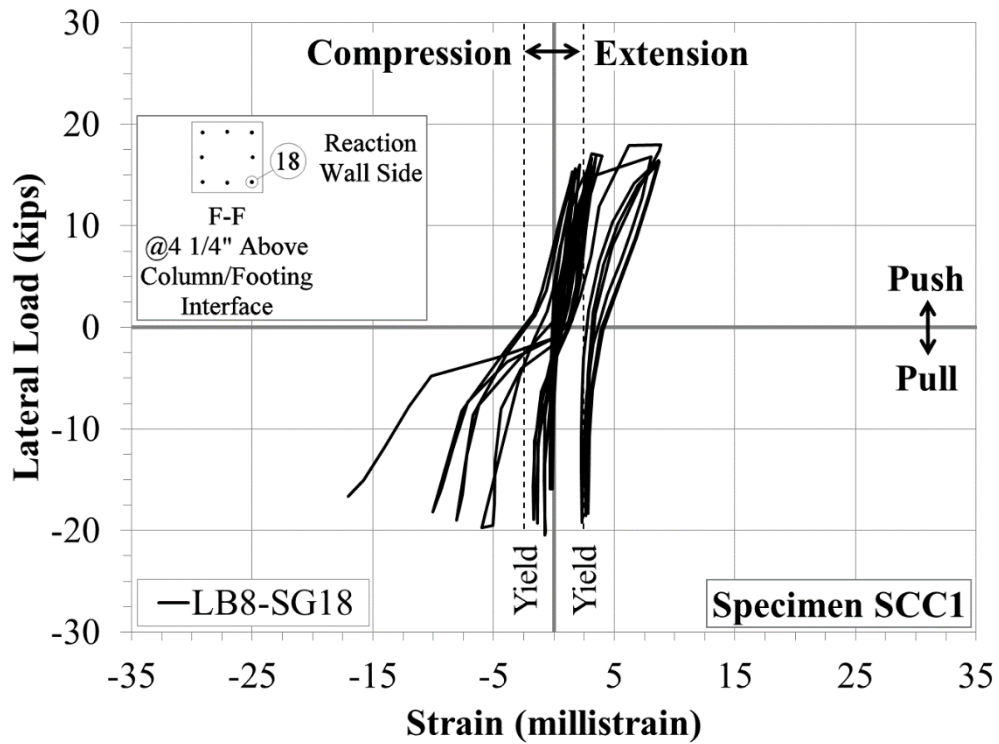
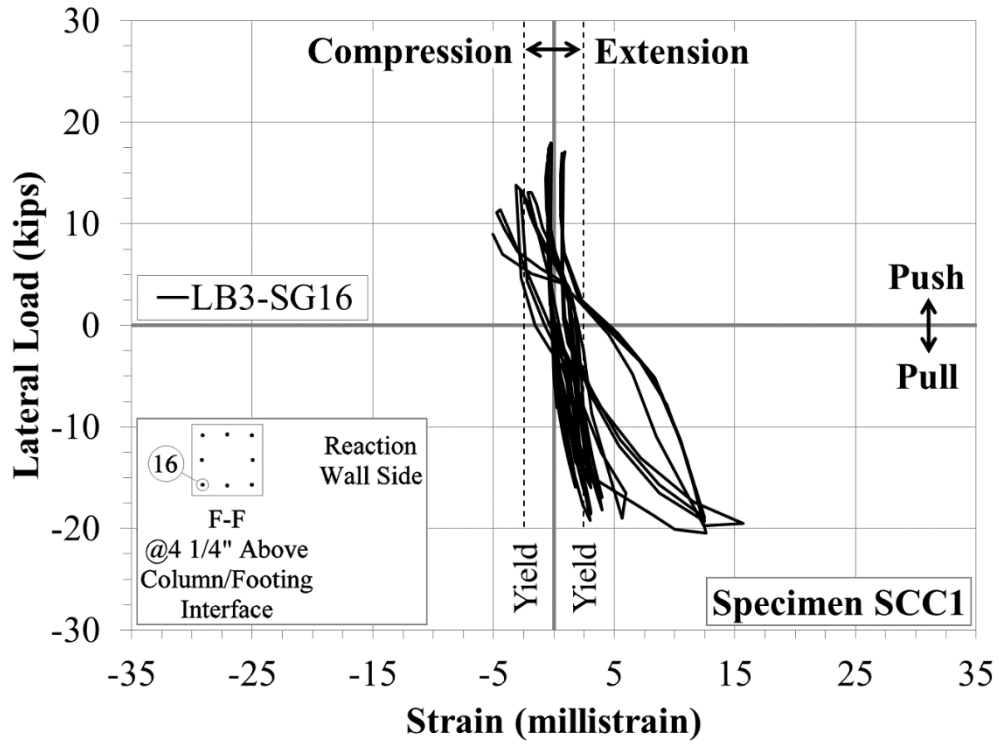


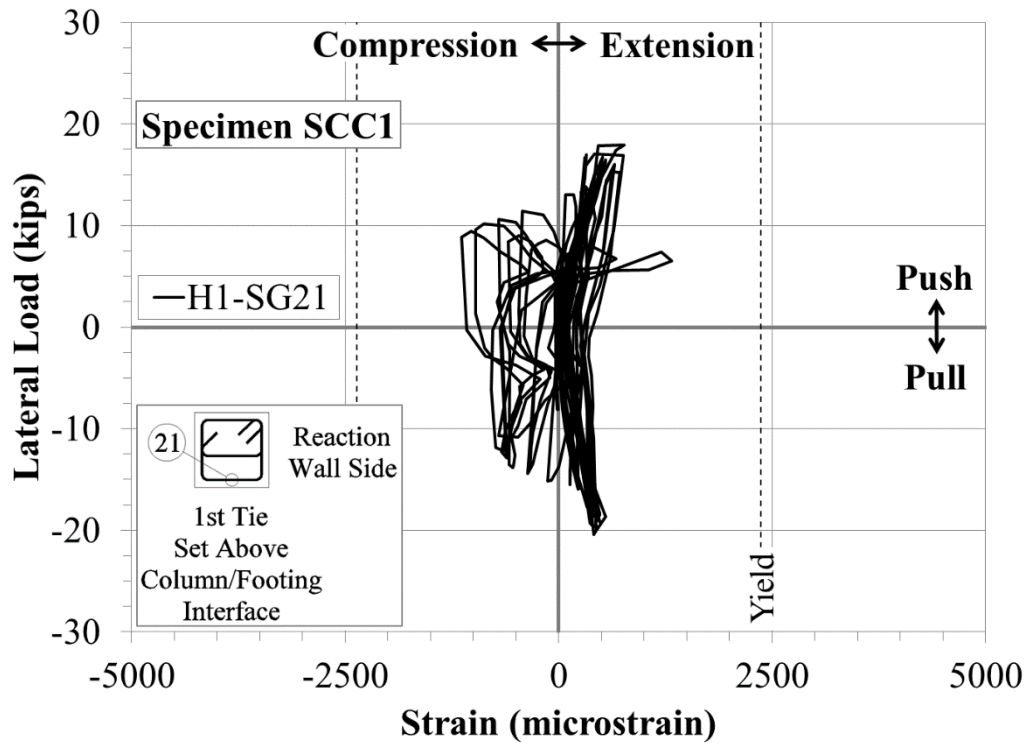
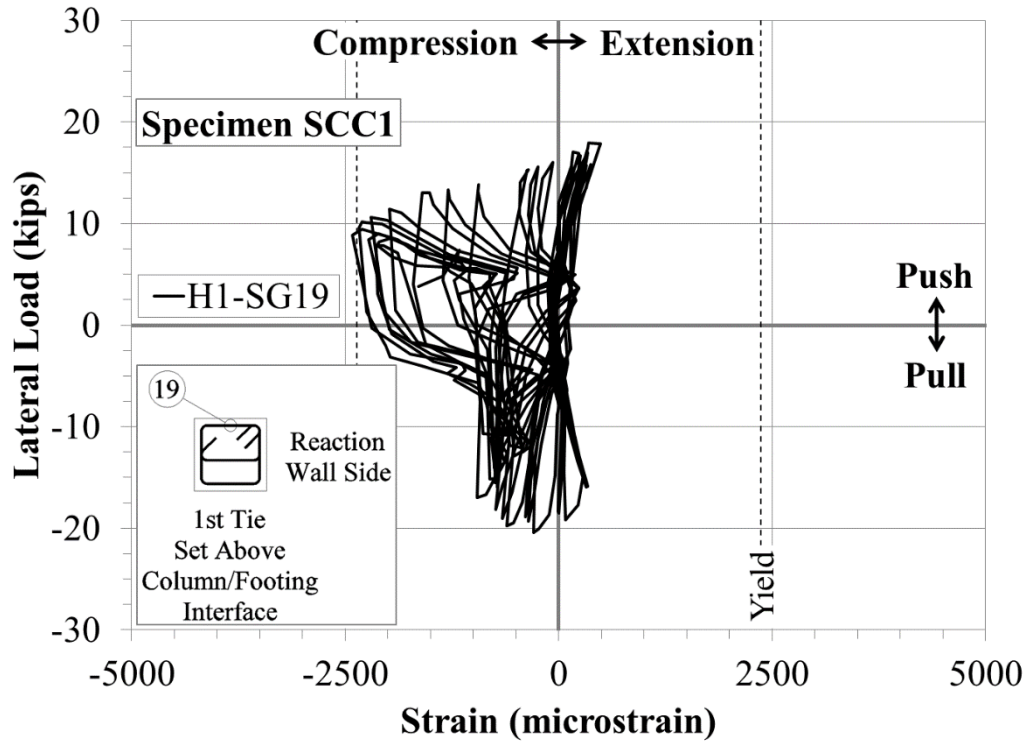


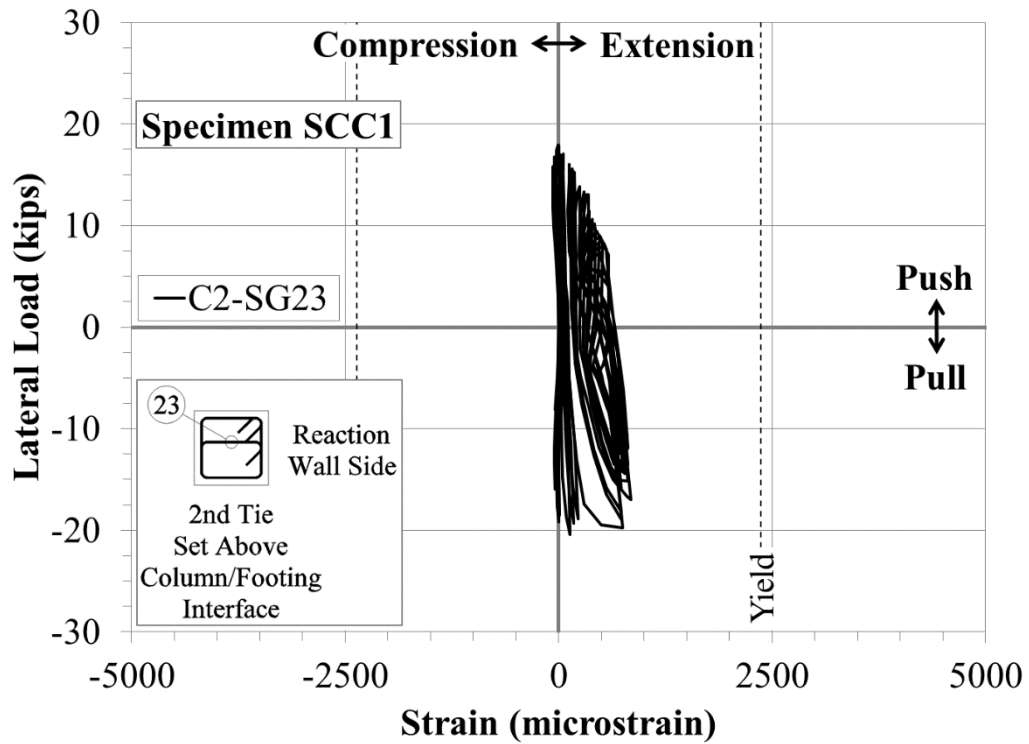
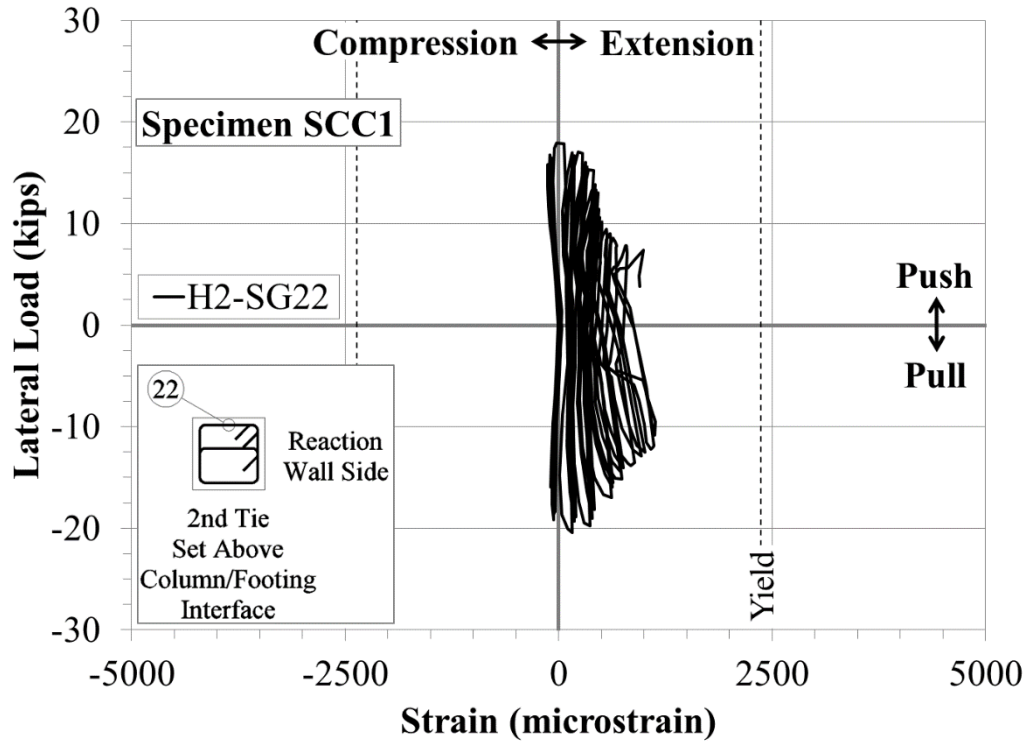


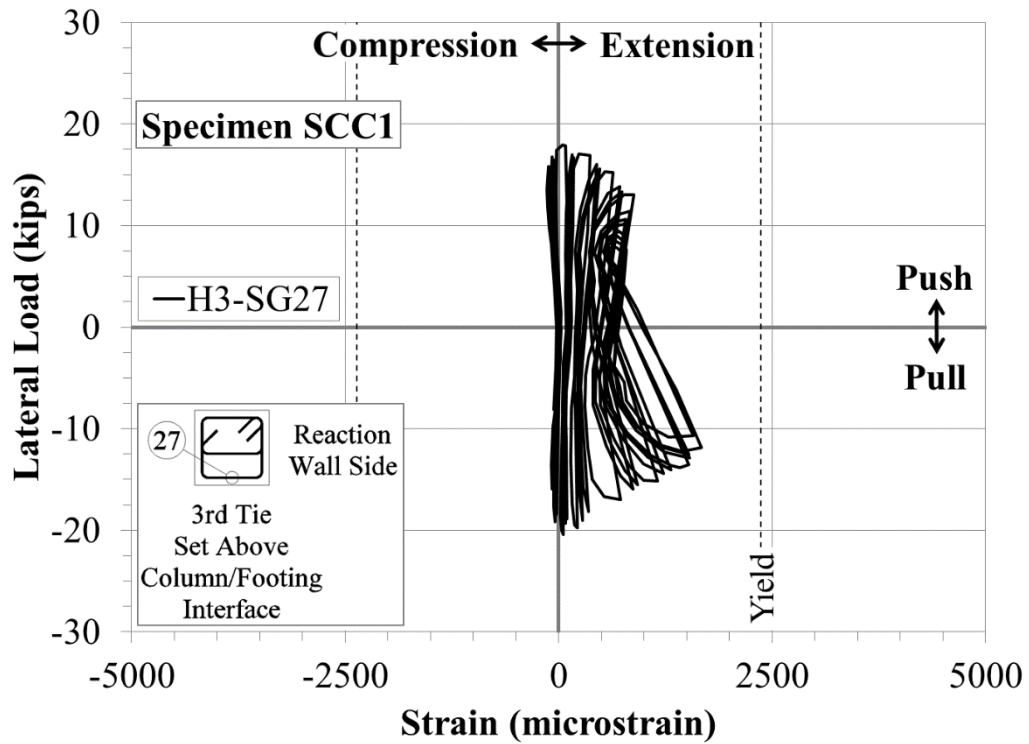
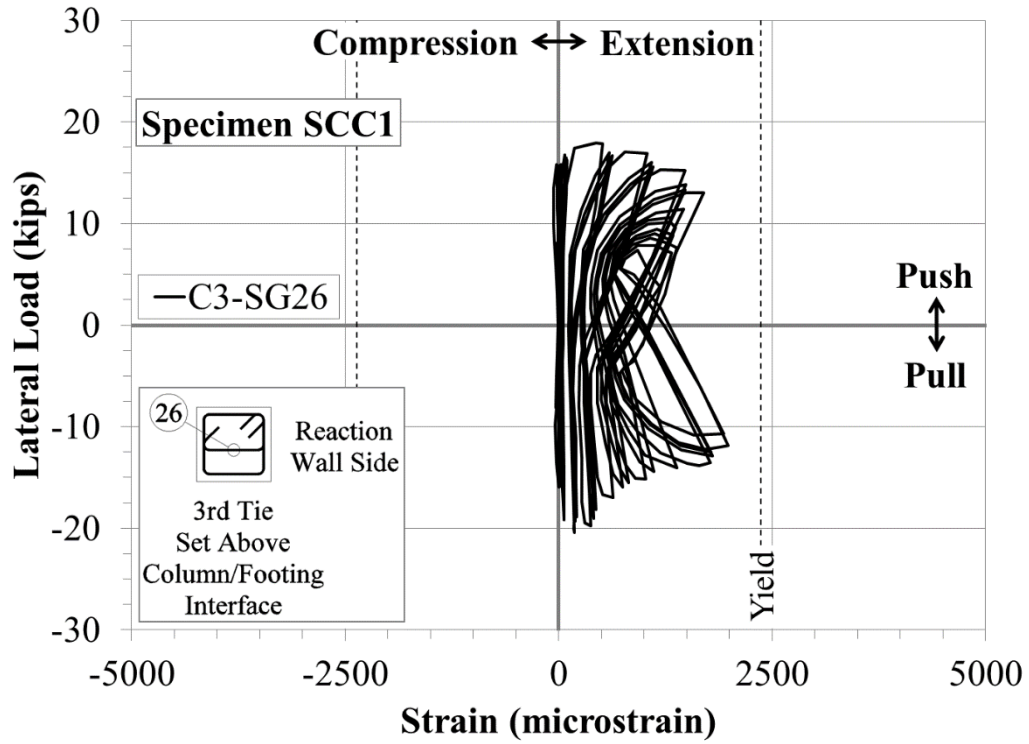












D-4: Specimen SCC2

